Integrated Railway Remote Condition Monitoring

By

Zheng Huang

A thesis submitted to

The University of Birmingham

for the degree of

DOCTOR OF PHILOSOPHY

School of Metallurgy and Materials

College of Engineering and Physical Sciences

University of Birmingham

December 2016

Synopsis

The rail industry is in a state of rapid growth around the world. However, there are a number of important challenges that rail industry will need to address in the foreseeable future if current growth is to become sustainable in the long-term. Firstly, the improvement in the safety of railway systems, which is probably the most immediate requirement that needs to be fulfilled to ensure the momentum in increasing passenger numbers and freight tonnage can be maintained further. Secondly, the introduction of measurable innovation in the rail industry, in order to maximise existing infrastructure capacity and increase profitability of railway assets and operations, and finally, the development of new railway lines to accommodate the continued growth in demand.

Railway infrastructure together with the rolling stock using it, compose a complex engineering system that consists of numerous critical components. The operation of large rail networks results in the generation of vast amounts of data related to inspection, remote condition monitoring, operation and maintenance activities on a daily basis. These data need to be processed, correlated and stored.

Deterioration of the structural integrity of critical railway components can result in emergency maintenance being required or even potential accidents, causing severe disruption on normal services, delays and unnecessary costs. Moreover, it can stretch the available human, equipment and spare parts resources to their limits. The effective and efficient application of advanced inspection and remote condition monitoring systems can help infrastructure managers and rolling stock operators to control the condition of critical assets efficiently and cost effectively. However, in order to achieve reliable evaluation of the condition of the assets being monitored the data generated by the inspection and remote condition monitoring

systems deployed on the network need to be accurate and of good quality. Otherwise, erroneous conclusions can be made.

Various wayside condition monitoring systems are used in the railway industry for diagnosing faults in rolling stock so as to reduce delays, damage to infrastructure, the likelihood of serious accidents and unnecessary financial losses. Existing wayside monitoring systems make use of different types of sensors such as strain gauges, infrared cameras, lasers, acoustic arrays etc. The data generated from these specialised wayside systems provide information regarding the condition of the wheel, axle bearing and bogie. However, such systems are expensive, prone to false alarms and many of them are able to detect serious faults only, just before final catastrophic failure occurs.

Rail infrastructure components such as rails and crossings, are predominantly inspected using conventional technologies based on visual inspection, ultrasonic testing and magnetic flux leakage. Inspection systems can be deployed using push trolleys, hi-rail vehicles or test trains. Unfortunately, with the exception of Fibre Bragg Grating sensors, which can be used to measure strain induced in rails, there are no other systems commercially available for monitoring rail infrastructure remotely.

This study has looked into the improvement of the overall reliability of rolling stock operations and infrastructure reliability, availability, maintainability and safety, through the development and implementation of a novel customised remote condition monitoring system based on the integration of acoustic emission and vibration analysis. The customised system can be further integrated by interfacing it with existing wayside systems such as hot boxes, wheel impact load detectors, etc., as well as inspection data acquired from inspection patrols or test vehicles.

In order to achieve maximum efficiency, collection, processing, trending, and efficient management of data acquired from existing wayside equipment with the customised acoustic emission and vibration analysis system have been considered in this work. The acoustic emission and vibration analysis system which has been developed in collaboration with other researchers from the University of Birmingham, Krestos Limited, VTG Rail and Network Rail makes use of inexpensive and robust sensors that can be easily installed on the rail track with minimal intervention required.

Experimental work carried out under actual conditions in Long Marston rail track and on the UK rail network at various testing sites has shown that these sensors are able to detect wheel and axle bearing related defects as well as monitor critical infrastructure components, such as cast manganese crossings. Interfacing of the customised system with existing wayside systems and data integration in the future can increase substantially the overall efficiency and value of wayside remote condition monitoring, hence improving the reliability of railway transport profoundly.

In addition to the above, a novel signal processing technique based on spectral coherence has been developed for the effective evaluation of data acquired from acoustic emission sensors and accelerometers used to monitor rolling stock and infrastructure. This particular signal processing approach is based on the identification of suitable templates containing features of interest. These templates can then be used to compare them with future signals and determine the extent of similarity. The higher the similarity index the more likely it is that a defect of similar nature is present. This technique can also be used to identify the damage severity, which is a very important requirement for rail infrastructure managers and rolling stock operators who are not satisfied with just detecting a particular defect but want to know when

maintenance should be carried out. In addition, a suitable approach for fusing information from various sensors has been investigated and is presented in detail.

Acknowledgements

I express my gratitude to my family. It is their love, and understanding that have made my life in Birmingham a wonderful time.

I am extremely grateful to my supervisor Dr Mayorkinos Papaelias, who has supported me throughout my study with great patience and guidance. His profound knowledge, experience and enthusiastic styles have encouraged me through many of the difficult times.

I would like to thank Mr Patrick Vallely and Dr Arash Amini for being good friends and their kind support. It was my pleasure to work with you two.

Publications

- M. Papaelias, A. Amini, Z. Huang, P. Vallely, D. Cardoso Dias, S. Kerkyras "*Online condition monitoring of rolling stock and axle bearings*". Proceedings of IMechE-Part F: Journal of *Rail and Rapid Transit Aug 2014.*
- M. Papaelias, Z. Huang, A. Amini, P. Vallely, N. Day, R. Sharma, Y. Kerkyras, S. Kerkyras, "*Advanced wayside condition monitoring of rolling stock wheelsets*". The 11th ECNDT 2014.
- Z. Huang, A. Amini, L. Wang, M. Papaelias, S. Kerkyras "*Online evaluation of railway axle bearing faults using acoustic emission and vibration analysis*". NDT 2014, BINDT, July 2014 Manchester, UK.
- Z. Huang, "Decision Support Tools and advanced signal processing approaches for RCM data analysis". Remote Condition Monitoring (RCM) on Railway workshop, March 2016, Istanbul, Turkey.
- A. Amini, M. Entezami, Z. Huang, H. Rowshandel, M. Papaelias "*Wayside detection of faults in railway axle bearings using time spectral kurtosis analysis on high-frequency acoustic emission signals*". Advances in Mechanical Engineering, 8(11), p.1687814016676000. 2016
- Z. Huang, P. Vallely, A. Amini, S. Shi, M. Papaelias, *"Structural health monitoring of cast manganese crossing using acoustic emission techniques"*. Birmingham Centre for Railway Research and Education, December 2015.

Table of Contents

List of Figures

List of Tables

Abbreviations

AE	Acoustic Emission
AVI	Automatic Vehicle Identification
CPSD	Cross Power Spectral Density
DAQ	Data Acquisition unit
EMI	Electromagnetic Interference
ESR	Emergency Speed Restriction
FFT	Fast Fourier Transform
HABD	Hot Axle Bearing Detector
HFRT	High Frequency Resonance Technique
KPI	Key Performance Indicator
PSD	Power Spectral Density
RAMS	Reliability, Availability, Maintainability and Safety
RCF	Rolling Contact Fatigue
RCM	Remote Condition Monitoring
RFID	Radio Frequency Identification
RMS	Root Mean Square
Sa/s	Samples per second
SCADA	Supervisory Control and Data Acquisition
SNR	Signal-to-Noise Ratio
TAAD	Track Acoustic Array Detector
WILD	Wheel Impact Load Detector
WMA	Wayside Monitoring Alliance
WPD	Wheel Profile Detector
FBG	Fibre Bragg Grating

Chapter 1:

Introduction

Chapter 1: Introduction

1.1 The industrial need

The growth prospect of international economy is closely linked with the level of mobility and its efficiency. The more efficient the national and international transport systems are, the more important their contribution to the general economy becomes. A smoothly operating transport system increases productivity and helps guard societal integrity at national and international level. It permits strong links to be formed with key economic hubs within a country, as well as with overseas states, ensuring goods and citizens can move around safely, reliably and on time. Maintaining existing business-levels and attracting new investments require by default a well-coordinated and reliable transport system.

The rail network is a key component of any surface transport network. It is relatively benign to the environment in comparison with road transport. It also helps decrease congestion in the already very busy roads of the world. Supporting the growth of rail transport has significant economic and environmental benefits, since it increases the potential of passengers and tonnage of goods that can be transported in a cost-efficient manner. For passengers, lower travel prices increase the level of mobility potential, both for business as well as leisure purposes, helping spread the wealth in all regions of a country and its neighbours. By reducing the cost of transporting goods across a country and beyond its borders, it is possible to lower prices and increase competitiveness of domestic industries. Therefore, rail transport is considered as the backbone of the entire transport system in several developed and developing countries.

Improving the efficiency of rail transport has profound positive consequences for the economy and society as a whole. However, in order for rail industry to increase its positive

impact it needs to move towards a 24-hour operation. This is currently impossible to implement due to the significant technical challenges that need to be overcome concerning reliability, availability, maintainability and safety (RAMS) of railway assets.

An additional problem that needs to be overcome is the eradication of delays and disruption due to rolling stock and infrastructure faults. Unfortunately, the nature of the rail network is such that faulty rolling stock and infrastructure components can result in considerable delays and disruption. It is very important for the rail industry to ensure that railway systems are reliable, minimising the likelihood of unpredictable faults, and in certain extreme cases, the occurrence of derailments.

Rolling stock traffic density has increased substantially over recent years in several countries (UIC, 2015). Any delays, unplanned disruption or reduction in availability due to maintenance required for repair of infrastructure defects or rolling stock faults have serious consequences for the mobility of passengers and freight using rail transport. Moreover, they result in significant costs being incurred unnecessarily. To effectively address the growing demand for rail transport, infrastructure managers invest heavily in the improvement of the rail networks respectively based on an extensive programme of track renewals and targeted upgrades, including the construction of new lines (UNIFE, 2016).

Although track renewals and upgrades contribute to the capacity increase of the rail network and improve efficiency, they cannot entirely address the problems associated with operational RAMS. The continuously growing traffic density coupled with higher axle loads and travel speeds means that any defects or faults in critical rail track and rolling stock components, such as cast manganese crossings, rails, wheelsets, and bogie suspensions, may lead to costly delays and disruption until emergency inspection and maintenance activities have been

completed. As the available capacity of the rail network becomes used up by the increasing numbers of passengers and freight, financial and mobility consequences arising from delays and disruption become rapidly magnified. Thus, additional improvements, other than track renewals and construction of new lines, need to be devised to further enhance capacity and enable the safe and cost-efficient transport of more passengers and freight over rail.

Railway infrastructure and rolling stock interact with each other at the wheel-rail interface through complex dynamic mechanisms. The rate of structural degradation sustained by rail track components (Andersson and Dahlberg, 1998, Grassie, 2005, Lewis and Olofsson, 2009, Grassie, 2012, Yilmazer et al., 2012, Shi, 2015) and rolling stock wheelsets and suspensions (Vallely, 2015, Amini, 2016) is strongly dependent on the wheel-rail interface quality, axle loads and rolling stock speed. Hence, maintenance and repair requirements for both rail track and rolling stock wheelset and bogie components are closely linked to the dynamic loads sustained.

Although current theoretical understanding of dynamic mechanisms influencing structural degradation in critical railway and rolling stock components has improved substantially, the need for effective Remote Condition Monitoring (RCM) remains. This is due to the stochastic nature of loading conditions that results in significant uncertainty. Advanced RCM technologies, which are capable of continuously and reliably evaluating critical railway assets, are yet to be used to their full potential.

1.2 Railway rolling stock operational reliability

The wheelset and bogie suspension are the most important components in the dynamics of rolling stock. The wheelset includes the wheel, axle bearing and axle. Any defects developing in these critical components if left unchecked can eventually result in extensive damage to

rolling stock and rail infrastructure and in extreme cases to serious derailments. A recent study published by DNV considered the railway accidents that have been reported in 23 countries over the past years (Andersen, 2011).

It was revealed that out of the 700 accidents considered, 37% of them were due to rolling stock faults (Figure 1-1). Moreover, 84% of all rolling stock-related accidents were confirmed to have been caused by wheelset and bogie defects (Figure 1-2).

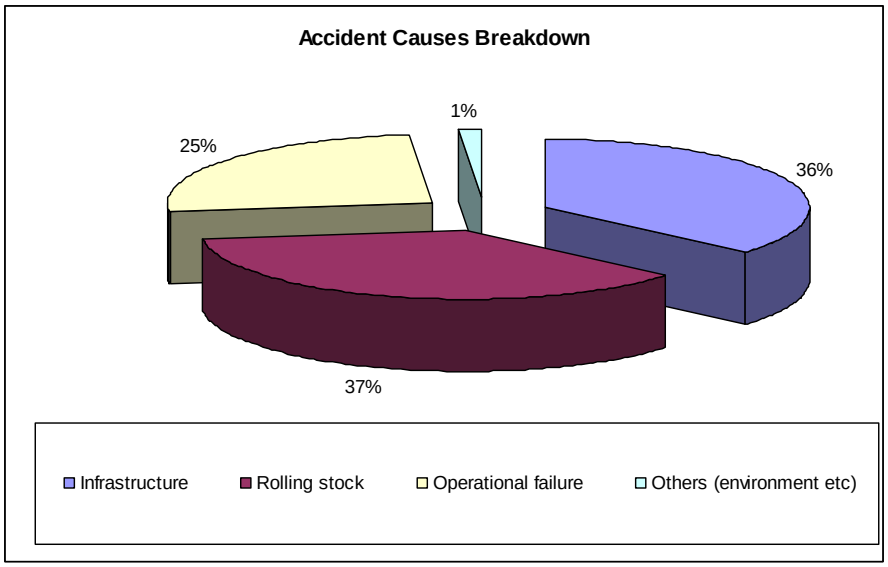

Figure 1-1: Railway accidents considered in the DNV study by cause (Andersen, 2011)

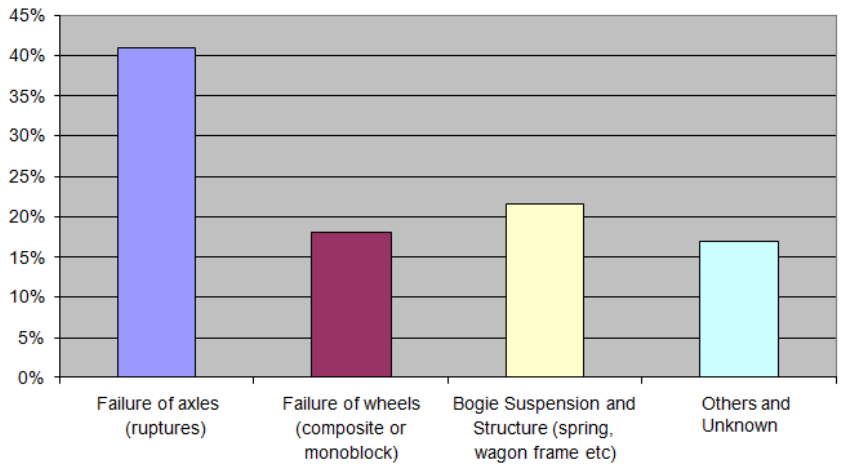

Figure 1-2: Rolling stock related accidents by cause (Andersen, 2011).

According to the findings of the DNV study 41 % of all rolling stock accidents were due to axle failure, which in the vast majority resulted from faulty bearings. Almost 60% of all rolling stock accidents were due to wheelset failure, thus accounting for one in five of all railway accidents considered in the study.

If a wheelset defect is not detected promptly, it will gradually become more severe, leading to more serious damage to other important rolling stock components as well as the rail track (Bladon et al., 2004). For example, an unattended wheel flat can result in failure of the primary suspension component of the bogie, damage to the axle bearing and damage to the rails. Furthermore, wheel flats can cause excessive vibration and noise, which are particularly undesirable in urban and sub-urban areas. Early detection of faults helps rolling stock operators to schedule maintenance activities more efficiently without compromising the minimum required fleet availability.

Poor maintenance scheduling can lead to reduced number of available trains, which in some extreme cases can cause disruption of normal train services giving rise to significant fines. In 2009, S-Bahn, the local train operator in Berlin, Germany, had to withdraw the majority of its fleet after a fractured wheel caused a Class 481 train to derail. Unscheduled emergency inspections and maintenance forced S-Bahn to leave only 165 out of the 630 units operational for several months (Railway Gazzette, 2009).

Wayside monitoring systems are installed in or next to the track to detect and identify faults in wheelsets and bogies before they cause a failure by measuring one or more parameters e.g. axle bearing temperature, impact loads applied on the rail, etc. (Barke and Chiu, 2005). The most common wayside systems currently in use include Hot Axle Bearing Detectors (HABD or hot boxes), Track Acoustic Array Detectors (TAADs), Wheel Impact Load Detectors

(WILDs), Weigh in Motion Detectors, Wheel Profile Detectors (WPDs), Automatic Vehicle Identification (AVI) units, track circuits and axle counters (Amini, 2016). Each wayside system is designed to monitor certain aspects of wheelset and bogie operation. Hence a significant number of various types of systems need to be installed throughout the network to monitor rolling stock condition.

Despite the large number of wayside monitoring systems currently in use, dangerous faults such as defective axle bearings or broken bogie suspensions are predominantly detected only after reaching a critical stage (Papaelias, 2013). The majority of wayside systems normally act as individual checkpoints for the detection of defects and only give an alarm if a pre-defined threshold is exceeded (e.g. HABDs). Data from individual wayside systems are not trended and integrated and as a result large numbers of false alarms are not uncommon for certain types of wayside systems. In contradiction to the U.S. and Australian railways, European rail networks only recently began using Radio Frequency Identification (RFID) tagging. This has made vehicle identification more complex and data trending more difficult in the past. Generally, there is no or very little trending of data for a particular train travelling on the network.

In this work, a novel integrated wayside condition monitoring system based on acoustic emission and vibration analysis was developed and studied in terms of its capability in detecting different types of faults and their severity in rolling stock wheelsets, and critical infrastructure components, such as cast manganese crossings. The customised system offers the possibility of being interfaced in the future with other commercial wayside systems such as HABDs and TAADs. Hence, different wayside systems can be correlated to each other to improve the accuracy of fault detection (Bladon et al., 2004).

1.3 Railway infrastructure reliability and availability

For any rail network, efficient operation requires good availability and reliability of the entire infrastructure. Structural damage influencing just a small section of a major rail line can cause significant disruption throughout the entire line in both directions. Severe rail defects (e.g 1A or 1B class) need to be replaced immediately or soon after detection. Certain defect types may be clamped using special fishplates until the rail section affected has been replaced. An Emergency Speed Restriction (ESR) of 20 MPH is normally applied for all rolling stock travelling over the damaged rail section until the necessary maintenance has been carried out (Papaelias et al., 2008, Vallely, 2015, Huang et al., 2015). ESRs imposed cause delays to normal traffic incurring additional costs to the rail infrastructure manager since rolling stock operators need to be reimbursed for the lost travel time.

Cast manganese crossings are particularly valuable assets, since they permit rolling stock to pass from one track to another. These particular rail infrastructure assets, in several cases form bottlenecks in the rail network. Structural damage of cast manganese crossings is far more complex to address, as these components are customised for the particular location. Hence, the time required in order to bring in a replacement crossing can range from a few days up to several weeks.

Rails are easier to replace but with increasing traffic density, inspection engineers have less time and opportunities to evaluate infrastructure condition in order to ensure severe defects are detected promptly. Furthermore, engineering crews have fewer opportunities to carry out the necessary maintenance. It is thus quite common that major maintenance campaigns take place during holiday periods such as Christmas, Easter and Bank Holidays to avoid disruption on normal workdays. However, these maintenance activities may still interfere with the travel

plans of holidaymakers trying to make their way from their homes to their holiday destinations, ports or airports.

Railway infrastructure is at the moment inspected using various inspection techniques mostly based on conventional technologies such as Ultrasonic Testing, Magnetic Particle and Liquid Penetrant Inspection, Automated Vision, Magnetic Flux Leakage and Eddy Current Testing. RCM techniques are limited to the occasional application of Fibre Bragg Grating (FBG) sensors, which are predominantly applied for the detection of unacceptably high axle loads or abnormal impacts on the rails.

One of the main objectives of this study has been to develop the necessary RCM technology that can be deployed easily and cost-effectively for the accurate assessment of critical railway infrastructure components in real time. This objective has been motivated by the increasing usage of rail networks around the world allowing far less time for inspection, the limitations of existing technologies (Papaelias et al., 2008) and the gradual implementation of the 24-hour railway being realised (e.g. London Underground).

1.4 Remote condition monitoring of railway assets

Practically all wayside RCM systems used by rail infrastructure mangers are designed to monitor rolling stock components and more specifically axle loads, wheel tread and axle bearing condition. Rail track infrastructure components are not monitored using RCM technologies.

Railway infrastructure managers rely instead on inspection campaigns, which are carried out by dedicated measurement trains and maintenance crews on foot. This inspection strategy is labour intensive and incurs a high cost. Effectively, inspection is performed only when the rail

section concerned is closed and at night. Even measurement trains, depending on the type of inspection performed cannot be used at the same speed as normal traffic due to the physical limitations of the non-destructive testing technique employed.

Moreover, the condition of the structural integrity of cast manganese crossings cannot be evaluated with conventional inspection technologies due to the physical limitations of these techniques. With the advent of 24-hour railway and the ever increasing demand for higher capacity and improved availability the need for implementing alternative inspection strategies becomes more evident.

Acoustic emission and vibration analysis are two powerful passive RCM techniques, which can be applied for the evaluation of the structural integrity of various railway assets including rails, cast manganese crossings, wheels, axle bearings and bogie suspensions. Both techniques apart from being extremely sensitive for detecting very small propagating defects of different types, including early initiation, they are relatively simple to implement and can be fully automated. More importantly, they can be interfaced with existing state-of-the-art systems resulting in a holistic RCM system with a feedback loop mechanism offering several advantages. The RCM data generated can be employed in a decision support tool helping improve maintenance efficiency and cost-effectiveness whilst maximising availability of both rail infrastructure and rolling stock.

RCM of critical rail infrastructure assets is a realistic alternative, which should be in place in time in order to accommodate the continuous growing demand for rail transport and avoid capacity bottlenecks in the short to medium term. However, there is also a clear requirement of addressing the question of how advanced rail infrastructure RCM systems are installed across the network since it is impossible, at least for the moment, to deploy sensors

throughout the network. This is not only due to the cost incurred, which would be unrealistic for any rail infrastructure manager, but also the amount of data that would need to be handled and processed.

1.5 Research objectives

The profound value of wayside monitoring in helping safeguard the RAMS of railway operations is undeniable. However, despite significant investments by the rail industry in this sector, the efficiency and reliability of wayside monitoring have not reached the desired level. Structural deterioration of the rail infrastructure and rolling stock faults, including axle bearing, wheel and bogie suspension defects still remain a significant problem which needs to be addressed as traffic density, train speeds and axle loads increase in rail networks around the world (Papaelias et al., 2012).

The main objectives of this study were to develop and evaluate an advanced wayside monitoring system based on acoustic emission and vibration analysis that can detect, identify and evaluate wheelset and suspension faults in rolling stock and structural deterioration in critical railway infrastructure components, e.g. rails and cast manganese crossings. The customised system developed employs open architecture to enable future integration with other systems. Various signal processing techniques based on conventional algorithms (e.g. moving RMS, moving kurtosis, HFRT), as well as more advanced approaches based on signal correlation and data fusion have been investigated in-depth.

The research aimed to assess the efficiency of the system developed as part of this study as well as exploit the opportunity of integrating and correlating data from various wayside systems in order to increase the reliability of results, improve accuracy and minimise the likelihood of false alarms. In this study, correlation between acoustic emission and vibration

data has been explored for the accurate detection and quantification of wheel and axle bearing faults and crack propagation in cast manganese crossings. The ultimate goal has been to feed the data generated from wayside systems in an intelligent decision support tool that can be used to decide the optimum maintenance process and schedule.

Certain types of RCM equipment used by rail infrastructure managers provide several synergies for data fusion. Thus, integration could potentially increase substantially the value of the information gained even from systems that are already installed and in use. In certain cases, the infrastructure manager has access to the low-level signals generated by a sensor. This can enable a more in-depth analysis or analysis in association with another type of sensor giving rise to far richer information.

Successful tests have been carried out under simulated conditions with the help of VTG Rail at the Long Marston test track and in the UK network with the support of Network Rail. The hardware employed together with the signal processing methodology and the main results arising from the present research are discussed later in this thesis. A number of alternative methods of signal processing and data correlation have been considered in order to improve data analysis and increase reliability of results. The main results of the research together with the experimental methodology employed are described in sufficient detail in the following chapters.

Chapter 2:

Rolling stock and infrastructure defects and inspection techniques

Chapter 2: Rolling stock and infrastructure defects and inspection techniques

2.1 Introduction

Rolling stock and infrastructure components are subjected to harsh operational conditions involving high and variable dynamic stresses, impact loads, corrosive media in the form of moisture and salts, debris contaminants and exposure to a wide temperature range. Before entering service all critical rolling stock and infrastructure components are subjected to stringent quality control to avoid any manufacturing defects which could lead to premature failure (Papaelias et al., 2008). Nonetheless, under prolonged in-service conditions, gradual wear, damage initiation and propagation will naturally develop. For this reason, rails, cast manganese crossings, rolling stock wheelsets and bogie suspensions are inspected at regular intervals to ensure no damage is present or if it is present that it has not exceeded the tolerance limit imposed by the standards.

The main challenge for the rail transport industry is to increase its operational capacity, cost-effectiveness and profitability by optimising RAMS. Rail transport needs to be efficient and reliable with a high level of asset availability. To enable this, the rail industry must adopt novel RCM technologies, which will help achieve optimum operational capability and contribute to a noteworthy reduction of operational costs as well as support the implementation of 24-hour railway. For that reason, the introduction of sufficient innovative technology into the rail industry is timely.

Infrastructure managers and rolling stock operators worldwide have invested significantly in RCM technologies in order to increase RAMS of railway operations. The main purpose of the RCM systems currently used is to evaluate the condition of the wheel tread and axle bearings

in order to prevent damage on rails from high axle and accidental impact loads due to the presence of wheel flats, derailments due to poor conformity of wheel tread with rail profile or failed bearings. Unfortunately, none of the RCM systems currently in use is designed to directly monitor rail infrastructure. Moreover, onboard systems in the scarce cases where they are used are restricted in measuring axle bearing temperature or acceleration (Jones and Southcombe, 2015, SKF, 2010).

For the evaluation of the structural integrity of rails and crossings, it is necessary to deploy inspection engineers and test trains on the network using specialised manual and automated equipment. Manual inspection equipment and test trains carry a high capital cost. However, the main disadvantage is that inspection needs to be scheduled when normal rail operations have seized. This reduces the maximum availability and capacity possible for the rail network and complicates further the implementation of 24-hour railway. There are also limitations in the defect resolution with increasing speeds which means certain types of defects even when severe may be totally missed. The advantage of the deliverables implemented in this study is that RCM technology can be used not only to monitor more effectively rolling stock components but also rail infrastructure, particularly rails and crossings.

2.2 Rolling stock wheelsets

2.2.1 Wheel defects

Wheels containing flats, shelling or metal build-up are sources of repeatable severe impact loads on the rail. Such defects have significant detrimental influence on the structural integrity of rails, sleepers, axle bearings, axles and bogie suspension (Nielsen and Johansson, 2000). Moreover, they can result in excessive vibration and noise. Wheel defects are usually related to tread wear, flange wear, fracture, profile damage and cracking (Burstow, 2010, Papaelias,

2009, EN 15313, 2007). The schematic in Figure 2-1 summarises the types of wheel defects commonly found in rolling stock.

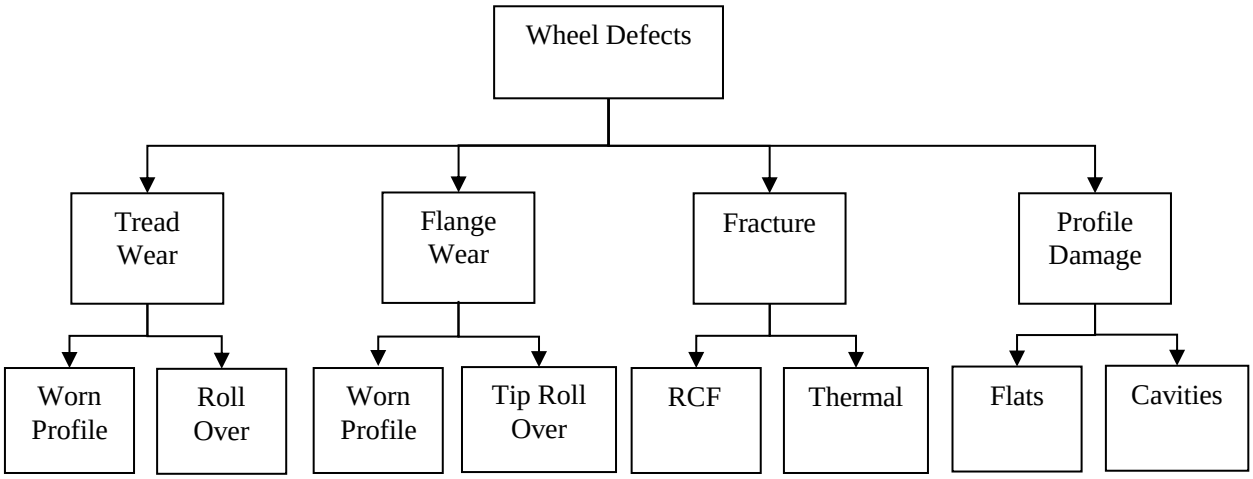

Figure 2-1: Schematic summarising the common types of wheel defects (Schmid, 2010).

Tread wear is most likely to occur as it is the area that constantly interacts with the rail surface and brake pads where these are employed. The condition of the tread has significant influence on wheel performance and wheel life. Flange wear is relatively uncommon, but rates of wear can be high at the interface where the wheel interacts with the rail. Flange wear can lead to worn profiles and tip rollover, which both generate sharp flanges.

There are two main causes of fractures in the wheel surface: Rolling Contact Fatigue (RCF) cracking and shelling (

Figure *2-2*), and thermal effects. Both of these require management by re-profiling to maintain the integrity of the wheel to prevent crack propagation (Burstow, 2010). RCF, thermal cracking and spalling are common in wheelsets using contact brake pads (Ekberg and Sotkovszki, 2001).

Figure 2-2: Shelling on the wheels of the test vehicle due to braking.

Wheel flats are a common type of profile damage on the running surface of a railway vehicle's wheel as shown in the photograph of Figure 2-3. They normally form due to locking of the wheels while the vehicle is braking. Flats always appear symmetrically on both wheels of a wheelset. Single or multiple flats covering the majority of the circumference of the wheel are possible. The maximum allowable size of flat spots for railway operation is dependent on the type of rolling stock and operational speed and is defined in the standards published by the International Union of Railways – UIC (Schöbel and Mirković, 2010).

Figure 2-3: Photograph showing wheel flats on the tread of a wheel.

Wheel flats can cause high impact stresses on the rail head, the bearings and other parts of the bogie, which can lead to damage initiation or rapid propagation of defects. The total amount of stress and potential damage depends on many different parameters, such as dimension and shape of the defect, wheel rotation speed, wheel load and type and properties of vehicle suspension.

2.2.2 Axle bearing defects

The axle bearing design considered in this study is the tapered roller bearing, as it is the one most commonly used in the rail industry. A tapered roller bearing assembly typically consists of an outer cup housing two tapered roller cone assemblies which are separated by a spacer (Zaretsky, 2010). The roller assembly consists of a race, rollers and a cage. Inboard and outboard seals, seal wear ring. A backing ring and an end cap complete the roller bearing assembly. The schematic in Figure 2-4 shows the configuration of a typical axle bearing (courtesy of Timken AP) (TIMKEN, 2015). This is similar to the axle bearings tested in Long Marston, which were also supplied by Timken AP.

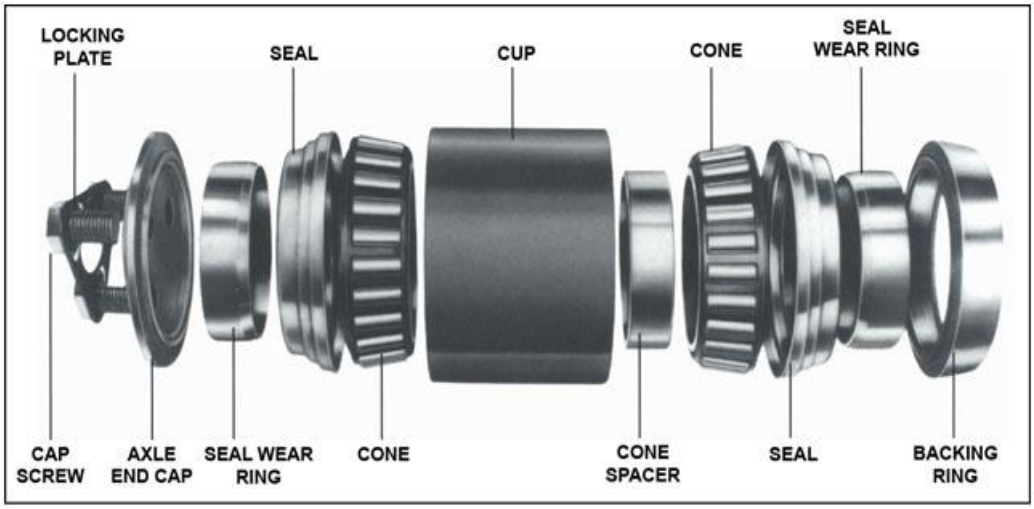

Figure 2-4: Schematic of a tapered roller bearing (courtesy of TIMKEN AP).

The normal service life of a rolling element bearing rotating under load is determined by material fatigue and wear at the running surfaces. Railway bearings can suffer from different types of faults including lubricant failure, lubricant contamination, loose bearing, roller spalling, corrosion, broken seals, missing cap screws, damaged backing rings and race damage (Howard, 1994, Radu, 2010). Often there can be overlap between factors for a particular bearing failure or a bearing may start to fail in one particular mode, which then leads on to other failure modes.

A bearing will eventually fail due to material fatigue. Fatigue damage begins with the formation of minor cracks below the bearing surface. As the load continues, the crack can progress to the surface and disturb the rolling motion of the bearing. Wear can also be caused by dirt and foreign particles entering the bearing through inadequate sealing or due to contaminated lubricant (Howard, 1994, Koyo, 2010). Examples of bearing faults are shown in Figure 2-5.

Failure of the axle bearing will cause it to seize, subsequently inhibiting the rotation of the train wheel. As a result, the affected wheelset will have a wheel that is rotating and one sliding along the track. Apart from the damage being inflicted on the surface of the rail and area of the wheel in contact with the rail from the heat, friction and contact stresses, the axle is exhibiting abnormal motion giving rise to very high stresses that eventually cause it to rupture in the centre after a while. Rupture of the axle will cause the wheels attached to it to lose adhesion with the rail and subsequently cause derailment of the affected carriage. This can then cause derailment of more carriages or even the entire train.

a)

b)

Figure 2-5: a) Roller showing multiple cone spalls and b) Multiple cone spalls (Koyo, 2010).

Several severe derailments around the world have been the result of faulty axle bearings, e.g. the Summit Tunnel accident in the UK in the 1980s (Rail Accident Investigation Branch, 2010). In the Summit Tunnel accident a freight train carrying fuel, sustained a failed axle bearing, which caused the axle of the affected wheelset to fracture, derailing it while going through the tunnel. The derailment caused fuel to be spilled which then ignited by a spark, most likely from the wheels braking and other wagons being derailed and sliding causing sparks to be produced. The fire caused extensive structural damage to the tunnel, whilst removal of the derailed wagons was far more difficult to be achieved due to the restricted area

available for deployment of heavy equipment needed to lift the heavy parts. Moreover, the structural damage on the tunnel itself needed to be addressed before maintenance crews could safely work their way to the derailed wagons.

2.2.3 Bogie suspension defects

The bogie is the structure that supports the superstructure of a railway car. In most cases, the bogie consists of two wheelsets, primary and secondary suspensions and brake system as shown in Figure 2-6. If the bogie is powered, then traction motors or torque converters are also included. The primary or axle box suspension consists of springs between the bogie frame and axle bearings used to absorb shocks. The secondary suspension consists of coil springs or rubber airbags and is responsible for absorbing shocks between the bogie and the rail vehicle body. Failure of the primary suspension can result in abnormal vibrations that can influence the stability of the train during movement, potentially resulting in derailment. It can also result in damage to the axle bearing itself. Similarly failure of the secondary suspension can also cause damage to the axle bearing (Okamoto, 1998).

Figure 2-6: Photograph showing a typical freight bogie.

2.3 Rail infrastructure defects

Rail infrastructure defects, if remain undetected, can gradually grow in size reaching critical dimensions, subsequently resulting into catastrophic failure. Rails and cast manganese crossings are exposed to harsh environmental conditions involving moisture, presence of salts and a wide range of temperature variations along with high dynamic bending and contact stresses, and impact loads. As a result, various flaws can initiate and propagate with time. To overcome this problem rails and crossings are regularly inspected using various traditional techniques. However, in the case of cast manganese crossings, due to the austenitic microstructure of the steel grade used, inspection is largely limited to visual observation and liquid penetrant inspection. These inspection techniques are capable of detecting surface-breaking damage only.

2.3.1 Rail defects

Rails can develop various types of defects including cracking in different orientations and parts of the rail including the head, web and foot (Cannon et al., 2003). Rail defects on the other hand can present themselves in various forms including rail head wear and RCF arising from contact stresses, sub-surface flaws in the head, web or foot arising from bending and lateral stresses, or foot corrosion. Crack initiation and propagation can be the result of bending or contact stresses, or may simply have arisen from accidental impact loads. Corrosion can also affect rails. However, this is a form of damage, which generally, is restricted to the foot of the rail. Furthermore, it occurs in sections of the network where there is water accumulation, e.g. tunnels. One of the most important damage mechanisms affecting modern steel grades used for manufacturing rails is RCF cracking (Schmid, 2010, Ringsberg, 2001). Since rail steel grades are much harder than older steel grades, having a predominantly

pearlitic microstructure, wear is much slower. This gives sufficient time for defects to initiate and propagate. Although sufficient grinding during the geometrical correction of the rail head profile can remove RCF initiation sites, sometimes cracks may have already propagated to a depth which cannot be removed by grinding alone. These cracks will continue propagating relatively rapidly every time a train goes over them, eventually causing shelling and possibly final fracture of the affected rail section. A very serious accident involving RCF cracking was the one that took place in Hatfield, UK, 2000 (Independent Investigation Board, 2006). Although the presence of the RCF defects was known, re-railing had been planned too late. This was probably due to an underestimation of the severity of the damage present by the maintenance engineers. As a result, one week before re-railing was due to take place a passenger train travelling at moderate speed derailed after a large damaged section of rail broke underneath it.

2.3.2 Cast manganese crossing defects

Crossings are manufactured of cast manganese steel grade that exhibits very high impact and wear resistance. However, its large gain austenitic microstructure means that it is also very difficult to inspect with conventional techniques and inspection is traditionally limited to visual observations with occasional application of liquid penetrant inspection. In most cases, damaged crossings have been found to have failed much earlier than their anticipated 20-year design lifetime, despite recent improvements achieved in manufacturing quality.

Cast manganese crossings can develop various forms of defects, including impact damage, shelling, cracking and lipping (Schmid, 2010, Cope and Ellis, 2002). Such defects can only be detected once they become visible to patrol engineers on foot occasionally monitoring infrastructure during the night when normal train traffic has seized. Therefore, there is a

profound need to be able to assess cast manganese crossings more effectively. An example of a damaged crossing is shown in the photograph of Figure 2-7.

Figure 2-7: Example of crack propagating in a cast manganese crossing.

Chapter 3:

Signal processing

Chapter 3: Signal processing

3.1 Fundamentals of acoustic emission

Acoustic emission is a passive technique which is based on the detection of stress waves emitted by propagating flaws within a material (Pao et al., 1979). As a technique, it has very few limitations in terms of the materials on which it can be applied for assessment. Its underpinning principle is the application of a load, which can stimulate damage growth. The detection of stress waves emitted from the tip of a growing crack for example is achieved by mounting one or more piezoelectric sensors on the surface of the test piece (Vallen, 2002). The stress waves will propagate towards all directions in the three dimensions, albeit not necessarily with equal energy. Therefore, some directionality may also be observed, i.e. more energy being emitted in a particular direction than others. As the stress waves propagate through the microstructure of the material, they will scatter and attenuate (Miller and McIntire, 1987). The level of scattering and attenuation with distance will depend on the type of material and its microstructural features (e.g. large grains, etc.). As distance from the source increases, the higher frequency content of the signal will attenuate and scatter faster than the lower frequency part. Therefore, lower frequency waves will travel further away from the source. Also certain types of waves such as the Rayleigh surface waves will be efficiently transmitted at far greater distances than compressive or longitudinal waves but will carry much less energy (Viktorov, 2014). The basic principles of the acoustic emission technique are shown in Figure 3-1.

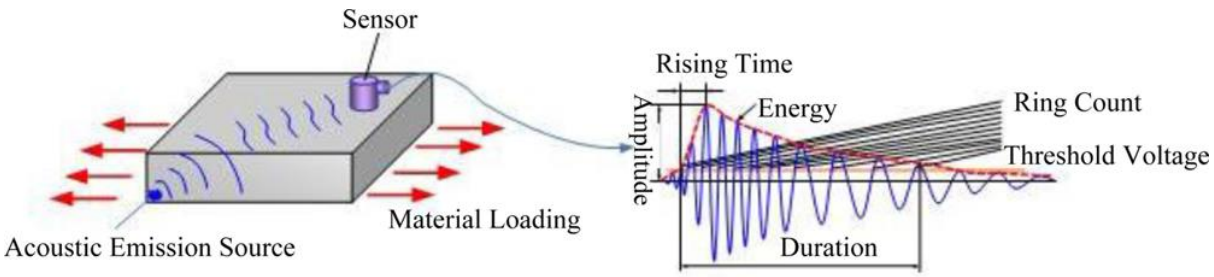

Figure 3-1: Principles of acoustic emission technique (Gao et al., 2011)

In the case of rotating machinery, acoustic emission is employed to record the waveforms of the noise produced from the interactions occurring at the interface of the rolling surfaces of the components of interest (Tandon and Choudhury, 1999). In simple situations where a single rolling element is involved, time domain analysis may be sufficient to detect a particular defect.

However, for more complex situations with multiple rolling elements and surfaces, analysis in the frequency domain is necessary in order to reveal the exact nature of the problem. To assess damage severity, in simple situations amplitude-based analysis of the signal may provide satisfactory results. Unfortunately, in components that are stochastically loaded far more complex analysis may be required, involving feature extraction, signal normalisation and statistical evaluation.

Acoustic emission signals have generally frequencies between 20 kHz – 1200 kHz although higher frequencies are possible (Vallen, 2002). However, due to the rapid attenuation of the energy of the emitted waveforms at higher frequencies, they are not particularly useful since the distance of the sensor from the source should be very small. Another important aspect of the acoustic emission measurement is the consistent quality of the coupling of the sensor to the structure being monitored. Any sensor movement or poor coupling may result in valuable

information being lost or the signal being contaminated by unrelated features, making analysis either impossible or giving erroneous results.

3.2 Fundamentals of vibration analysis

Vibrations can generally be described as oscillations exhibited by a structure around a point of equilibrium after being excited by a stimulating source (Taylor, 1994, McFadden and Smith, 1984). Vibrations have much lower frequencies in comparison to acoustic emission, with the typical useful range falling between 0 Hz – 18 kHz. Piezoelectric accelerometers are commonly used to detect vibrations. However, care needs to be taken when selecting accelerometers to ensure that they have an appropriate operational frequency range for the application concerned. For example, if low-speed rotational machinery is to be monitored, e.g. the main bearing of a wind turbine rotor which revolves at a rotational speed of as low as 8-9 RPM in larger industrial turbines, an accelerometer with an operational range starting as low 0.1 Hz will be required to detect the bearing tone. Accelerometers with a frequency range starting from a few Hz will fail to detect the bearing tone, meaning damage in the main bearing can go undetected. The typical features of an industrial accelerometer are shown in the schematic in Figure 3-2.

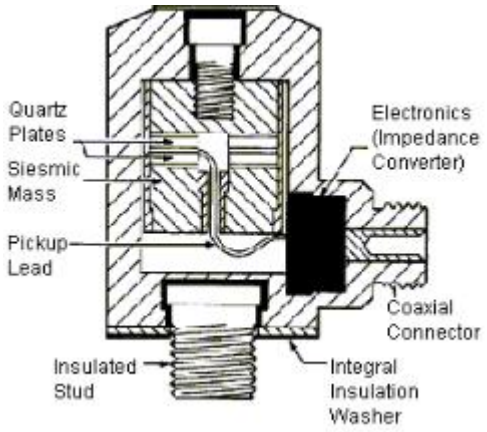

Figure 3-2: Schematic showing the main features of typical industrial accelerometers (YILMAZ and ÇETİN, 2004).

The maximum useful operational frequency of an accelerometer apart from being dictated by the characteristics of the piezoelectric crystal employed, also depends on the way that the accelerometer is mounted on the structure of interest. For example, if the accelerometer is mounted using a magnet then the maximum useful frequency will not exceed 5 kHz due to damping effects from the magnet's structure. If adhesive pads are used instead, then the maximum operational frequency can reach up to 11 kHz. For detecting higher vibration frequencies, then mounting should be done by using threads, screwing the accelerometer directly on the structure under investigation.

3.3 Signal characteristics for wayside monitoring

In order to achieve better understanding and analysis from the acquired acoustic emission and vibration data, it is essential to investigate the mechanism of the wayside bearing defect detection as well as the contents of the signal and its features collected by track-mounted acoustic emission sensors and accelerometers.

Acoustic emission is generated by rapid release of energy from localised sources within a material during transient changes in the local stress and strain fields. Acoustic emission is produced at the source as a short pulse of elastic and kinetic energy that travels through the material as an elastic wave. Two types of acoustic emission signals are normally seen: transient and continuous signals (Li, 2002, Kaphle et al., 2012). These signals have distinctly different characteristics. Transient signals occur only for a short duration and often arise from fracture or crack growth in metal, whereas continuous signals occur for a longer period of time and are associated with wear, motion of dislocations and noise (Vallen, 2002). A defective bearing tends to generate more acoustic emission energy than a healthy one. The more serious the defect is, the more energy it will generate.

The signal produced by the defective bearing is transferred through the wheel-rail interface, along the track, and eventually collected by the sensor. Data analysis is then preformed to extract the information about the nature of the source. The signal transmission path is illustrated in the following diagram (Figure 3-3).

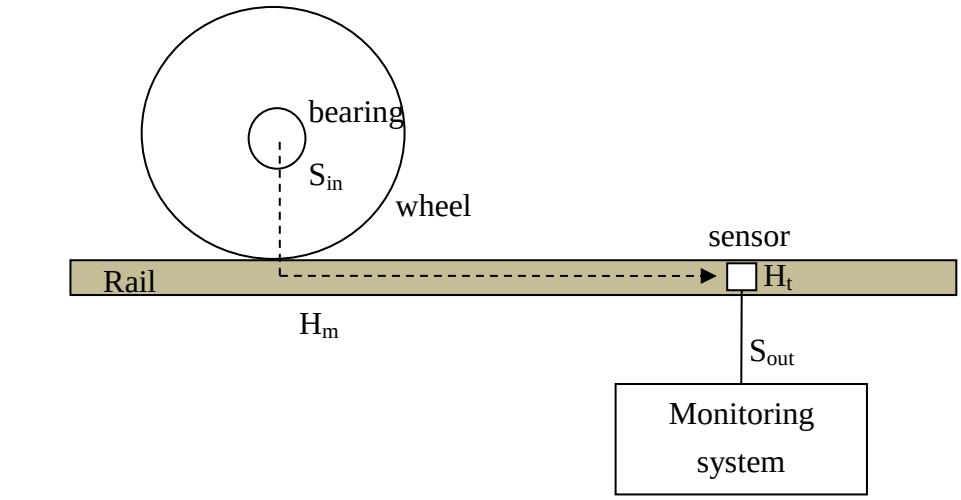

Figure 3-3: Sketch showing the transmission path from a faulty bearing to the acoustic emission sensor.

Taking into account the effect of the sensor characteristics and the transmission path, a transfer function equation can be used to describe the system mathematically as follows (Ono, 2005, McLaskey and Glaser, 2012, Mba and Hall, 2002):

$$S_{out}(\omega) = S_{in}(\omega) \cdot H_m(\omega) \cdot H_t(\omega) \quad (3\text{-}1)$$

Where $S_{out}(\omega)$ is the Fourier transform of the recorded signal, $S_{in}(\omega)$ is the Fourier transform of the source, $H_m(\omega)$ is the transfer function for the propagation medium, and $H_t(\omega)$ is the frequency response of the acoustic emission sensor.

As the waveform is affected by both the complex transmission path and the sensor characteristics, the frequency spectrum of the acoustic emission signals generated at the point

of release does not necessarily equal to what has been recorded. According to previous research, acoustic emission waveforms are influenced mainly by three factors; the source type, medium of propagation, and sensor characteristics (Ono, 2005). More explanation about each of these factors will be provided in detail later on in the present thesis.

3.3.1 Spectrum features of bearing defects

Railway bearings can suffer from different types of faults including lubricant contamination, roller spalling, corrosion, broken seals, damaged backing rings and race damage. The bearing acoustic emission signal can generally be regarded as being produced by three types of possible sources; localised defect, fatigue, and sliding friction respectively.

Localised defects of rolling element bearings include cracks, pits and spalls on the rolling surfaces, of which the dominant mode of failure is spall of the races or the rolling elements (Howard, 1994, SKF, 1994). This type of defect produces transient acoustic emission signals for each strike, and multiple bursts can be recorded as the bearing rotates. In this study, the proposed localised defects are the artificially induced roller and race defects.

The rest of two sources are considered as continuous signals. They can be influenced by speed, load and lubrication condition of the bearing. Fatigue damage begins with the formation of minor cracks below the bearing surface. As the loading continues, the crack can progress to the surface and disturb the rolling motion of the bearing. Besides, during the bearing movement, a combination of sliding and rolling occur on the running surface. The sliding of mating surfaces is a continuous process leading to gradual wear and structural deterioration.

The acoustic emission signal signature arising from a bearing often comprises overlapping transients. It is likely to be predominantly continuous with superimposed burst emissions due

to the presence of localised defects. A typical example of a wayside bearing acoustic emission signal is provided in Figure 7-26.

The spectrum of the bearing signal is also worth investigating, as each type of defect has its unique frequency distribution. By analysing the frequency content, it is possible to discriminate signals that correspond to particular defect mechanisms. The frequency distribution of the acoustic emission signals changes depending on the mode of deformation and fracture. The common frequency range for acoustic emission testing for structural monitoring is in the range of 100 kHz - 300 kHz (Fu, 2005).

To be more specific, the impact of a localised defect triggers the resonance of the bearing structure and most energy lies at frequencies below 250 kHz (Rogers, 1979, Hase et al., 2012, Marfo et al., 2013). In the case of mild wear, where the emissions originate from rolling of wear particles between the sliding surfaces, the primary frequency domain groups are in the region from 80 kHz to 200 kHz. In addition, frequency peak for sliding friction occurs at around 100 kHz. Each defect mechanism produces its unique type of frequency spectrum, which is not dependent on the nature of the materials involved (Hase et al., 2012). The activity of specific frequency band of acoustic emission wave is increasing with the gradual evolution of fatigue damage (Roberts and Talebzadeh, 2003).

To sum up, based on the different frequency characteristics of each defect mechanism, a frequency range of 100 kHz - 250 kHz has been selected for bearing acoustic emission signal processing. This frequency range should be sufficient to cover the most important bandwidth that contains the bearing defect information.

When a localised defect impacts on the mating element, it generates a transient bust of high frequency energy at the bearing resonance frequency (Adams, 2000). As the bearing rotates,

this transient signal will repeat itself at a unique frequency called the characteristic frequency, as shown in Figure 3-4. The characteristic frequency is of much greater interest for the detection of bearing defects in comparison with the resonance frequency of the bearing. Such frequency can be determined with the information of bearing rotational speed and geometrical characteristics. Bearing defects will result in an amplitude modulation effect on the bearing signal at the characteristic frequency (Randall and Antoni, 2011, Lacey, 2008).

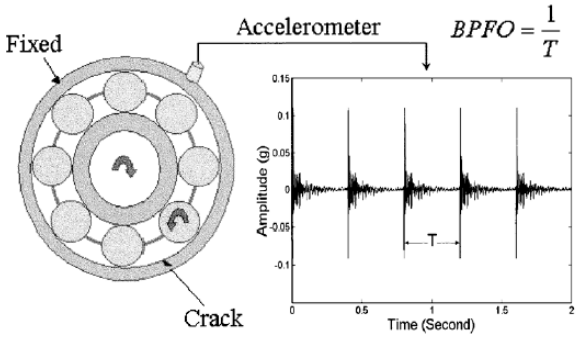

Figure 3-4: Raw waveform showing an outer race bearing defect (McInerny and Dai, 2003).

Therefore, bearing defects can be identified by detecting any of these frequencies. The amplitude of the signal will indicate the severity of the defect detected. The information about the characteristic frequencies of the bearing is provided by the manufacturer. The formulas for calculating these specific frequencies are the following (Bosso et al., 2012, Bently et al., 2001, McInerny and Dai, 2003, Randall and Antoni, 2011).

$$
\begin{aligned}
BPFI &= \frac{N}{2} \times F \times (1 + \frac{B}{P} \times Cos\theta) \\
BPFO &= \frac{N}{2} \times F \times (1 - \frac{B}{P} \times Cos\theta) \\
FTF &= \frac{F}{2} \times (1 - \frac{B}{P} \times Cos\theta) \\
BSF &= \frac{P}{2B} \times F \times [1 - (\frac{B}{P} \times Cos\theta)^2]
\end{aligned}
\qquad (3\text{-}2)
$$

where N is Number of balls, F is Shaft frequency (Hz), B is Ball diameter (mm), P is Pitch diameter (mm) and θ is Contact angle. BPFI is ball pass frequency inner race (Hz), where defect is on the inner race; BPFO is ball pass frequency outer race (Hz), where defect is on the outer race; FTF is fundamental train frequency –Frequency of the cage (Hz), where defect is on the cage; BSF is ball spin frequency circular frequency of each rolling element as it spins (Hz), where defect is on the rolling element.

Roller and race defects will give rise to a fundamental frequency. The fundamental frequency is very useful in the diagnosis of the root cause of the defect. The dominant peak at 1 RPM in Figure 3-5 (also called 1X or fundamental shaft frequency) is due to imbalance. The presence of the 2 RPM (or 2X) component in the spectrum is very likely to be caused by shaft misalignment, asymmetry or bent shaft (Muszyńska, 1989).

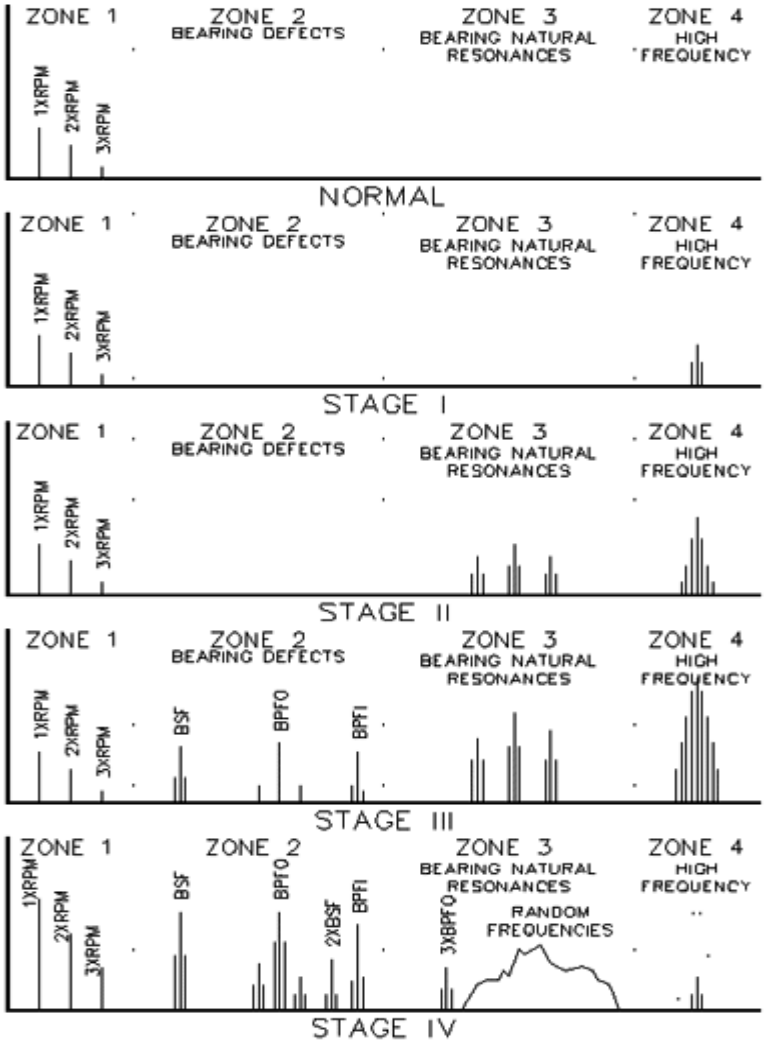

Figure 3-5: Frequencies of growing bearing defects (Salvan et al., 2001).

Figure 3-5 shows the diagram of the frequencies changes as a bearing defect grows. When a discrete outer race defect is present, the signal only contains the BPFO frequency as the outer ring is stationary and the amplitude of the signal is identical. In contrast, an inner race defect will generate not only BPFI frequency, but sidebands at fundamental shaft frequency (1X) as well. This is because when the defect leaves the load zone, the amplitude of the signal reduces, leading to amplitude modulation at inner ring rotational frequency. When a rolling element defect occurs, the frequency contents can be a mixture of BSF frequency, twice the BSF frequency, harmonics and the 1X. The double BSF frequency is generated by a defect striking

both raceways. However, such frequency is not consistent, as it may not show up when the rolling element is not in the load zone. Lastly, FTF frequency is generally not evident as cage defects do not usually excite specific frequencies (Lacey, 2008, Randall and Antoni, 2011, McInerny and Dai, 2003, Konstantin-Hansen and Herlufsen, 2010, Felten, 2003, McFadden and Smith, 1984).

Due to the fact that the bearing defect signal is repetitive, it will manifest itself throughout the spectrum. Inter-harmonic frequencies are common due to the sliding effect of the rolling elements (Lacey, 2008). It should be noted that as these formulas are theoretical, the measured frequencies can differ from the actual calculation due to effects such as sliding of rolling elements, different contact angle and misalignment. This can lead to 1 – 2 % change in frequency (Randall and Antoni, 2011).

3.3.2 Transmission path

The transmission path refers to the geometry of the wheel-rail structure from the bearing to the sensor, as shown in Figure 3-3. It includes the bearing house, wheel, wheel-rail interface, and the track. The bearing acoustic emission signal is transferred through this complex transmission path to the sensor. It has already been proven that acoustic emission signals are capable of passing through the connections between two jointed components, even though the contact surface is not constant (Grosse and Ohtsu, 2008).

However, in terms of a structure with complex geometry, the effect of reflection, attenuation and mode dispersion can make it extremely difficult to restore the information about the nature of sources. Complications arise as acoustic emission signals can travel in different wave modes with various speed. This greatly depends on the complexity of the transmission path and can be regarded as a changing transfer function.

Due to the lack of clear understanding about wave propagation in this application, it is impossible to describe the complex transmission path quantitatively. As a result, the signal source at the selected 100 kHz - 250 kHz frequency will be gradually attenuated and distorted with increasing distance from the sensor. Thus, it makes discrimination of the defective bearing signal directly from the collected data extremely difficult.

3.3.3 Sensor characteristics

Resonance acoustic emission sensors are more sensitive at specific frequencies leading to a complex frequency response. The main advantage is that mechanical noise lying at lower frequency will have a smaller effect on the recorded signals. The drawback is that the signals collected will be distorted as discussed in more detail in Chapter 6.

3.3.4 Signals from other sources

Since acoustic emission sensors detect the elastic waves emitted passively, any signals propagating towards the sensor will be collected as long as they exceed the background noise level. In other words, signals produced by spurious sources, including the adjacent bearing, locomotive, wheels and tracks, can be acquired as well apart from the target bearing.

Signals generated by the adjacent bearing can cause interference to the one monitored, as the distance between two bearings from the same bogie is only 2.1m. Signals generated by these two bearings will be collected by the acoustic emission sensor. Any peaks arising will be mixed and can overlap with delays and intervals. Wheel imperfection is another major source of possible interference. When a wheel defect, for instance wheel flat, is present causing impacts on the rail head it generates a transient burst of acoustic emission energy. Besides, spurious signals can be produced by rail defects as well, for example RCF cracking caused by contact fatigue stresses between the rail and wheel. When the rolling stock weight loads RCF

cracks, the contact stresses arising can cause crack growth causing acoustic emission signals to be emitted for the duration that the train is loading the affected rail section. This also applies to the sliding motion at the wheel-rail interface, as the wheel is not only rotating, but also sliding on the surface of the track. Finally, the effect of acceleration and brake can generate a considerable amount of energy in the form of transient signals.

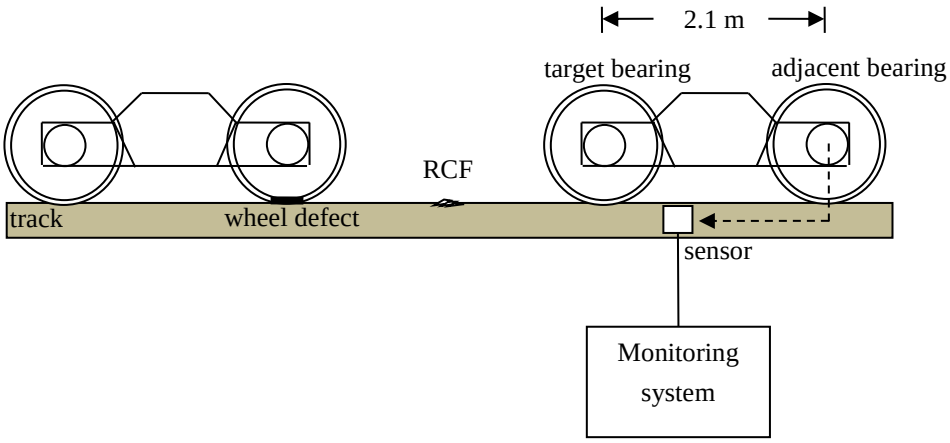

Figure 3-6: Schematic showing possible interferences during wayside measurement.

All these sources introduced above can be regarded as interferences when detecting bearing defects. Therefore, it is expected that the gathered waveform can be represented as a sum of acoustic emission signals from various sources containing different mechanisms of acoustic interferences and noise.

There are two main challenges that need to be addressed in acoustic emission monitoring of axle bearings. Since the mechanism and the effect of the transmission path remains unknown, it is not possible to establish a direct link between the collected acoustic emission signal and the dynamic properties of the bearing source. Therefore, it is difficult to identify the defect by recovering the original signal. On the other hand, due to the passive nature of the acoustic emission sensor, a lot of noise and interferences are also collected. These unwanted

components overlap with the bearing signal, greatly reducing the signal-to-noise ratio and making it more difficult to detect defects. Relevant research showed that it is ineffective to detect bearing defects in the test field (Zhang, 2011). An alternative method is thus developed to differentiate signals from different acoustic emission sources and minimise the effect of complex transmission path.

3.4 Data analysis techniques of bearing signals

3.4.1 State-of-the-art analysis technique

Since railway dynamics are highly non-linear, signal-based methodologies are more appropriate than model-based ones to analyse data acquired by wayside RCM systems (Ngigi et al., 2012). Fault detection and data analysis of bearing acoustic emission signals in steady state rotating machinery is well-developed and widely used in many industries. Current signal processing techniques of bearing acoustic emission signals can be divided into two categories: parameter-based and waveform-based approach (Tandon and Choudhury, 1999, Grosse and Linzer, 2008, Kaphle et al., 2012).

In parameter based approach, a number of signal parameters are recorded and analysed to assess the extent of damage, such as threshold, hit, amplitude, rise time, duration, energy and counts (Grosse and Ohtsu, 2008, Tandon and Nakra, 1992). On the other hand, waveform based approach acquires the entire raw data, so that more information can be kept. By using signal processing techniques, better data interpretation capability can then be achieved (Grosse et al., 2004, Taha et al., 2006, Jardine et al., 2006). Some commonly used signal processing methods include time domain statistical analysis (Heng and Nor, 1998, Miettinen and Pataniitty, 1999, Usgame, 2013, Li, 2002), such as kurtosis, RMS and crest factor, and frequency domain processing. Nowadays, time-frequency domain analysis gradually becomes

more popular, including spectrogram, spectral kurtosis (SK), empirical mode decomposition (EMD) and wavelet transform, so as to condition the signal and thus improve the SNR for better results (Grosse et al., 2004, Pandya et al., 2013, Ruiz-Cárcel et al., 2014, Chacon et al., 2015, Eftekharnejad et al., 2011, Elasha et al., 2016, Shiroishi et al., 1997). Techniques like adaptive filter and feature extraction are also applied to reduce noise and improve the effectiveness of defect detection (James Li and Li, 1995). These include auto-regression (AR) coefficients, Morlet wavelet, Mahalanobis distance and approximate entropy (ApEn) (Caesarendra et al., 2016, Patil et al., 2016). In addition, various Artificial Intelligence (AI) approaches are considered to improve the performance of defect diagnosis (Jardine et al., 2006), including artificial neural networks (ANN) and evolutionary algorithms (EA) and expert systems (ES) (Siddique et al., 2003, Li et al., 2000, Jayaswal et al., 2011).

No matter what methods are used, the core idea of frequency domain analysis for stationary bearing is to improve signal quality so that the characteristic frequency of the localised bearing defect can be identified.

By examining the repeating frequency, it is able to determine the type of the bearing defect (McFadden and Smith, 1984, Tandon and Choudhury, 1999). However, all these state-of-the-art research require the bearing to be stationary with acoustic emission sensor attached as close as possible, so that the effect of the transmission path can be minimised and thus the condition of the experiments does not change over time. In reality, such premises do not apply to wayside condition monitoring of bearings, largely due to the fact that the fast moving train results in limited number of impacts recorded and the effect of dynamic transmission path.

The waveform of the wayside measurement only contains a small portion of repeating impacts generated by the bearing defect. It is very difficult to recover the repeating frequency of the bearing component directly from the original waveform in order to identify the characteristic frequency.

3.4.2 Proposed methodology of defect detection

The track-mounted acoustic emission sensor can effectively collect signals generated by a defective bearing. However, the complex transmission path and interferences make it hard to identify the defect accurately. Instead of attempting to find the characteristic frequency of the defects, it is more feasible to discriminate peaks that have similar frequency distribution to the defect. It has been suggested that different types of acoustic emission sources have their individual unique spectral characteristics. This feature should apply to all signals generated by the same source at different time instants. Searching for similarity among signals can help to discriminate various sources (Grosse et al., 2004).

Therefore, an alternative approach is proposed using correlation processing to separate signals from different sources. Assuming the feature of the bearing defect is known in advance, it can be used as a template to perform source differentiation with the wayside data by identifying all segments from the original waveform that are similar to it. These segments with the identical feature are very likely to be generated by the same defect. Hence, correlation analysis can be used as a powerful tool not only to identify the presence of a defect, but also to discriminate signal generated by different sources of acoustic emission.

There are two vital parts in the proposed correlation analysis: the template and the selected feature required for the correlation processing. Templates are of great importance to achieve accurate and reliable results in correlation analysis. It normally consists of a set of signals

which are generated by a specific defect. It is selected from tests under a controlled environment, where the information of the location and vehicle is known, such as train speed, bogie geometry and wagon weight. Figure 3-7 shows an example of how to effectively select a template. The spectrogram results match the time instant when the defective bearing passes the sensor. As the train speed is around 8 m/s and the diameter of the wheel is 0.91m, one revolution of the wheel can be calculated as 0.35 s. This is used as the length of the template signal. As a result, the segment of 5s to 5.35s of the raw signal is selected as the template.

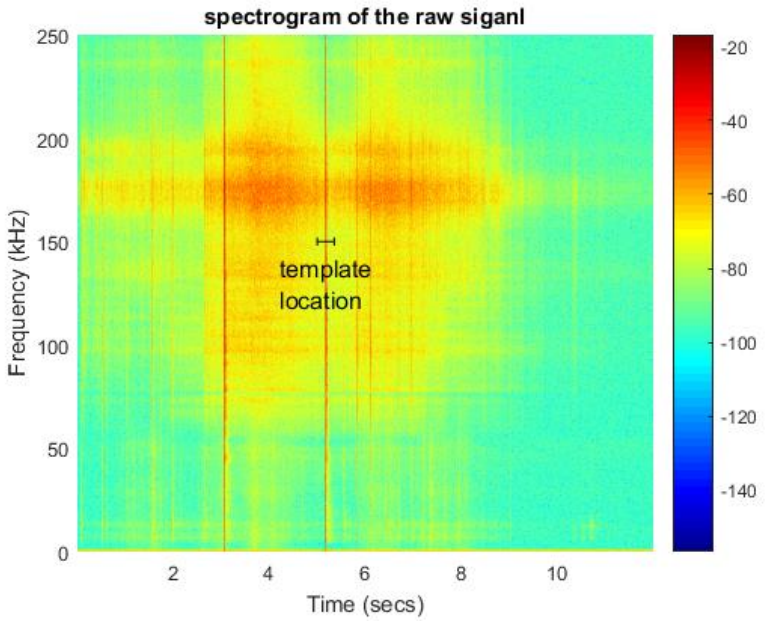

Figure 3-7: Spectrogram of the raw AE signal for the tests involving axle bearings with lubricant contamination.

It has been well-established that the frequency and power distribution analysis can be effective methods for processing acoustic emission signals (Wadley et al., 1980, Grosse et al., 2004). Defective axle bearings generate unique spectral information and are not correlated with other acoustic emission sources. Therefore, the power spectrum density (PSD) can be used as the feature to perform correlation processing. By calculating the similarity between

the PSD of both template and the acquired acoustic emission data, it is able to determine whether such signal is generated by a defective bearing.

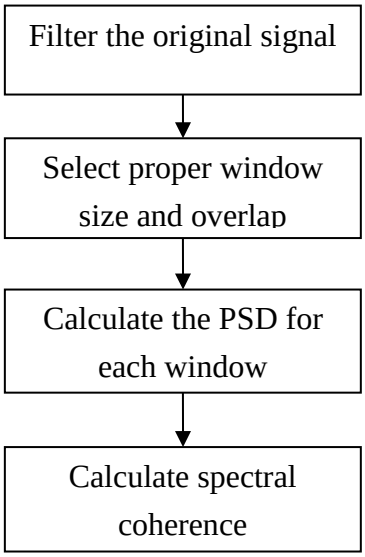

Figure 3-8: procedures for correlation processing

The detailed procedure of correlation processing is shown in Figure 3-8. It includes 4 steps described next:

1. Filtering the signal

As explained earlier, the frequency band of interest lies between 100 kHz to 250 kHz. Although the pre-amplifier has an analogue bandpass filter built-in, the energy of the low frequency signals from spurious sources can still be high enough to appear in the spectrum. As a result, the collected data needs to be filtered again to remove the low frequency contents.

2. Selecting window size and overlap

The raw data is divided into a number of segments that is determined by the value of the window size and overlap. The more segments it has, the better resolution it can achieve. However, it is a trade-off between the accuracy and computing time. The window size

generally covers the duration of a complete impact signal, while 50% overlap is sufficient. These settings can be determined according to (Carter et al., 1973).

3. Calculating the PSD for each window

As the bearing signal acquired is non-stationary, an appropriate technique needs to be selected to estimate the power at different frequencies. In this scenario, Welch's method is used based on the concept of periodogram spectrum estimates. It can be calculated by breaking the time series into segments with overlap, performing periodogram for each segment and finally averaging the results.

4. Performing the correlation processing

Spectral coherence analysis is performed to calculate the similarity between template and each window. As suggested, signals that contain same features with the template should have higher similarity results. More details about these methods will be introduced in the next chapter.

Cross-correlation processing is aimed to identify signals that have similar frequency contents with high energy. However, cross-correlation itself is not enough, since the energy of each windowed signal can affect the result causing it to fail. The accuracy of detection can be compromised by an interference signal with higher energy than the target signal with much lower energy. Therefore, coherence processing is also performed to reduce such effects by removing the interference of the energy of the signal, and focusing more on the frequency information itself.

The correlation processing method can also be applied to process the data from the stationary bearing. Impact signals from the same source can be identified with high similarity with the

correlation processing. Then, the characteristic frequency of the defect can be calculated from the similarity sequence.

3.4.3 Signal processing techniques used in the work

3.4.3.1 Correlation analysis

In order to identify the bearing signal that embedded as a segment of the raw data, correlation processing is considered to be a suitable solution (Kumar et al., 2005). The concept is to create a reference signal and determine the similarity between the reference and the input signal. The method applied in this work is spectral coherence analysis.

3.4.3.1.1 Cross-correlation

Cross-correlation calculates similarity of two series as a function of the time-lag shift. In signal processing, it reflects the various frequency components held in common between the two signals (Kaphle et al., 2012). The absolute maximum value indicates the maximum correlation of the two signals at certain time shift. The equation of cross-correlation for continuous signals is shown below.

$$R_{12}(\tau) = \int_{-\infty}^{+\infty} f_1(t) \cdot f_2^*(t-\tau)dt \qquad (3\text{-}3)$$

The equation of a finite length discrete cross-correlation is provided:

$$R_{12}(m) = \sum_{n=-N}^{N} f_1(n) \cdot f_2{}^*(n-m)\,,\ n = 0, \pm 1, \pm 2 \ldots \pm N \qquad (3\text{-}4)$$

As cross-correlation is conjugate symmetric, which is:

$$R_{12}(\tau) = R_{21}^*(-\tau) \qquad (3\text{-}5)$$

Therefore,

$$R_{12}(m) = \begin{cases} \sum_{n=0}^{N} f_1(n) \cdot f_2{}^*(n-m), & m \geq 0 \\ R_{21}^*(-m), & m < 0 \end{cases} \qquad (3\text{-}6)$$

where N is the size of the signal, f_1 can be the template signal, f_2 can be the input signal.

Giving the Fourier transform pairs of $f_1(t) \leftrightarrow F_1(\omega), f_2(t) \leftrightarrow F_2(\omega), R_{12}(\tau) \leftrightarrow R_{12}(\omega)$, the cross-correlation can be calculated as (Lewis, 1995):

$$R_{12}(\tau) = \int_{-\infty}^{+\infty} f_1(t) \cdot f_2^*(t-\tau)dt$$

$$= \int_{-\infty}^{+\infty} f_1(t) \cdot \left[\frac{1}{2\pi}\int_{-\infty}^{+\infty} F_2(\omega)\, e^{j\omega(t-\tau)}d\omega\right]^* dt$$

$$= \frac{1}{2\pi}\int_{-\infty}^{+\infty} f_1(t) \cdot \left[\int_{-\infty}^{+\infty} F_2^*(\omega)\, e^{-j\omega(t-\tau)}d\omega\right]dt$$

$$= \frac{1}{2\pi}\int_{-\infty}^{+\infty} F_2^*(\omega) \cdot \left[\int_{-\infty}^{+\infty} f_1(t)\, e^{-j\omega t}dt\right]e^{j\omega\tau}d\omega$$

$$= \frac{1}{2\pi}\int_{-\infty}^{+\infty} F_2^*(\omega) \cdot F_1(\omega)e^{j\omega\tau}d\omega \qquad (3\text{-}7)$$

Therefore,

$$R_{12}(\tau) \leftrightarrow R_{12}(\omega) = F_1(\omega)F_2^*(\omega) \qquad (3\text{-}8)$$

In reality, interferences with high energy can greatly affect the results of cross-correlation processing. In order to minimise such effect, cross-correlation coefficient is recommended. It is achieved by subtracting the mean and dividing by the standard deviation of two signals.

3.4.3.1.2 Cross power spectral density

The cross power spectral density (CPSD) function is defined between two signals $f_1(t)$ and $f_2(t)$ as

$$S_{12}(\omega) = \int_{-\infty}^{+\infty} R_{12}(\tau)e^{-j\omega\tau}d\tau \qquad (3\text{-}9)$$

where R_{12} is the cross-correlation sequence introduced above. It serves as an indication of the frequencies held in common between $f_1(t)$ and $f_2(t)$. In addition, the PSD is a special case of the CPSD function where two input signals are identical. It can be seen that CPSD and cross-correlation are seen to be Fourier transform pairs as described below:

$$S_{12}(\omega) = F\{R_{12}(n)\} = f_1(f) \cdot f_2^*(f) = |f_1(f)| \cdot |f_2(f)| \cdot e^{-i(\emptyset_{f1} - \emptyset_{f2})} \quad (3\text{-}10)$$

3.4.3.1.3 Spectral coherence

The spectral coherence is another indicator of the similarity between two signals (Carter et al., 1973, Seker, 2000). It is defined as

$$C_{12}(\omega) = \frac{|S_{12}(\omega)|^2}{S_{11}(\omega)S_{22}(\omega)} \quad (3\text{-}11)$$

where C_{12} is the cross-spectral density between f_1 and f_2, while S_{11} and S_{22} is the PSD of f_1 and f_2 respectively. The result of spectral coherence is a function of similarities for all frequencies that covered. Each value represents the similarity at that specific frequency. According to the Cauchy–Schwarz inequality, it has $0 \leq C_{12} \leq 1$.

Moreover, the function of spectral coherence can be represented by a single value as:

$$\overline{C_{xy}}(f) = \frac{1}{f_2 - f_1} \int_{f_1}^{f_2} C_{xy}(f) df \quad (3\text{-}12)$$

Considering that each frequency is of the same priority with equal weight, spectral coherence can be described as the average value of spectral similarity between f_1 and f_2. Therefore, it provides a method to quantify the spectrum similarity between two different spectra (Grosse et al., 2004).

3.4.3.2 High Frequency Resonance Technique (HFRT)

High frequency resonance technique (HFRT), also known as envelope demodulation processing, is carried out to identify the characteristic frequency of the defective bearing (Segla et al., 2012). The detailed procedure used to apply HFRT analysis is shown Figure 3-9.

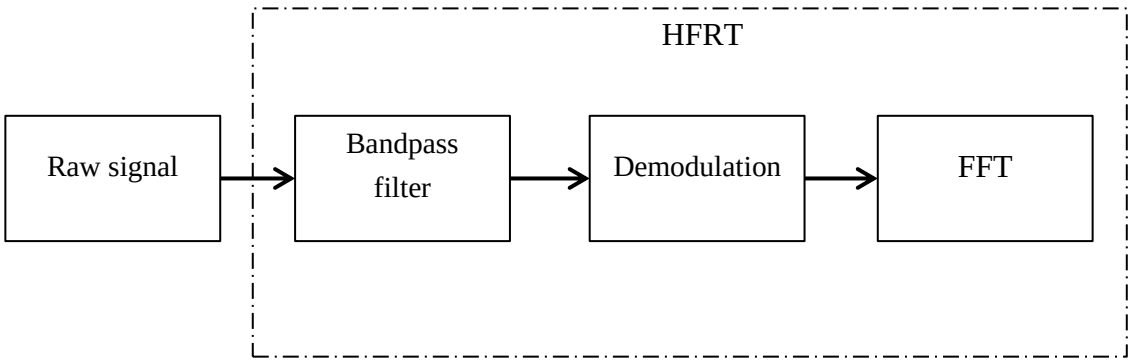

Figure 3-9: Schematic showing the procedure employed in high frequency resonance technique analysis.

The main idea of HFRT is to eliminate interferences by using band-pass filtering around the resonance frequency and demodulating the bearing signal to identify the sideband frequency from the raw signal (McFadden and Smith, 1984, Tandon and Choudhury, 1999, Tandon and Nakra, 1992, Xu, 1999). The bandpass filter needs to be carefully designed. The bandwidth is suggested to allow five times of the sideband at each side, so that the characteristic frequency can be restored with good signal-to-noise ratio (McFadden and Smith, 1984). Then, the Hilbert transform is applied to demodulate the filtered signal. The Hilbert transform of g(t) is the convolution of g(t) with the signal $\frac{1}{\pi t}$. The equation is provided as followed (Kschischang, 2006):

$$[g(t)] = g(t) * \frac{1}{\pi t} = \frac{1}{\pi} \int_{-\infty}^{\infty} \frac{g(\tau)}{t-\tau} d\tau = \frac{1}{\pi} \int_{-\infty}^{\infty} \frac{g(t-\tau)}{\tau} d\tau \qquad (3\text{-}13)$$

The result of Hilbert transform is the magnitude of the envelope of the input signal which only contains the characteristic frequency. A final step of Fast Fourier Transform (FFT) can easily reveal the characteristic frequency of interest.

3.4.3.3 Sensor fusion techniques

The customised RCM system makes use of multiple sensors to improve the reliability of the system and performance of defect detection. A weighted sensor fusion technique is applied to achieve sensor-level correlation, which will be explained in Chapter 5. The equation is provided below (Zubair et al., 2012):

$$\bar{x} = \sum_{i=1}^{N} w_i \, x_i \qquad (3\text{-}14)$$

Where $\bar{x}$ is the fused signal, w_i is the weight coefficient for each sensor signal, x_i is the data from each sensor.

$$w_1 : w_2 : \cdots : w_N = E_1 : E_2 : \cdots : E_N$$

$$w_1 + w_2 + \cdots + w_N = 1$$

$$E_i = \sum_{j=1}^{N} [R_{ij}]^2 \qquad (3\text{-}15)$$

where E_i is the energy coefficient from each sensor, R_{ij} is the cross-correlation result of two sensor signals and the weight value is normalised so that the sum equals to one.

The weight is calculated as the sum of cross-correlation results among all sensors (DHILLON, 2011). The higher the cross-correlation result is, the greater weighted value is assigned. The advantage of using such method is that no prior information is required for sensors and weights can be updated with the real-time data. In addition, due to the effect of averaging, large errors can be effectively supressed.

3.4.3.4 Moving RMS

The moving RMS (root mean square) algorithm is the most fundamental yet powerful analysis approach in time domain to calculate the energy of the signal. The equation of RMS is provided below (Lebold et al., 2000):

$$RMS = \sqrt{\frac{1}{N}\sum_{n=1}^{N} x_n^2} \quad (3\text{-}16)$$

where N is the number of data in the signal.

Since RMS only provides a single value output, the information of how the energy changes over time is lost. Instead, the moving RMS divides the signal into small windows of a specified size and then calculates RMS values for each window. Therefore, the time information of the signal is reserved after moving RMS processing with better resolution and flexibility as well. Analysis of the bearing raw signal using the moving RMS can provide the preliminary understanding of dominant peaks that are very likely to be generated by bearing defects.

3.4.3.5 Moving Kurtosis

Kurtosis is another powerful statistics indicator to quantify the degree of sharpness of peaks in the raw signal. The equation of how to calculate Kurtosis is provided below.

$$K = \frac{\mu_4}{\sigma^4} = \frac{\sum_{i=1}^{n}(X_i - \bar{X})^4}{(\sum_{i=1}^{n}(X_i - \bar{X})^2)^2} \quad (3\text{-}17)$$

where $X_i - \overline{X}$ is the difference between each value and the mean, μ^4 is the fourth moment about the mean and σ^4 is the fourth moment about standard deviation of the signal.

For signals generated by healthy bearings with normal distribution, the kurtosis value is 3. Any value greater than that indicates the presence of a defect (Tandon and Choudhury, 1999). A threshold is normally predefined for the specific monitoring system.

Moving kurtosis, like moving RMS, provides the flexibility to analyse the signal in terms of time variance. It is calculated by dividing the raw signal into windows of a specified size and performing Kurtosis with each segment. However, the limitation of Kurtosis is that it is not effective in noisy environments.

Chapter 4:

Wayside remote condition monitoring systems

Chapter 4: Wayside remote condition monitoring systems

4.1 Introduction

Rail networks consist of several critical subcomponents related to both infrastructure and rolling stock. Many of these components interact dynamically with each other. The type of dynamic interactions sustained by each component influences the way its structural integrity deteriorates with time. Regardless of the component concerned, if structural degradation is allowed to progress uncontrolled, it will eventually result in failure of the affected component. Therefore, unexpected failures can subsequently give rise to delays, network disruption and potentially derailments.

It is of utmost importance that faults initiating and propagating in various infrastructure and rolling stock components are diagnosed promptly so that necessary remedial actions can be carried out in time to prevent disruption and minimise the likelihood of catastrophic failure. The prompt detection of faults offers significant advantages to rail infrastructure managers and rolling stock operators in terms of improved RAMS (TSLG, 2012). To achieve this rail infrastructure managers and rolling stock operators have been relying on various types of RCM systems installed at different parts of the network.

This chapter discusses the categories of RCM systems that are currently in use with detailed explanations regarding their key principles and main limitations provided. Therefore, it emphasises the need of introducing system correlation and decision support tool to current architecture of RCM systems, which will be elaborated in the next chapter.

4.2 Categories of RCM systems

Various types of RCM systems are currently employed in order to enable the assessment of different problems associated with the infrastructure or rolling stock. The use of RCM systems evaluating rail infrastructure is limited, predominantly relating to track stiffness measurements based on vibration in predefined network sections of interest. Commercial RCM systems can be broadly categorised into four groups based on the installation point and the type of assets to be monitored as shown in

Table *4-1* (Tucker and Hall, 2014).

		Asset types	
		Infrastructure	Trains
installation point	trackside	Trackside monitoring infrastructure	Trackside monitoring trains
	Onboard	On-board monitoring infrastructure	On-board monitoring trains

Table 4-1: the main categories of RCM technology used on the UK Rail Network

Any RCM systems mounted on hi-rail vehicles, test trains or deployed manually for the evaluation of rail wear and damage, etc. are classified as onboard (Schmid, 2010). Systems designed to continuously monitor critical rolling stock components are also classified as onboard. An example of such a system is SKF's Axletronic which is capable of monitoring the condition of individual axle bearings under in-service conditions (Papaelias et al., 2014, SKF, 2010).

4.3 Wayside RCM systems

A wayside monitoring system is typically installed in or next to the track to detect and identify deterioration before it causes a failure by measuring one or more parameters of the system. Any potential defects can be identified after appropriate analysis of the available data has been carried out. The raw data generated by different RCM systems can vary considerably in complexity and nature. This has important consequences on the way data are acquired, analysed, transmitted and stored. In most cases, the rail infrastructure managers are interested in detecting abnormal events indicating a possible problem. These can then depending on their severity be classified under an appropriate alarm level so the decision-making can be simplified and automated, reducing human subjectivity to an absolute minimum. Depending on the type of defect under consideration state-of-the-art RCM technology may be less or more effective. For example, although wheel flats or overweight carriages can be detected with a relatively high level of confidence and accuracy, this is not the case for axle bearings.

Wayside RCM systems capable of monitoring critical rolling stock components offer significant advantages. First of all, they can monitor the wheels, axle bearings and bogie suspensions of every train passing through the instrumented site. In order to do this using onboard RCM technology, each wheelset and bogie should be monitored individually. This involves very high costs associated with sensors and acquisition units required to be installed on each train. Although the data quality and accuracy of onboard RCM systems is likely to be by default superior to that achieved by wayside equipment, the cost together with maintenance requirements normally proves prohibitive. The only exception to this are high-speed passenger trains which by law above a certain speed (≥250 km/h) are required to have as a minimum a temperature sensor monitoring individual axle bearings.

Although infrastructure-related condition data are predominantly acquired using conventional inspection equipment and methods, wayside RCM systems can provide continuous in-depth monitoring capability offering distinct advantages over current state-of-the-art. The main issue to overcome is the meaningful deployment of such systems. Due to the very large length of the rail network, the number of infrastructure components to be monitored and various types of defects to be detected, it is very important to rationalise instrumentation in the sections of most importance or interest. Various approaches can be considered in order to address this matter including risk of failure evaluation based on statistical analysis using Weibull distribution, maintenance history, available inspection data and rolling stock traffic density or tonnage (Lidén, 2016, Chattopadhyay and Kumar, 2008).

4.4 Wayside systems monitoring rolling stock components

Wayside RCM systems monitoring rolling stock are diverse in nature. Not only they can be used to measure abnormal impacts of the wheel tread on rails, but also check the level of wheel tread wear and detect surface abnormalities such as flats, squats, shelling and spalling. Quite often, WILDs are installed near the entrances of depots so damage can be detected before the train enters operation or when it returns from its daily service minimising the likelihood of damage (Schmid, 2010). Unfortunately, there is still need to instrument parts of the rail network itself since abnormal heavy braking can result in the formation of wheel flats at any time.

Rolling stock RCM technology can be classified as reactive or predictive (Lagnebäck, 2007). Reactive systems detect actual faults on the vehicles. In most cases the information from these systems is not suitable for trending, but is of importance to protect further damage from occurring due to the fault's presence. Examples of such systems are HABDs and WILDs.

The operational principle of HABDs (shown in Figure 4-1) is based on measuring the temperature of axle bearings using the infrared radiation emitted when a train is passing over an instrumented site. HABDs are reactive-based systems that are designed to report an alarm only after a predefined critical threshold has been exceeded. Hence, they are not optimal for long-term observation. Unfortunately, if an axle bearing is overheating then it has already failed. Therefore, HABDs are actually "last line of defence" RCM systems since they are only able to detect a failed axle bearing shortly before it actually seizes and potentially causing a derailment as a consequence. If sufficient HABDs are installed along a certain rail section, temperature trending may be possible. This can help minimise the likelihood of a false alarms. One major drawback of HABDs is that measurements can be affected by the temperature of the surrounding components. Heavy braking just before passing through a section instrumented with a HABD can give rise to temporary local overheating, resulting in a false alarm being generated. Although modern HABDs perform better, false alarms are still inevitable.

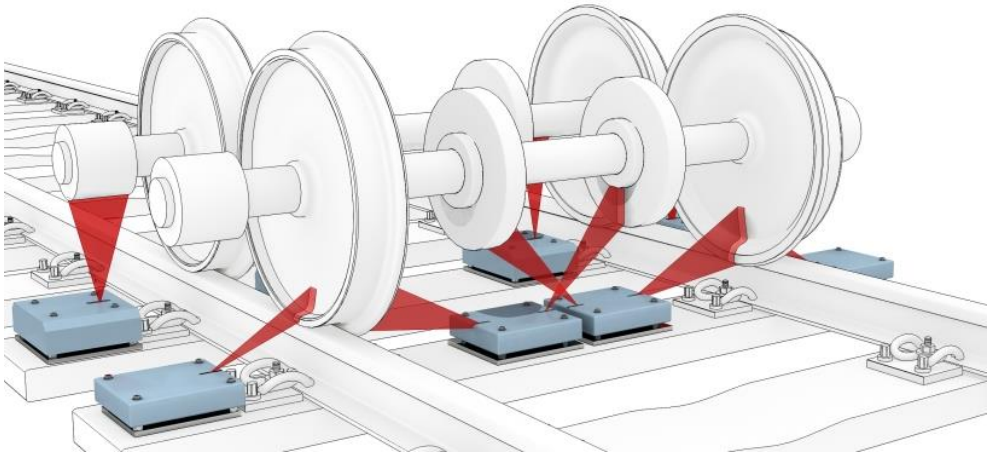

Figure 4-1: Schematic of the Pegasus hotbox detector by MER MEC. The schematic is courtesy of MER MEC Group.

Predictive systems, on the other hand, are capable of measuring, recording and trending the ride performance of the vehicles and also specific components. It is possible to analyse the condition of the equipment to predict potential failures and faults that may occur in near or distant future from the collected information. Typical systems include acoustic array detectors for the detection of faulty axle bearing and wheel profile monitors for the detection of wheel tread geometric irregularities.

Predictive systems offer long-term trending of vehicle parameters by providing root data instead of effects or symptomatic results. A low-level alarm can be raised if any early defects are detected. Such systems achieve the prediction of component failure and hence contribute to the proactive scheduling of relevant checks and repairs of vehicles before they suffer further collateral damage as well as inflict damage on rail track. Such sophisticated systems are more expensive and thus the sites to be instrumented need to be carefully decided to maximise the benefits drawn.

There are over 20 types of state-of-the-art wayside monitoring systems available on the market. These can be classified into 5 groups based on the component they are used to monitor (Brickle et al., 2008, Ngigi et al., 2012, Barke and Chiu, 2005, Schmid, 2010).

Table *4-2* provides detailed information about various wayside monitoring systems currently in use.

Wheel	Wheel profile detector	WheelView	M: multicamera and stereo machine vision technology P: Flange height, flange width, flange slope, tread hollow, rim thickness, wheel width and wheel diameter; additionally, back-to-back gauge, groove tread, tracking position and wheel temperature measurements S: 65 mph O: AVI compatible, data storage and automated email reporting;
		FactIS	M: cameras P: flange height, flange width, tread hollow, rim thickness and back-to-back gauge S: Low- speed (~30 mph) or medium-speed (~60 mph)
		WheelCheck	M: laser beam and a high-resolution camera P: flange height, flange thickness, flange angle, back-to-back gauge, rim thickness, hollow tread, tread taper and wheel diameter S: 60 mph
		WheelSpec	M: laser illumination with high-speed cameras P: flange height, flange thickness, rim thickness and tread hollow measurement S: 60 mph
		Argus	M: laser beam with cameras P: wheel profile, roundness and flat spots, wheel diameter and surface cracks S: <7 mph O: database sever
		Model 2000 Wheelset Parameter Measurement and Control Facility EVA Module	M: Laser beam with Cameras P: flange height, flange thickness, qR factor, distance between inner sides, distance between active sides and wheel diameter S: 10 mph
		TreadVIEW	M: cameras and lasers with image analysis software P: flange height, flange width and tread hollow Data storage, low-speed applications (<10 mph)
	Tread condition monitoring system	Model 2000	M: surface wave-based ultrasonic detector P: surface-breaking discontinuities on the surface of the wheel material S: 6 mph O: interface with Model 2000 wheelset parameter measurement and control facility; data storage
		Argus	

			M: ultrasonic scanning heads integrated into the track P: transversal cracks, surface cracks, material splintering on the tread and metal building up at the outer profile edge S: 7 mph; depth of 4 mm O: the crack detection module of Argus
Bearing	Acoustic bearing detector	TAADS	M: array of microphones P: discrete defects in internal bearing components, multiple defects and generalised noise
		RailBAM	M: array of microphones P: surface faults (spalls, water etching and brinelling on internal bearing components), loose or fretting components S: 20 ~ 75 mph
	Hot axle/wheel box detector	Pegasus	M: multi-element infrared sensors P: the temperature of bearings, brakes and wheel discs S: 310 mph with bearing temperature of 0-150℃ and brake/wheel temperature of 80-650℃ O: web-based database
		FUS II	M: four-element HgTdCe infrared sensor P: the temperature of bearings and wheels S: 310 mph with bearing temperature up to 180℃ and brake/wheel temperature up to 650℃
		Micro Hot Bearing Detector	M: P: bearing temperature O: GE Advanced Concepts Scanner; voice radio talker output, several serial protocols and dial-out modem connection
		MULTIRAIL	M: infrared tech P: bearing temperature and critical brake condition O: AVI and web-based reporting
Bogie	Bogie performance detector	MATTILD	M: optical sensors P: dynamic axle, bogie imbalance and wheel vertical and lateral loads O: compatible with automatic tamping machines
		HTD	M: lateral strain gauge array P: hunting, flange-climb derailments S: 10-180 mph
		TPD	

			M: strain gauges and/or optical angle of attack sensors P: vertical lateral loads and/or axle angle of attack S: 10-180 mph
		TBOGI	M: laser sensors P: hunting bogies, subtle defects in bogie performance (skewed, warped and misaligned bogies) S: high-speed passenger, freight and intermodal traffic
Wheel – rail interface	Wheel Impact detector	GOTCHA	M: optical sensors P: wheel defects
		WheelChex	M: array of strain gauges P: running surface defects e.g. skid flats and out-of-round wheels
		RoundChex	M: vertical deflection of the flange tip P: out-of-round wheels O: threshold alarms with trending data
M: type of measuring sensor P: measured parameters; S: applicable speed O: Others to be mentioned.			

Table 4-2: Commercial wayside systems currently in use around the world.

As a comparative example of the use of wayside RCM systems, Network Rail currently maintains 206 HABDs, 34 WILDs (including 8 GOTCHA systems) and 3 TAADS (including 2 RailBAM systems) installed across the UK (Vallely, 2015). The majority of these RCM systems are installed on the most heavily travelled parts of the network such as the West Coast Main Line (e.g. London-Euston-London route).

4.4.1 Wheel monitoring

The objective of a wheel check system is to measure the critical dimensions of the wheel such as flange height and width, wheel profile, defect trends, wheel flats, thickness of the rim as

well as recognise surface cracks, and pitting. Wheel profile distortion can occur as a result of braking process, poor adhesion or incorrect brake lock settings.

Wheelset RCM systems are designed to inspect and identify worn wheels on passing trains by using non-contact sensors, such as high-speed cameras and lasers. Two types of such systems are available; WPDs and tread condition monitoring systems (Brickle et al., 2008). Further data analysis of WPD data can provide useful information regarding several wheel profile parameters, including flange height and slope, tread hollowness, wheel width and wheel diameter. Tread condition detectors are capable of detecting discontinuities in the running surface of the wheel, such as surface-breaking and subsurface cracks. Figure 4-2 shows an example of the typical output of a WPD (Bladon et al., 2004).

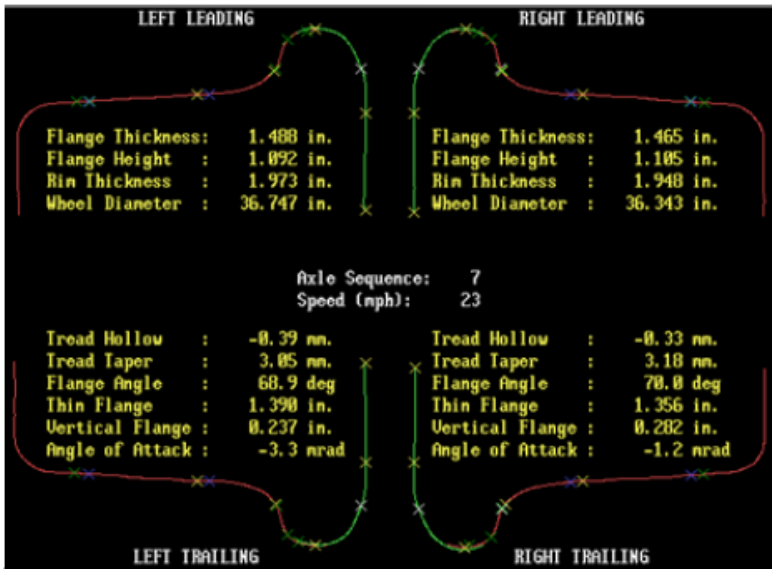

Figure 4-2: Typical output of wheel profile detector (Bladon et al., 2004).

The technology used by different RCM system manufacturers can vary considerably. The WILD WheelChex systems (shown in Figure 4-3) use strain gauges attached on the web's surface to assess the condition of the wheels. These strain gauges measure the change in resistance arising from the increasing deflection of rails under higher impact loads caused by

the presence of irregularities in the wheel tread such as wheel flats. Other systems make use of accelerometers measuring vibration and the level of acceleration instead to assess the loads exhibited on the rail by passing rolling stock.

Figure 4-3: Photograph showing a WheelChex System installed on the UK rail network (the photograph is courtesy of Network Rail).

WPDs are based on the use of scanning lasers in order to determine the exact profile of the wheel tread. All the information is then compared against standard healthy profile. The use of WPDs eliminates the need for manual profile inspection (Barke and Chiu, 2005). WPDs are real-time measurement systems using a combination of lasers and video cameras to automatically measure the wheel profile, while rolling stock is in motion. WPDs are mounted wayside in the track area. The system acquires relevant data and analyses them. Some prediction is also possible with respect to the time remaining prior to re-profiling. The data acquired from WPDs include, wheel profile and wear, wheel diameter, height and thickness of the flange, back-to-back distance and wheel inclination (Danneskiold-Samsoe et al., 1993). The FactIS system (mostly found in Canada, USA, Brazil, and Australia) is based on the use of cameras for capturing images of the wheels as they pass. This is similar to the Argus system, which uses a combination of scanning lasers and cameras.

When the geometry of the wheel-rail interface changes, this can have result in significant impact to the vehicle as well as infrastructure components (Jones and Jones, 2010). The shape and size of flats or shelling, wheel and rail profiles, axle load, vehicle speed and rail pad stiffness are parameters affecting the level of loads arising after each wheel revolution. Since WILDs can detect the impact loads generated from the wheels of the train while it travels over them, train drivers can be alerted promptly of any wheelset problems. Most importantly detection of abnormal wheel impact loads in time can help prevent structural damage on rails and crossings (Fu and He, 2001). The photograph in Figure 4-4 shows the strain gauges of a WILD attached on the rail.

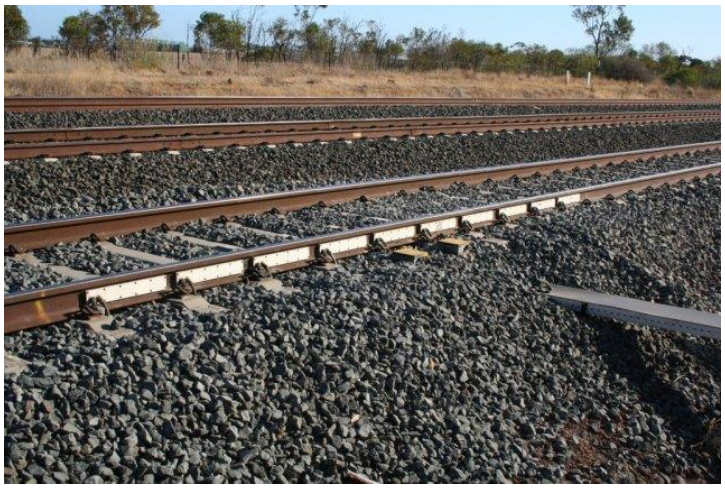

Figure 4-4: WILD based on strain gauges (photograph courtesy of Markus Wong).

WILD data can be analysed to detect, locate, and measure the size of defects, such as shelling, spalling, wheel flat and out-of-roundness. If the preset threshold is exceeded an alarm is given. In extreme cases of excessive impact load amplitudes the driver may be asked to stop the train to prevent excessive damage on rail infrastructure and subsequently asked to proceed slowly to the nearest siding in order to have the affected wheel replaced (Yang et al., 2005). High-impact wheels are most often wheels that have a flat spot on the tread surface, known as

a slid flat (Stratman et al., 2007). It should also be noted that wheel impacts can act as precursors to axle bearing faults.

4.4.2 Axle bearing

Increased levels of vibration, noise and temperature produced by the axle bearing are likely signs of a developing defect. TAADs use acoustic arrays to record the noise produced by the bearing as the train passes along the instrumented site. TAADs are potentially capable of detecting the acoustic signature of developing bearing defects much earlier than HABDs. Hence, they can be employed as predictive monitoring systems. However, they are dependent on trending.

HABDs make use of thermal sensors that normally mounted on a specially designed hollow sleeper to monitor axle boxes of passing rolling stocks and detect any bearings with unusual temperature. A red alarm will be given whenever wheels are overheating beyond a pre-defined threshold which is normally 90 ℃. A HABD alarm indicates imminent failure of the bearing as a reactive monitoring system.

As mentioned earlier HABDs are reactive systems. Hence, an alarm generated by a HABD indicates imminent failure of the bearing. Moreover, HABDs are not capable of detecting the cause of the fault but just its result. Although currently there is no trending for HABD data (Tucker and Hall, 2014), limited predictive capability could become possible through data (alarm) trending from multiple instrumented sites in sequence provided that the distance between each HABD is small enough so derailment has not already occurred.

The distance between two HABDs is normally based on the available budget to buy, install and maintain such systems, the type of rolling stock travelling along a particular line (mixed,

passenger or freight only), the operational speed, traffic density and distance between stops (Blakeney, 2001).

Trackside acoustic detection systems are predictive maintenance tools. They make use multiple microphone arrays placed trackside listening to the audible noises produced by the axle bearing of passing rolling stock. The microphones identify sound characteristics emitted by bearing defects such as roller or ring surface defects. The maximum operational frequency is limited to 22 kHz or 44 kHz (i.e. close to the audible range for humans).

There are two main types of TAADs which are currently used in the rail industry. The first one is RAILBAM (Rail Bearing Acoustic Monitor) designed by Track IQ, Australia (Siemens in the UK) and the other acoustic system is TAADS (Trackside Acoustic Array Detection System seen in Figure 4-5 (Watson et al., 2007) designed by TTCI, US. Since 2012 TAADs have been installed in three locations on the UK rail network undergoing evaluation (Southern et al., 2004).

Figure 4-5: TAADS system in the U.S. (the photograph is courtesy of TTCI).

Since the operating frequency of the microphones is restricted to the audible range, the acoustic signals captured can be contaminated by the sounds from the surrounding

environment as well as the measured train itself (e.g. wheel flats or noise from the engine). Therefore, such systems are theoretically prone to errors due to the aforementioned reasons.

Another drawback of TAADs is the clearance required for the microphone arrays to be installed, The housing structure that needs to be installed trackside is of substantial size and this can be particularly problematic when a third rail is present or when the clearance between two lines is too small (e.g. four-foot).

Wayside acoustic systems should be more effective than HABDs since they are designed to detect bearing faults in an earlier stage. With proper signal processing techniques, they are able to trend individual wheelsets every time they pass the instrumented site. Although wayside acoustic systems are more expensive than HABDs in terms of equipment and installation cost, fewer systems are required to be deployed over the network to effectively monitor rolling stock.

In the case of TAADs if a defective bearing is detected in time, sufficient time for maintenance planning can be made available in order to avoid disruption and delays caused by faulty axle bearings. Unfortunately, there is very little information available on the public domain regarding the actual capability in terms of sensitivity and accuracy of TAADs. The photographs in Figure 4-6 show examples of a TAAD and HABD system respectively. Even if TAADs are effective in detecting damage much earlier, HABDs are still required as a last resort against potential defects that may be missed by TAADs.

a)

b)

Figure 4-6: a) The RAILBAM system installed on the UK rail Network (photograph is courtesy of Siemens) and b) a HABD installed in Portugal.

4.4.3 Bogie geometry

The definition of bogie geometry here indicates the angle of attack and tracking position, which is relevant to vehicle hunting. By using optical sensors, bogie condition monitoring system is able to measure static and dynamic loads applied to the rail, such as dynamic axle, bogie imbalance and wheel lateral load. It is feasible to combine bogie condition monitoring system with WILDs to get better understanding of the relationship between overall dynamic loads and wheel/rail force (Lamari, 2008). The photograph in Figure 4-7 shows an example of bogie monitoring systems installed on the rail network.

a)

b)

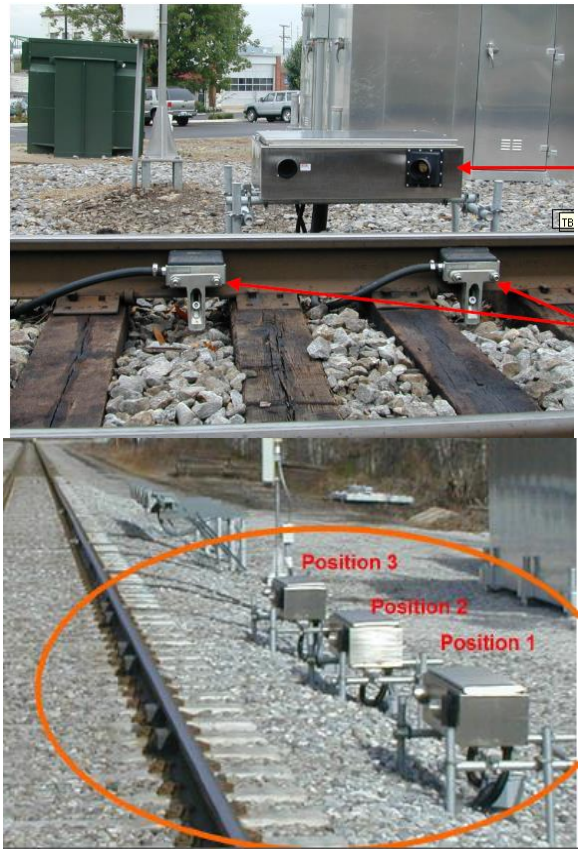

Figure 4-7: Single bogie monitoring system (upper); sets of such systems (lower). The photograph is courtesy of TrackIQ).

4.4.4 Automatic vehicle identification

The Automatic Vehicle Identification (AVI) system provides a means of tracking individual vehicles at a particular location, date and time. An example of AVI is shown in Figure 4-8. They operate based on Radio Frequency Identification (RFID) principles. The tag readers installed next to track send out the message. The tags on the wagon reflect the signal back to the readers. Each tag has a unique identification code to indicate a certain wagon so that the information can be recorded. The advantage of AVI systems makes it possible to do trend analysis from wayside inspection systems for individual vehicle.

Figure 4-8: Example of AVI system (Photograph courtesy of Citycom).

4.4.5 High-frequency acoustic emission

High-frequency acoustic emission is based on the detection of ultrasonic signals which are normally in the range between 20 kHz – 1200 kHz. Due to the high-frequency of the detected signals passive piezoelectric transducers used to detect them need to be mounted on the side of the rails. Acoustic emission sensors are capable of detecting the stress waves generated by the various possible flaws on the wheel tread, such as, flats, or other surface defects, which generate huge impact load on the rail while the wheel is turning, faulty axle bearings and bogie suspensions. Acoustic emission can also be employed for the detection of crack initiation and crack growth in infrastructure components such as rails, crossings and sleepers.

By using resonant acoustic emission transducers it is possible to eliminate the effect of environmental mechanical noise not associated with the presence of defects (Papaelias et al., 2014). The effective filtering of unwanted environmental noise can be further enhanced by using suitable signal processing algorithms.

4.4.6 Vibration analysis

Vibrations are random or periodic mechanical oscillations of a body or system. Abnormal vibrations in a system can signify the evolution of damage (Watson et al., 2007). Piezoelectric accelerometers are typically used in order to measure vibration in rotating machinery. Typically, the operational frequency of accelerometer ranges between 0 Hz - 18 kHz. The level of sensitivity at higher frequencies is directly dependent on the way that the accelerometer is mounted, i.e. magnetic hold down, glue or thread since it affects the level of damping of the accelerometer (Taylor, 1994).

Vibration analysis usually requires data trending in order to be accurate, thus data measurements in the good and deteriorated states are required. Accelerometers have been used in WILDs but they are also evaluated as a means of detection of faulty axle bearing and profile irregularities, such as ovality shape (Madejski, 2006, Dukkipati and DONG, 1999).

4.5 Infrastructure monitoring infrastructure

Rails are generally monitored using train-mounted sensors. This involves dedicated test trains that can cover large sections of infrastructure in a single inspection campaign as they run along the track. Unfortunately, due to the nature of the crossings test trains cannot be used for inspecting them. Instead, infrastructure managers rely predominantly on visual and dye penetrant inspection to assess the condition of such assets (Weston et al., 2014). Any internal defects are practically impossible to detect with conventional inspection techniques due to the nature of the microstructure of cast manganese steel (large austenite grains) which cause scatter and attenuation of ultrasonic waves. In addition, austenite is non-magnetic so magnetic flux leakage commonly employed on conventional rails is not applicable. Low frequency

eddy current testing could be used but at the expense of sensitivity making detection of even relatively significant defects practically impossible.

The structural integrity of cast manganese crossings is of paramount importance to ensure effective RAMS. According to Network Rail's statistics, about 900 crossings are ordered and installed per year. Approximately 25% of the ordered crossings are used to replace old defective crossings. The remainder are used for new build project work. The intended lifetime of cast manganese crossings on the UK rail network is anticipated to be a minimum of 20 years. However, many of these crossings fail earlier, with some failing as early as within 1 to 3 years in-service. A crossing costs between £15k - £30k depending on size, with installation costs reaching between £10k - £40k depending on location and complexity. Thus, the cost of renewing an existing crossing can range from £30k - £130k depending on whether it is completed as a planned or reactive renewal (up to £200k if delay costs are included). A recent Network Rail report showed that 20 instances of crossing failures (replacements required) were recorded on the London NorthWest (LNW) Route from April 2015 to May 2016. On LNW South alone, more than 15 crossings failed and were replaced over this 12-month period. Another significant cost associated with crossing failures are the Train Delay Attribution minutes. Crossing-related failures resulted in 81,137 delay minutes at a cost of £8.3m (Delay Attribution Board, 2015). Because of the disruption that can result from failure, some of the crossings can be considered to be golden assets for rail infrastructure managers.

Chapter 5:

Systems correlation and decision support tool

Chapter 5: System correlation and decision support tool

5.1 Introduction

As discussed earlier in the present thesis, there are a number of wayside monitoring systems used by railway infrastructure managers in order to monitor critical rolling stock and infrastructure components. These RCM systems are manufactured by different companies and designed to monitor a single component, such as bearings and wheels. In almost all cases these systems are designed as black boxes, offer very few, if any, interactive functionalities to their supervisors.

Existing systems are designed to operate as individual checkpoints. Therefore, there is no correlation among different individual systems and data are not shared (Tucker and Hall, 2014). An interesting RSSB report looking into this particular topic showed that there is a strong demand by the rail industry to bring individual RCM systems and the data they generate together in order to improve the reliability and maintenance efficiency of rail systems (Brickle et al., 2008). This would also support the realisation and effective implementation of condition-based maintenance strategies.

5.2 Decision support tools

One example of decision support tools used by railway infrastructure asset managers is RAMSYS. This particular software package has been developed by MERMEC S.p.A., Treviso, Italy (Swift et al., 2011). This commercial maintenance system provides a single platform to integrate and manage data related to railway asset maintenance. It can perform such functions as data validation, condition-based and predictive maintenance planning.

However, there is currently no relevant software focusing on integrating information and data generated from the various numerous commercial RCM systems found on large railway network. This is also technically more complicated than asset management alone since interfacing of the various systems is required.

One of the interests of the present study is to create an intelligent platform based on the customised RCM system developed, which is capable of integrating multiple wayside monitoring systems of different types into a single operational network. Such an integrated network of RCM systems can be developed based on the technology of database systems and can incorporate several unique features including, data trending, sensor fusion and data correlation (Yam et al., 2001, Palo et al., 2014).

The decision support tool considered in this study can improve the reliability of current in-service RCM systems and implement condition-based maintenance by providing comprehensive information regarding the actual condition of key rolling stock and infrastructure components.

Moreover, it has the potential to consolidate an efficient strategy of where and what to install on the existing and future rail network. This can be decided using a proper network optimisation model that is capable of selecting cost-effective installation sites for wayside monitoring systems (Ouyang et al., 2009). The schematic in Figure 5-1 shows the basic principles of an integrated decision support tool capable of integrating several monitoring systems of different types into a single centrally managed operational platform.

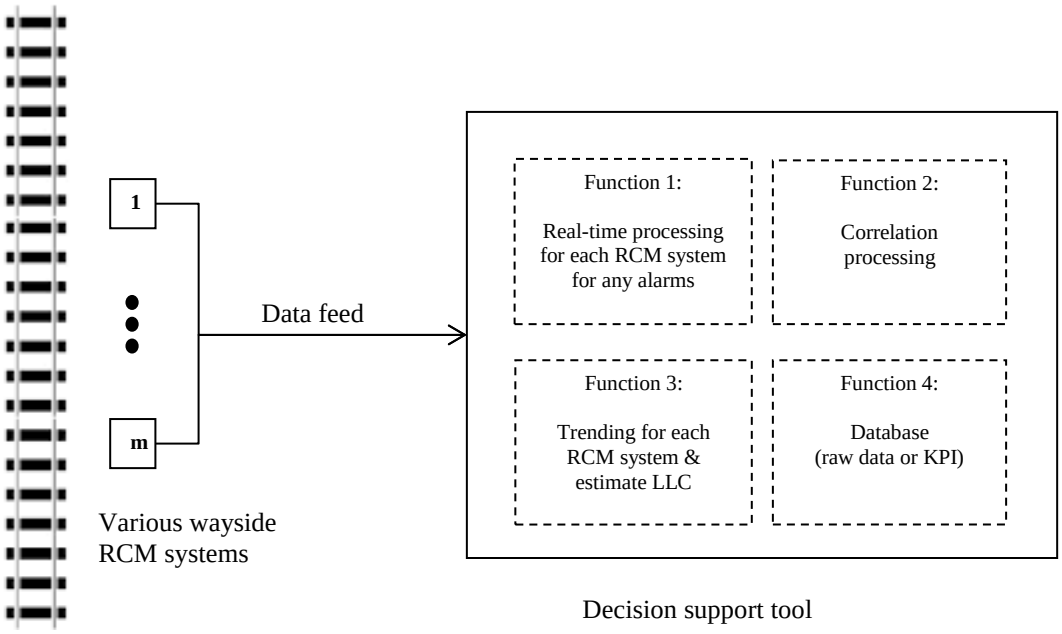

Figure 5-1: Simplified schematic showing the main architecture of a decision support tool capable of integrating various RCM systems into a central platform.

The data collected by individual wayside RCM systems can be transmitted to a central database serving as a remotely operated Supervisory Control and Data Acquisition (SCADA) Centre (or Dispatch Centre) (Marquez et al., 2008). High-rate data transfer can be achieved using optical fibres, which are in several locations already available on the rail network. Alternatively, where appropriate coverage exists, wireless connections can be used instead.

The decision support tool considered herewith consists of four main functions as detailed next (Swift et al., 2011):

Function 1: Real-time processing is essential to identify any incipient faults. Where data processing is required to be carried out will depend on each system. Data processing can be done at the trackside directly after data acquisition has been completed. Subsequently, the processed results can be transmitted to the central database. This is especially useful when the dataset is too large to be transmitted in a short period of time or where data transfer comes at a

significant cost. Other datasets can be analysed by the decision support tool after transmission. Any alarm can then be issued immediately after detecting incipient defects.

Function 2: Correlation processing is the most important part of the decision support tool. It plays a vital role in the drastic improvement of the accuracy of detection. More information can be obtained from the existing database by fusing data generated by the various RCM systems in use as explained later on.

Function 3: Data trending can be achieved by data mining of historical datasets for each RCM system. This method provides the ability to identify defects in the early stage and schedule maintenance with minimum disruption to the live railway traffic (Hajibabai et al., 2012). Currently, there is no or very little trending of data for a particular train travelling on the network. As discussed before practically all wayside systems act as individual checkpoints for the detection of specific defects, only giving an alarm once a pre-defined threshold is exceeded (e.g. HABDs, GOTCHAs, WPDs, etc.). Data from individual wayside systems are not trended and integrated and as a result large numbers of false alarms are not uncommon for certain types of wayside systems.

Function 4: Since each wayside system produces datasets of significant size on a daily basis, a properly functioning database system needs to be capable of effectively handling data collection, storage and accessibility on-demand. It is also important that individual RCM system are compatible with other wayside systems, providing a generic interfacing protocol and allowing the system operator to flexibly access and distribute the information to engineering, maintenance or train control (Bladon et al., 2004, Tucker and Hall, 2014). By adopting a uniform interface, system extension and upgrading becomes easier and more cost-effective in time (Maly et al., 2005).

5.3 Data correlation and data fusion

Data correlation is the most important feature in the decision support tool. It is a feature that allows the decision support tool to be clearly distinguishable from normal database systems. The purpose of the decision support tool is to correlate and analyse the synergistic differences in various types of data, reducing the number of false alarms, and thus, improving the reliability of RCM systems. Three levels of correlation will be introduced following a bottom-up architecture.

5.3.1 Sensor-level correlation

There are a number of advantages in using multiple-sensor systems. It is obvious that the more sensors used can provide additional independent observation with an increase in both spatial and temporal coverage. Moreover, systems with multiple sensors have an inherent redundancy. When one or more sensors fail, the system is still functional. Therefore, using multiple sensors can improve system performance and reliability (Alfaro and Cayo, 2012, Dong et al., 2009, Liggins II et al., 2008, Hall and Llinas, 1997).

Perhaps the most important benefit of using multiple-sensor systems is that signals acquired can be correlated to each other using sensor fusion techniques to provide more information about the components being monitored (Castanedo, 2013, Steinberg et al., 1999). Since the signal source is the same, either from rolling stock or infrastructure, signals obtained by multiple sensors are inherently correlated. Hence, they can be effectively processed with appropriately selected sensor fusion and signal processing techniques (Xuejun et al., 2009). If signals from different sensors are fused correctly, the information provided by the combination of individual sensors is more accurate and valuable than that obtained by each sensor individually.

5.3.2 Object-focused correlation

Critical railway components, such as wheels and axle bearings, can be monitored by more than one type of RCM systems. Different types of sensors are used so that they can provide information from different physical perspectives, such as temperature, shape, load impact and acoustic noise. It is advantageous to synthesize and analyse data from numerous sources to provide deeper insight into the effective evaluation of different defect types. In this way, a certain type of defect can be more effectively detected and accurately quantified in terms of its severity by potential correlation of several systems rather by a single one.

For example, systems that are capable of detecting wheel defects include acoustic emission systems, acoustic detectors, WILDs and WPDs. Although each of the aforementioned systems measure different parameters, they can all detect the presence of the wheel flat (Hajibabai et al., 2012, Schöbel and Mirković, 2010, Palo et al., 2014, Lagnebäck, 2007). The relationship between indirect measurements of these systems and wheel flats can be improved with the help of correlation processing of the acquired data. The architecture of the decision support tool framework is shown in Figure 5-2. By analysing all these individual datasets in combination, it is possible to generate a comprehensive understanding and evaluation of the actual condition of the wheel tread. Other possible correlation includes axle bearing monitoring (Huang et al., 2014, Papaelias et al., 2014) and track geometry monitoring (Faiz and Singh, 2009).

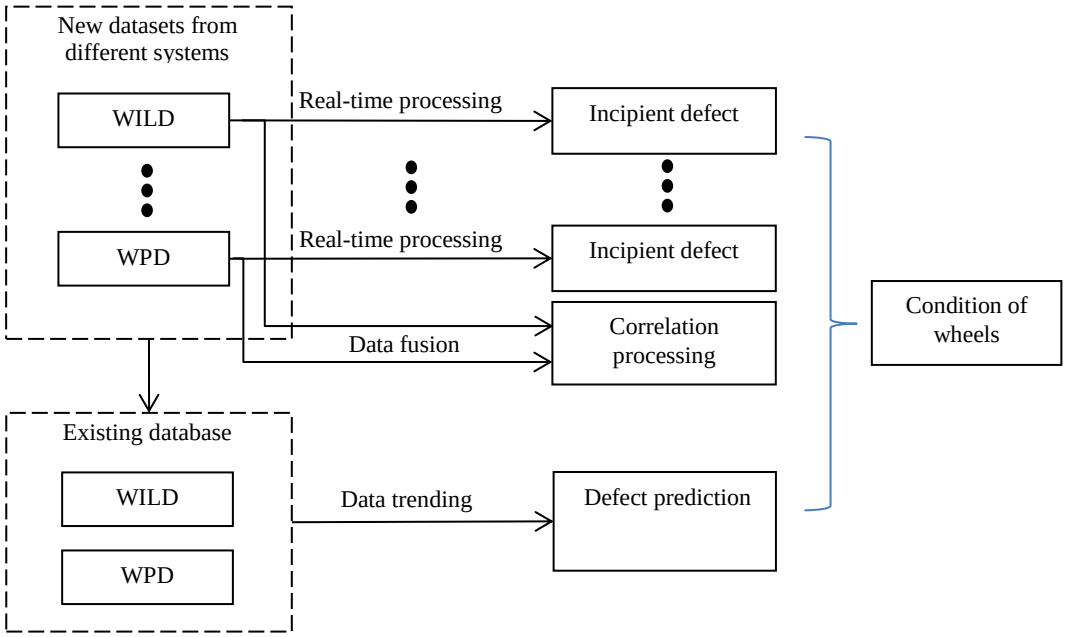

Figure 5-2: Schematic showing the basic architecture of the decision support tool framework for wheel conditioning systems.

5.3.3 System-level correlation

As rolling stock and infrastructure form a highly-integrated and dynamically interacting system, any localised defect developed in one component can affect the dynamics of the whole system, leading to the initiation and evolution of defects in other components if left unattended (Vale, 2014, Barke and Chiu, 2005, Palo et al., 2014). Due to the fact that no system-level correlation has been implemented so far, data collected by each RCM system are processed separately. Moreover, there is no information available from relevant components where defects can develop from.

Therefore, a strategy of system-level correlation needs to be implemented to link different components and faults affecting them for better understanding of potential failures and improving remote monitoring capabilities. This approach of system-based correlation has several advantages. It can improve the reliability of defect detection by cross-validating the

results, provide detailed information about the integrity of the entire fleet, and reduce the maintenance effort due to centralised function checking (Maly and Schobel, 2009).

The inner-relationship of the rolling stock and wheel-rail dynamics is shown in Figure 5-3. Any defect in the graph will start the cycle and propagate to other components. For example, a skid on the wheel can cause early fatigue of the wheels, and eventually damage the axle bearings and bogie suspension as well as cause structural damage on the rails (Schöbel and Mirković, 2010, Bladon et al., 2004, Bladon and Hudd, 2008). On the other hand, a defect in bogie geometry can lead to bearing defects due to strong vertical force, and later cause wheel defect because of the imbalance load. Other research also indicates that noisy wheels can cause axle bearing damage since this can be an indication of higher than normal stresses being sustained by the axle bearing due to poor conformity of the wheel contact area with the rail head (Bladon et al., 2004).

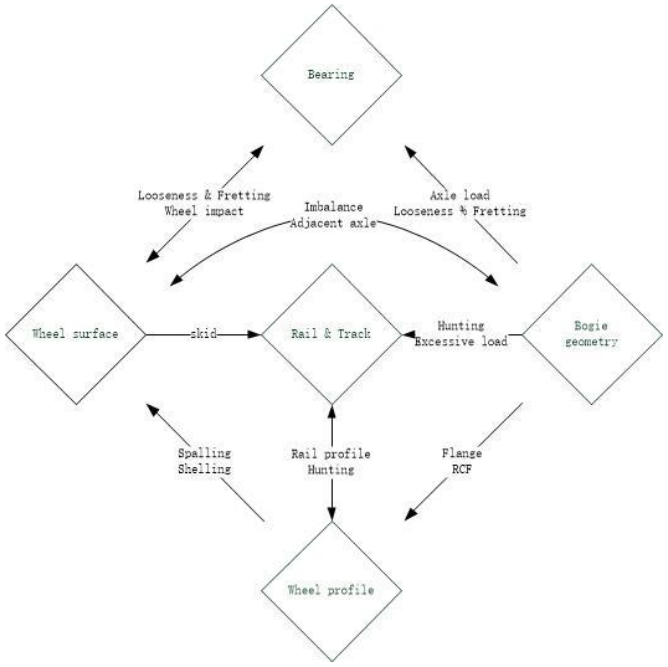

Figure 5-3: Schematic showing the inner-connection of rolling stocks and wheel-rail dynamics (Bladon et al., 2004).

Some pilot trials have been carried out to address the aforementioned issues. The Wayside Monitoring Alliance (WMA) was formed to monitor rolling stock, offering long-term trending of vehicle parameters. Systems correlated include WPDs, wheel condition detectors and axle bearing acoustic detectors (Bladon et al., 2004). However, the limitation of the WMA is the lack of advanced signal processing with raw signals, since data trending is performed with data that have already been processed by each RCM system.

5.4 The customised RCM system

The difficulties of carrying out system correlation of wayside RCM systems effectively have been identified in a number of studies reported that have been reported previously (Brickle et al., 2008, Tucker and Hall, 2014). System correlation does not only require different parties to agree in sharing information and data, but also requires a widely accepted database platform and systematic level of approach to integrate and manage data and equipment. In addition, the decision support tool should be granted high-level access so that it can retrieve raw data from each RCM system for more advanced processing if necessary. The effectiveness of data correlation processing using processed data is limited as the information contained by raw data is lost after processing is completed by each RCM system.

In order to solve this problem, the author proposed a customised RCM system that integrates different types of sensors to record data from rolling stock and infrastructure. Data will be transmitted to a decision support tool for correlation processing. The prototype system currently makes use of acoustic emission and vibration techniques to monitor bearing, wheel and cast manganese crossings. This will be expanded in the future to include other wayside systems.

The customised system can carry out cross-correlation and spectral coherence processing on acoustic emission and vibration raw data to identify defects in each component. If no defect is defected, KPIs will be stored in database for future trending. Otherwise, truncated raw signals will be stored instead so that the original information of the component can be kept.

Three levels of correlation processing, as introduced before, are also integrated in the decision support tool, which will be elaborated with case studies. In terms of sensor-level correlation, multiple acoustic emission sensors and accelerometers are used in all test trials. The schematic in Figure 5-4 shows the sensor layout for the Cropredy test site which is more thoroughly discussed in chapter 6.

Sensor fusion is carried out among 4 acoustic emission sensors as a case study. The results indicate that sensor fusion processing is able to provide the ability of self-testing for each sensor, calculate the train speed, detect axle load imbalance and identify the time instance for each wheel passing through from the raw signal.

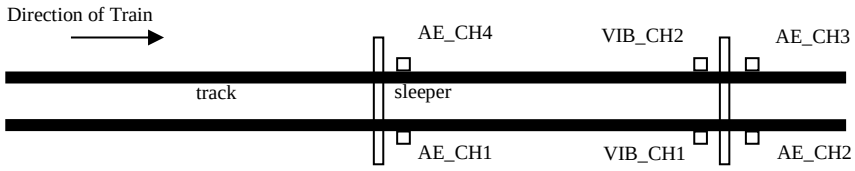

Figure 5-4: Schematic of sensor layout at Cropredy test site.

Axle bearing monitoring is selected as the scenario for object-focused correlation, which can be monitored by means of acoustic emission, vibration and temperature data. The schematic in Figure 5-5 shows the architecture of system correlation for wheel and axle bearing monitoring. By analysing the AE and vibration signals, wheel and bearing defects can be

distinguished, while temperature signals obtained from the HABD can be used to validate the results of acoustic emission signals in the case of severe axle bearing damage.

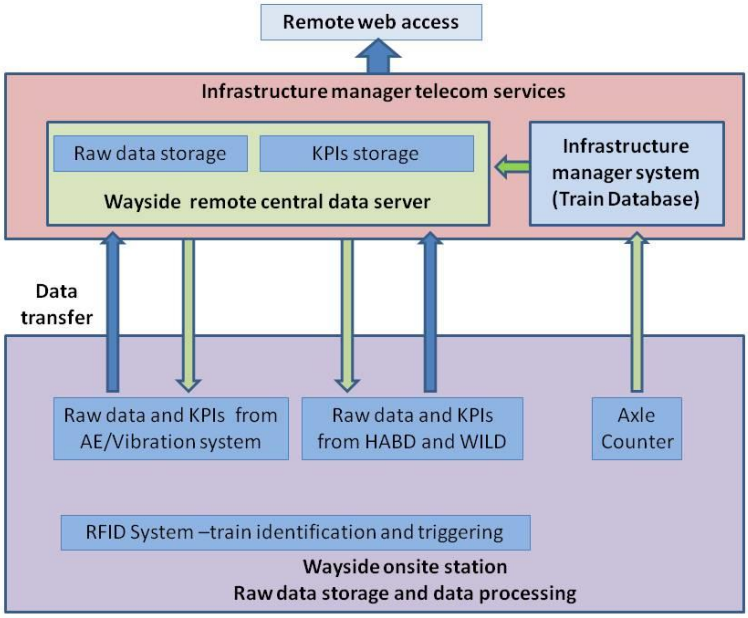

Figure 5-5: Schematic showing system correlation for wheel and axle bearing condition monitoring.

The case study for system-level correlation is carried out by comparing acoustic emission data generated from the interactions at the wheel-rail interface and crossing crack growth. Since the monitoring of crack growth in cast-manganese crossings makes use of the wagon load as the source, interference from the rolling stock is inevitable for wayside crossing monitoring. However, the interference can be minimised by correlating acoustic emission signals collected in both cases. Detailed discussion about this scenario will be provided in Chapter 7.

Chapter 6:

Experiment methodology

Chapter 6: Experimental methodology

This chapter discusses the experimental procedure employed in the study. Testing was performed under realistic railway operational conditions at the Long Marston test track and various sites of the UK rail network. Short and long-term testing at the Long Marston test track was carried out with the support of VTG Rail, Motorail Logistics, Krestos Limited and Network Rail. The short and long-term trials on the UK rail network were carried out with the support of Krestos Limited and Network Rail. For all tests performed, a customised RCM system developed by the author in collaboration with other members from the NDT and Condition Monitoring Group at the School of Metallurgy and Materials of the University of Birmingham was used.

In order to enable the commissioning of the customised RCM system on the UK rail network, a safety study needed to be submitted to Network Rail for approval. The safety study was required to identify the main risks arising from the instrumentation of rail infrastructure and overall operation of the customised RCM system once commissioned. The approval of the safety study by Network Rail engineers was granted in the form of a Certificate of Acceptance with Number PA05/06524, valid since 1st September 2015. The Certificate of Acceptance allowed tests to be carried out practically anywhere on the UK rail network. Experiments outside the Long Marston test track focused on the West Coast Mainline, and more specifically, the heavily travelled London-North West route. The system architecture, key characteristics, selection of rolling stock tested, selection of sites instrumented, components monitored, together with the experimental methodology employed in each scenario are described in detail in the following sections.

6.1 Customised RCM system

A customised RCM system that integrates acoustic emission sensors and accelerometers has been developed in collaboration with other researchers. The customised system consists of two main parts; a) the data acquisition unit and data storage component and b) the signal processing and decision support tool.

The data acquisition unit is responsible for digitising the analogue signals generated by the piezoelectric acoustic emission sensors and accelerometers and subsequently transmit them to the control PC where data are logged and stored for further analysis. The data acquisition unit consists in its most basic form of a commercial Agilent 2531A USB data acquisition card (DAQ) with a maximum sampling rate of 2MSa/s at 12 bits. If the maximum sampling rate is to be used then the DAQ is able to support only one data acquisition channel. However, in the case there lower sampling rates are used up to four channels can be supported. The limitation is that all channels should be logging the same output signals, which is either acoustic emission or vibration. Therefore, in the cases where acoustic emission and vibration data need to be collected simultaneously then two DAQs are required, one recording acoustic emission data from up to four acoustic emission sensors and one recording vibration data from up to four accelerometers. The two DAQs can operate at independent sampling rates to accommodate the different requirements of the acoustic emission and vibration measurements.

Once the acoustic emission and vibration signals have been digitised, a conventional PC running a customised data logger and signal analysis software written by the author in LabVIEW® and MATLAB® is used to log and store the data for subsequent analysis. All data

generated are given an identifying filename which is based on date and time of acquisition and subsequently stored in a central database.

The database serves as the platform for system integration and correlation using advanced signal processing algorithms. The developed system has a broad range of applications since the same methodology can be employed to monitor both railway rolling stock and infrastructure components. Figure 6-1 shows the general architecture of the customised integrated RCM system employed in this study. The same architecture applies for measurements on infrastructure components such as rails, cast manganese crossings and sleepers.

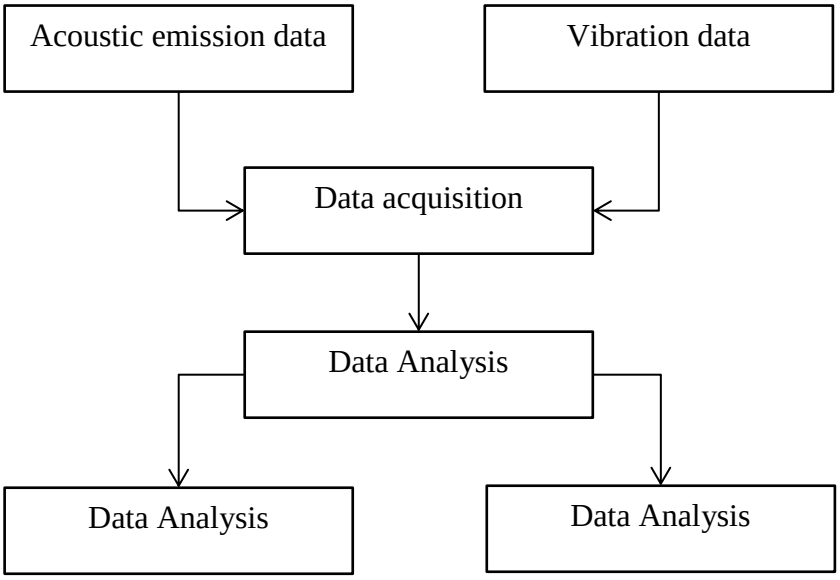

Figure 6-1: Simplified schematic showing the basic architecture of the customised integrated acoustic emission and vibration analysis RCM system for rolling stock measurements

The customised RCM system has been designed in such a way so it is possible to be triggered using various techniques. In the simplest method, the RCM system can be triggered to acquire manually. Alternatively, if automated acquisition is required, there are two different options

depending on the requirements of the measurement. Firstly, acquisition can be performed using time. This is done by entering the start time for the first acquisition and subsequently the time intervals that the measurement should repeat itself. The acquisition intervals can be adjusted to take place every few seconds or up to every few hours. Secondly, acquisition can be initiated by an external triggering signal. In this research two different triggering systems have been considered; a customised optical system consisting of two pairs of infrared (IR) transmitter-receivers, and an industrial electromechanical treadle already certified for use on the rail network for detecting the presence of a train as they pass through different sections. The purpose of either triggering system used in this study was to automatically start the data logging whenever a train approached the instrumented site. The duration of the measurement itself is adjusted beforehand and can be altered depending on the requirements of the system operator. Normally, the measurement duration is sufficient for the entire train to be captured but not excessively higher so as to avoid the generation of unnecessarily large data files which may require further manipulation before signal processing can be carried out due to memory and CPU limitations.

The IR optical gates were selected for the Long Marston trials due to their simple and quick installation. The optical triggering system apart from being able to automatically start the acquisition, it also allows the counting of the number of axles passing over the sensors as well as calculating the train speed. Despite its simple installation procedure, the IR gates are prone to progressive movement due to vibrations arising from passing trains. In addition, windy conditions may also contribute to the gradual misalignment of the transmitter-receiver pairs causing the triggering system to fail. To align the transmitter-receiver pairs, manual intervention would be required. In the railway environment, this was not straightforward, since minimum number of visits to check the operation of the system was required. For this

reason, an electromechanical treadle was employed instead for the Cropredy site trials. This choice was made based on the inherent higher long-term operational reliability of the treadle and its readily acceptable use by Network Rail since it is proven not to interfere with track circuits.

Figure 6-2 presents a flowchart that illustrates the basic operational concept of the customised RCM system developed as part of this study. Certain secondary operational details such as error handling and message display have not been included in the flowchart.

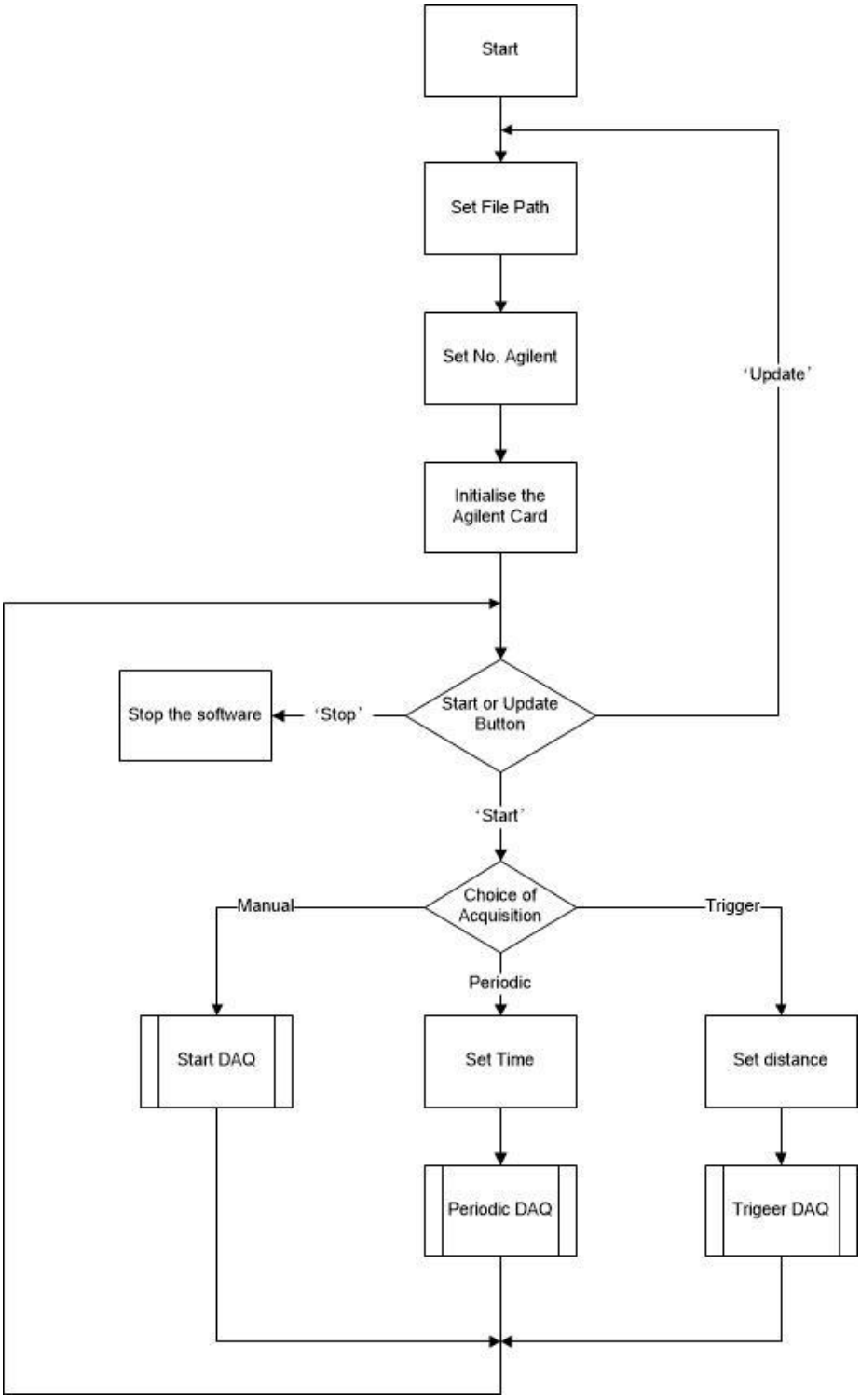

Figure 6-2: Flowchart showing the basic architecture of the customised RCM system.

The simplified schematic in Figure 6-3 provides a more detailed overview of the main functionalities incorporated in the system including data file creation and storage in TDMS format, etc.

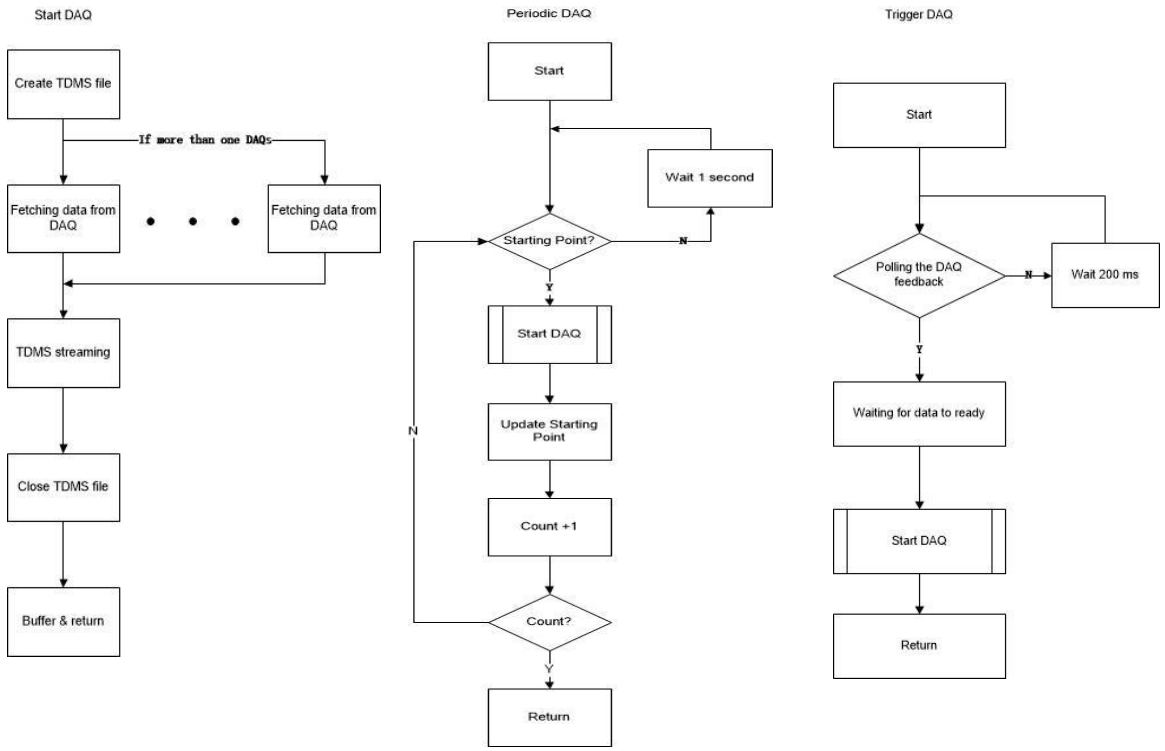

Figure 6-3: Simplified schematic showing the main functionalities of the customised RCM system.

6.2 Hardware equipment

6.2.1 AE sensors

Standard commercial acoustic emission sensors employ a single piezoelectric crystal, which is typically manufactured of Lead Zirconate Titanate (PZT). These piezoelectric crystals are very robust and ensure consistent long-term performance over a wide-range of temperatures of interest from -65°-175°C. The piezoelectric crystals are elastically deformed due to the surface movement caused by the propagation of high-frequency elastic waves along the

structure they are mounted on. These crystal deformations give rise to the generation of tiny electric signals which can subsequently digitised following appropriate amplification (Vallen Systeme, 2015b). In order to protect the piezoelectric crystals, they are placed behind an Al_2O_3 ceramic wear-resistant plate. Apart from protecting the piezoelectric crystal, the wear plate thanks to its very high stiffness (Young's Modulus) is also an ideal transmitter of the elastic waves from the structure to the piezoelectric crystal. This is a very important factor in ensuring that the raw waveforms to be processed are captured without any damping effects, which could generate erroneous results following analysis.

The acoustic emission sensors can be typically divided into two main groups depending on their operational characteristics; wideband or differential sensors, and resonance (narrow-band) sensors. The acoustic emission sensor type needs to be selected carefully as it is of particular importance to measure the waveform correctly but also minimise unwanted environmental noise, which may contaminate the signal and make signal processing far more difficult or even impossible. Wideband sensors have a largely flat-frequency response curve. In comparison, resonance sensors are generally more sensitive at particular frequencies, which are basically known as the resonant frequencies of the piezoelectric crystal. At the resonant frequencies the response of the piezoelectric crystal is amplified. Therefore, unwanted mechanical noise that normally lies at lower frequencies (i.e. below 100 kHz) can be filtered much more effectively using resonant sensors rather than wideband ones.

Research reporting on the advantages of resonant over wideband sensors has been reported in various studies published previously (Anastasopoulos et al., 2010, Bollas et al., 2010, Amini, 2016). In the present study, R50α resonant sensors manufactured by Physical Acoustics Corporation (PAC – now MISTRAS) were employed. The R50α resonant sensor has an

operational frequency range of 100 - 700 kHz. Its main resonant frequencies lie at 170 kHz, 220 kHz and 350 kHz as shown in the plot in Figure 6-4 (MISTRAS, 2011).

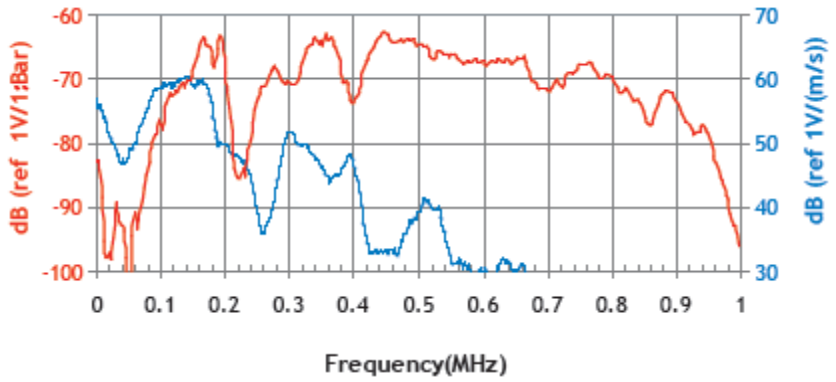

Figure 6-4: Typical response (red) of an R50α AE sensor (PAC R50α product sheet, http://www.physicalacoustics.com/content/literature/sensors/Model_R50a.pdf).

The condition of rolling stock wheelsets was monitored using acoustic emission sensors mounted on the web of the rails using magnetic hold-downs. Magnetic hold-downs permit the rapid installation and removal of the acoustic emission sensors. Coupling between the acoustic emission sensors and the rail structure was achieved either using grease or Vaseline. In the case where cast manganese crossings were required to be monitored, the use of magnetic hold-downs was not possible since the microstructure of cast manganese steel is austenitic and hence paramagnetic. Therefore, Araldite^{TM} was used instead in order to glue the sensors permanently on the crossing. In addition, Araldite^{TM} provides excellent coupling efficiency between the test piece and the acoustic emission sensor.

One disadvantage of resonant acoustic emission sensors, which oughts to be taken into consideration, is that the signals collected will be inevitably distorted due to its unique frequency response. This results in partial loss of spectral information contained in the original waveform emitted by the defect. However, it is possible to restore the actual input waveform by spectral calibration with the help of the sensor manufacturing datasheet or better

through calibration measurements carried out using a Hsu-Nielsen acoustic emission source (pencil lead breaks). The principles of the Hsu-Nielsen source calibration test are shown in Figure 6-5.

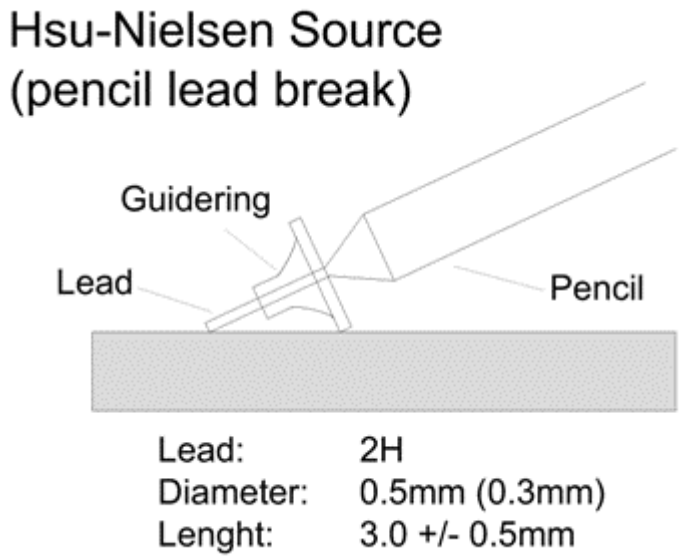

Figure 6-5: Schematic showing the basic principles of the Hsu-Nielsen source test (http://www.ndt.net/ndtaz/content.php?id=474).

Spectral calibration permits the original information contained in the raw waveform to be recovered for more in-depth analysis in the frequency domain. The plot in Figure 6-6 shows an example of the actual frequency response of the R50α sensor.

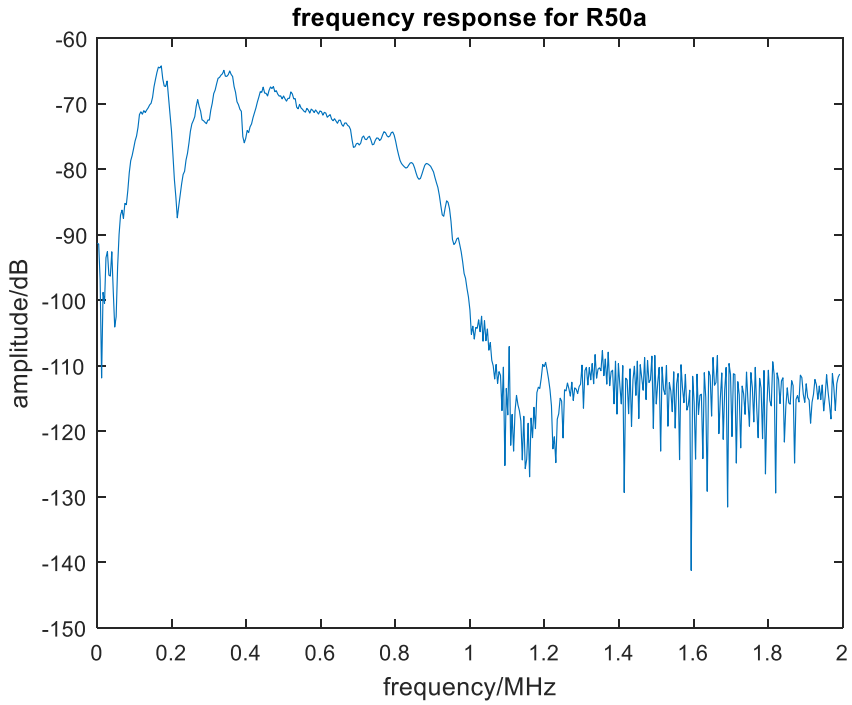

Figure 6-6: Plot showing the actual frequency response of an R50α AE sensor (S/N: AB49).

The Hsu-Nielsen source calibration tests require the breaking of pencil lead tips with a hardness of 2H on the surface of the structure on which an acoustic emission sensor is mounted. It is very important that the correct pencil lead hardness is used since 2H ensures the emission of a signal over a very wide range of frequencies from a few kHz up to several MHz. This is a significant feature of the test for confirming that acoustic emission sensors with high-frequency operational range are properly coupled and calibrated. The use of pencil leads with hardness other than 2H may result in signals emitted only over a low frequency range which may not exceed 50 kHz. Up to 50 kHz is normally the maximum range of a significant percentage of unwanted mechanical noise. Pencil lead tip breaks simulate an impulse signal similar to that emitted by a propagating crack (McLaskey and Glaser, 2012). The emission of an ideal impulse signal is constant over the entire frequency spectrum. This matches the calibration requirements for a broadband spectrum with the same frequency emission (Breckenridge et al., 1975). Pencil lead breaks were used in order to evaluate the responses of

the R50α AE sensors employed in this study. The waveform containing the impulse produced by a single pencil lead break (top plot) and the calibrated response of the sensor (bottom) are shown in Figure 6-7.

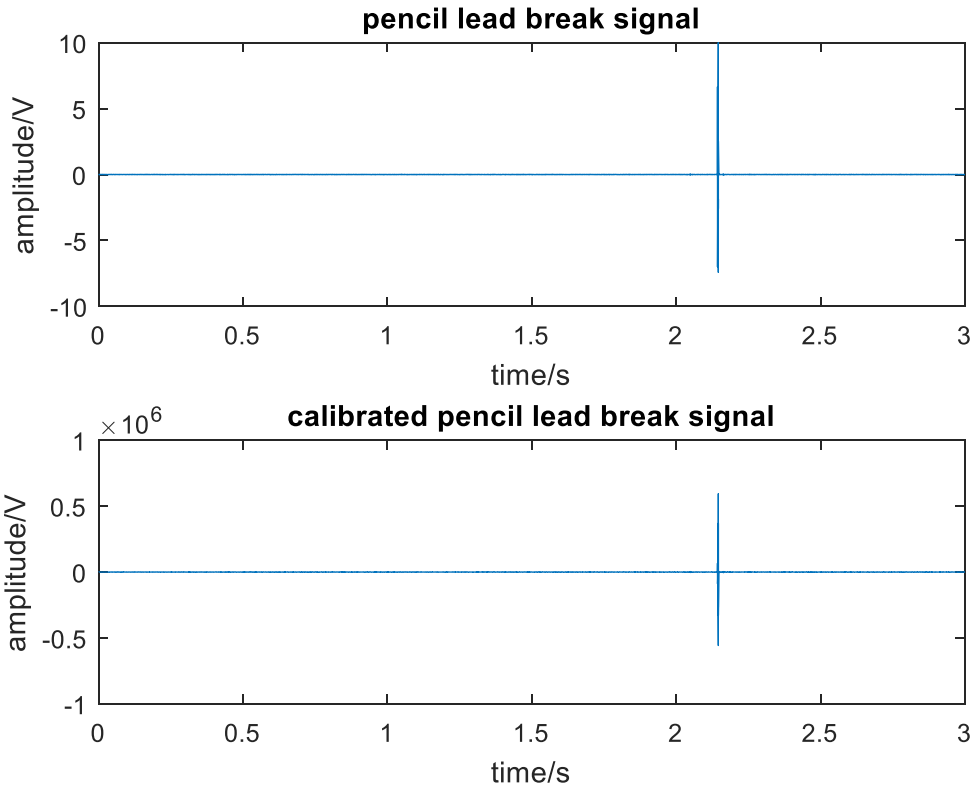

Figure 6-7: Comparison of raw (top) and calibrated (bottom) pencil lead break signals

Figure 6-8 show the spectral difference before and after calibration. Since the operating frequency starts from 100 kHz, the zoomed-in plot is shown in Figure 6-9. The frequency response becomes flat after calibration, which matches the frequency response of an impulse signal generated by pencil lead break.

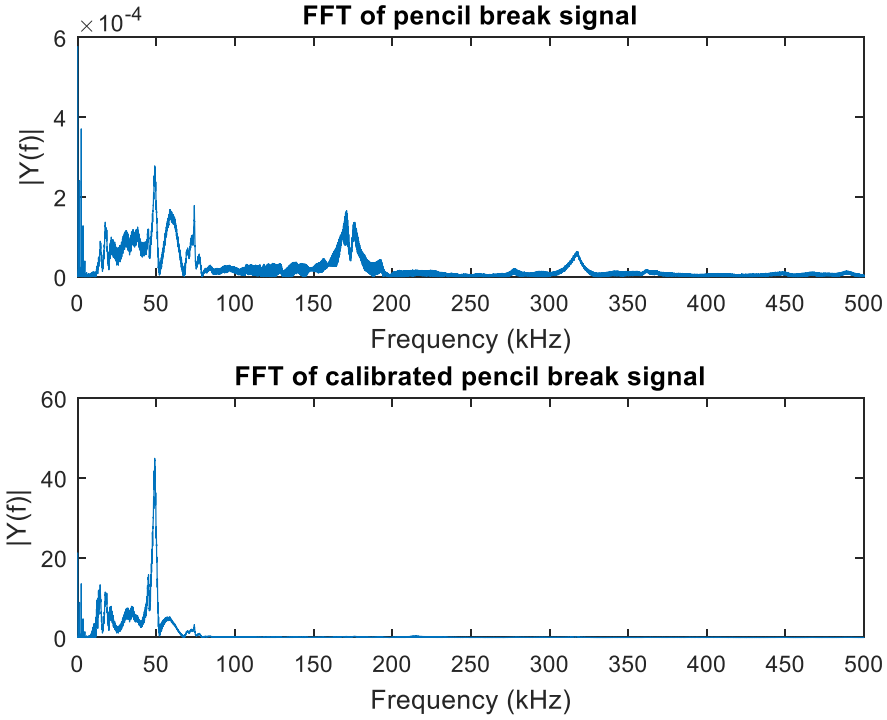

Figure 6-8: Spectrum of raw (top) and calibrated (top) of the pencil lead break signal.

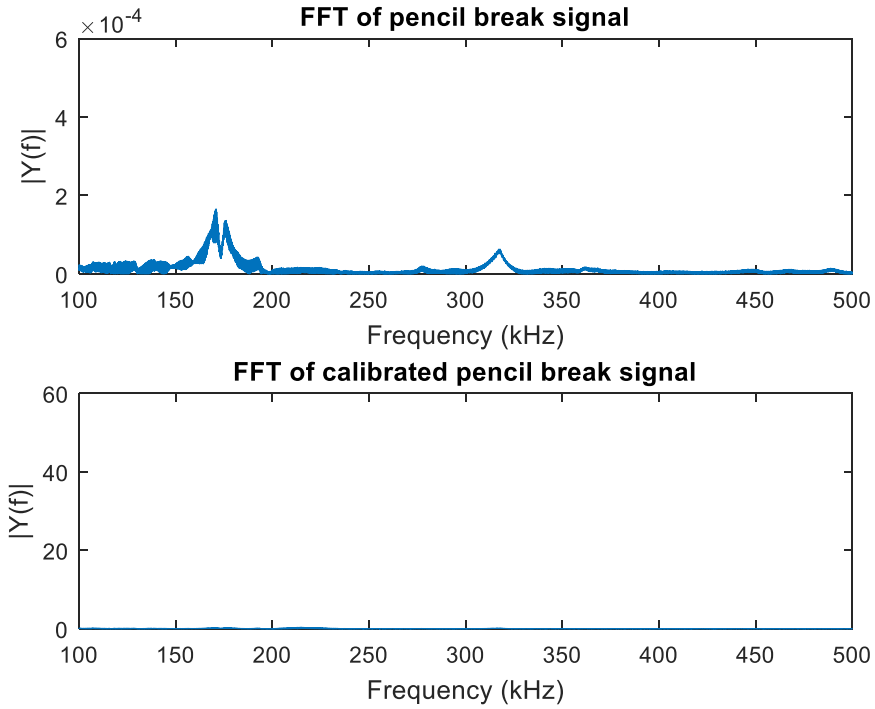

Figure 6-9: Zoomed-in spectrum of raw (top) and calibrated (bottom) pencil lead break signal from 100-500 kHz

6.2.2 Accelerometers

Wilcoxon 712F industrial piezoelectric accelerometers with integrated BNC cable were employed for the measurement of vibration signals as part of the customised RCM system. Wilcoxon 712F accelerometers are designed to operate within a frequency range of 9 Hz to 15 kHz. This type of industrial accelerometers is suitable for use in the field under harsh operational conditions. It has a nominal sensitivity of 100 mV/g and a linear frequency response. A twelve-channel power supply with 18 VDC manufactured by Vibrametrics is used in order to power the accelerometers. The photograph in Figure 6-10 shows the calibration process of one of the accelerometers used during this study.

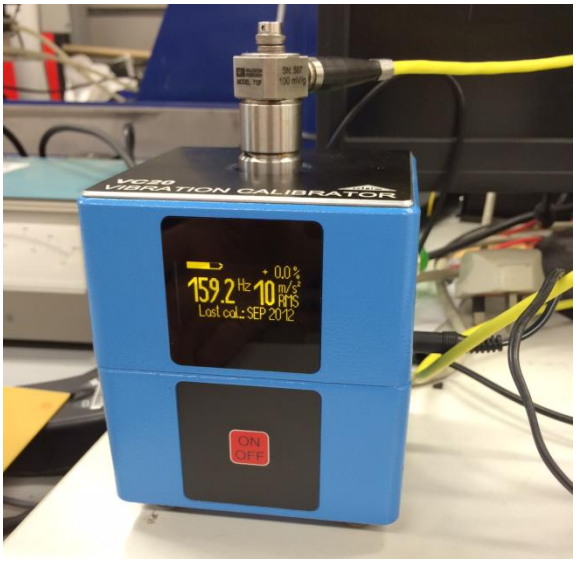

Figure 6-10: Photograph showing the calibration process of one of the Wilcoxon accelerometers used in the study.

The accelerometers were attached to the rail web next to the acoustic emission sensors using built-in magnets as shown in the photograph of Figure 6-11. Since sensors are mounted rather than glued or threaded, the upper operational frequency range is limited to 5 kHz due to dampening effects from the magnet.

Figure 6-11: Photograph showing a pair of acoustic emission sensors together with an accelerometer mounted on the rail web at the Long Marston test track.

6.2.3 RCM system hardware architecture

The hardware architecture of the customised RCM system consists of the following basic components apart from the aforementioned acoustic emission sensors, accelerometers and triggering equipment; a) pre-amplifiers manufactured by PAC, b) main amplifiers manufactured by Krestos Limited or PAC, c) four-channel hub manufactured by Agilent, d) two Agilent 2531A four-channel USB cards and e) a PC for logging, storing and analysing the acoustic emission and vibration signals acquired. The customised software running on the PC has been written in LabVIEW ® and MATLAB® and is capable of both logging and analysing the datasets acquired. The photograph in Figure 6-12 shows the main hardware of the customised RCM system.

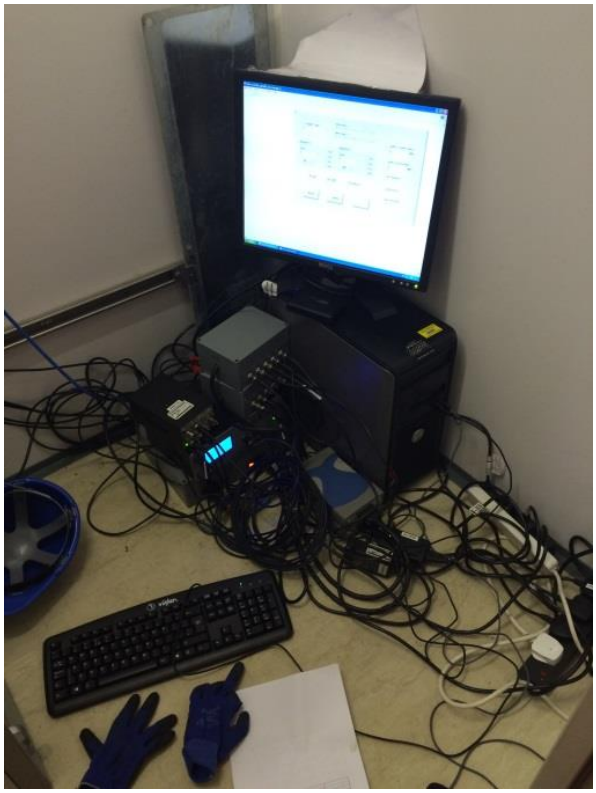

Figure 6-12: The customised RCM system installed in Cropredy.

The amplitude of the output signal produced by the acoustic emission sensor is relatively small, with an amplitude range of a few mV. Hence, amplification is required before the signal can be transferred to the DAQ unit. In order to amplify the acoustic emission signals two amplification stages are required. The amplification is provided by the pre-amplifier and main amplifier units (Vallen Systeme, 2015a). The pre-amplifier is required to be placed close (normally no more than 1.5 metres away) to the acoustic emission sensor to reduce any noise that can arise during the amplification of the signal. It also provides low impedance for signals to be transmitted over long distance with minimal loss. In addition, the pre-amplifier has an analogue band-pass filter built-in that can filter the signal from 100 kHz - 1000 kHz, which is the operating frequency range for the R50α acoustic emission sensor. Further amplification is achieved by the use of a main amplifier located near the DAQ unit. The gains

in both the pre-amplifiers and amplifiers can be adjusted. In the case of the pre-amplifier there are three possible settings for gain at 20, 40 and 60 dB.

The desirable amplification settings need to be carefully selected based on the experimental parameters of each test, including wagon load, train speed and distance from the acoustic emission sources of interest as well as undesirable noise. The total amount of gain can be calculated as the sum of gain (in dB) from both amplifiers. The AE and vibration signals transmitted from sensors are digitised using Agilent U2531A DAQs (Keysight Technologies, 2009). The Agilent DAQs can be set to acquire using various trigger modes and sources as discussed earlier.

6.2.4 Trigger systems

Two types of trigger systems were installed wayside and connected to the customised RCM system in order to start up the data acquisition automatically. At the Long Marston test track, experiments were carried out under controlled environment with uninhibited access to the rail track. For this reason, a semi-permanent trigger system consisting of two pairs of transmitter-receiver IR optical sensors were installed next to the rail track. The operation of the IR optical system is based on the following principle; whenever there is a train passing in front of each transmitter-receiver pair then each wheel blocks temporarily the transmitted IR beam giving rise to an electric pulse. The electric pulse generated by the IR system sets the DAQ card to acquire. Subsequently each time a wheel blocks the transmitted IR beam is register as an axle, allowing the system to count the number of axles passing from the instrumented site and the exact time that this happened, helping improve the reliability of the analysis. Since the exact distance between each IR transmitter-receiver pair is known, by recording the exact time that the first wheel passed in front of them, it is possible to accurately

calculate the speed that the train was travelling during the data acquisition process. Since both the speed and exact location of the wheelsets can be ascertained using the information generated by the optical triggering system, it becomes possible to correlate the AE and vibration waveforms acquired with the position of any defects detected. Knowing the exact location of possible defective wheels is advantageous as data processing of signals correlated to each wheelset can be isolated and processed separately by truncating them over the time range during which a particular wheelset passed over the location of each sensor. The photograph in Figure 6-13 shows one of the transmitter-receiver pairs of the IR optical triggering system used in the Long Marston test trials after being installed next to the track.

Figure 6-13: One of the IR transmitter-receiver pairs comprising the optical triggering system after installation at the Long Marston test track.

For the trials taking place on the actual rail network at the Cropredy site, a Type 59 Cautor electromechanical treadle was used instead for triggering data acquisition. The installation of the electromechanical treadle is shown in the photograph of Figure 6-14. The operation of the

treadle is based on the detection of the presence of a train by its actuating arm which is pressed down by the flange of the first wheel as the train passes through the instrumented site (Network Rail, 2007).

Figure 6-14: Installation of the type 59 Cautor electromechanical treadle at the Cropredy site by Network Rail engineers.

Once the arm is in lower position, an electric signal is generated by the relay inside the treadle, which is subsequently transmitted to the DAQ unit causing it to be triggered and start acquisition as illustrated in the schematic of Figure 6-15. The arm gradually returns to the original position setting up for the next train. This means that the treadle only produces one activation signal for each train. Although the treadle can no longer identify the position of each wheelset and calculate the train speed directly, it is more robust and reliable as a triggering system in comparison with the customised optical IR system used for the Long Marston trials. Electromagnetic Interference (EMI) effects on the electromechanical treadle are also minimised. In addition, it is possible to identify the positon of wheelsets and calculate train speed through advanced signal processing of acoustic emission data as discussed in detail in the following chapter.

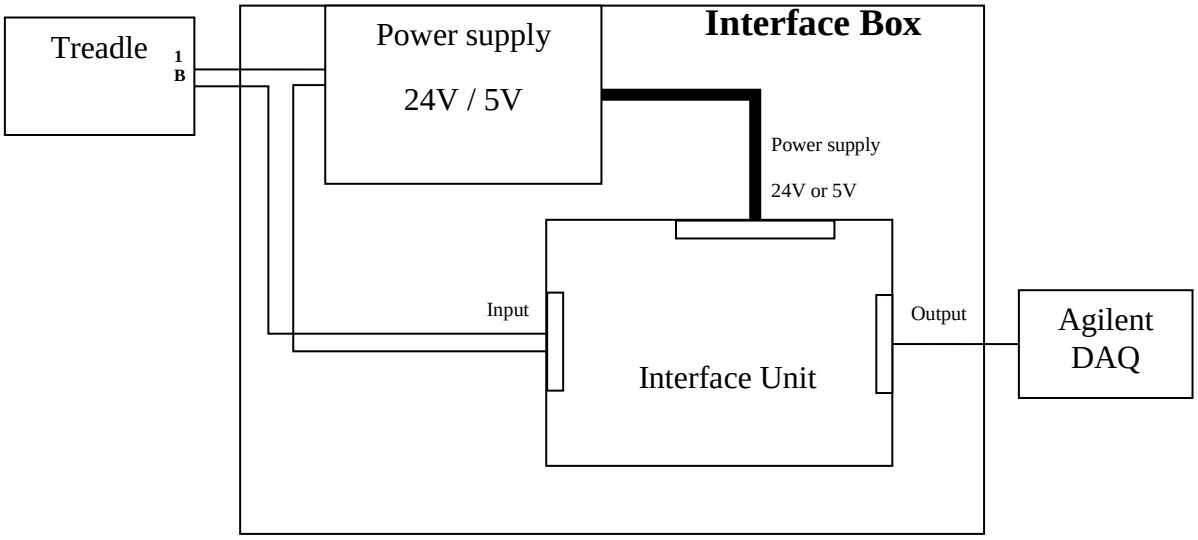

Figure 6-15: Simplified schematic showing the treadle connection to the Agilent DAQ.

6.3 Software design

6.3.1 Main data logging system

Different versions of customised software for data logging, storage and analysis were created using LabVIEW® and MATLAB®. Print screens of the data logger used to control the Agilent DAQ unit are shown in Figure 6-16 and Figure 6-17. The software was programmed based on the concept of state machine, as shown in Figure 6-18.

The main features of the data logger include different triggering modes, error logging, high throughput data streaming, multiple DAQ systems compatibility, and self-testing for error diagnosis. An executable file was created so that the data logger can be used on standalone PCs and if required to self-start-up in case of power failure. The datasets logged are stored in advanced TDM Streaming (.TDMS) format with all test information written in the data file properties. This data format is also compatible with MATLAB®, where datasets can be loaded for further advanced signal processing.

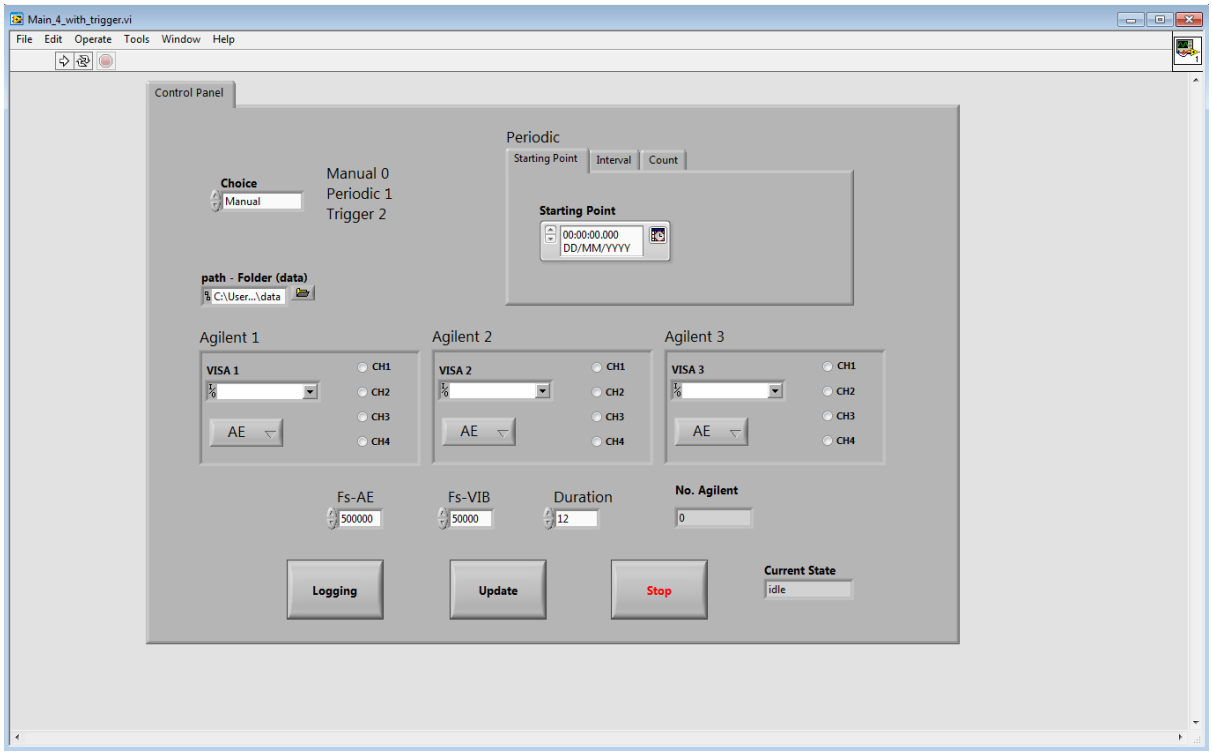

Figure 6-16: Print screen showing the customised data logger version used in the Long Marston trials.

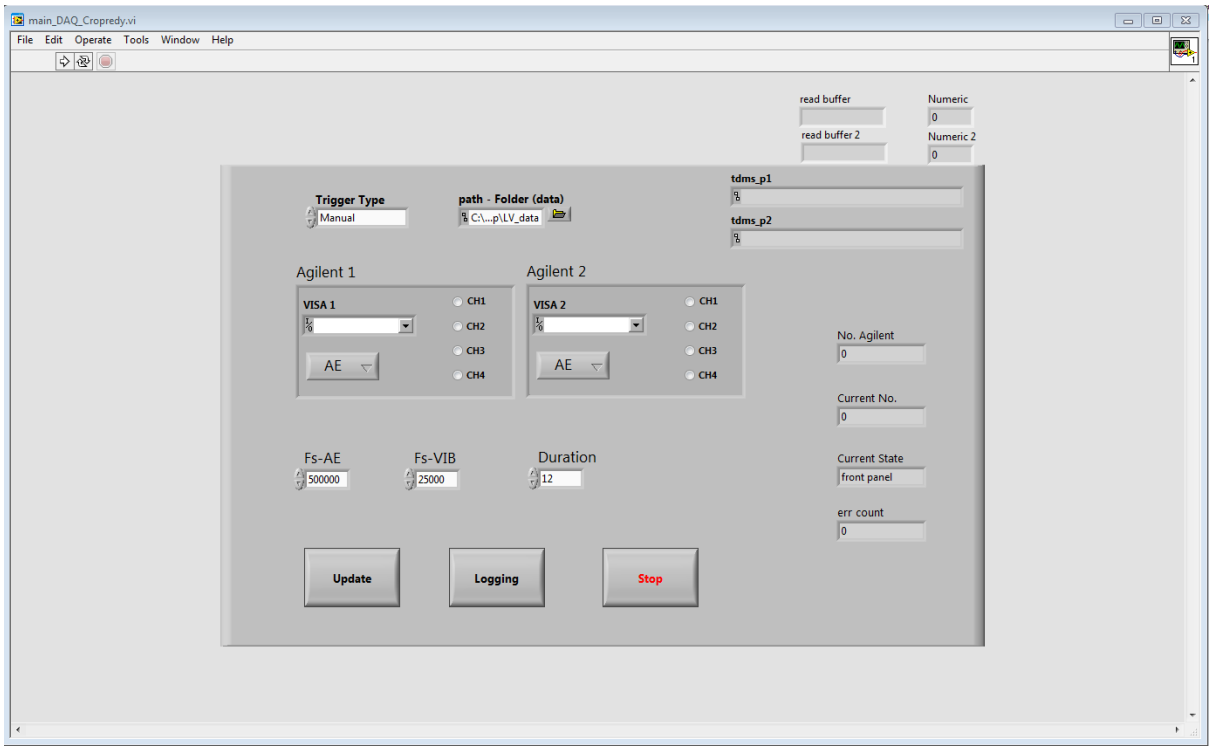

Figure 6-17: Print screen of the fully automated data logger version used in the Cropredy site installation.

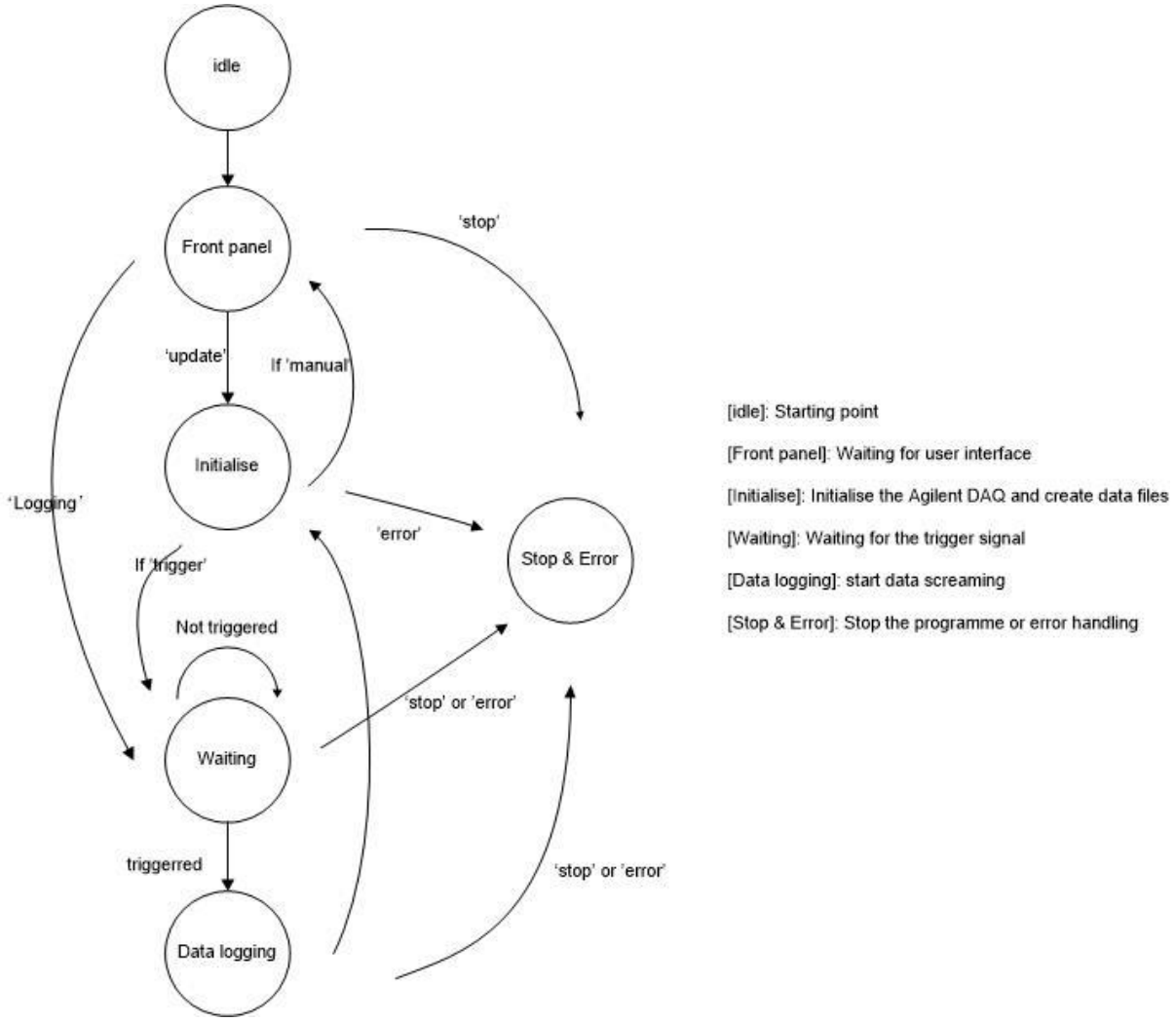

Figure 6-18: Schematic showing the state machine for the DAQ software application.

6.3.2 Optical trigger system software

For the Long Marston trials, an independent software application also created using LabVIEW® was used to control the optical IR system. The optical IR system software used to trigger the main DAQ application is shown in the print screen of Figure 6-19. This software application also allows the counting of the total number of axles and registering the exact time that each wheelset passed from the instrumented site. By knowing the distance between the two pairs the train speed is also accurately calculated and displayed on screen for each measurement. There was no need for creating a separate triggering software application for

the Cropredy trial as the generic DAQ software was hardware triggered by the output from the treadle.

Figure 6-19: Print screen of the optical system software application for the Long Marston trials.

6.4 Experiments

The customised RCM system developed for this study was used for a large number of different experiments for the detection of both rolling stock and infrastructure components. Tests were carried out at the Long Marston test track as well as several sites on the UK rail network, with a permanent system installed at Cropredy for monitoring the condition of rolling stock wheels and axle bearings. Temporary installations were carried out for the evaluation of cast manganese crossings at Hatton, Wembley and Watford on the West Coast Main Line. Thus, the performance of the customised RCM system has been evaluated under different operational conditions and setups.

Supplementary tests were also carried out to calibrate the system. These included control impact tests used to evaluate the response of the acoustic emission sensors by impacting the instrumented rail with a hammer and locomotive-only tests to evaluate the AE signals generated by the train engine alone.

6.5 Rolling stock trials

Feasibility tests for assessing the capability of the customised acoustic emission and vibration analysis RCM system to detect bearing and wheel defects was initially carried out using a spinning test rig and a motorised trolley under laboratory conditions (Amini, 2016). The results indicated that acoustic emission and vibration techniques were indeed able to detect and distinguish bearing and wheel-related defects (Amini, 2016, Papaelias et al., 2014). Two rounds of field tests were then proposed to further investigate the capability of detection under a realistic operational environment. The Long Marston trials were designed to test the customised RCM system under controlled environment with manually induced defects of different severities. The Cropredy trial, on the other hand, is a blind test to monitor in-service passenger and freight trains.

6.5.1 Long Marston testing

The purpose of the Long Marston trials was to evaluate the capability of the customised acoustic emission and vibration RCM system in detecting various artificially-induced wheel and axle bearing defects and quantifying their severity in order to validate its detection reliability. The tests held at the Long Marston test track were carried out using freight tanker wagons provided by VTG Rail. Various test wagons were employed with no and artificially induced axle bearing and wheel defects. A locomotive with no wheelset defects provided by

Motorail Logistics was used to pull the test wagons during these trials. The photograph in Figure 6-20 shows one of the experimental configurations used.

During testing at Long Marston, the test train run forwards and backwards over the instrumented section for several hundred metres at a constant speed of 48 km/h and 32 km/h respectively. Thus in the forward tests the engine was in front, pulling the wagons while in the backward tests the engine was in the back pushing the wagons. The train was required to coast through the test zone in order to eliminate any interference arising from wheelset sliding or braking. In addition, since the track was continuously welded there were no impact noises arising from the wheels going over any rail joints.

Figure 6-20: One of the experimental configurations used in Long Marston.

Various bearing defects and a wheel flat were simulated during the Long Marston trials. These defects were manually induced by VTG Rail. During the experiment, three sets of tests were carried out considering different types of defects. The first set of trials focused on bearing lubricant contamination. The second set of tests was carried out on a freight wagon with axle bearings with roller defects of different severities (2, 4 and 8 mm deep) induced using a power tool. All defects were induced only from one side of the wheelsets with the

other side kept defect-free for comparison purposes. The photograph in Figure 6-21 shows the axle bearing containing an artificially induced 8 mm roller defect.

Figure 6-21: Photograph showing one of the faulty axle bearings with an artificially induced 8 mm deep roller defect.

Figure 6-22: Photographs showing aspects of the experimental configuration employed for the Long Marston trials. On the left one of the bogies with one faulty axle bearing containing a roller defect (right wheelset) and a healthy axle bearing (left wheelset). The photograph on the right shows an acoustic emission and vibration sensor pair mounted on the rail web.

The schematics in Figure 6-23 show the experimental configuration of the testing conditions (lubricant contamination and faulty axle bearings with roller defects).

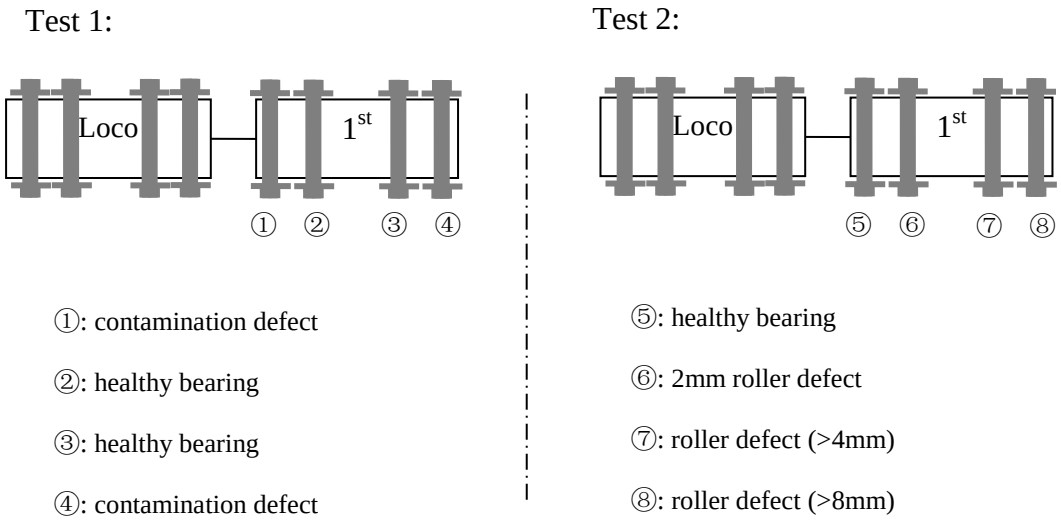

Figure 6-23: Schematic of Experimental Setups 1 and 2 with all defects listed.

As mentioned before, acoustic emission and vibration sensors were mounted on the web of the rail using magnetic hold-downs. The area where the sensors were mounted was slightly grounded to improve contact. Vaseline was applied to couple the acoustic emission sensors on the surface of the rail web so as to minimise the effects of acoustic impedance mismatch at the interface and increase signal transmissibility from the fault sources to the acoustic emission sensors. The acoustic emission and vibration sensors were installed above sleepers to reduce the effects on the signals caused by the bending moments of the rail as the rolling stock travelled above it. Four R50α acoustic emission sensors and two Wilcoxon 712F accelerometers were used. The location of each sensor is shown in the schematic of Figure 6-24. Acoustic emission and vibration data were transmitted and collected separately by two Agilent DAQ boards. The sampling rates used for acoustic emission and vibration were 500 kSa/s and 25 kSa/s respectively. Data were acquired for 12 seconds in order to capture the complete waveform for the entire train passage.

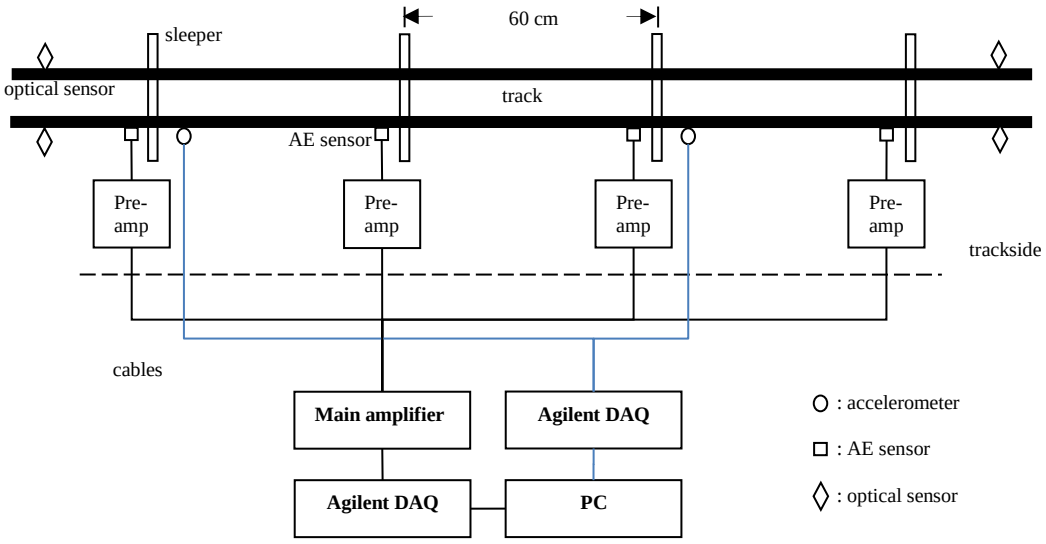

Figure 6-24: Schematic showing the installation of the wayside RCM system with sensor locations during the Long Marston trials.

The optical IR triggering system discussed earlier was placed at either end of the instrumented section as shown in the schematic of Figure 6-24.

The optical system was used to trigger data acquisition, correlate acoustic emission and vibration signals with the position of each wheelset and calculate speed. By knowing the exact position of each wheel it is possible to truncate the acoustic emission and vibrations signals at the exact times during which each wheelset passes through the detection zone and above each sensor location.

6.5.2 Cropredy trial

The same customised RCM system was installed at the Cropredy test site, on the Chiltern rail line connecting London Marylebone with Birmingham Moor Street stations. The 8-channel system installed in Long Marston has been able to successfully monitor passenger and freight trains passing through the instrumented sited since September 2015. The Cropredy trial, as a

blind test, is the ultimate stage of the present study in an effort to evaluate the effectiveness and reliability of the designed RCM system under actual operational conditions.

The installation of the RCM system at Cropredy consists of the same sensors as those used in the Long Marston trials, i.e. four R50α acoustic emission sensors and two Wilcoxon 712F industrial accelerometers as shown in the photograph of Figure 6-25.

Figure 6-25: Acoustic emission and vibration sensor pair mounted on the rail at the Cropredy site.

The schematic in Figure 6-26 shows the overall installation. The Cropredy instrumented site has been selected adjacent to a Network Rail HABD detector for comparison and validation purposes. The Cropredy RCM system is triggered by the electromechanical treadle positioned 18.5 metres in front of the first sensor pair.

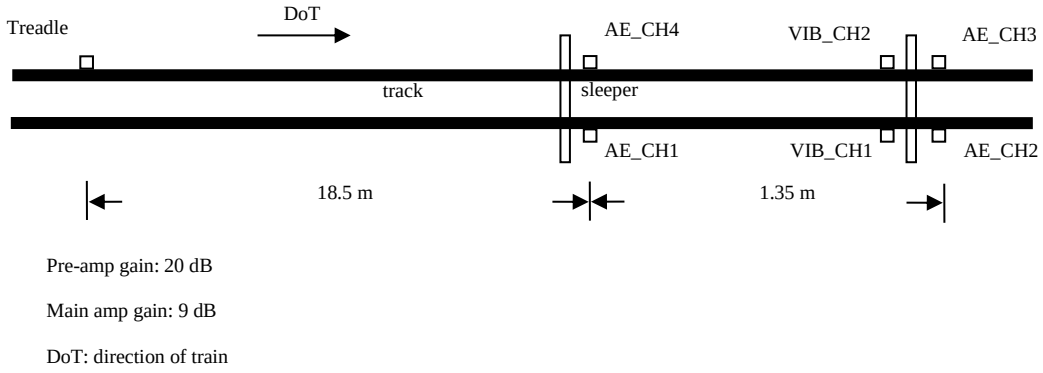

Figure 6-26: Sensor layout for the Cropredy site installation.

The rails are continuously welded so there are no rail joints from which unwanted impact noise could arise. The instrumented line is mainly used by class 168 DMU Chiltern passenger trains and Type 66 freight trains. The number of carriages and train speed varies. The passenger trains normally consists of 3 or 5 carriages and running up to a maximum speed of 160 km/h. Freight trains can have more than 25 wagons and reach a maximum speed of about 90 km/h. The Chiltern Rail Line does not have any track circuits as it uses magnetic axle counters instead. It is also not electrified.

Prior to the installation at Cropredy a safety study was submitted to Network Rail with all the details required in order to obtain authorisation. Upon approval of the safety study a Certificate of Acceptance with reference number PA05/06524 (shown in Figure 6-27) was issued by Network Rail authorising installation of the customised RCM system in any suitable location on the UK rail network, including Cropredy.

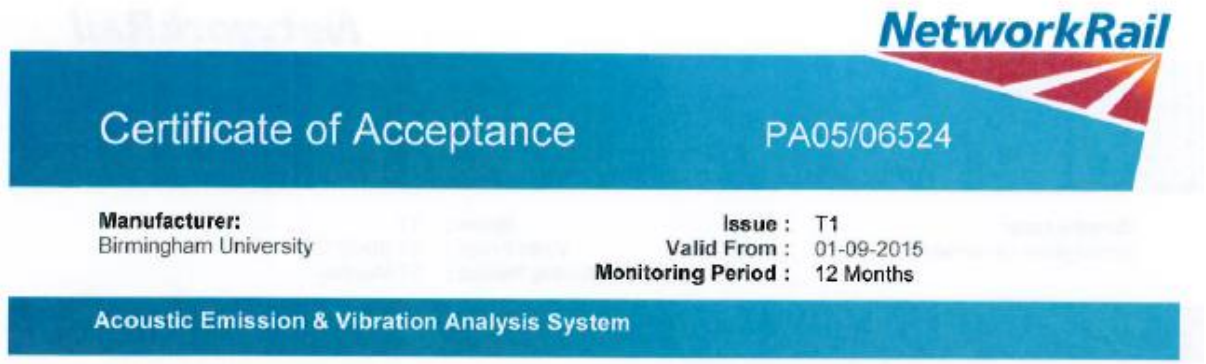

Figure 6-27: Certificate of Acceptance issued by Network Rail granting installation of the customised AE and vibration analysis system on the UK rail network.

The RCM system is set up to record acoustic emission and vibration data once triggered by the electromechanical treadle when trains pass over the instrumented section. The photographs in Figure 6-28 show aspects of the installation at Cropredy during line possession.

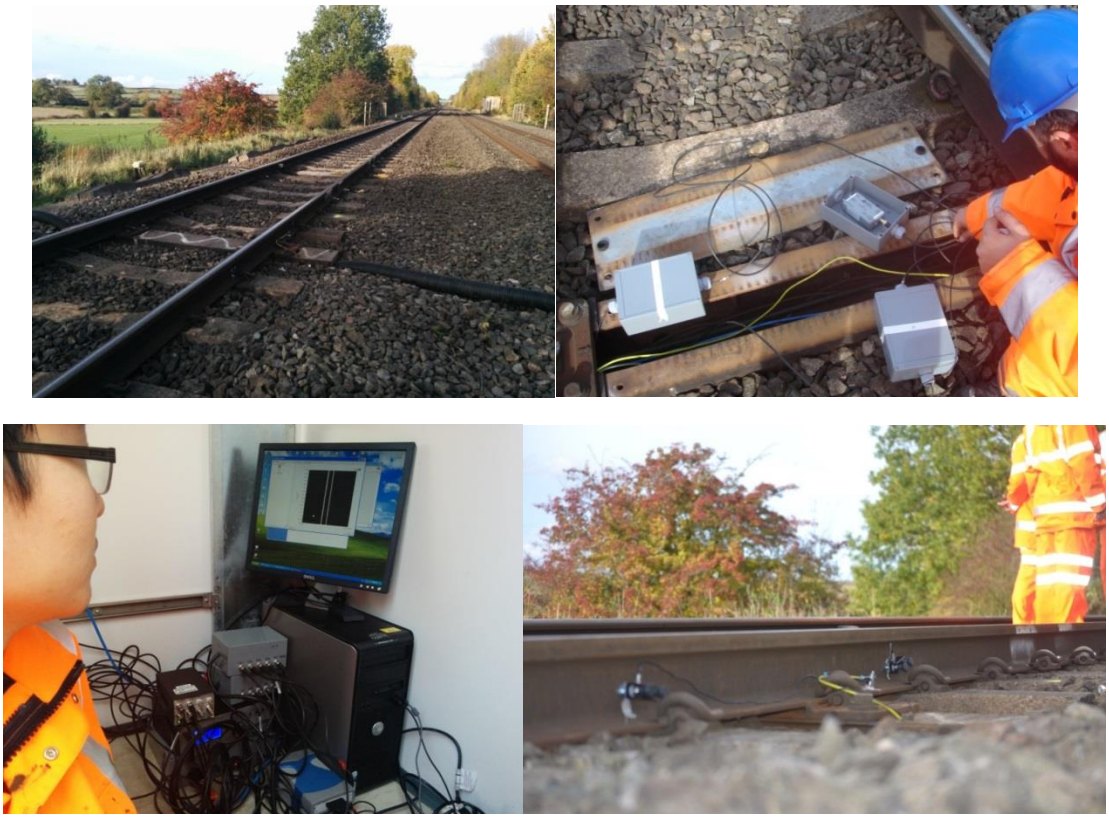

Figure 6-28: Aspects of the installation at Cropredy.

The treadle has to be placed at some distance before the first sensor pair to ensure data acquisition can initiate in time. There is a delay of approximately 0.3 s before acquisition actually starts. It takes about 0.5 s for the first bogie to travel from the treadle position to the first sensor pair for passenger trains travelling at 160 km/h. The sampling rate used in Cropredy was the same as the one used in Long Marston, i.e. 500 kSa/s for acoustic emission and 25 kSa/s for vibration. However, the recording time was reduced to 6 s, as the train speed is much higher so the time it takes for a train to go through the instrumented site is much less. This also minimises the storage space used in the hard disk of the PC logging each dataset.

6.6 Cast manganese crossing tests

As discussed earlier the customised RCM system is able to monitor cast manganese crossings by detecting acoustic emission signals generated from propagating cracks. Although vibration could also be measured, in this particular instance work focused only on acoustic emission sensors due to their much higher sensitivity to crack initiation and propagation during loading from passing rolling stock. Any cracks initiating and propagating in cast manganese steel will cause stress waves to be emitted. Differences in the vibration signature of the crossing may also arise but only once a defect has propagated to very large dimensions by which time the crossing is most likely to be considered to have failed already.

For these tests, acoustic emission sensors were mounted on the crossings of interest using Araldite^{TM}. Araldite^{TM} provides very good long-term and stable sensor adhesion since magnetic hold-downs are not applicable on the austenitic cast manganese steel grade. It also provides very good quality long-term coupling ensuring optimum transmissibility of any AE signals generated from propagating cracks. The other significant advantage of Araldite^{TM} is its

excellent electrical insulating properties ensuring no interference with electric track circuits. It also prevents any sensor damage from the large traction return current in electrified lines.

The most likely location where damage can initiate and propagate in crossings is at the nose. This is also the location sustaining the maximum impact loads from the wheels going over the crossing. To ensure optimum coverage of the crossing, a pair of acoustic emission sensors was installed on both sides of the nose of each crossing tested as shown in the photographs of Figure 6-29.

Figure 6-29: Photographs showing acoustic emission sensor installation on one of the crossings. The adhesive Araldite™ is visible on the left.

Several temporary installations were carried out during this study to evaluate crossings under different conditions ranging from healthy to severely damaged (i.e. replacement of the crossing imminent). In all test scenarios, the crossings evaluated were installed on mixed lines used by both passenger and freight trains. Acoustic emission signals generated by both types of rolling stock were recorded. The first test was carried out on a recently installed healthy crossing near Wembley Stadium on the West Coast Mainline. No damage was identified on the Wembley crossing through visual inspection before the experiment. Trains can go over the

crossing up to a maximum speed of 160 km/h. The second set of tests were carried out on a defective crossing near Hatton Railway Station on Chiltern rail line. Visual examination of the Hatton crossing revealed surface damage (cracking and lipping) as shown in Figure 6-30. No speed restrictions had been set at the Hatton crossing so the line speed of 160 km/h still applied. The final set of tests were carried out at Watford Junction where a severely damaged crossing was instrumented. Visual examination of the crossing revealed a major crack which had also been confirmed by Network Rail maintenance personnel. The defective crossing was scheduled to be replaced within two weeks. An ESR of 32 km/h was imposed and visual checks were scheduled for every night to monitor crack growth. The crack started from the bottom of the crossing as shown in the photograph of Figure 6-31. Network Rail maintenance personnel suspected that the root cause of the crack initiation and subsequent propagation was due to installation conditions (track wet beds causing excessive movement and vibration of the crossing).

Figure 6-30: Surface breaking crack on the crossing nose at Hatton.

Figure 6-31: Severe cracking in the crossing at Watford Junction (left) and AE sensor installation (right).

As the customised acoustic emission RCM system was temporarily installed for all crossing trials, no trigger system was used. Acquisition was initiated instead manually every time a train approached the instrumented site. The sampling rate was set to be 1 MHz and the duration of recording was 8 s. The higher sampling rate was necessary as most energy released by cracks propagating in cast manganese steel lies at frequencies around 300 kHz.

6.7 Difference between rolling stock and crossing monitoring

Although the main body of the RCM system remains the same for both rolling stock and crossing monitoring, there are some differences that need to be taken into account. Signals generated by rolling stock are more complicated than those from crossings. This is because the stress waves have to propagate through a very complex transmission path from the axle box to the sensor. Hence more sophisticated signal processing techniques are required for the

effective analysis of rolling stock signals. However, it should also be noted that in the case of wheel tread defects the transmission path is simpler.

Since both the acoustic emission and vibration sensors can easily detect wheel tread defects, acoustic emission and vibration signals need to be correlated to dismiss the possibility of a faulty axle bearing. Accelerometers are able to detect axle bearing faults only in very severe cases. Therefore, any vibration signals are more likely to be related to a wheel tread defect. This can be easily confirmed by relating the frequency of occurrence of the impact noise to the wheel RPM using appropriate signal processing.

Both AE and vibration sensors are used in rolling stock monitoring, while only acoustic emission was deployed for crossing monitoring. Using both sensors provides the ability to distinguish signals generated by bearing and wheel defects by means of signal correlation. However, as the crossing monitoring is focused on the crack growth in the metal with no vibration movement, accelerometers are no longer needed.

For rolling stocks monitoring, 500 kHz was selected as mechanical noise is the dominance signal. Over-sampling would only result in huge file that is not necessary. In contrast, crossing monitoring is focused on crack growth, where 1 MHz is more appropriate. The schematic in Figure 6-32 shows the basic principles of crossing monitoring using the customised RCM system.

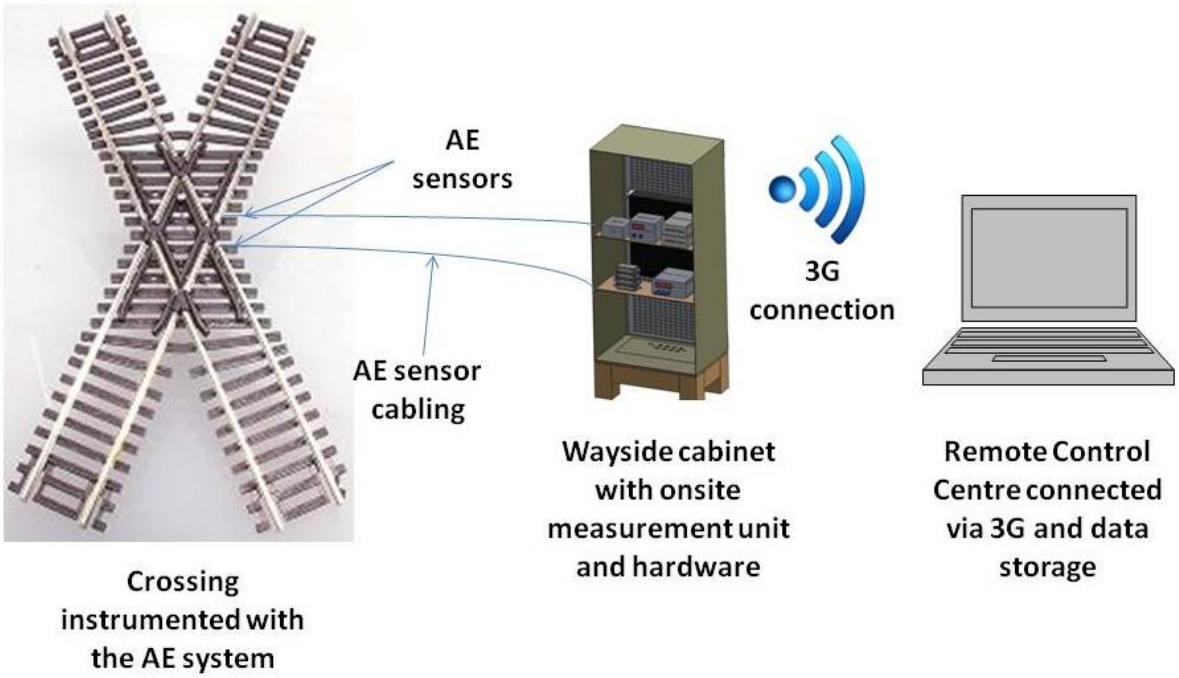

Figure 6-32: Simplified schematic showing the customised RCM system installation for crossing monitoring purposes.

Chapter 7:

Results and analysis

Chapter 7: Results and analysis

In this chapter, the details regarding the main results arising from this study and data analysis techniques employed are discussed. The first part looks into basic signal processing techniques and their effectiveness in detecting axle bearing defects. Onboard measurements carried out for validation purposes are also presented. The next section of the results chapter is concerned with the validation of the effectiveness of spectral coherence processing, which is the most important technique used for the analysis of the data obtained from the various measurements carried out in the field. The following part presents the detailed analysis with respect to the methodology used in identifying rolling stock defects and crack growth in cast-manganese crossings. The fourth and last part is concerned with the case study of a three-level system correlation.

7.1 Technique validation

During the Long Marston trials, onboard measurements were conducted in order to assess the actual condition of the axle bearings and wheels using the customised monitoring system that introduced in the previous chapter. One accelerometer and one acoustic emission sensor was attached using magnetic hold-downs on each bearing casing. The result shows that acoustic emission can effectively detect various bearing defects, while vibration is good at detecting wheel flat defect (Amini et al., 2017, Huang et al., 2014, Papaelias et al., 2014, Amini et al., 2016).

7.2 Correlation of acoustic emission and vibration

Acoustic emission has been proven to be able to detect bearing defects, while vibration can be used to detect and measure wheel flats and other types of tread defects. In the case that more than one defect is present, it can be of great benefit to combine acoustic emission and

vibration to improve the accuracy of detection. An example is provided below which includes two bearing defects of the same type and a 1 mm wheel flat simultaneously. Figure 7-1 shows the correlation of acoustic emission and vibration data.

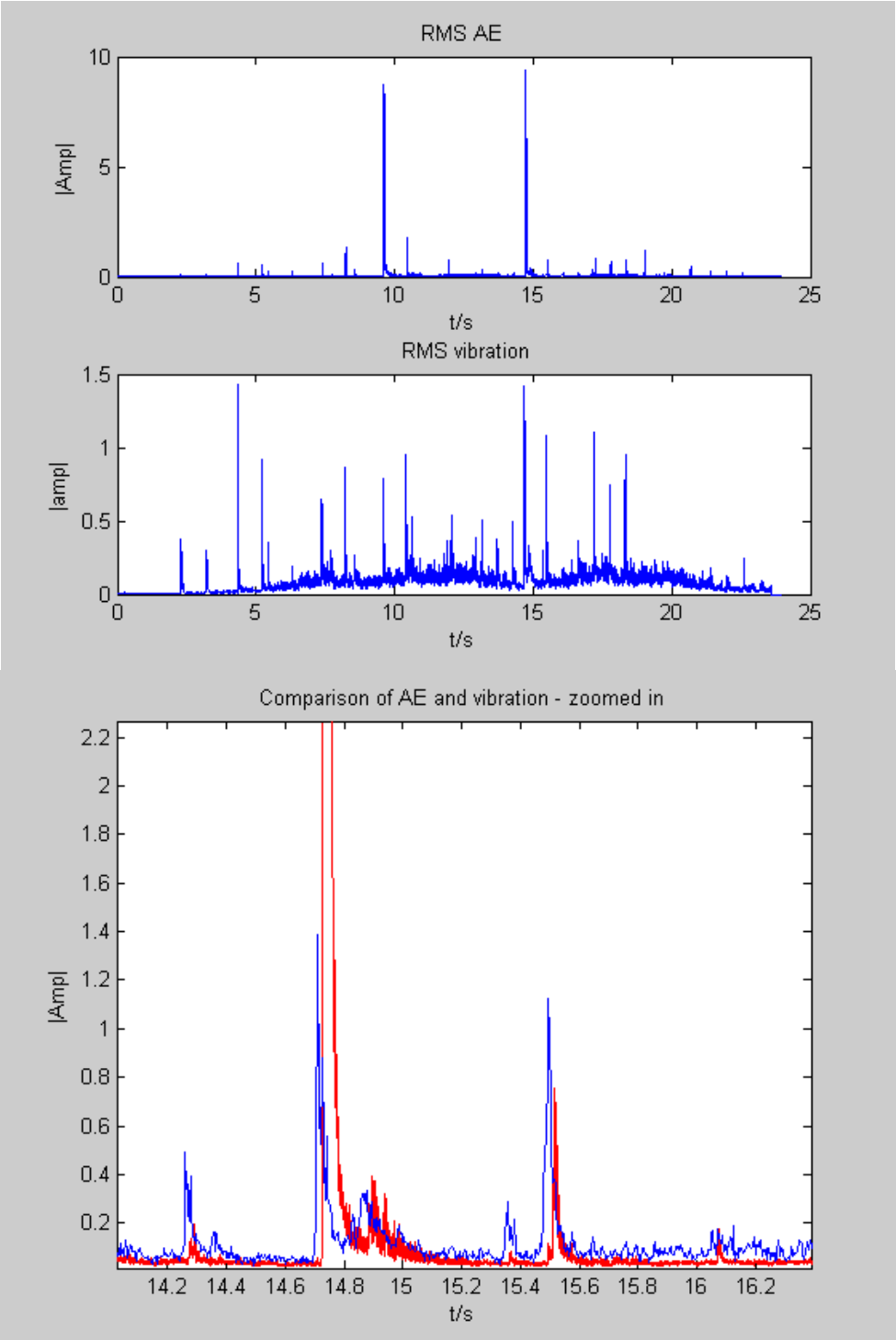

Figure 7-1: Acoustic emission and vibration signal from faulty bearing with a 1 mm flat defect using correlation analysis.

It can be seen that acoustic emission detects two bearing defects and picks up a small spike beside the larger one. This small peak is identified as a wheel flat by looking into the vibration measurement with the help of timing to pinpoint the wheelset positions. The slight delay between acoustic emission and vibration data is caused by the distance between sensors. Wheel flats can give rise to peaks which are similar to those arising from severe bearing defects in the acquired acoustic emission signal. However, by correlating vibration and AE measurement, it is possible to effectively determine the nature of the defect detected.

7.3 Validation for correlation-based processing

As discussed earlier, the similarity of two signals can be calculated by performing spectral coherence of two signals. This technique is based on the concept that signals generated by the same source have consistent spectral characteristics. Two calibration examples based on impact testing and locomotive noise measurements have been considered to validate this hypothesis.

7.3.1 Impact test

The aim of the impact test is to check whether the acoustic emission sensors and accelerometers have been installed properly. Also to ensure that the acoustic coupling quality achieved for all acoustic emission sensors is comparable. Impact signals can be generated by impacting the rail with a hammer. This simulates an impulse signal, which is equivalent to that produced by a wheel flat impact event. The plot in Figure 7-2 shows an example of multiple impact signals measured with acoustic emission. Subsequently the original raw acoustic emission signal has been truncated separating the individual impact events after a high-pass filter of 100 kHz has been applied (Figure 7-3). The frequency spectrum of each impact is shown in Figure 7-4 for comparison. It can be seen that the shape of the three PSDs

is similar. This is reasonable, since all three waveforms arising from each individual impact event have been generated in the same way.

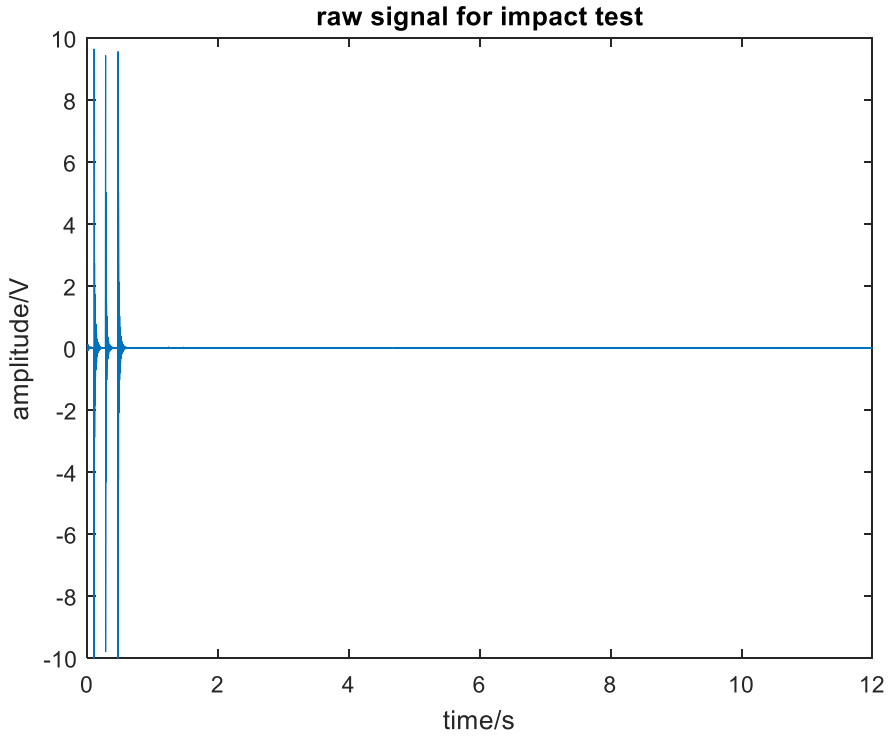

Figure 7-2: Raw AE signal captured during impact testing. Each peak indicates a separate impact event.

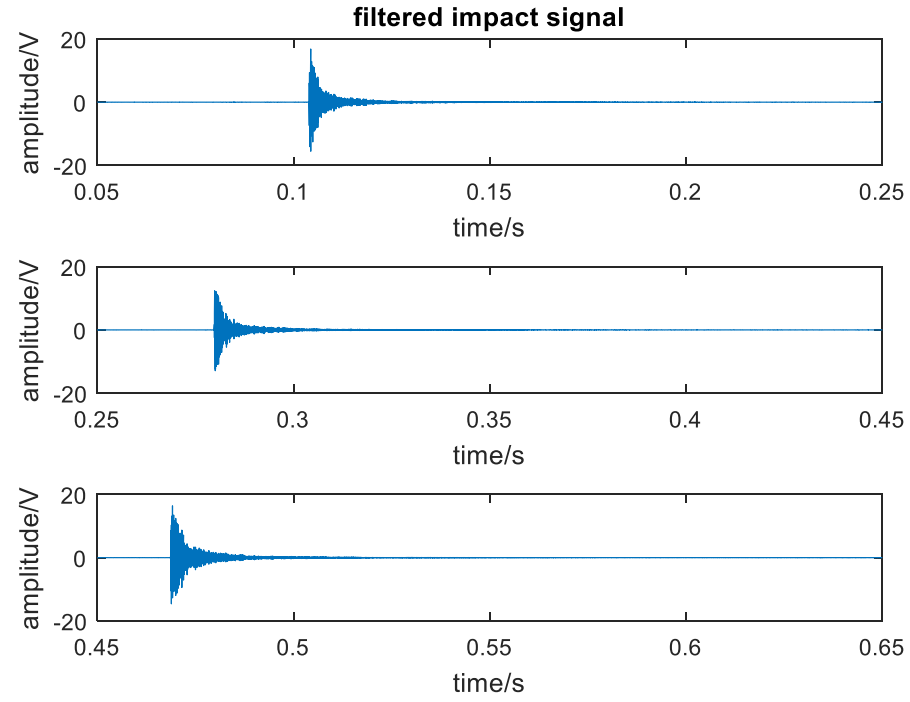

Figure 7-3: Individual impact signals truncated after a high-band pass filter of 100 kHz has been applied.

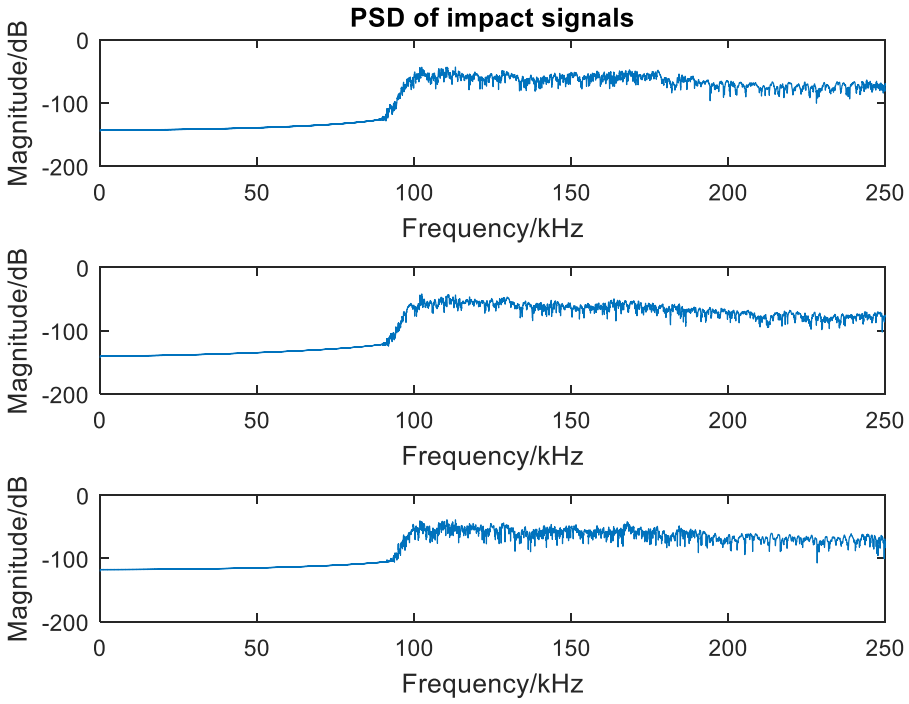

Figure 7-4: PSD plots for each of the previous impact signals.

By using the PSD of the first impact as the template, the similarity of the impact signal can be calculated with spectral coherence processing. The plot in Figure 7-5 shows the normalised results. Since the first peak is basically correlated with itself, the similarity is equal to 1.

The results for two other peaks are around 0.5, since their PSDs are not completely identical to that of the template. This is expected since after the first impact, ultrasonic waves are still travelling within the structure which mix up and interact with the ultrasonic waves produced by the second event.

Constructive and destructive interference may also occur. This also applies for the third impact event where the ultrasonic waves from the first two impacts are still travelling within the structure attenuating with time. The rest of the signal remains zero as background noise is not correlated to the impact.

The results produced when using the second or third peak as the templates, yield the same response as seen in Figure 7-6 and Figure 7-7. Therefore, the level of effectiveness of the correlation-based processing can be verified.

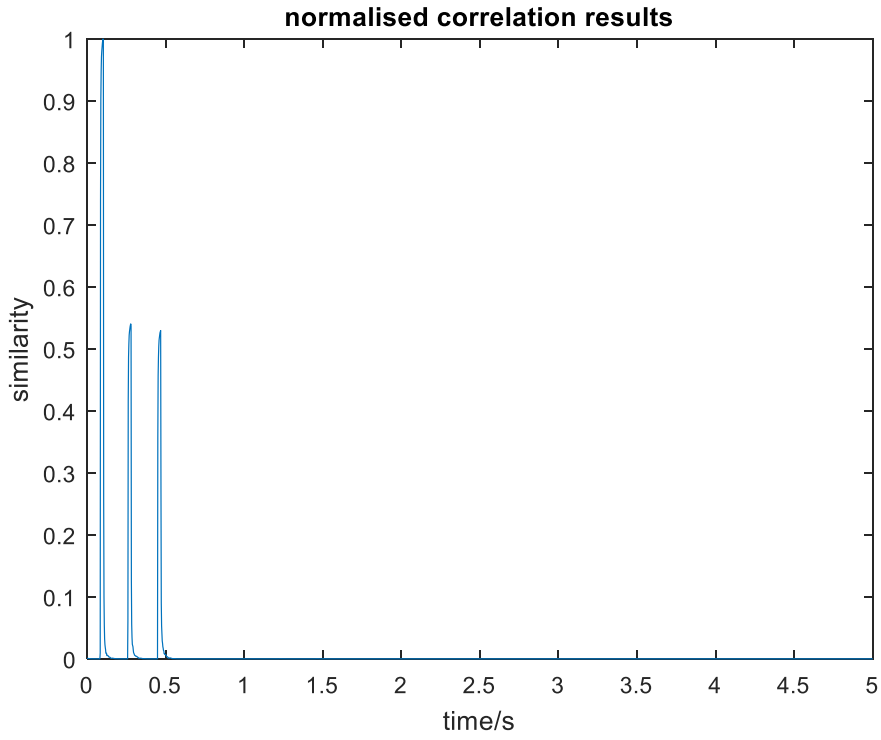

Figure 7-5: Plot showing the normalised correlation results with the first peak used as the template.

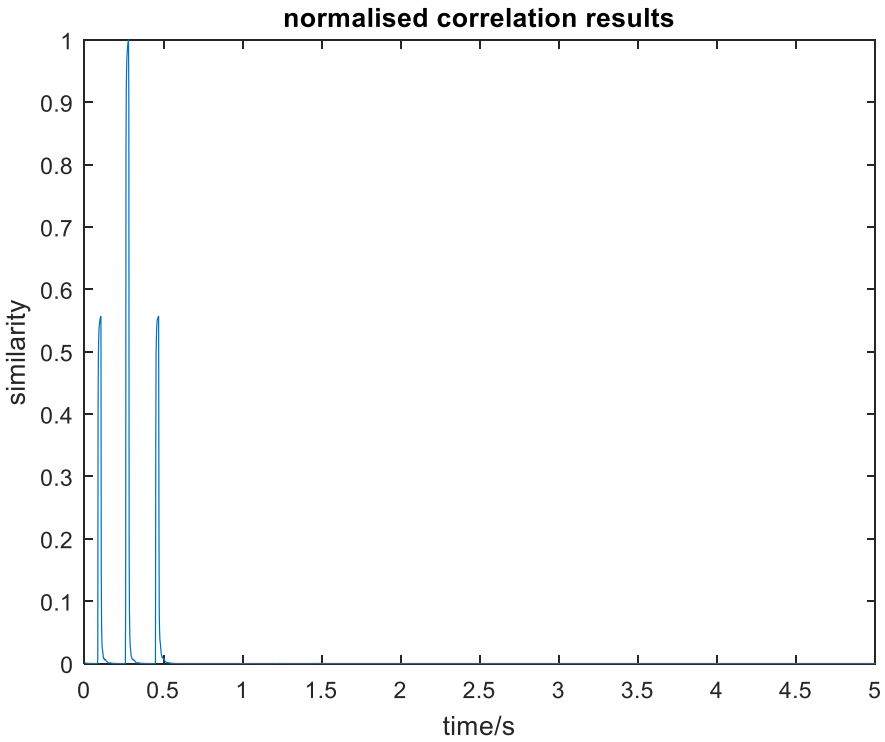

Figure 7-6: Normalised correlation results with the second peak used as the template

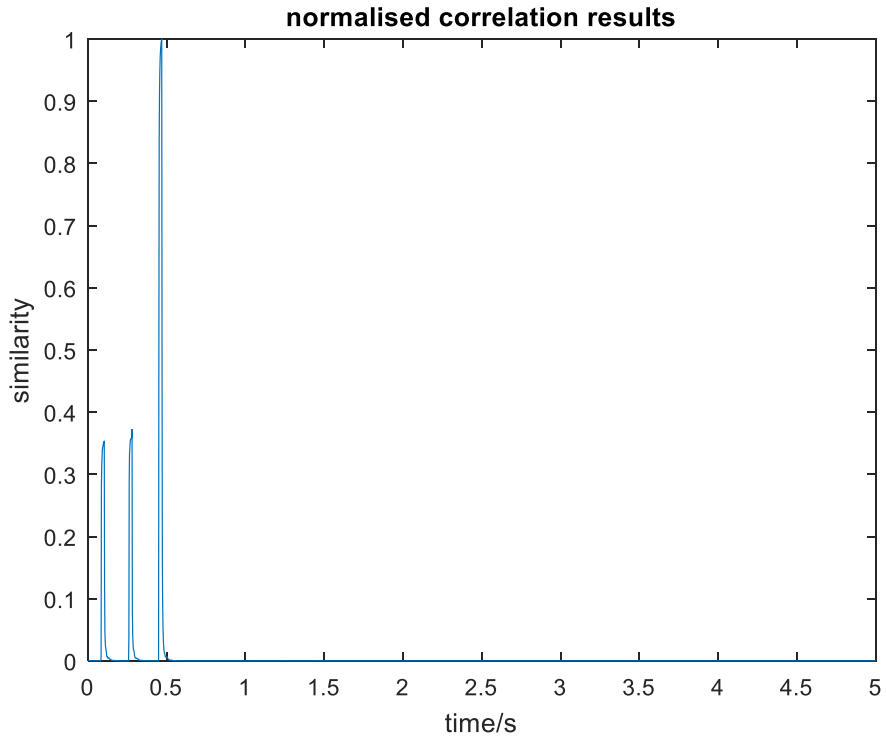

Figure 7-7: Normalised correlation results with the third peak used as the template.

7.3.2 Locomotive test

As part of the Long Marston test plan, the effect of the locomotive on the wayside signal was investigated. For this reason calibration tests were carried out using only the locomotive to obtain reference acoustic emission signals. The plot in Figure 7-8 shows the raw signal generated by the locomotive recorded from the defect-free side of the track. Looking into the moving RMS of the recorded signal (shown in Figure 7-9), a certain pattern can be recognised due to a number of repeating peaks spaced at the same interval.

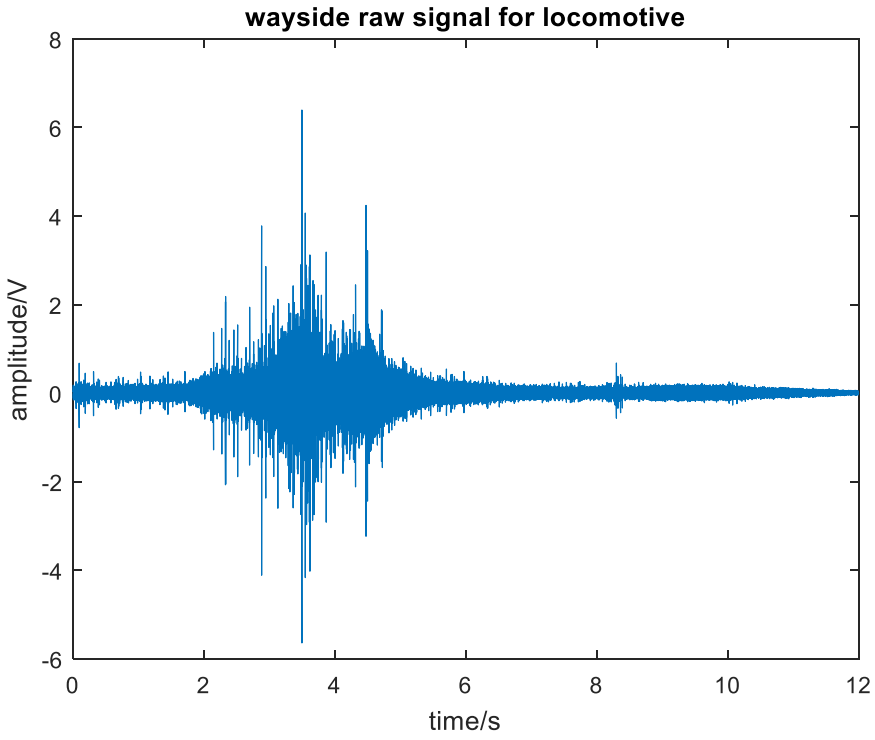

Figure 7-8: Wayside raw acoustic emission signal obtained from the locomotive only.

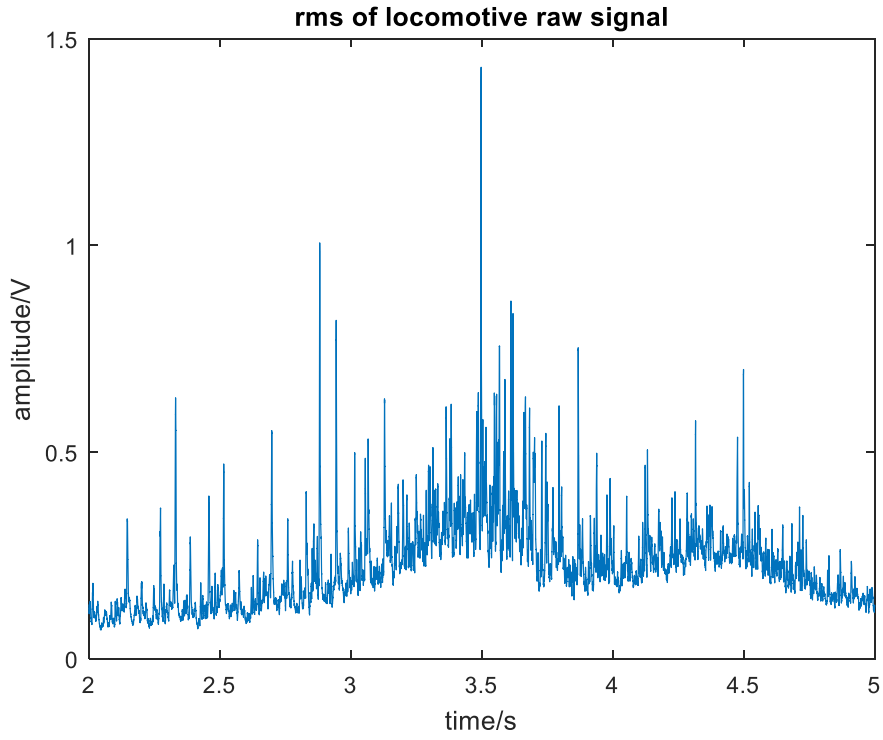

Figure 7-9: Moving RMS results for the locomotive acoustic emission signal.

Since the locomotive wayside signal is amplitude-modulated, by performing HFRT analysis, a frequency of 5.4 Hz can be detected from the spectrum of as shown in Figure 7-10. It is speculated that this particularly frequency has arisen from a loose engine pipe on the defect-free side, as it was vibrating and generating loud audible noise during the measurements. This particular frequency did not show up in the acoustic emission signals acquired by the sensors installed from the defective side of the track. This is due to the fact that the signal source, i.e. the defective engine pipe, is isolated. Thus, any high-frequency acoustic emission signals generated from it would not be able to be transmitted to the other side due to attenuation and complex transmission path.

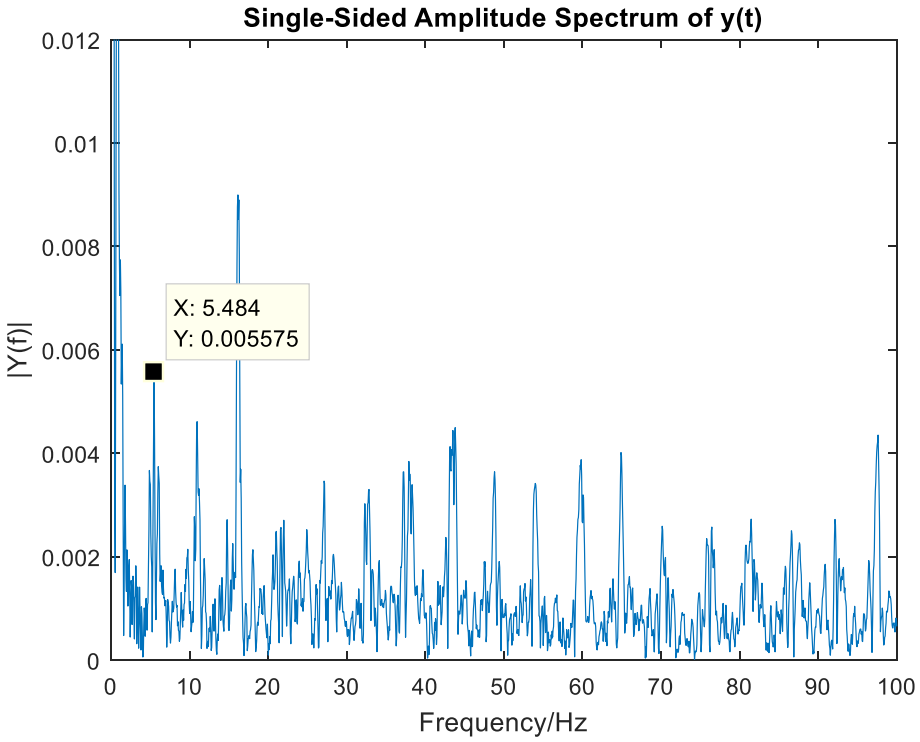

Figure 7-10: Plot obtained after processing the raw signal using the HFRT algorithm. A frequency of 5.4 Hz and its harmonics are clearly evident.

Since these peaks are generated by the same source, their frequency contents should have a high degree of similarity. Spectral coherence processing should be able to identify the

defective frequency as well by picking out peaks with the same feature. Therefore, it can be used an example to validate the effectiveness of the spectral coherence method. A detailed comparison between these two methods is provided in

Table *7-1*.

Method 1: HFRT	Method 2: Spectral Coherence
1. Performing bandpass filter to pick out the frequency range with sidebands 2. Performing Hilbert transform to demodulate the filtered signal 3. Performing FFT to identify the frequency of the envelope signal	1. Using one typical spike in the raw data as a template 2. Performing spectral coherence to identify any other spikes in the signal that are generated by the same source 3. Performing FFT on the similarity result to identify the frequency of repetition

Table 7-1: Comparison of HFRT and Spectral Coherence

Figure 7-11 shows the result of the spectral coherence processing. The template is selected as a random peak generated by the defective engine pipe around 2.2 s in the graph. After performing FFT, the frequency spectrum of the correlation result is shown in Figure 7-12. The frequency of 5.4 Hz can be clearly identified, which matches with the result of HFRT processing. It further proves that spectral coherence method is a powerful tool to process wayside acoustic emission and vibration data.

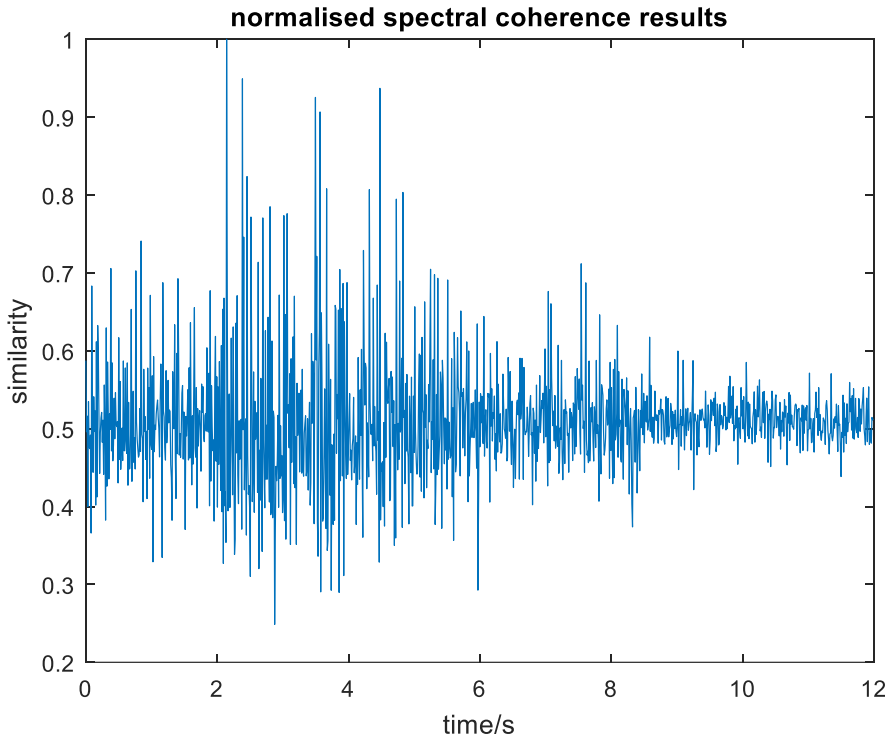

Figure 7-11: Normalised results for the spectral coherence processing.

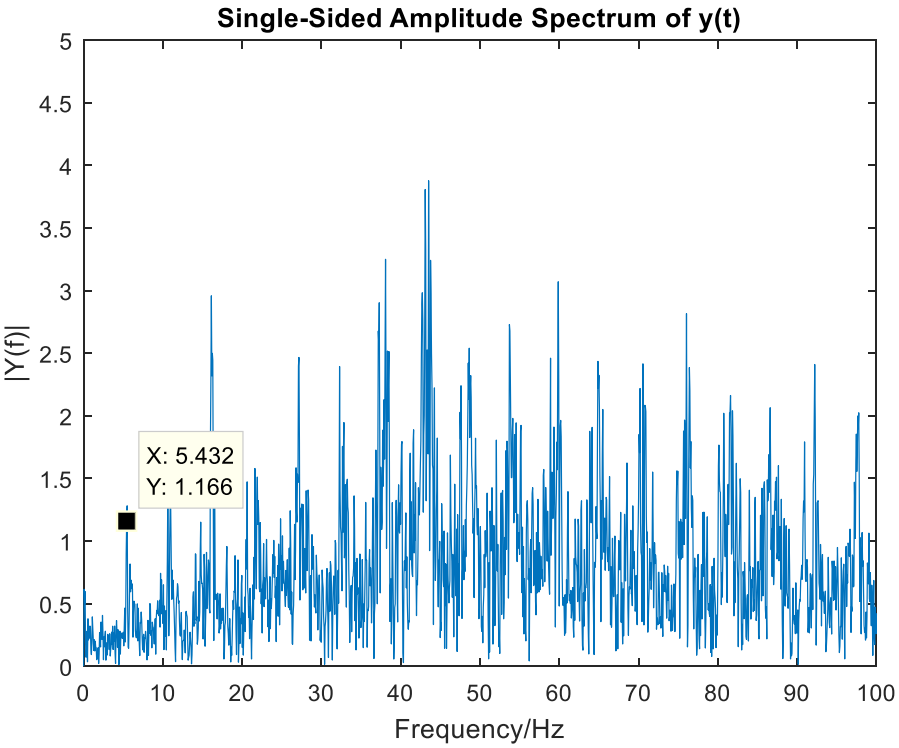

Figure 7-12: Frequency spectrum showing the spectral coherence results.

The signal analysed above is recorded when the locomotive travelled at an approximate speed of 48 km/h or approximately 13 m/s. In the next run the locomotive was running at the opposite direction (Figure 7-13) with a speed measured to be 32 km/h or approximately 9 m/s. Hence, the unique frequency of the engine pipe vibration can be calculated using the simple equation below:

$$\frac{5.484\ \text{Hz} \times 9\ \text{m/s}}{13\ \text{m/s}} = 3.79\ \text{Hz}$$

Therefore, the 3.79 Hz should be able to be identified by both HFRT and spectral coherence processing, which is illustrated in Figure 7-14 and Figure 7-15. It is clearly evident that the spectral coherence technique can be realistically applied for the identification of features of interest in the acquired acoustic emission signals.

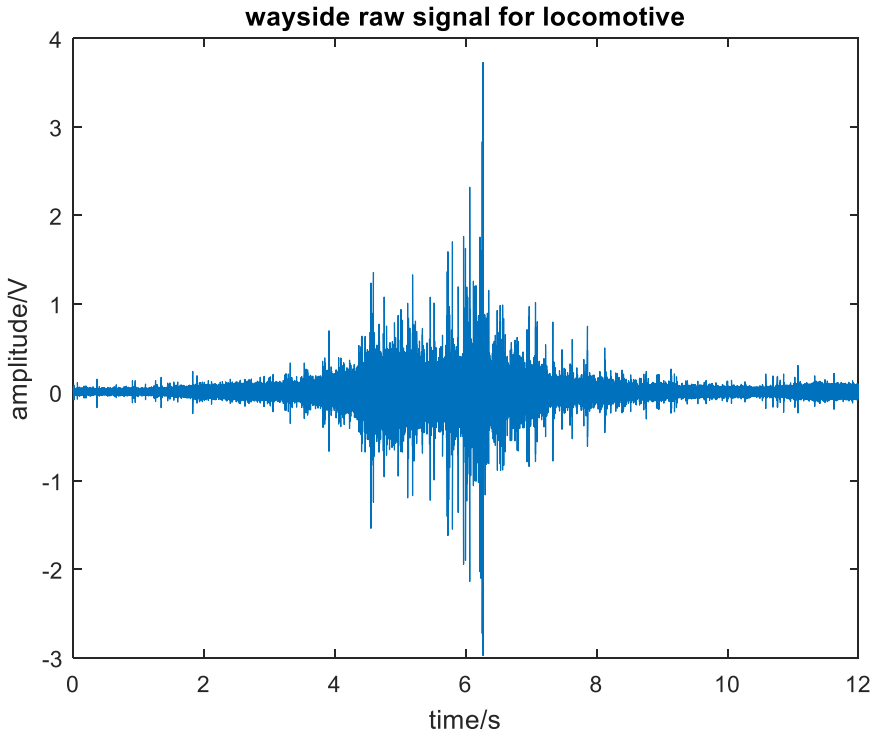

Figure 7-13: Wayside raw acoustic emission signal obtained for the locomotive while travelling in reverse.

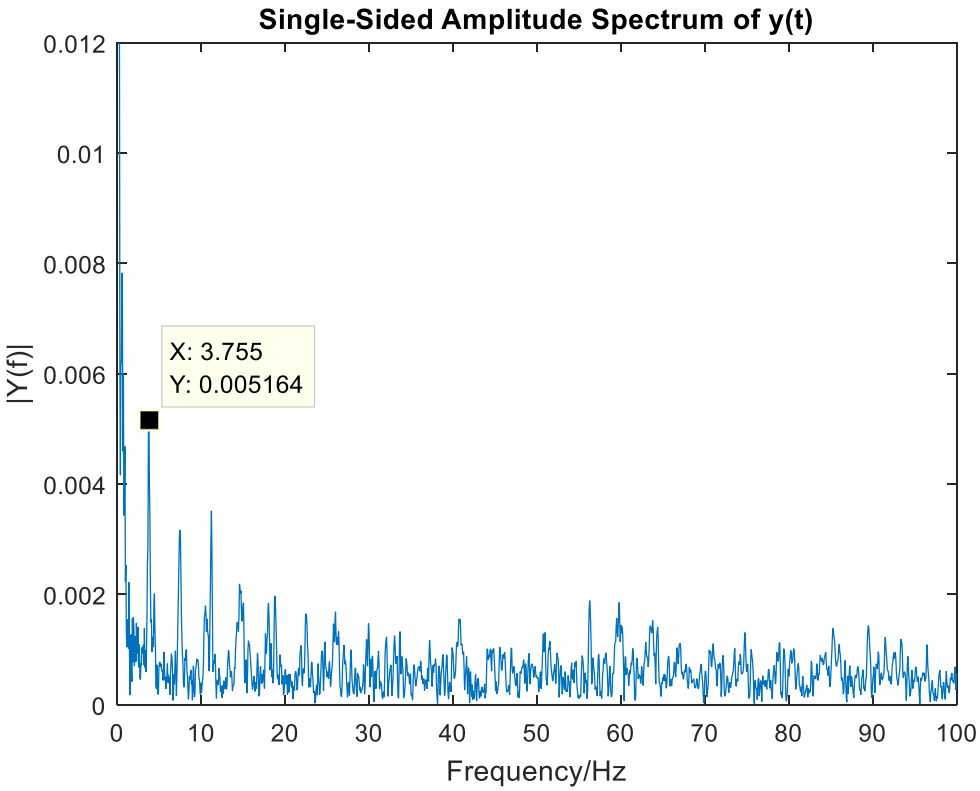

Figure 7-14: Plot obtained after HFRT processing of the raw acoustic emission signal.

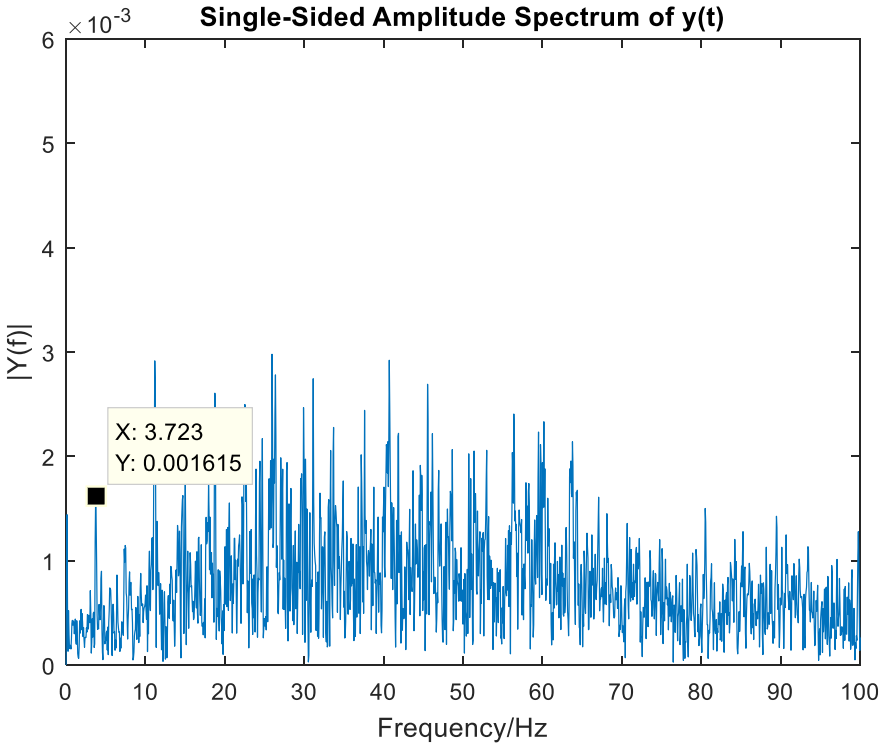

Figure 7-15: Frequency spectrum of the spectral coherence results.

7.4 Signal processing for rolling stock data

7.4.1 Long Marston trials

Long Marston tests were carried out under a relatively controlled operational railway environment that minimises environmental interference. This helped in accurately evaluating the performance of the acoustic emission and vibration techniques in detecting different wheel and axle bearing defects induced in the test rolling stock. It should be noted that two different locomotives were used during the various Long Marston trials, where the latter has the defective engine pipe.

7.4.1.1.1 Lubricant contamination test

The lubricant of two of the axle bearings of one of the test freight tanker wagons were purposely contaminated with sand and water jetted in the exposed bearings. Both defective bearings were from the same side of the track but in a different bogie. Therefore, each bogie of the test freight wagon contained one healthy and one faulty bearing from the defective side of the track.

The plot in Figure 7-16 shows the raw acoustic emission signal obtained from the defect-free side of the track. The main signal content is the noise generated when each wagon passed through the detection zone. Discrete peaks shown in the raw signal are generated by the vertical impact load of the wheel and rail joints present (re-railing took place shortly afterwards with the new track being continuously welded as mentioned earlier). In contrast, the plot in Figure 7-17 shows the raw acoustic emission signal from the defective side of the track with the two contaminated bearings present.

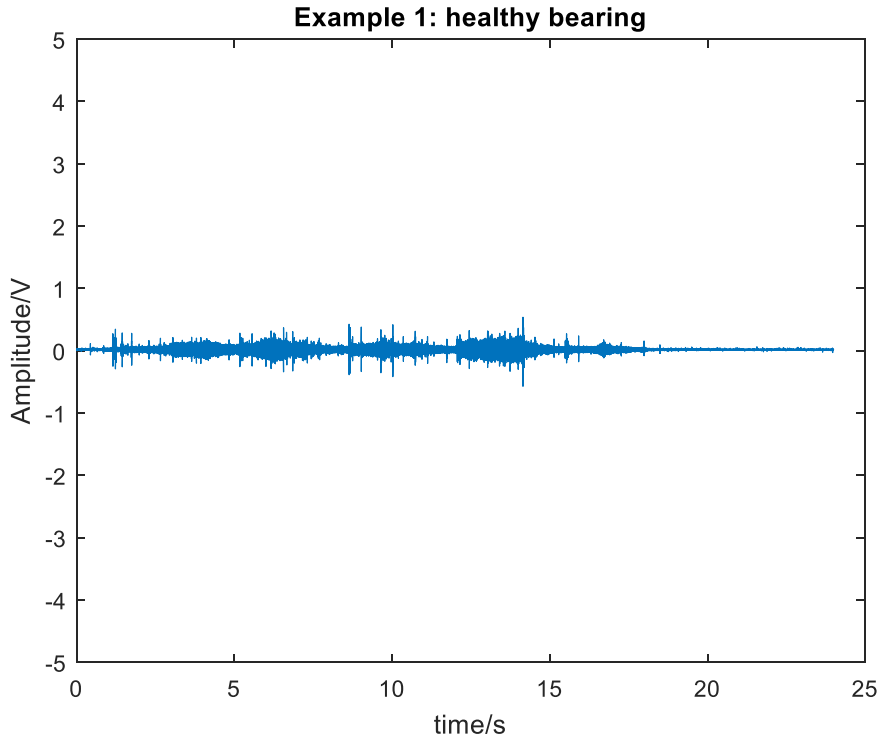

Figure 7-16: Wayside raw AE signal from the defect-free side of the track.

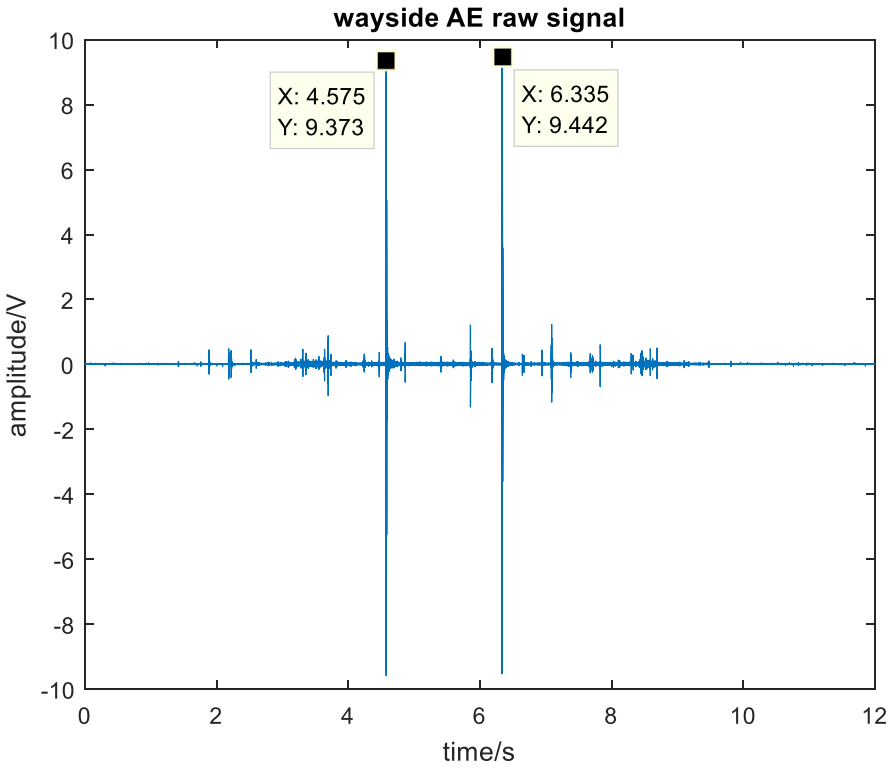

Figure 7-17: Wayside raw acoustic emission signal from the defective side of the track. The differences are evident.

The plot in Figure 7-18 shows the results after processing the raw acoustic emission signal using the moving RMS algorithm. The peaks related to the defective bearings are clearly visible.

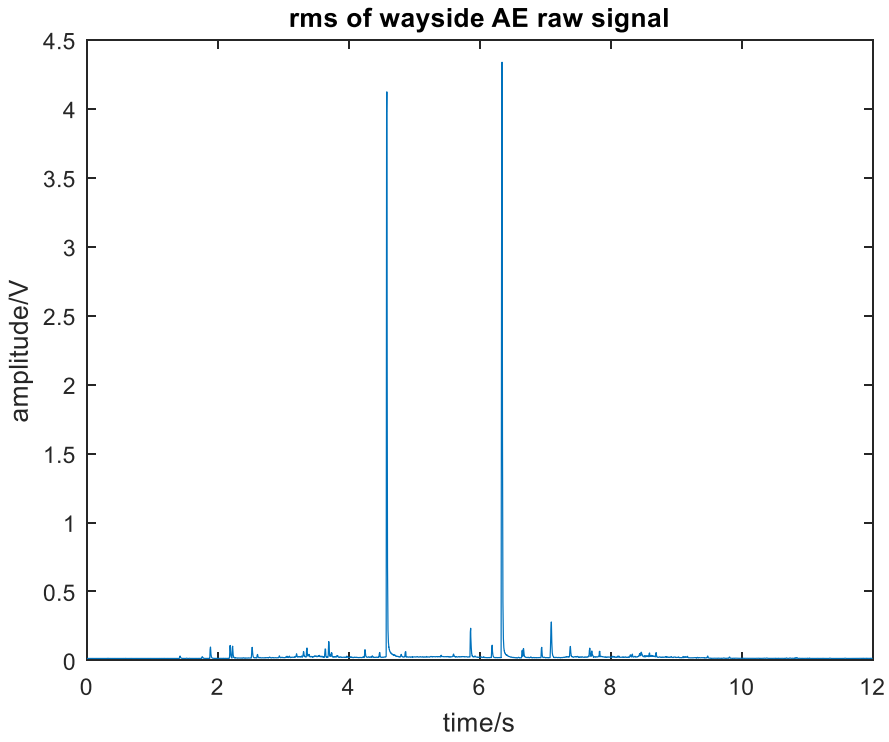

Figure 7-18: Analysis of the raw acoustic emission signal from the defective side using moving RMS. The two faulty bearings are clearly visible as two distinct peaks of high amplitude.

The spectrogram shown in Figure 7-19 further confirms the presence of the two defective axle bearings.

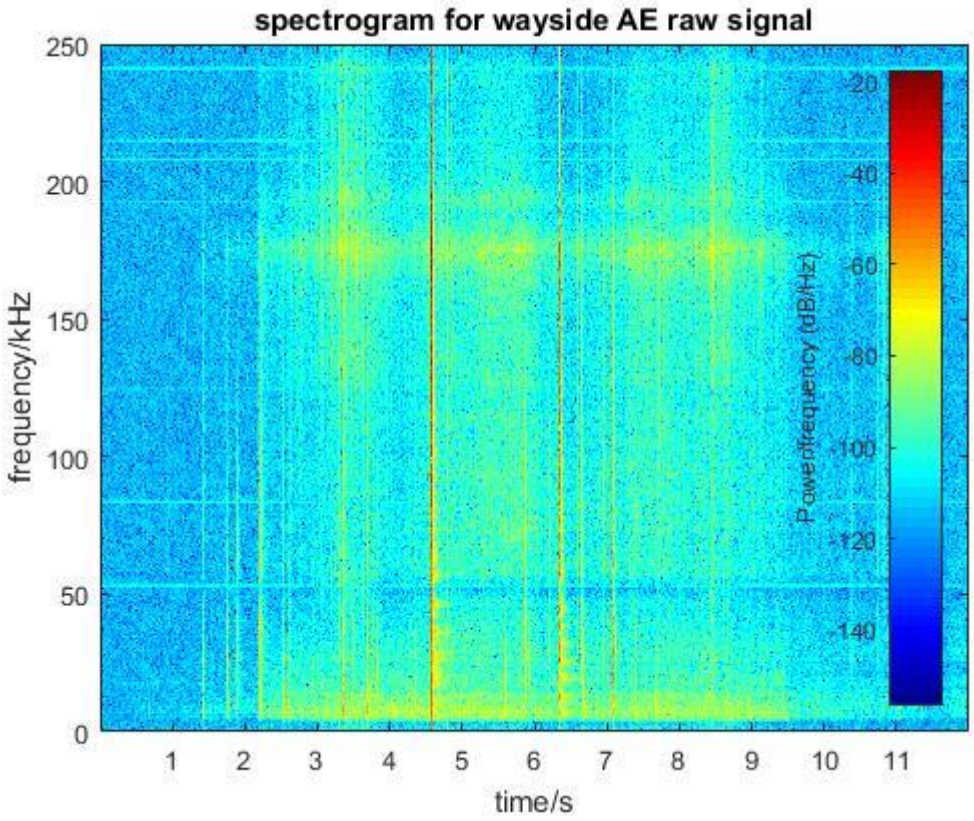

Figure 7-19: Spectrogram obtained for the acoustic emission signal from the defective side. The presence of the two faulty axle bearings is clearly visible.

Two distinct peaks can be clearly identified at 4.575 s and 6.335 s. The amplitude of these peaks is around 9.3 V. As seen by comparing the plots in Figure 7-18 and Figure 7-19 respectively these two peaks have much higher energy spread over the entire spectrum than the rest of the signal. Despite the two discrete peaks, the rest of the background raw signal has the same amplitude range, which indicates that the two peaks are generated by the contaminated bearings causing the affected wheels to rotate irregularly. This result can be further verified by considering the train speed and geometrical characteristics of the freight wagon (wheelset distances and wheel diameter). As the train speed remained constant at approximately 30 km/h (8.3 m/s) when travelling in the forward direction and the distance between two defective bearings is 14.5 m, the time difference, when the two bearings pass over the acoustic emission sensor can be calculated as 1.74 s. This matches well with the 1.76

s identified from the plot in Figure 7-17. Therefore, these two distinct peaks can be ascertained to have been generated by the two faulty axle bearings.

Further experiments were conducted on the same test wagon after inducing a wheel flat in one of the wheels from the side where the two defective axle bearings were present. This was done in order to assess the capability of the system in distinguishing two completely different types of defects present at the same time. The plot in Figure 7-20 shows the acoustic emission signal acquired for this scenario.

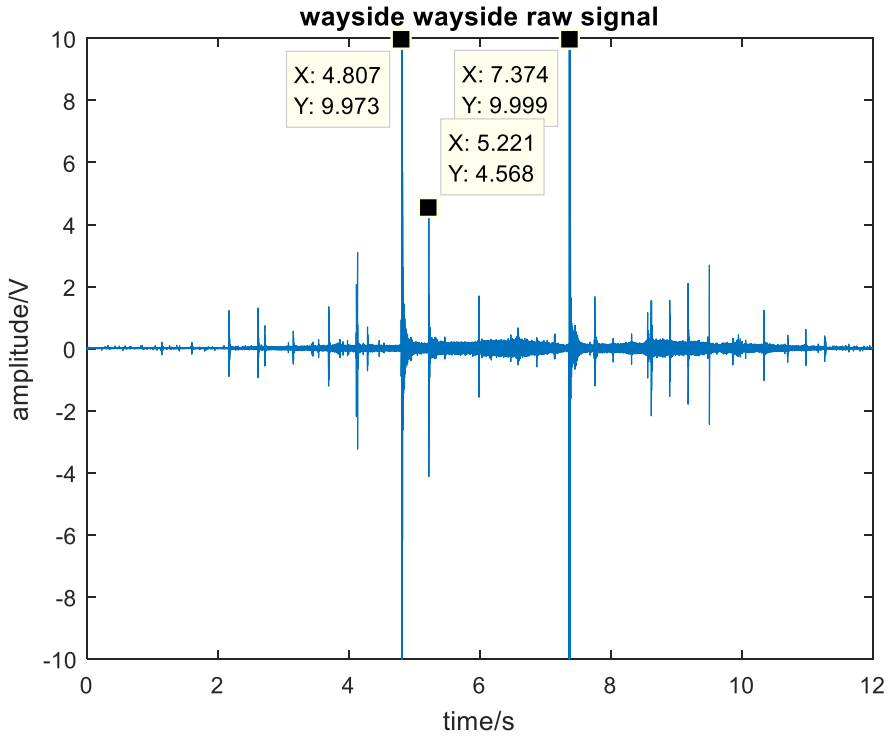

Figure 7-20: Wayside raw acoustic emission signal with defective axle bearing and an artificially induced wheel flat present at the same time.

In the Figure 7-20 an additional discrete peak can be identified at 5.2 s. As the dataset was recorded with the train moving in the opposite direction (backwards), the train speed was approximately 20 km/h (5.56 m/s). Given the train geometry, the time difference between the

two main peaks associated with the faulty axle bearings can be calculated to be equal to 2.6 s. This matches well with the value of 2.567 s calculated from the plot in Figure 7-20.

As discussed in Chapter 6, the wheel flat was artificially induced on the third wheel with a grinding tool. The lower amplitude peak on the right of the first dominant peak is thus considered to have been generated by the wheel flat impact. This can be examined in more depth using the same methodology described earlier. The time interval has been calculated to be 0.38 s from the train geometry and 0.414 s from the plot in Figure 7-20. This shows that the acoustic emission technique is capable of both detecting axle bearing faults and wheel flats. Although it is possible to ascertain the nature of the defect by the aforementioned technique, correlating the results with the vibration analysis signals helps increase the confidence level of the conclusions drawn.

Since the acoustic emission sensor is passive, it records any stress waves transmitted to the sensor including the ultrasonic energy generated by wheel flat impacts and faulty bearing. However, the main difference between the wheel flat and the contaminated bearings is that the spectrum distribution is different. As shown in Figure 7-21 and Figure 7-22, the majority of the energy generated by the wheel flat impact is distributed below 100 kHz. The frequency spectrum of the contaminated axle bearings has a wide bandwidth instead.

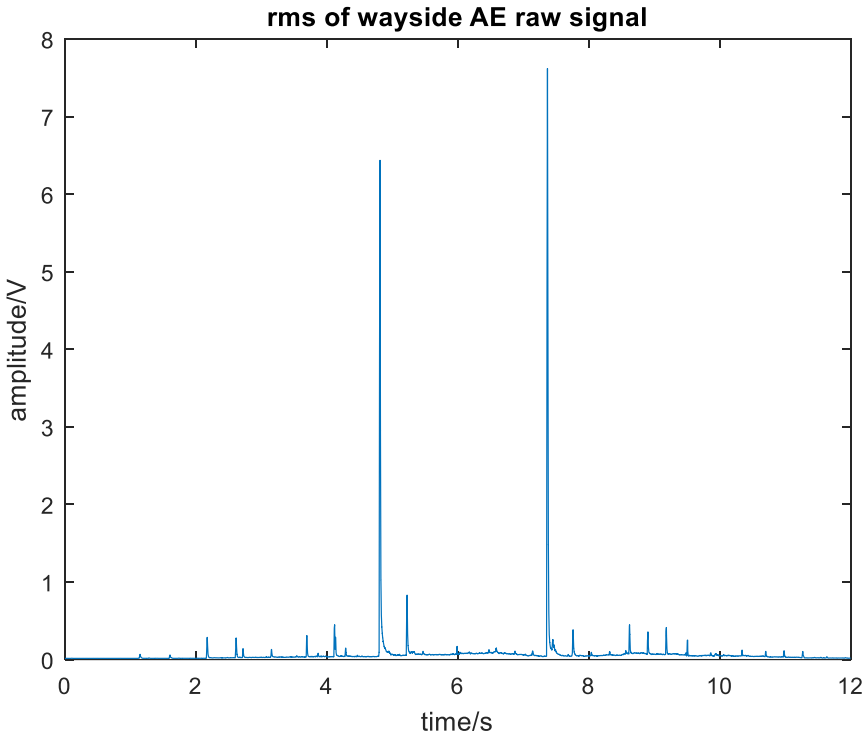

Figure 7-21: Moving RMS result for defective side signal with wheel flat present.

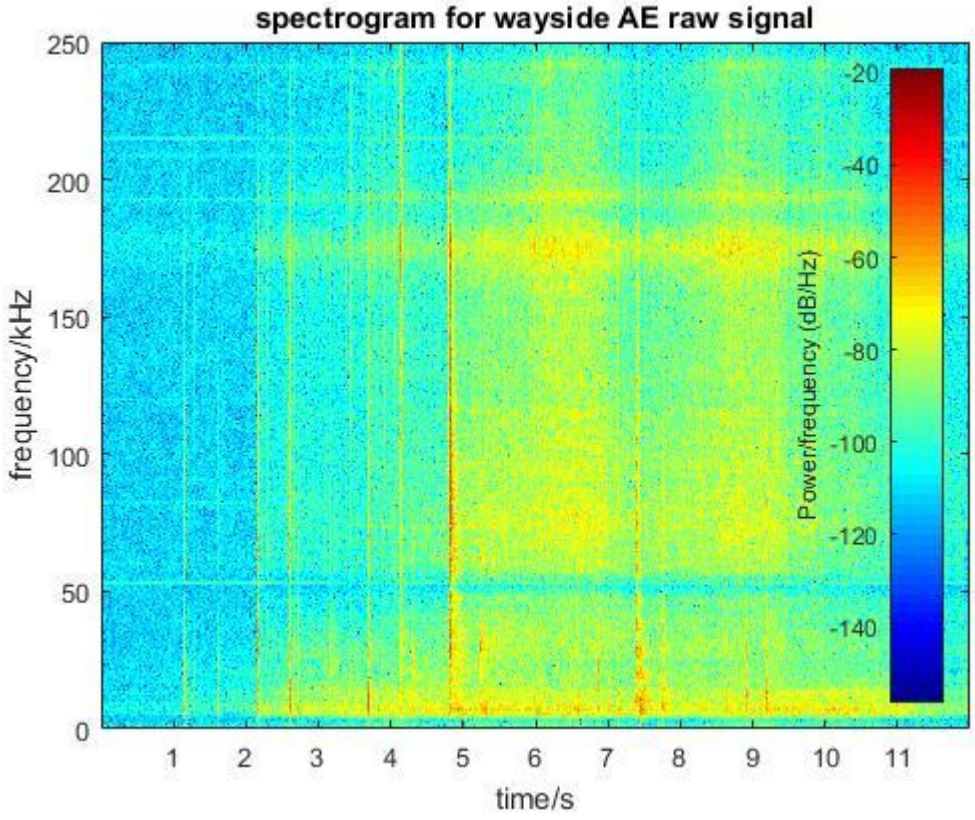

Figure 7-22: Spectrogram for the defective side signal with wheel flat present.

In addition, the contaminated axle bearings can be identified by using correlation-based processing. Due to the same nature of the defect affecting both faulty axle bearings, the spectral feature of peaks generated by the lubricant contamination are expected to be similar and correlated well to each other. The template is selected as the second dominant peak from 6.3 to 6.4 s from the filtered raw signal without the presence of the wheel flat as shown in Figure 7-17. The filtered template is shown in Figure 7-23 below.

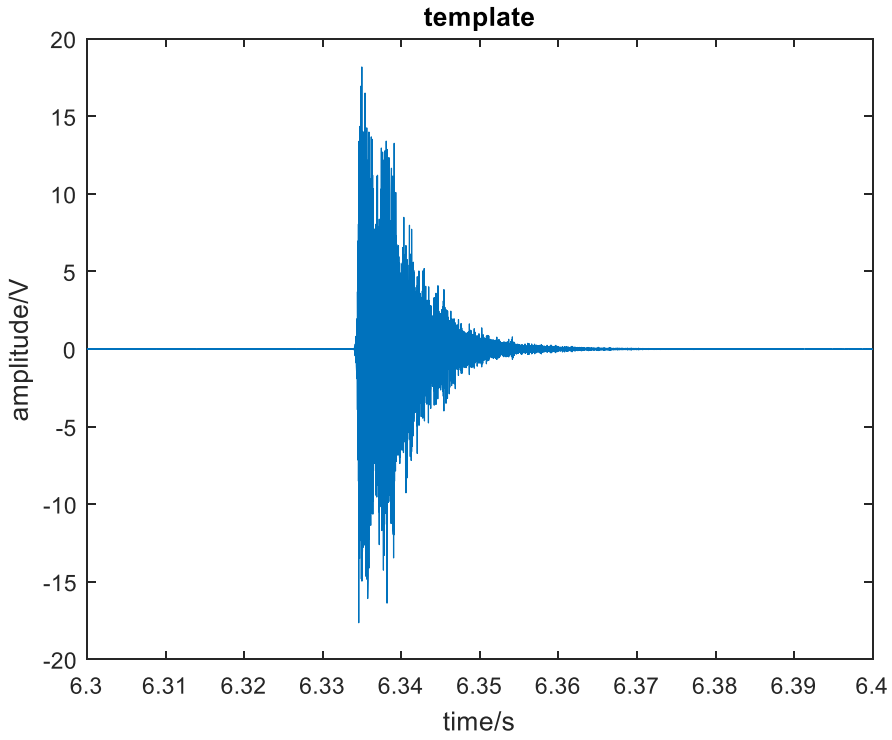

Figure 7-23: The template used for wayside bearing defect and wheel flat detection.

The normalised spectral coherence results for both scenarios are shown in the plots of Figure 7-24 and Figure 7-25. In the plot of Figure 7-24, the highest amplitude is 1, which corresponds to the template selected for analysis. The other discrete peak generated by the first defective bearing can be easily distinguished from the graph with a high similarity index. The plot in Figure 7-25 illustrates the result using the selected template on the dataset with bearing defect and wheel flat present simultaneously.

It also proves the fact that train speed does not affect the result of spectral coherence processing. Such technique can be applied to signals acquired with test train running in both directions.

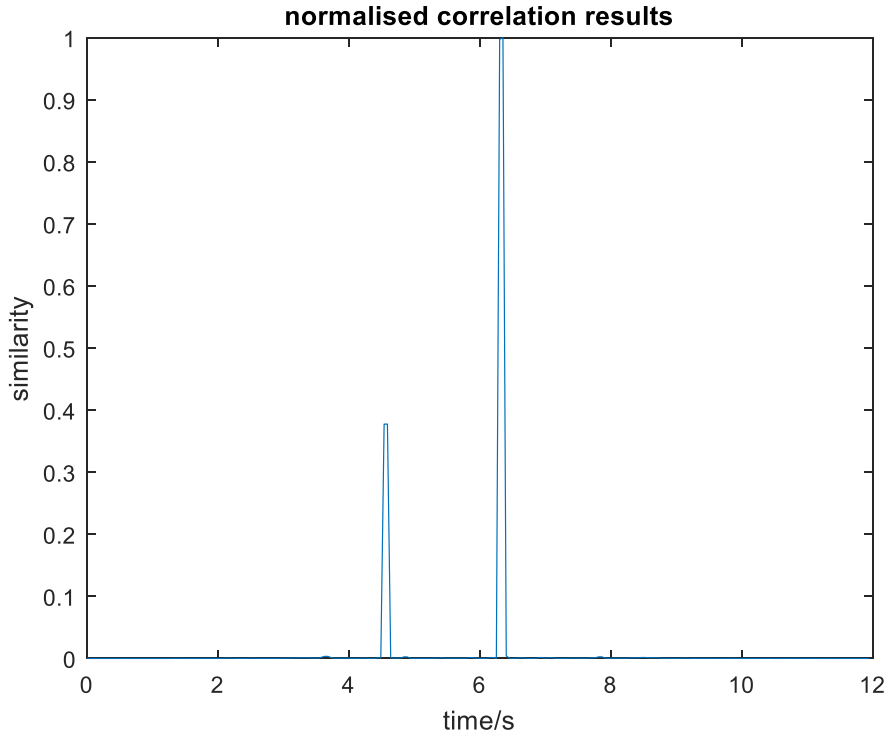

Figure 7-24: Normalised spectral coherence results without wheel flat.

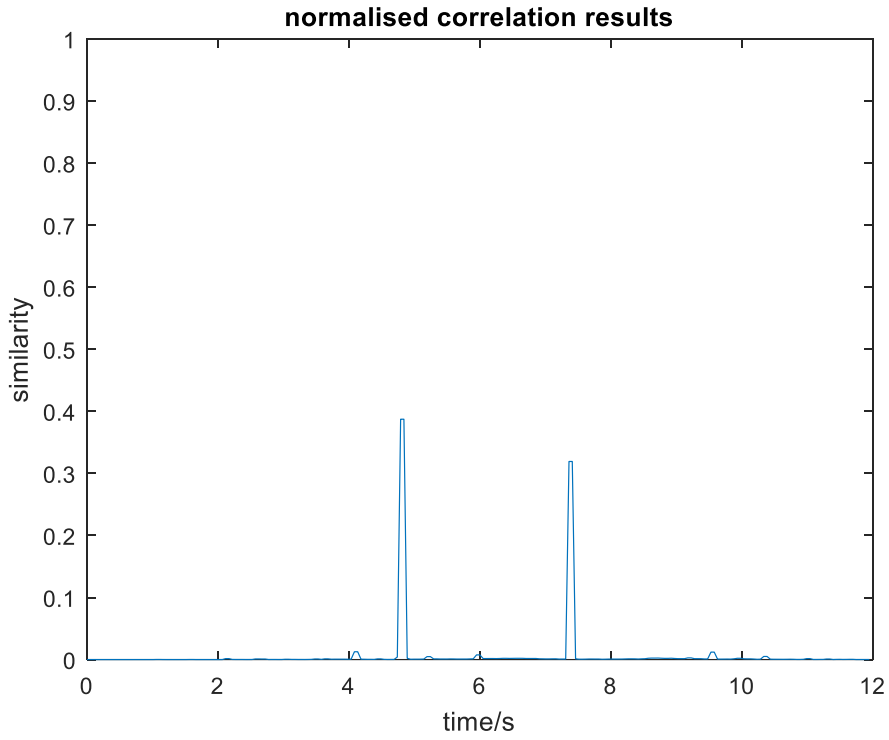

Figure 7-25: Normalised spectral coherence results with wheel flat present.

7.4.1.1.2 Roller defects test

In addition to the tests carried out on the axle bearings with lubricant contamination, experiments were carried out on bearings with roller defects of varying severity present to further evaluate the acoustic emission technique. One of the testing configurations considered, involved the locomotive and the freight wagon with 2, 4 and 8 mm roller defects present. Details of the experiments were also discussed in detail in Chapter 6.

The plot in Figure 7-26 shows an example of wayside raw signal generated by the test train. With the help of optical sensors, time distances when each wheel ran over the acoustic emission sensor were recorded, so that the location of the test train can be identified from the waveform, as annotated in Figure 7-26.

The lubricant contamination defect in the bearings was rather straightforward to detect because it releases significant acoustic emission transient energy. It is more difficult to identify bearing roller defects simply by looking at the raw signal, as the mechanism is complex, leading to a mix of both transient and continuous acoustic emission signals.

Thus, analysis based on spectral coherence has been performed to analyse the raw AE signals acquired during experiments. The process of template selection is illustrated in Figure 7-26 and Figure 7-27. The peak used as the template has been confirmed to be generated by 8 mm roller defect. This particular template will be used in spectral coherence processing on other datasets in order to prove the template is time invariant.

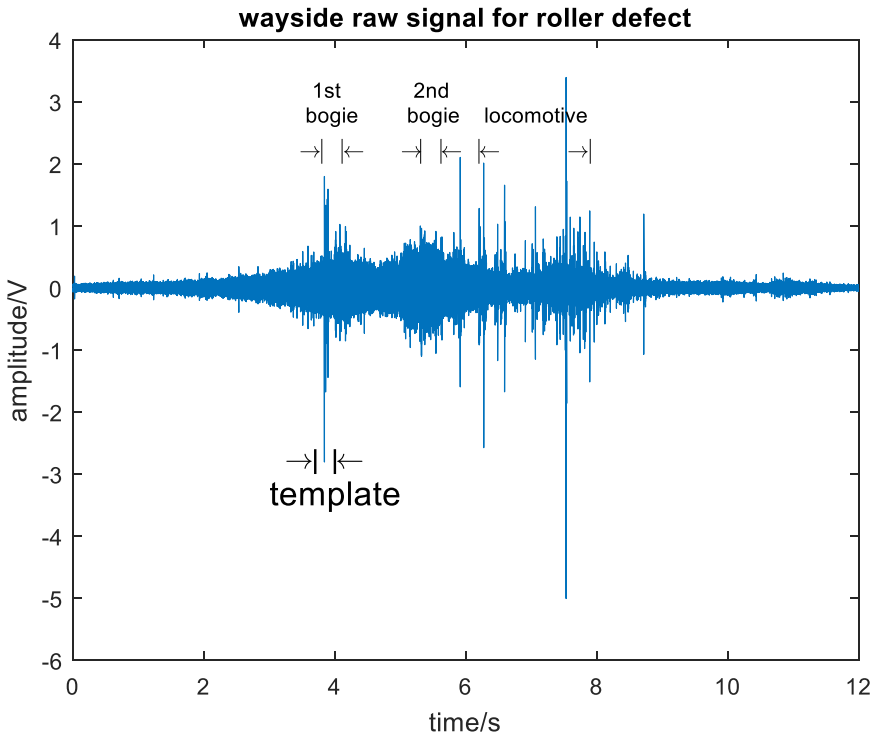

Figure 7-26: Wayside raw acoustic emission signal for the test configuration with the axle bearings containing roller defects of various severities.

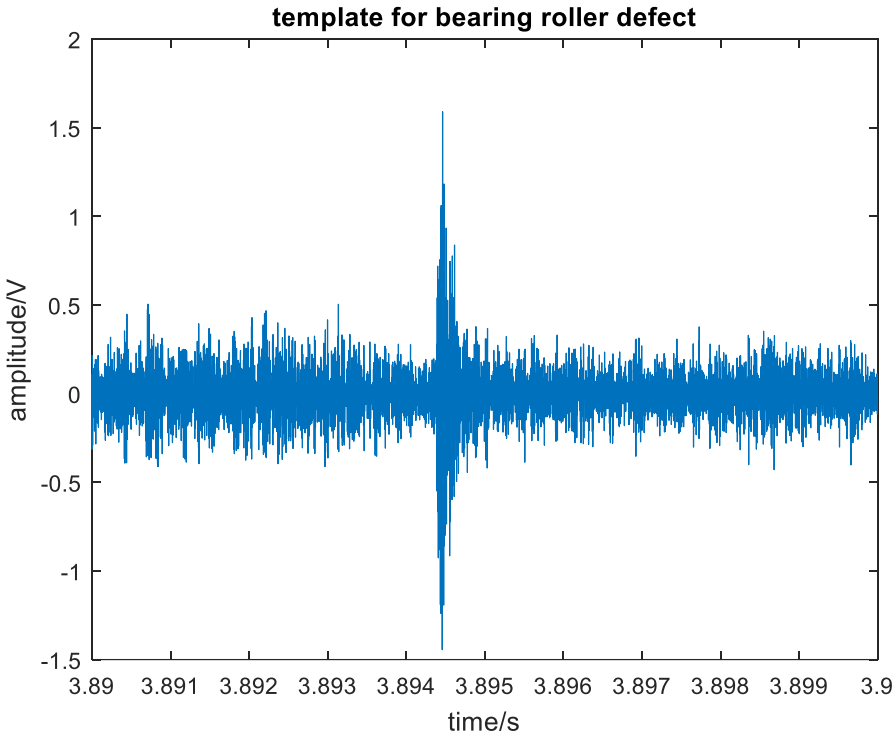

Figure 7-27: Template selected for the assessment of bearing roller defects.

The raw acoustic emission signal of the first example is provided in Figure 7-28 with the position of the train shown. This dataset was recorded when test train was moving backwards (i.e. the test freight wagon is in the front), with the speed recorded to be approximately 7.8 m/s. The correlation result is shown in Figure 7-29.

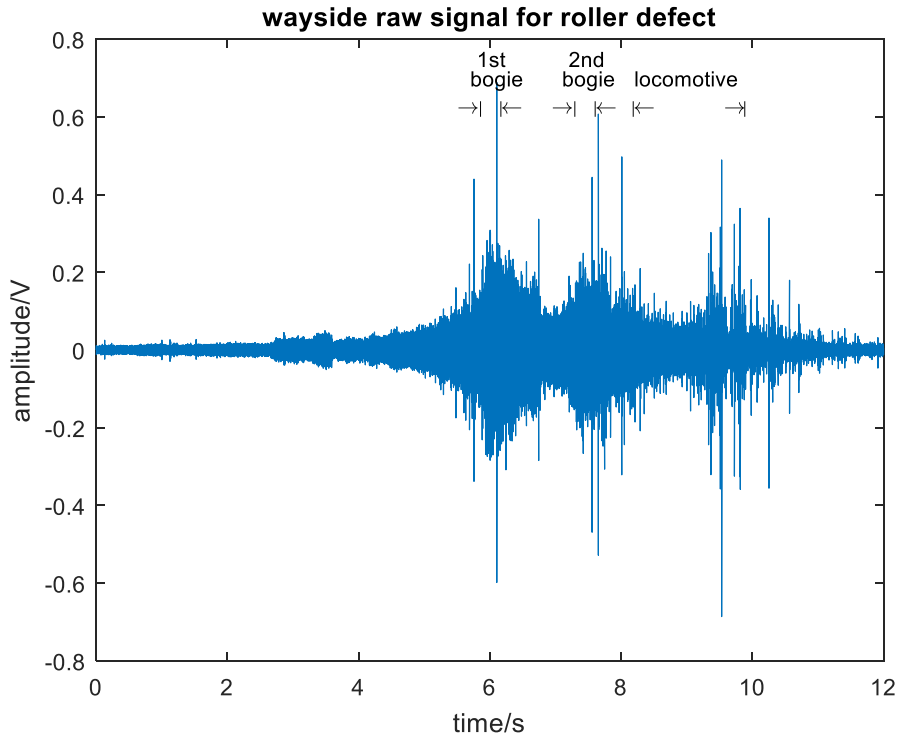

Figure 7-28: Wayside raw acoustic emission signal for the testing configuration with the roller axle bearing defects present.

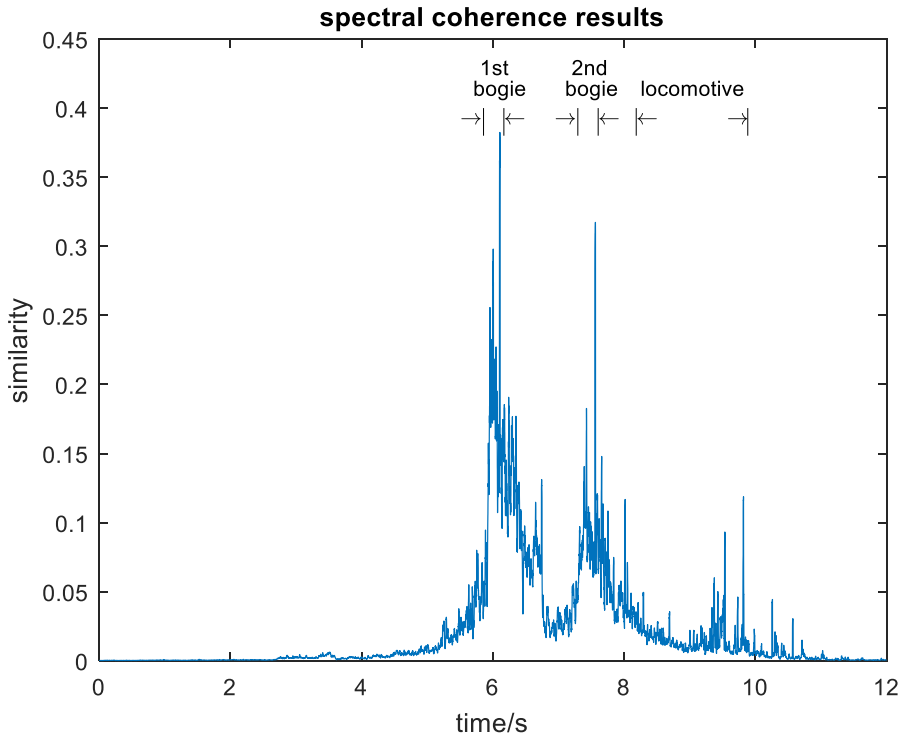

Figure 7-29: Results of the spectral coherence analysis.

It is difficult to determine the source of individual peaks in time domain only by checking interval and location of the raw signal, as acoustic emission bursts by nature are random. A better solution is to use spectral coherence processing, which is able to supress signals of less similarity (interferences), as shown in Figure 7-29. The severity of the defect can be evaluated by the score of similarity. Since the first bogie consists of 4 and 8 mm roller defects, the overall correlation result is higher than the second bogie. The result for the locomotive should yield a smaller similarity index, as the spectrum does not correlate with the template of roller defect even if the amplitude is high in raw signal.

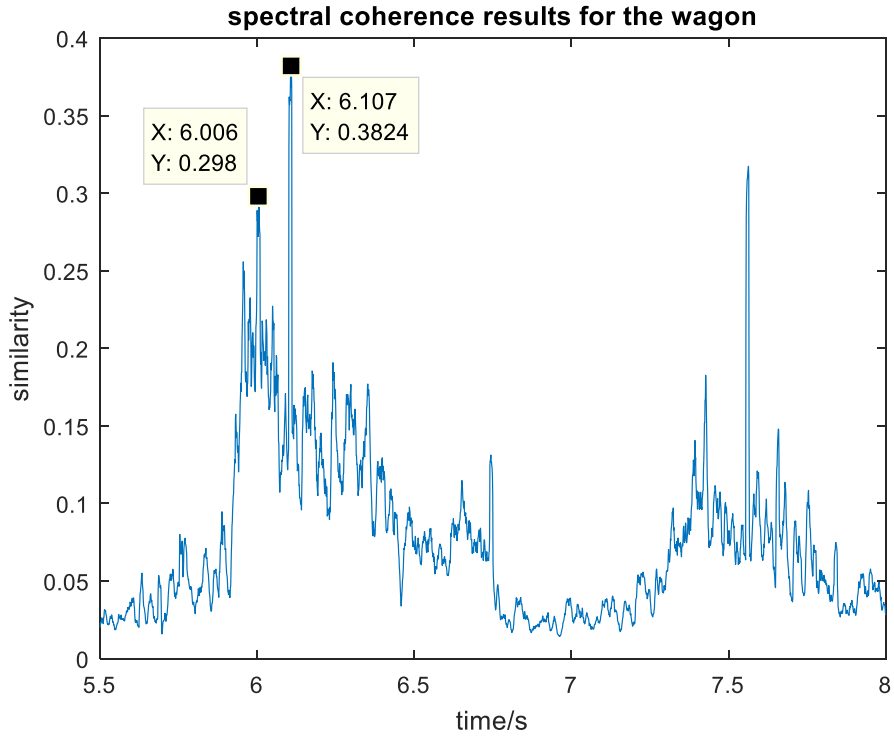

Figure 7-30: Spectral coherence result for the freight wagon with roller defects.

The plot in Figure 7-30 shows the zoomed-in correlation results for the freight wagon from 5.5 s to 8 s. Since limited number of impacts were recorded from the defective bearing when it passed over the sensor, the HFRT technique is no longer suitable to calculate the BSF directly from the raw acoustic emission signal. Instead, it can be recovered by identifying the

same type of impacts, firstly, through spectral coherence processing, and then by calculating the time interval of potential peaks. As shown in Figure 7-30, the time difference between the two marked peaks is 0.101 s, which indicates a frequency of 9.9 Hz. Since the shaft frequency is $f_s = \frac{v}{\pi d} = \frac{7.8}{\pi * 0.91} = 2.73$ Hz, the BSF can be calculated as $f_{BSF} = {f_0}/{f_s} = \frac{9.9}{2.73} =$ 3.6 Hz, which matches the frequency of 4.2 Hz provided by the manufacturer (Appendix A).

Another example presented here is a dataset where the locomotive is at the front running at around 12 m/s (Figure 7-31). The position of the train is also annotated on the figure. The correlation result is presented in Figure 7-32. Both results have identical waveform shape and the conclusion from the previous example still applies.

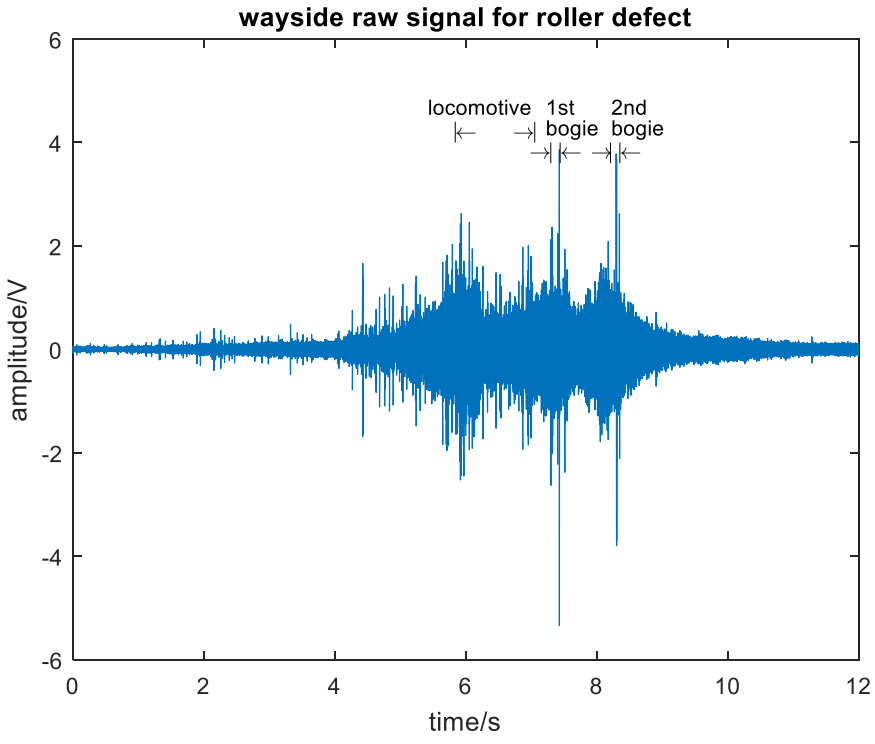

Figure 7-31: Wayside raw acoustic emission signal for roller defects with train moving forward.

The zoomed-in result for the freight wagon is shown in Figure 7-33. The time difference between the two peaks is 0.046 s, which indicates a frequency of 21.74 Hz. Since the shaft

frequency is $f_s = \frac{v}{\pi d} = \frac{12}{\pi * 0.91} = 4.2$ Hz, the BSF can be calculated as $f_{BSF} = {f_0}/{f_s} = \frac{21.74}{4.2} =$ 5.17 Hz, which also false close to the frequency of 4.2 Hz calculated by the manufacturer's product sheet.

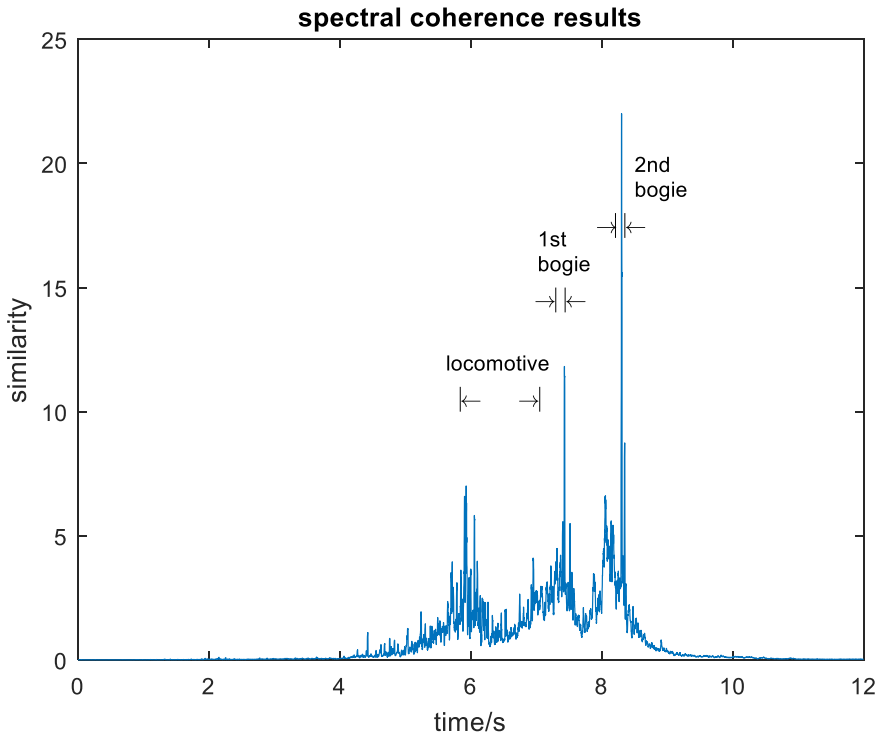

Figure 7-32: Spectral coherence results.

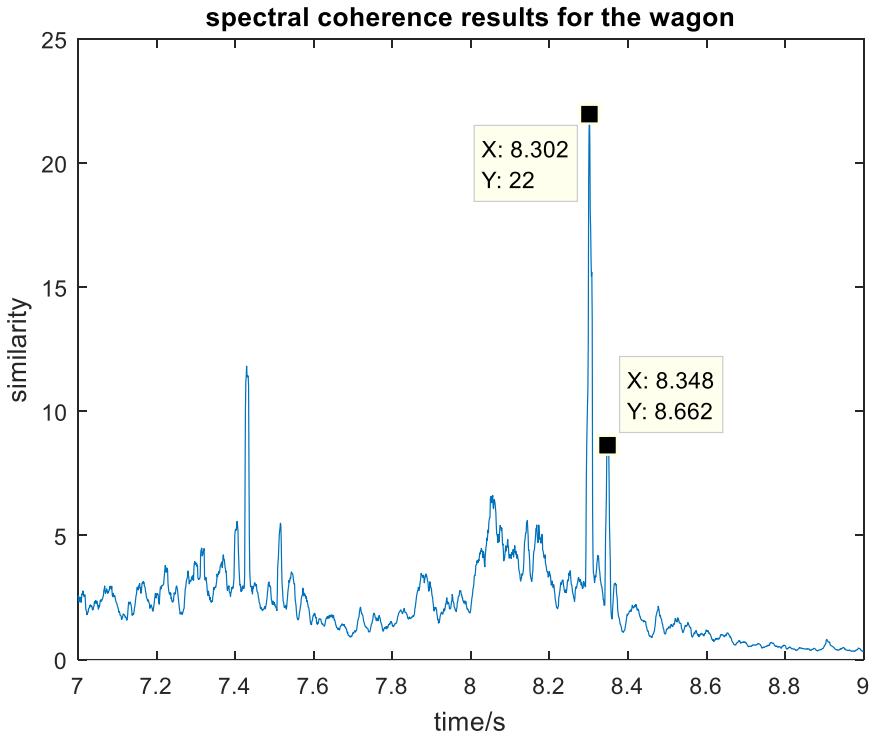

Figure 7-33: Spectral coherence result for the freight wagon with roller defects only (zoomed in signal).

7.4.2 Cropredy trial

Field trials monitoring actual railway traffic have been performed at the Cropredy site, which is part of Chiltern rail line connecting London with Birmingham. These trials serve as blind trials for the evaluation of the customised monitoring system and data processing techniques applied under realistic operational condition. The results so far show no sign of rolling stock defects as it is expected for in-service fleet. The chance of having incipient defect is very low.

However, there is one particular dataset that could indicate an inner race defect. The relevant raw acoustic emission signal generated by a slowly moving freight train locomotive passing through the instrumented site at Cropredy, is shown in Figure 7-34. After preliminary analysis, it was found that a segment of the raw acoustic emission signal has strong modulation. This falls in the time range of 3.2s to 4.4s (Figure 7-35). It was generated by one of the bogies in

the locomotive, which indicates that the specific bogie suffered from strong impacts from a rotating component.

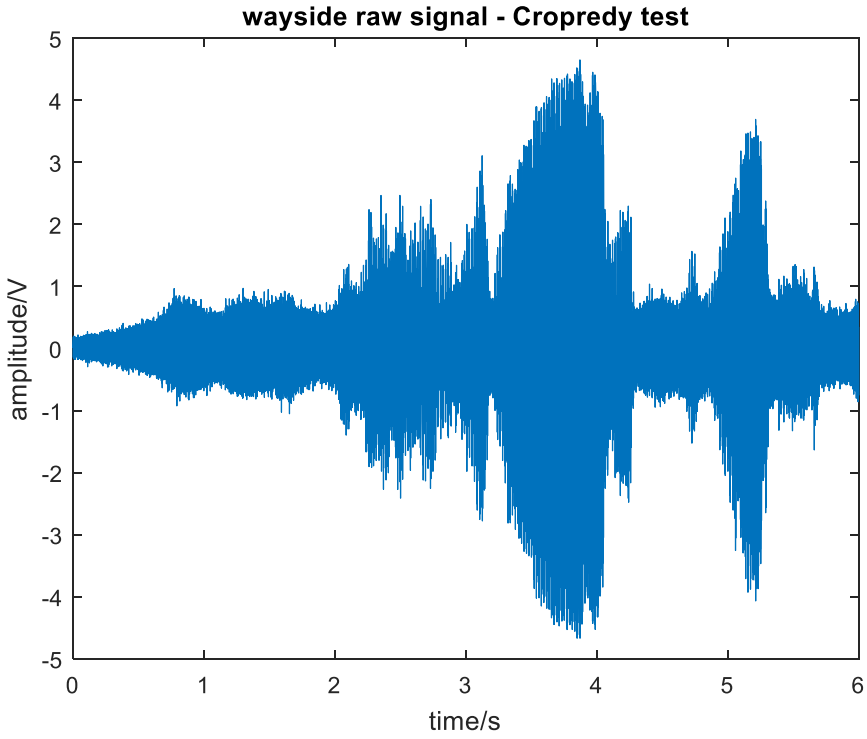

Figure 7-34: Wayside raw acoustic emission signal for the slowly moving freight train locomotive passing through the Cropredy site.

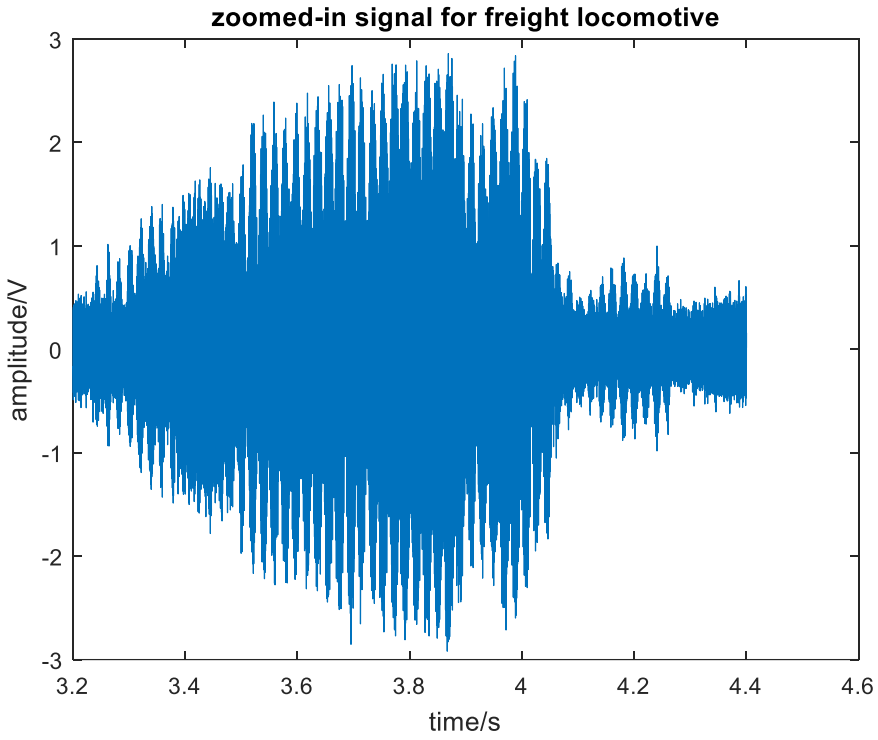

Figure 7-35: Zoomed-in signal for freight locomotive.

After filtering, the HFRT algorithm was applied to process the raw acoustic emission signal. The result is shown in Figure 7-36 and Figure 7-37. According to the definition of localised inner race defect, it generates BPFI frequency that is amplitude modulated at fundamental rotational frequency (1X). The pattern of the spectrum results matches the definition, which contains BPFI of 1 kHz with sidebands at fundamental rotational frequency of 50 Hz. The result still needs to be confirmed with help from Network Rail.

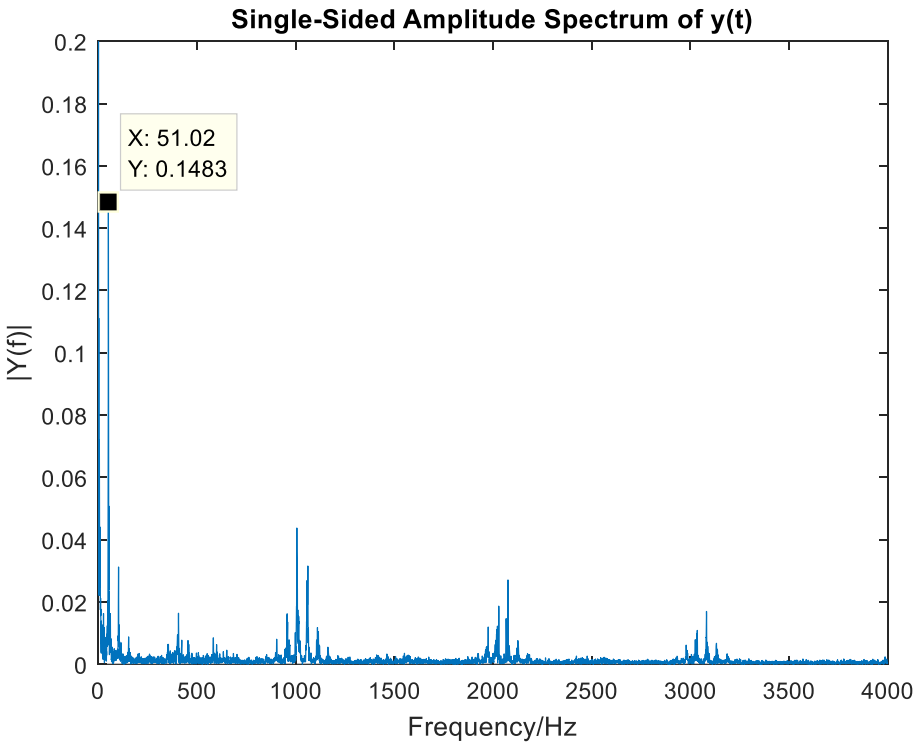

Figure 7-36: HFRT results for the freight locomotive showing clear side-bands and bearing tone harmonics indicating the presence of a bearing defect.

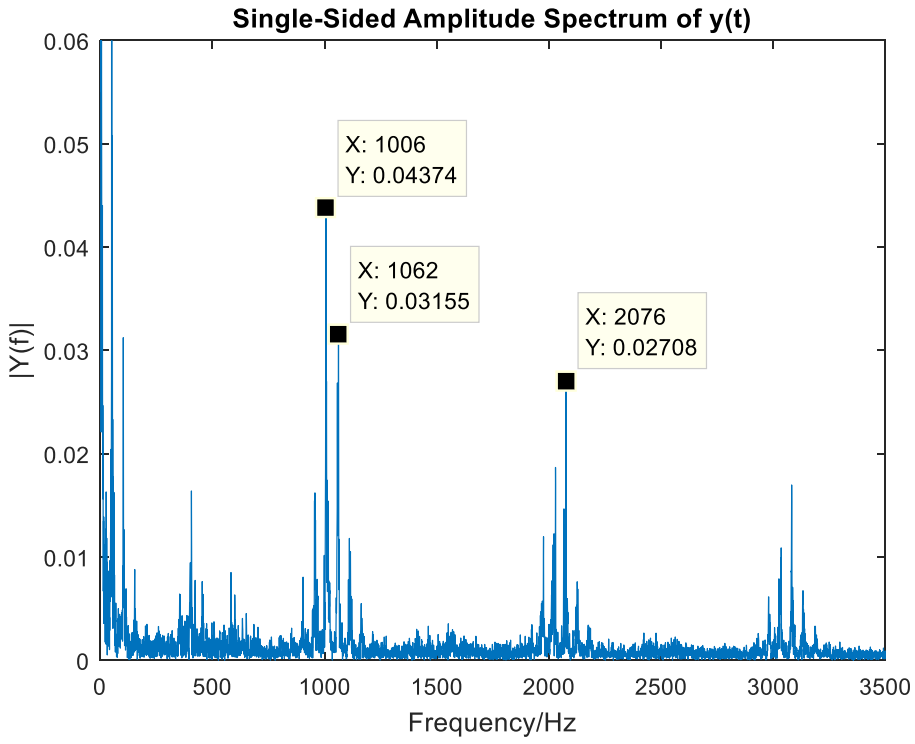

Figure 7-37: Zoomed-in HFRT results for the freight locomotive.

7.5 Signal processing for cast manganese crossing data

Three sets of experiments were carried out on three different cast manganese crossings with varying conditions ranging from healthy to severely damaged. The customised RCM system with spectral coherence processing was deployed to identify damage evolution in the form of crack growth in the crossings considered as well as evaluate the speed of deterioration. The templates used were selected from laboratory experiments carried out on fatigue samples manufactured from cast manganese steel. The same set of templates was used for correlation processing of the data obtained from all three sets of tests on the individual crossings. The crossings were loaded by both passenger and freight trains passing over them. Each of the wheels periodically loads the crossing. If damage is present and propagating, loading cycles will cause stress waves to be generated which are detectable using acoustic emission sensors.

7.5.1 Templates

Laboratory tests were carried out on cast-manganese samples to investigate the nature of acoustic emission signals generating from the crack growth events during loading cycles. Data were recorded throughout each test using interrupted acquisitions of few seconds in duration. Two templates were selected to represent the initial and later stage of the crack growth. Figure 7-38 shows the raw acoustic emission signal for one of the samples tested with a small growing crack present. It indicates crack growth at early stage in every loading cycle. Figure 7-39 shows the template selected from the raw signal which is the first peak from 0.99 s to 1.01 s.

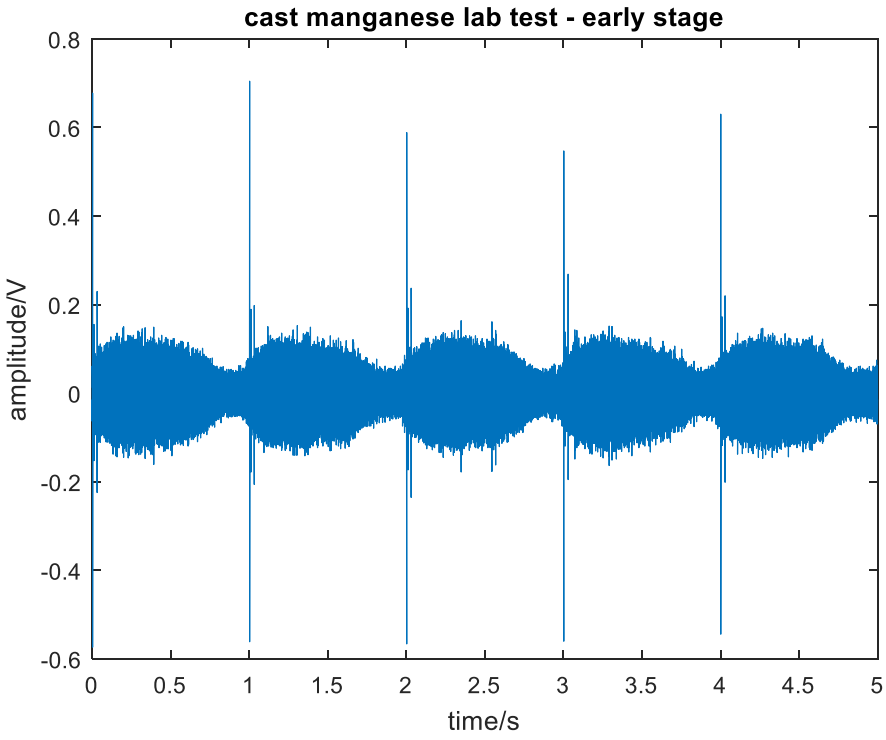

Figure 7-38: Raw acoustic emission signal acquired from one of the cast-manganese steel fatigue samples with crack growth still at an early stage

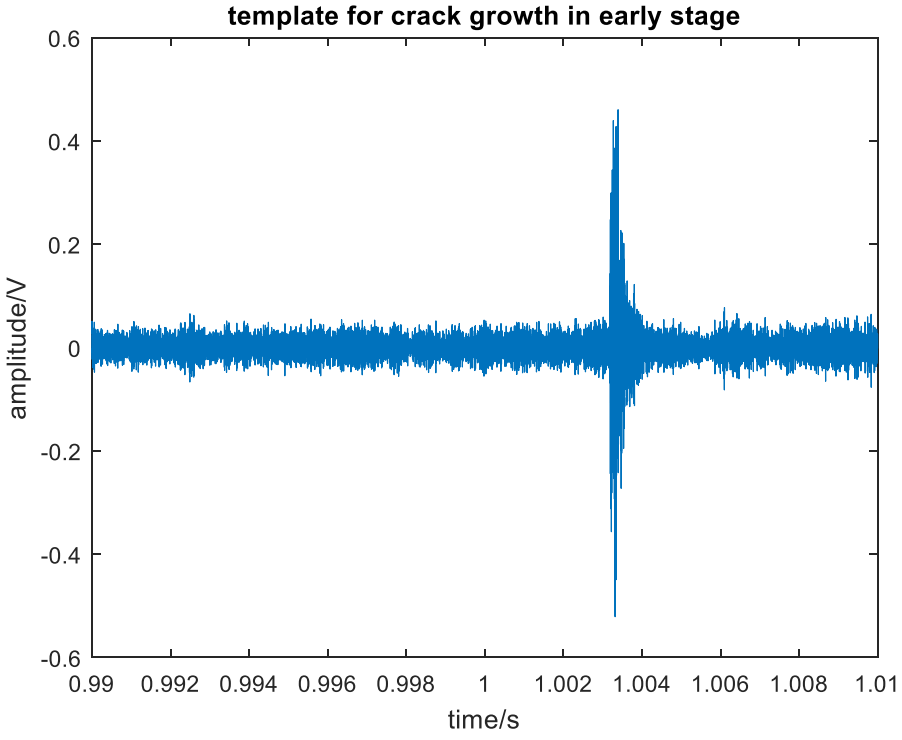

Figure 7-39: Selected template indicative of acoustic emission signal related to early stage crack growth.

Figure 7-40 shows the raw acoustic emission signal when crack propagation has accelerated and is considered to be in the middle stage of its evolution. The plot in Figure 7-41 shows the selected template truncated from 2.6 s to 2.62 s. By comparing these two templates, it can be observed that crack growth can not only result in burst-type AE signals with increasing amplitude as more energy is released with increasing crack growth rate. This can also change the spectral distribution as shown in Figure 7-42 and Figure 7-43. These two templates have been used to evaluate the condition of the actual cast-manganese crossing measured in the field.

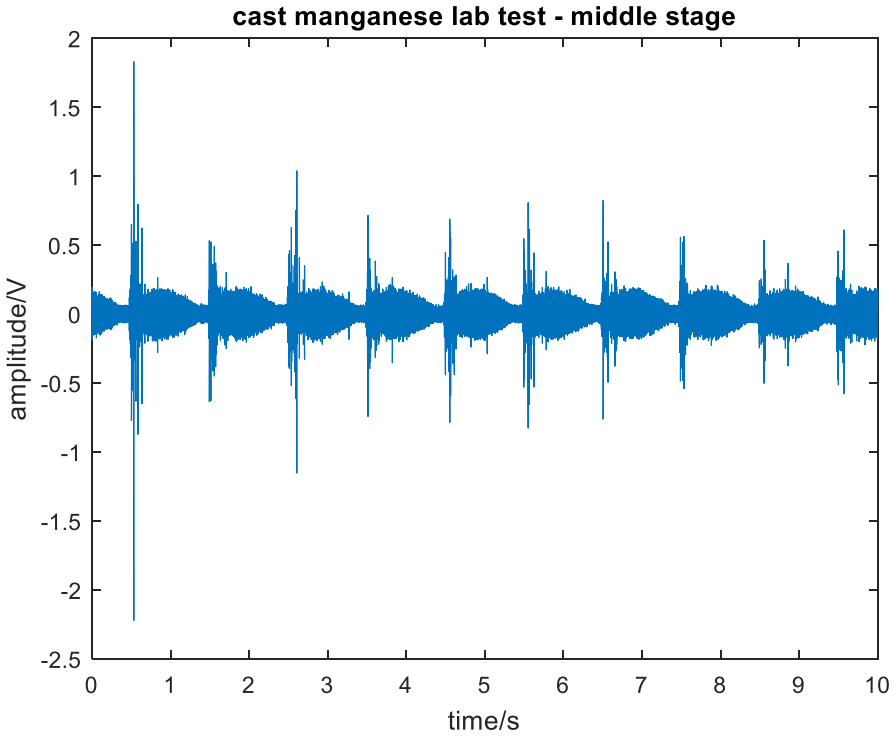

Figure 7-40: Raw acoustic emission signal of cast-manganese sample with crack growth at middle stage of evolution.

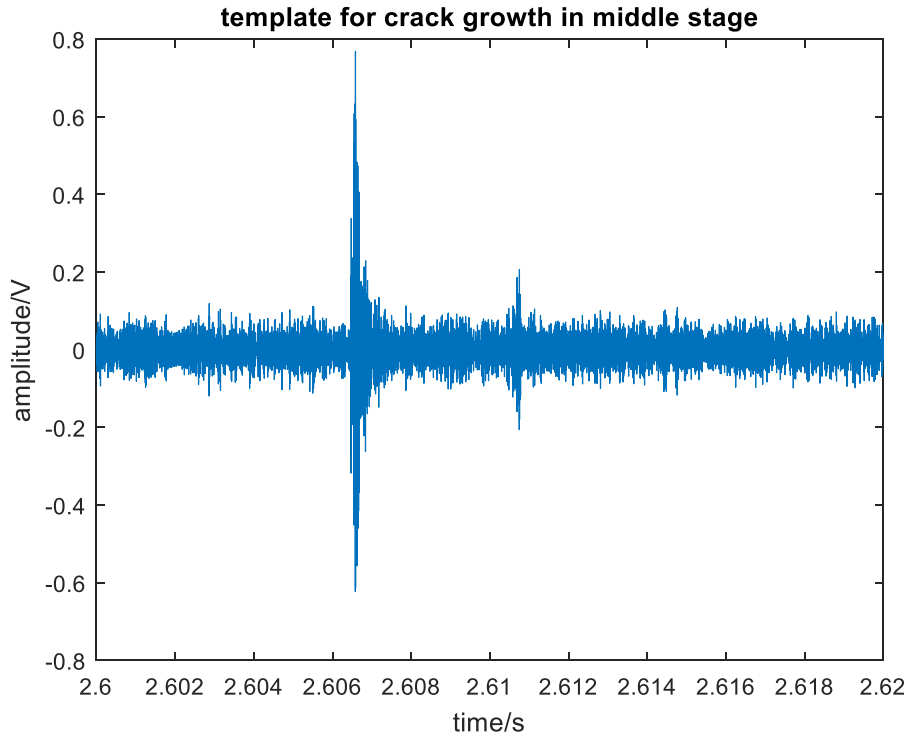

Figure 7-41: Selected template indicative of middle stage crack growth.

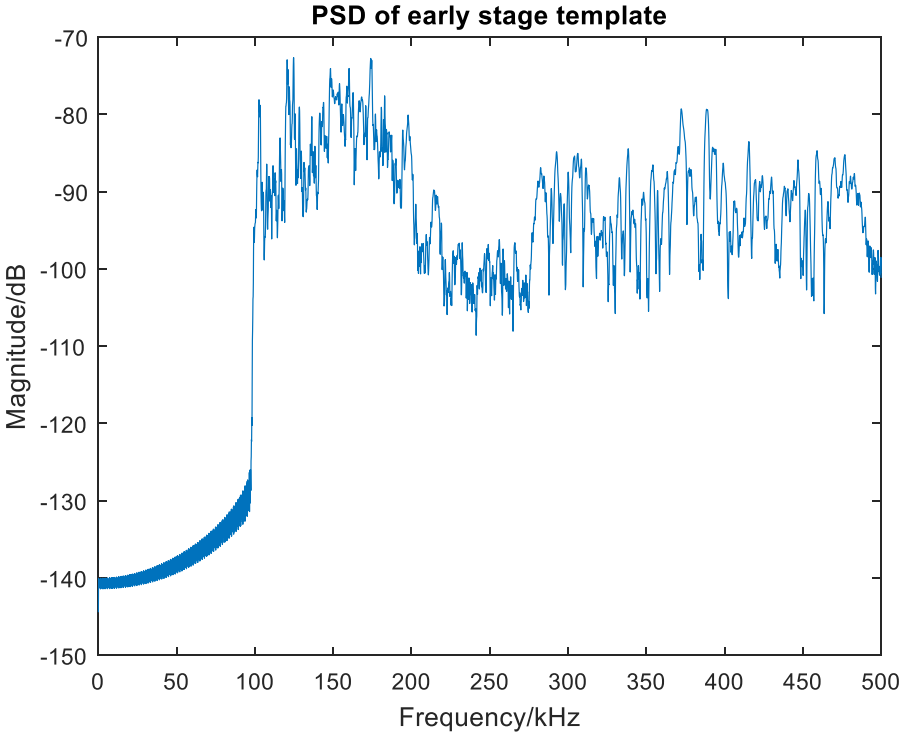

Figure 7-42: PSD of the selected template for early stage crack growth.

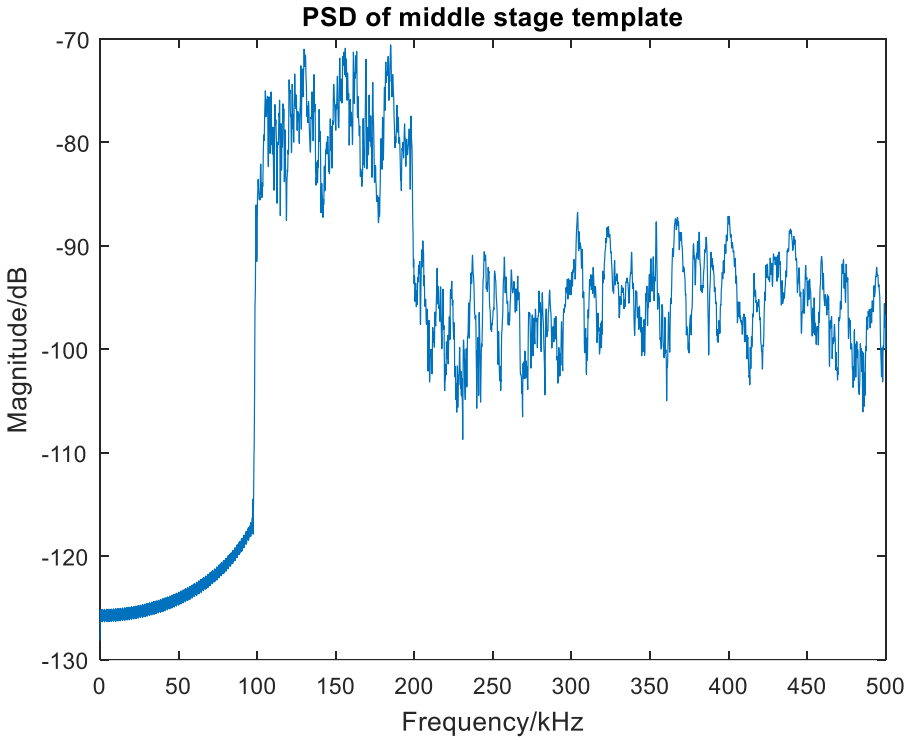

Figure 7-43: PSD of selected template for middle stage crack growth.

7.5.2 Wembley trial

As introduced in the previous chapter, a crossing on the West Coast Main Line near Wembley station known to be in good condition was considered for evaluation of the healthy condition. The selected crossing was visually inspected prior to testing with no visible defects evident. Therefore, no indication of crack growth was expected from the data analysis.

The plot in Figure 7-44 shows an example of raw acoustic emission signal generated by a passenger train. The four peaks of high amplitude are predominantly generated from the powered axles which cause sliding of the wheels. As the passenger train was passing through the detection zone of the instrumented crossing, no wheel impacts are visible in the raw signal.

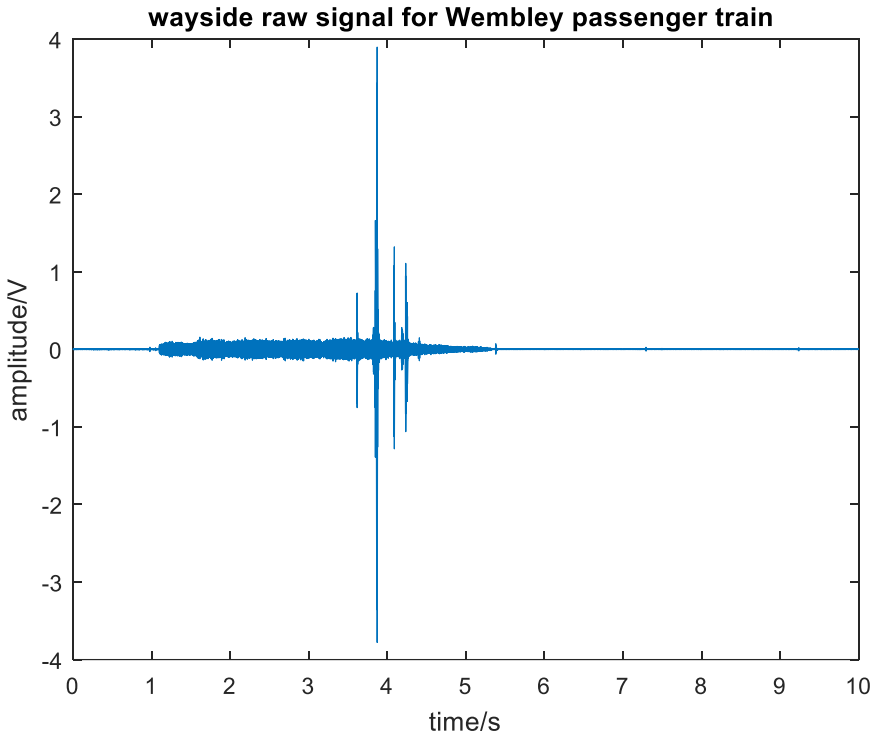

Figure 7-44: Raw acoustic emission signal obtained from passenger train going over the Wembley crossing.

The spectral coherence result using early stage template is provided in Figure 7-45. The result shows that the correlation is higher when a train runs over compared with the result obtained for purely background noise.

This result indicates that no crack damage is present in the crossing. The conclusions are validated by the results using middle stage template, shown in Figure 7-46.

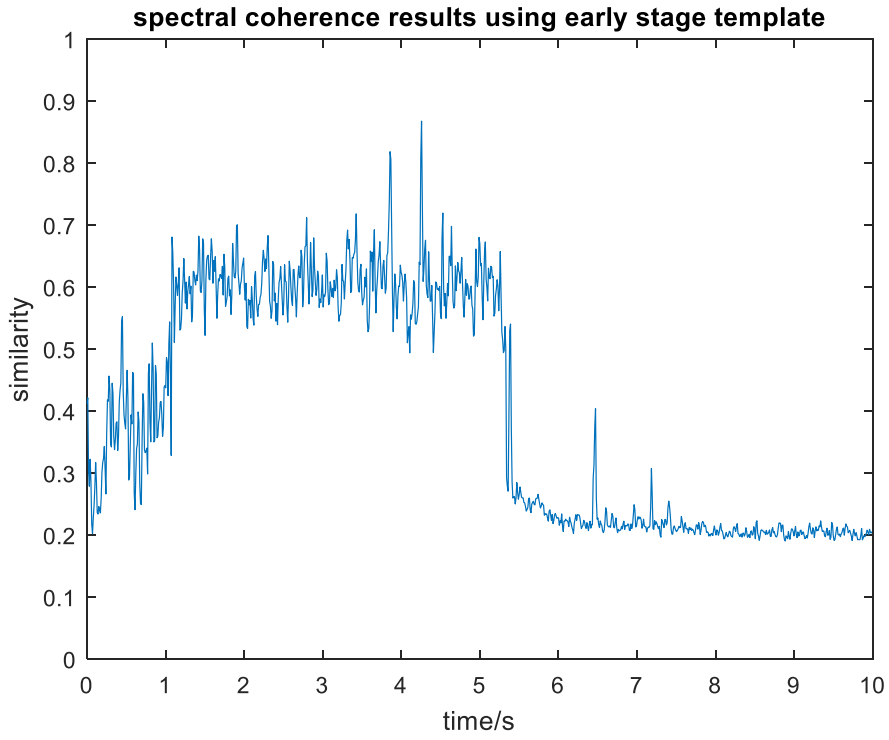

Figure 7-45: Spectral coherence result for the Wembley crossing loaded by a passenger train using the early stage template.

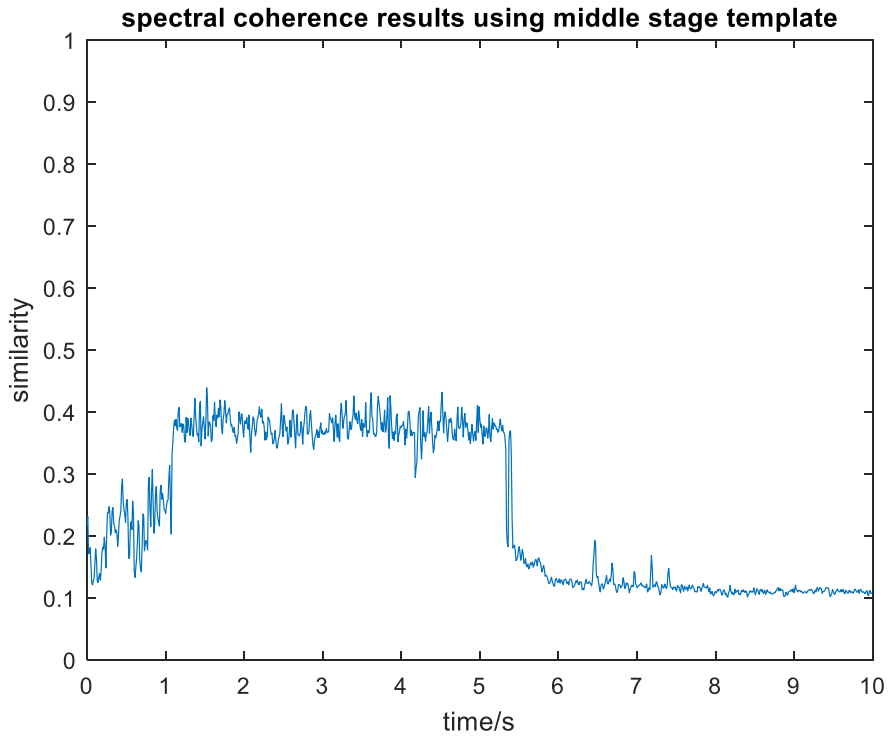

Figure 7-46: Spectral coherence results using the middle stage template.

A raw signal from a freight train is shown in Figure 7-47. Only part of the freight train is seen in this measurement due to the length of the entire train. The high-amplitude peaks seen at the start of the signal are caused by the powered axles of the locomotive. Spectral coherence results using both templates are provided in Figure 7-48 and Figure 7-49. There is no indication of crack growth from the results obtained. Figure 7-48 also indicates that the PSD of the dominant peaks at the start of the signal is so different from the middle stage template that the similarity result is even smaller than the background noise.

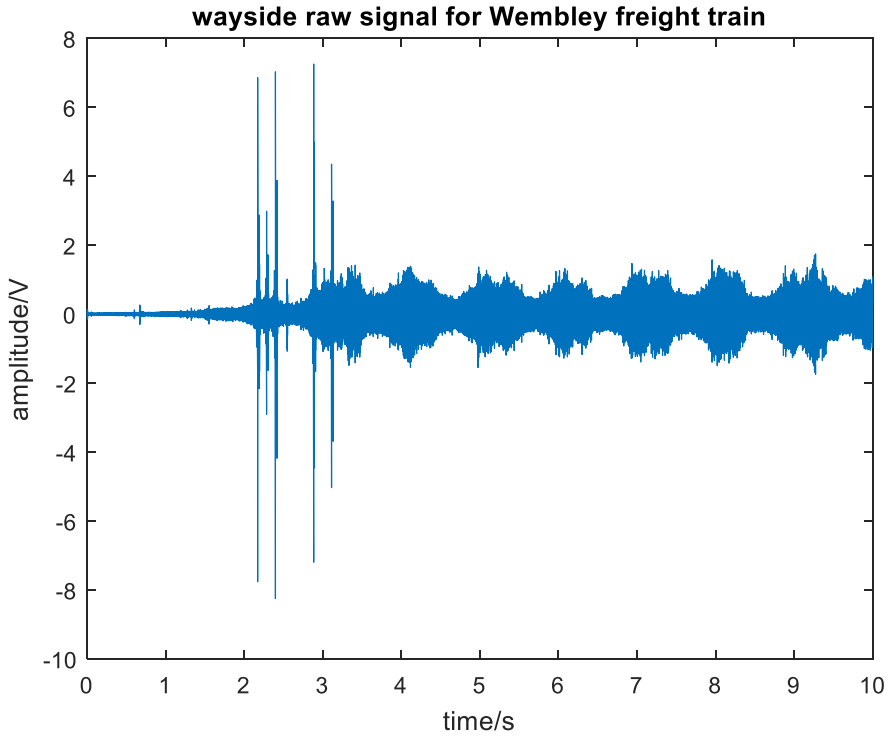

Figure 7-47: Raw acoustic emission signal of freight train loading the Wembley crossing.

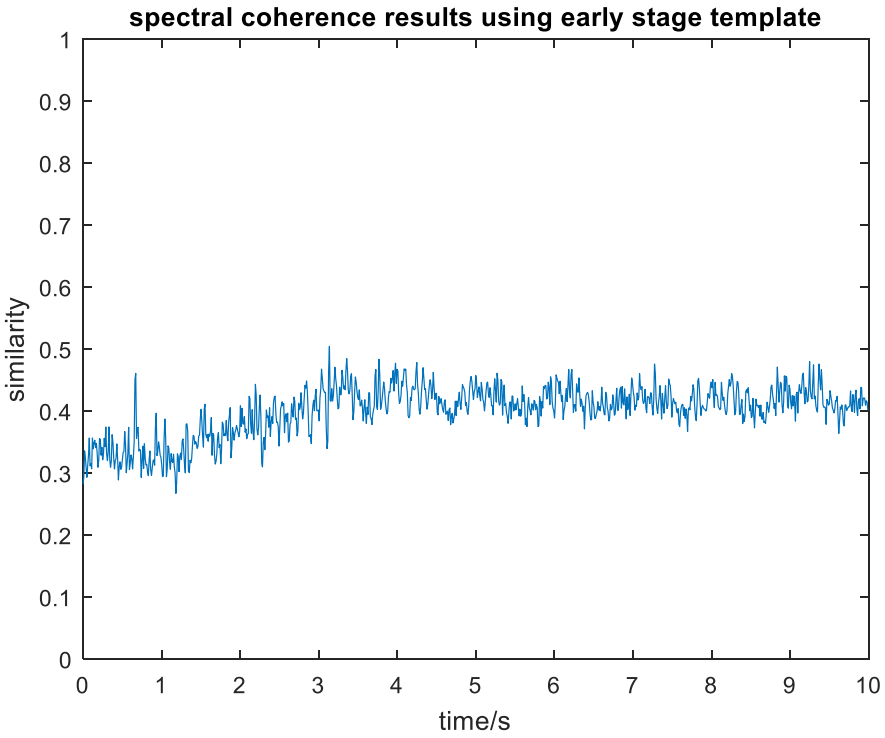

Figure 7-48: Spectral coherence results using the early stage template.

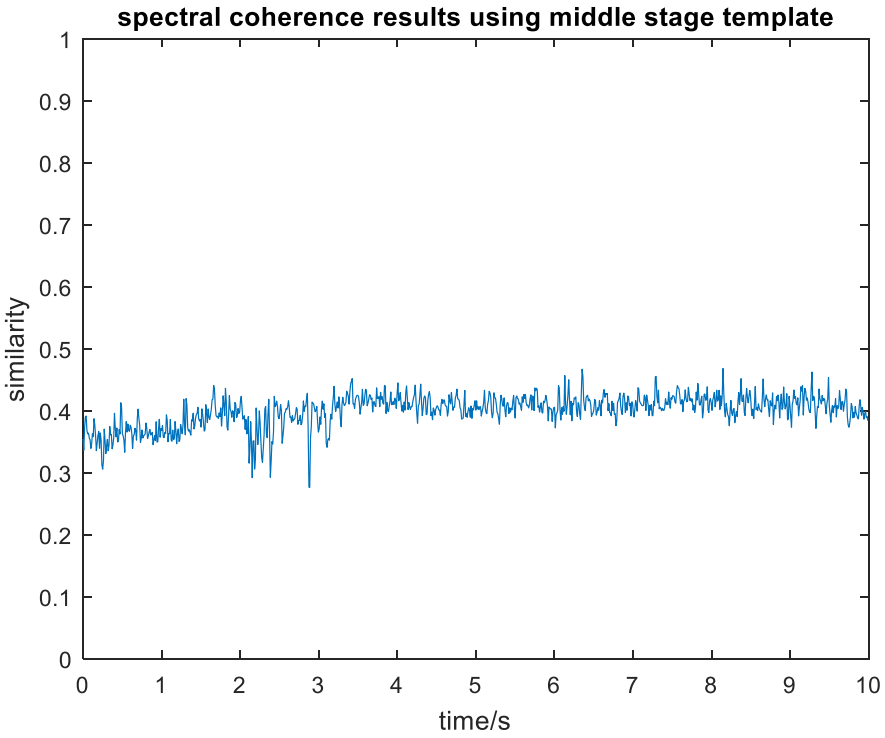

Figure 7-49: Spectral coherence results using the middle stage template.

7.5.3 Hatton trial

The cast-manganese crossing monitored at Hatton has been visually examined and identified to have minor surface damage. The same data analysis and templates used in Wembley trial are also applied here to evaluate the severity of the crack.

Figure 7-50 shows the raw signal for a passenger train loading the instrumented crossing. Amplitude of acoustic emission bursts are much higher compared to the Wembley test despite the fact that it is the same type of the train operating on both line. The plot in Figure 7-51 shows the correlation results using the early stage template. There are clear peaks indicating crack growth when the bogie is loading the crossing. Figure 7-52 shows the results based on the use of the middle stage template. A dominant peak is visible at around 0.5 s indicating crack growth damage that happens in moderate stage. Therefore, the results suggest that the Hatton crossing has early stage crack damage which is gradually developing when the crossing is loaded.

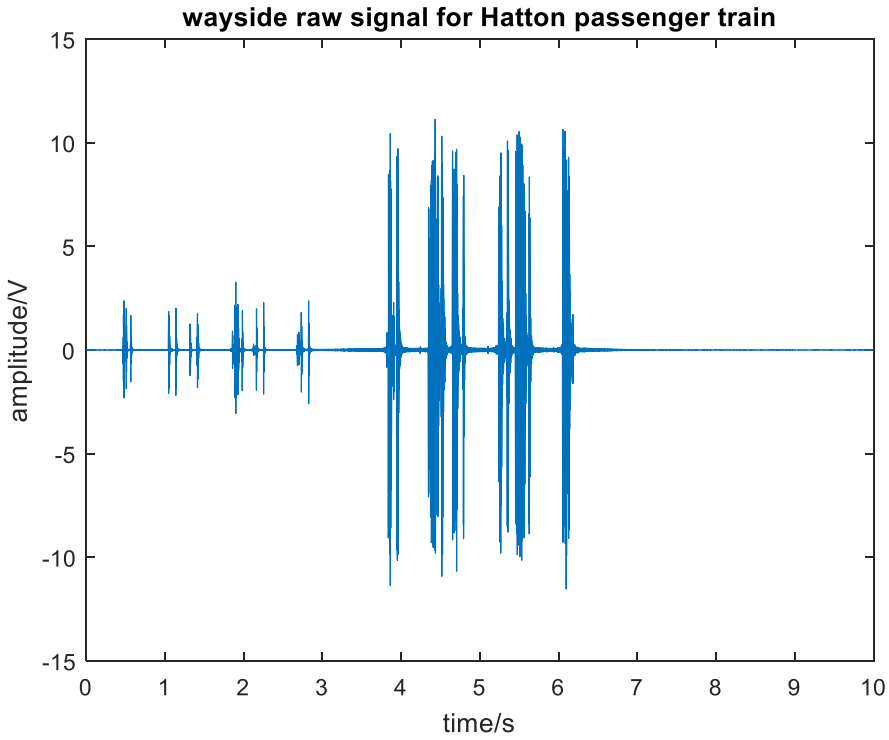

Figure 7-50: Raw acoustic emission signal generated from a passenger train loading the Hatton crossing.

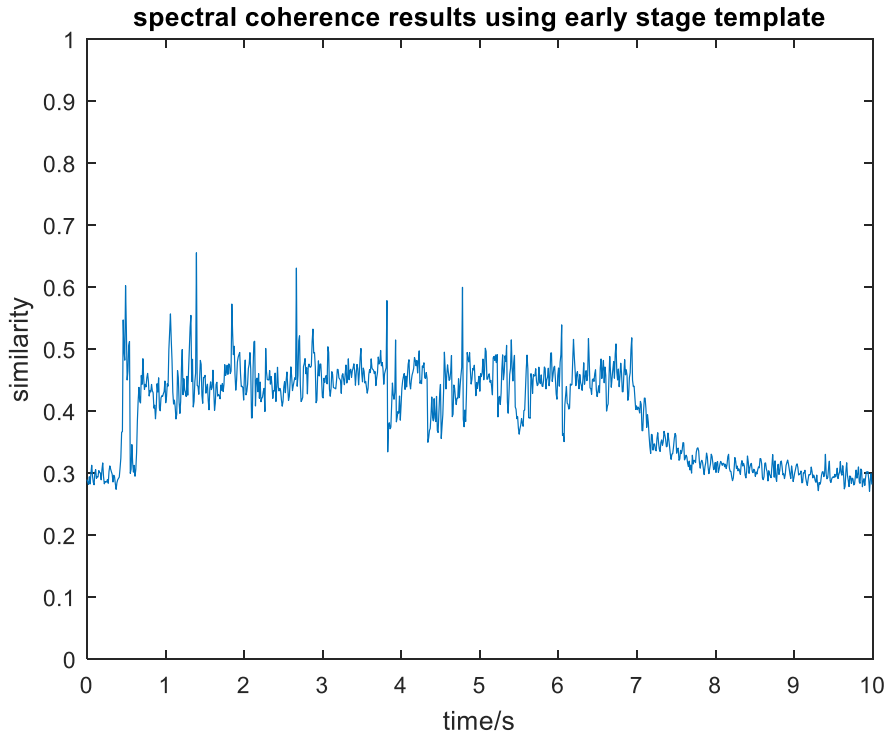

Figure 7-51: Spectral coherence results using the early stage template.

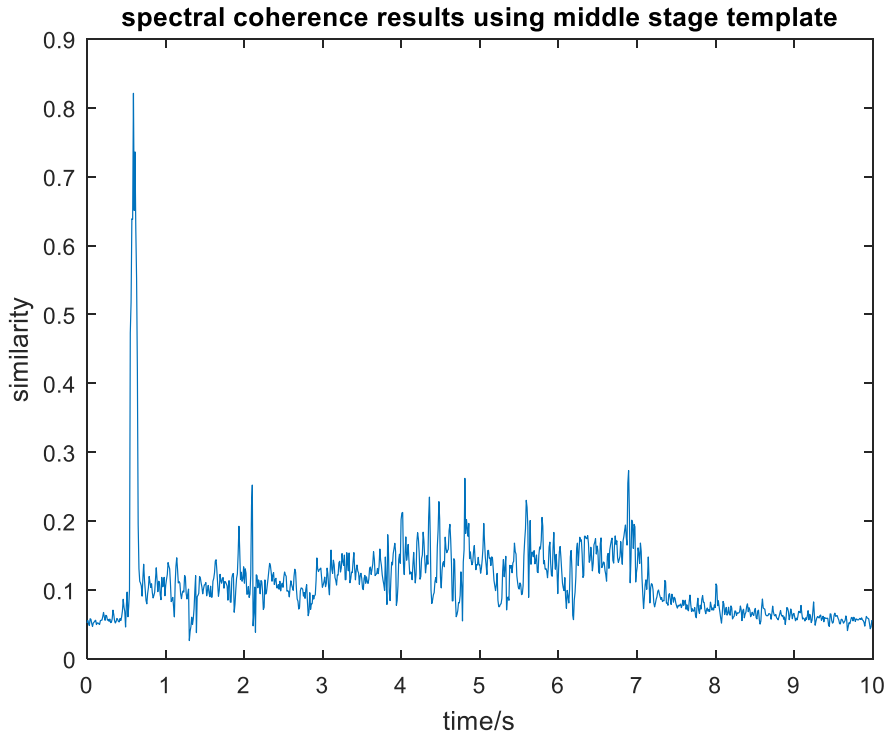

Figure 7-52: Spectral coherence result using the middle stage template.

Figure 7-53 shows the raw acoustic emission signal generated when the crossing was loaded by the wheels of a passing freight train. Each low-amplitude peak is related to the loading from each wheel. The high-amplitude peaks in the middle of the signal are most likely caused by the heavy wheel impact. Sometimes it is difficult to identify whether a peak is produced by crack growth in the crossing or wheel impact from the vehicle. If such is the case, spectral coherence technique can provide better insight by comparing normalised spectral distribution.

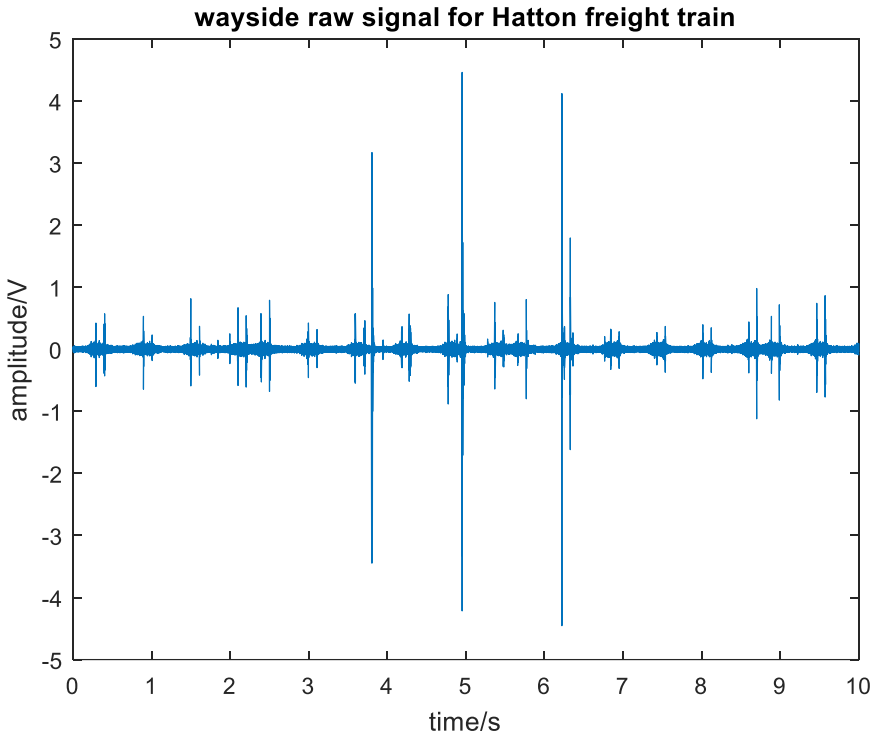

Figure 7-53: Raw acoustic emission signal generated by a freight train loading the Hatton crossing.

Figure 7-54 shows the spectral coherence result when using the early stage template. Peaks are evident in the plot generated, indicating that damage growth in at the early stage. Figure 7-55 shows the result after applying the middle stage template. The smaller peaks are no longer visible in the graph, as they are not caused by the middle stage damage mechanism. However, the dominant peak at the 5 s shows up with high similarity results. It indicates faster damage evolution for that particular loading event.

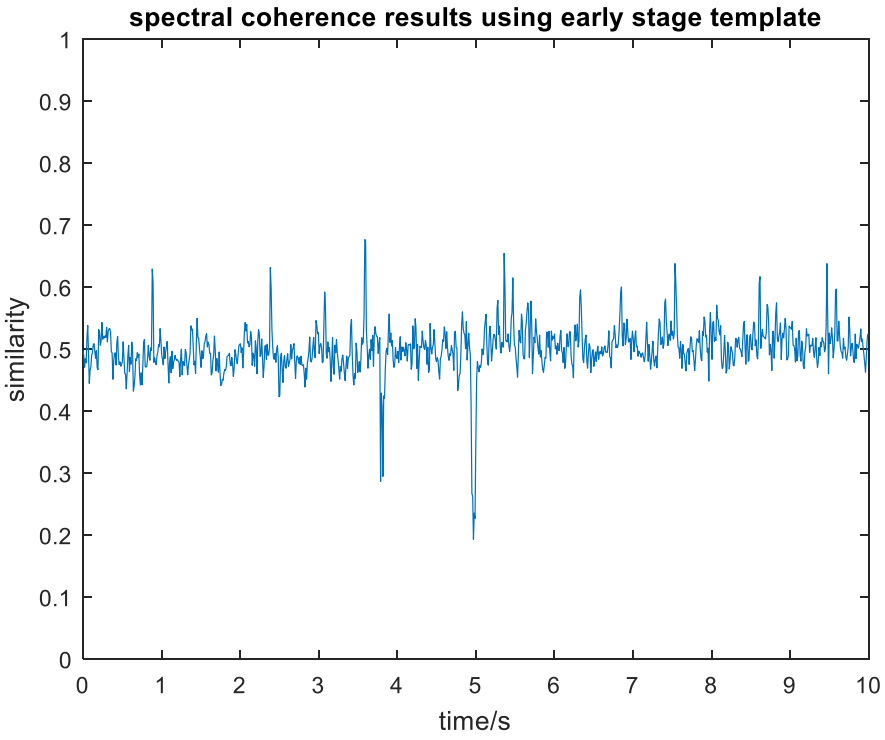

Figure 7-54: Spectral coherence results using the early stage template.

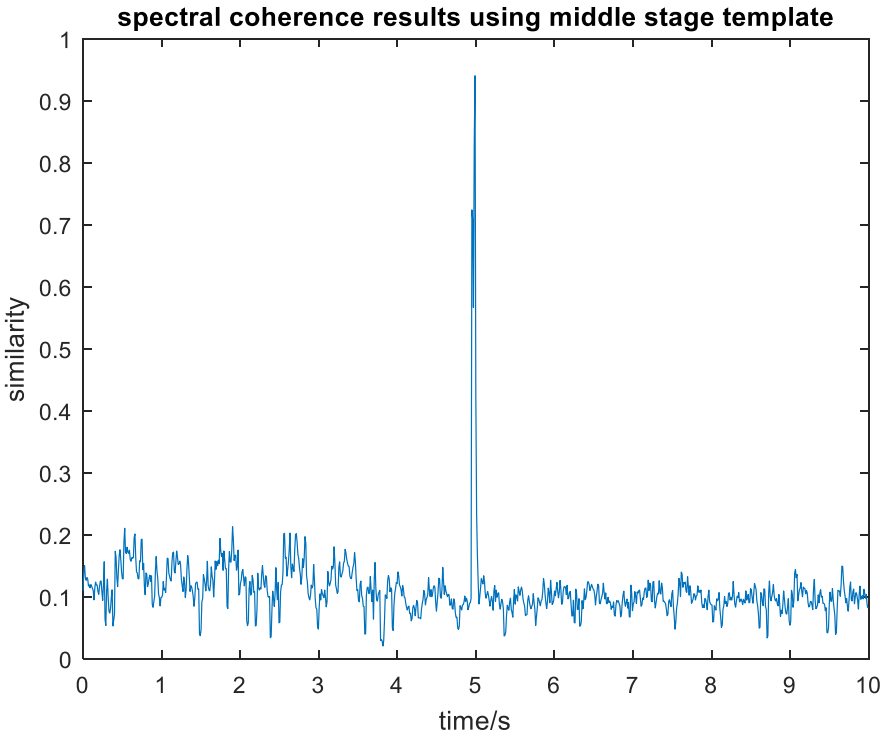

Figure 7-55: Spectral coherence results using the middle stage template.

Based on the results of the analysis presented above, it is plausible to conclude that the Hatton crossing is affected by damage at early stage, gradually propagating with subsequent loading cycles from passing trains.

7.5.4 Watford trial

A severely damaged crossing was reported by the Network Rail maintenance department on the West Coast Main Line in the area of Watford Station. Visual inspection revealed a large crack in the foot of the crossing. The crossing had been scheduled to be replaced within two weeks-time depending on the speed of deterioration. An ESR of 32 km/h (20 MPH) had also been imposed. Traffic passing over the crossing involved both passenger and freight trains.

Figure 7-56 shows the raw acoustic emission signal generated by a passenger train passing over the instrumented crossing in Watford. Peaks with high amplitude are clearly present in the graph. Spectral coherence processing was carried out to process the data with both early and medium stage templates. Figure 7-57 and Figure 7-58 show the similarity results obtained following the analysis.

The results obtained indicate that the crack damage does not belong to the early stage category with similarity results lower than the background level. On the contrary, it fits well with the middle stage template with evident high amplitude peaks present in the graph.

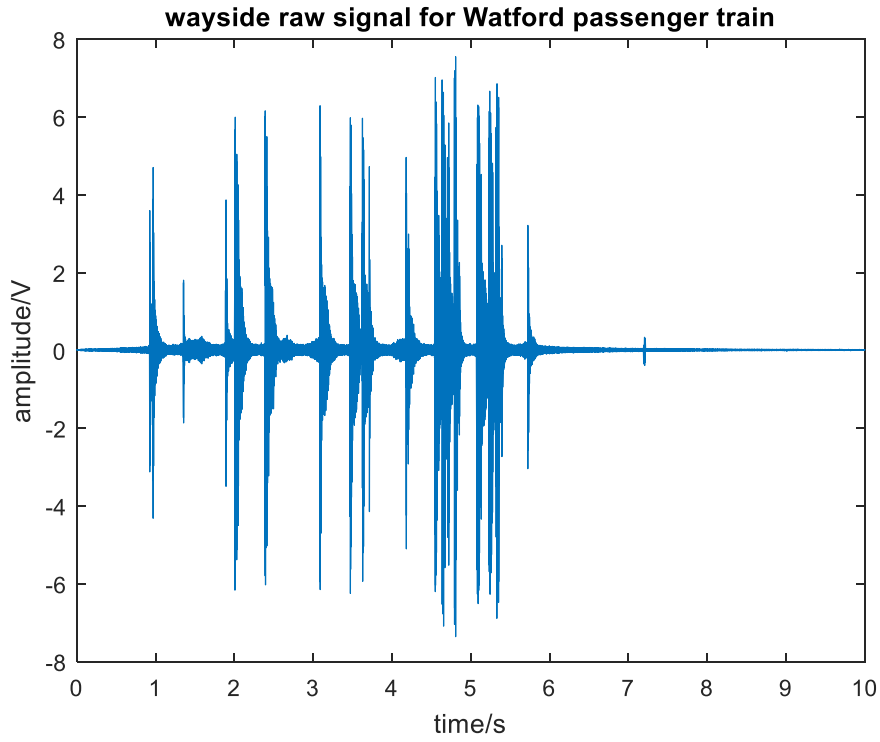

Figure 7-56: Raw acoustic emission signal of passenger train loading the Watford crossing.

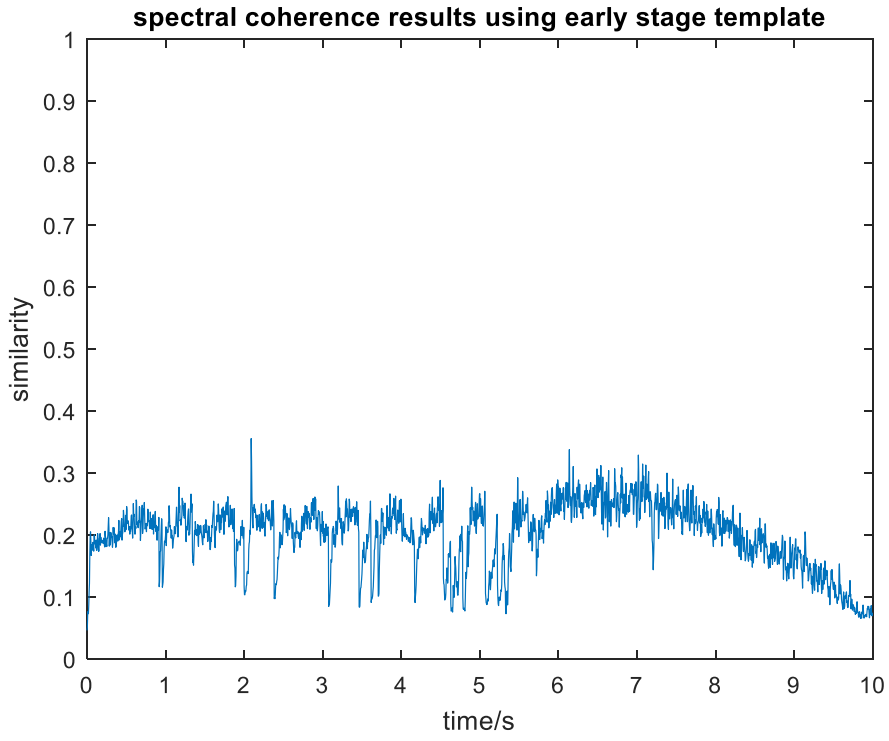

Figure 7-57: Spectral coherence results using the early stage template.

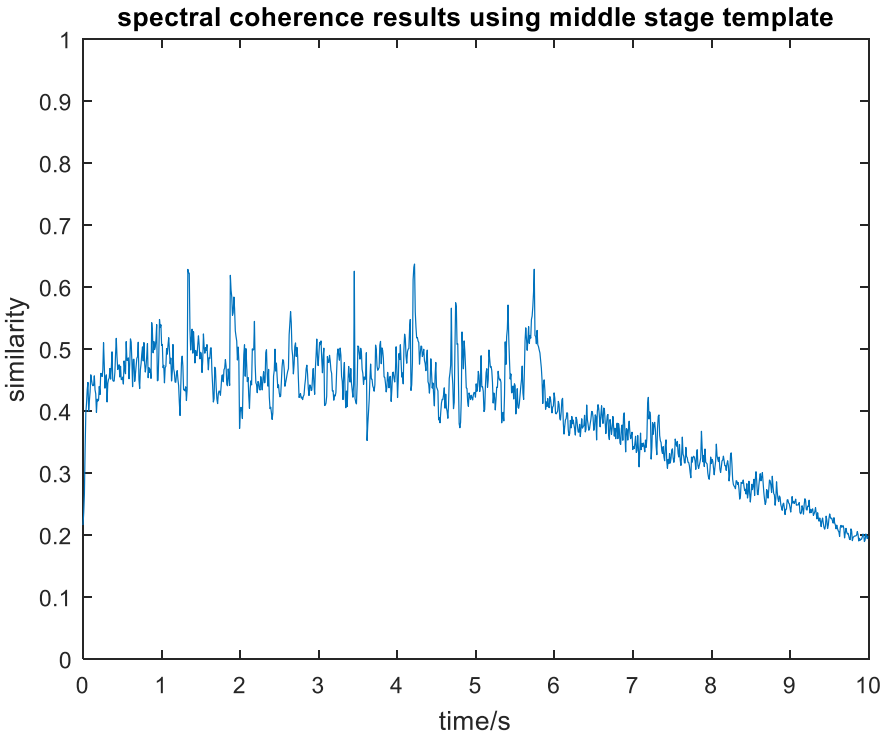

Figure 7-58: Spectral coherence results using the middle stage template.

The same processing technique was applied on the raw signal generated by a freight train loading the crossing. The raw acoustic emission dataset obtained is shown in Figure 7-59. The plot resembles the raw signal from the laboratory test with peaks indicating crack growth under loading events. Figure 7-60 shows the result using the early stage template. It clearly shows that the raw signal does not have any peaks related to early stage damage mechanism. Instead, as shown in Figure 7-61, the crack damage is much more likely to be in the middle stage with damage growth peaks evident for almost every loading cycle. The high-amplitude peak at around 7.8s in Figure 7-59 appears to be related to wheel impact as the spectrum feature does not match either early stage or middle stage template.

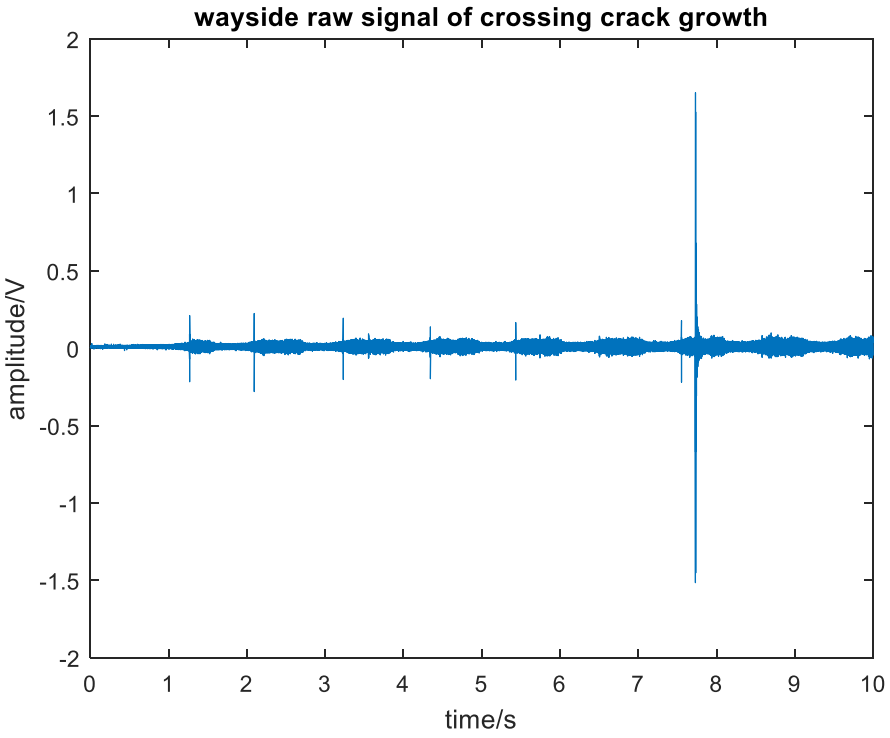

Figure 7-59: Raw acoustic emission signal generated by freight train loading the Watford crossing.

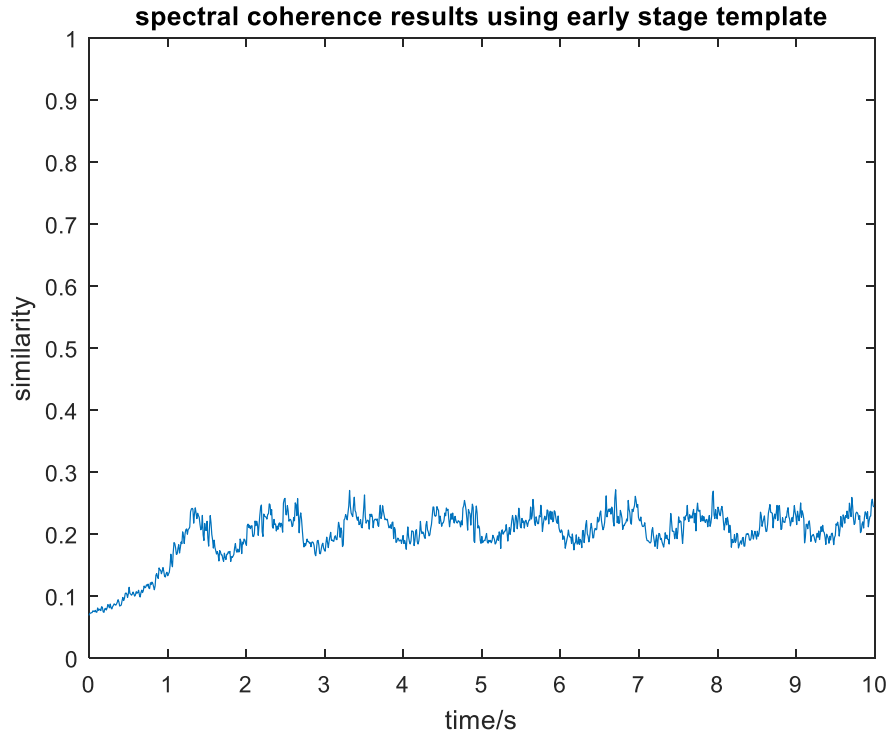

Figure 7-60: Spectral coherence results using the early stage template.

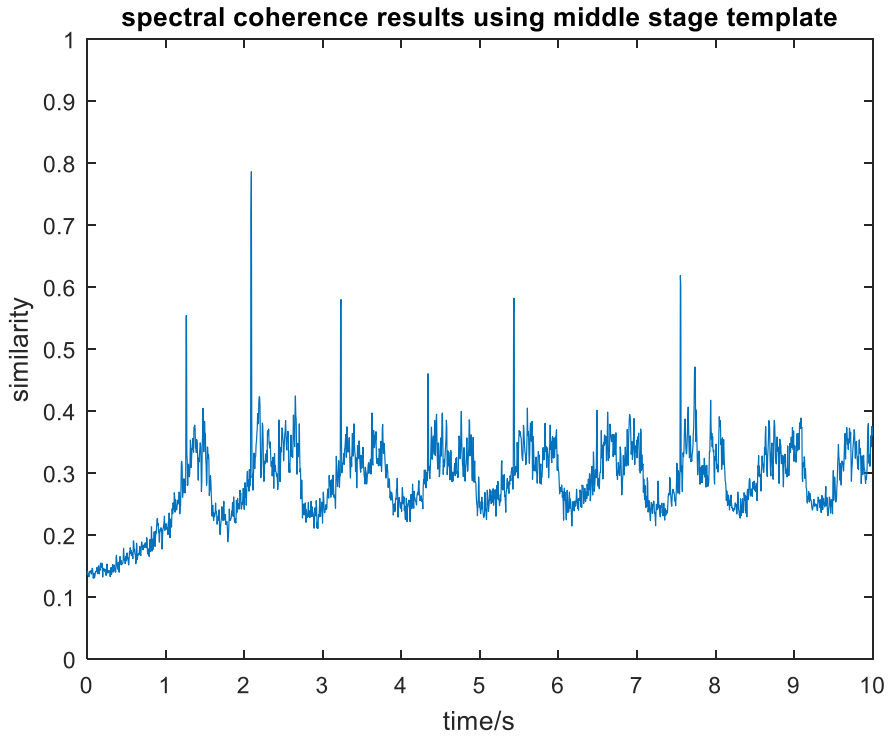

Figure 7-61: Spectral coherence results using the middle stage template.

As a conclusion, with the help of accurate templates, spectral coherence technique has been proven to be a possible technique for processing complex acoustic emission signals that can be used to identify crack growth and evaluate damage severity.

7.6 Case study for system correlation

Three levels of system correlation have been introduced in the previous chapter in order to establish the decision support tool. Details of each system correlation will be provided using a case study. The idea of sensor-level correlation is explained by applying sensor fusion technique to datasets obtained by multiple acoustic emission sensors. Object-focused correlation is elaborated with the help of rolling stock monitoring using acoustic emission, vibration and temperature signals. The system-level correlation is briefly introduced with the idea of combining rolling stock data with crossing data.

7.6.1 Sensor-level correlation

The system installed at Cropredy consists of four acoustic emission sensors, which have been installed to monitor the wheelsets of passing passenger and freight rolling stock. The sensor layout was presented in Chapter 6. Spectral coherence technique based on individual AE sensors was introduced and proven earlier in this chapter.

In addition, more information about the rolling stock can be discovered by applying sensor fusion techniques, including train speed, bogie position and axle load imbalance identification.

Figure 7-62 to Figure 7-65 show the raw acoustic emission signal obtained for each individual sensor or channel. It should be noted that when this dataset was recorded the Channel 1 of the amplifier had failed and thus the signal acquired is just background electrical noise. However, from the remaining channels in operation it can be seen from the graph obtained that the acoustic emission signals collected from each side do not match, indicating strong axle load imbalance.

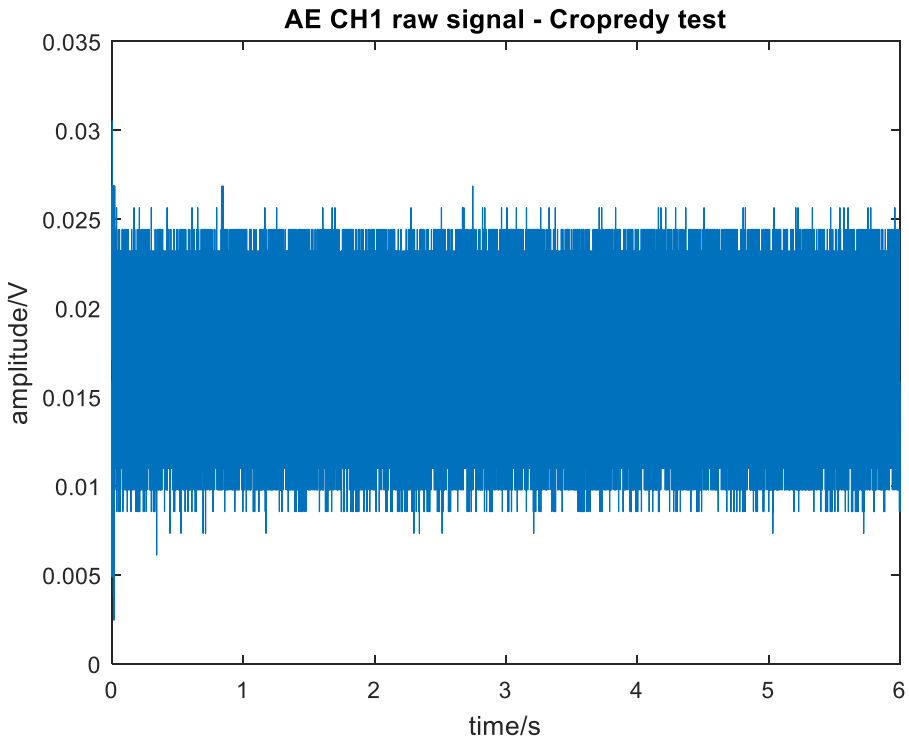

Figure 7-62: Raw acoustic emission signal from faulty Channel 1 sensor.

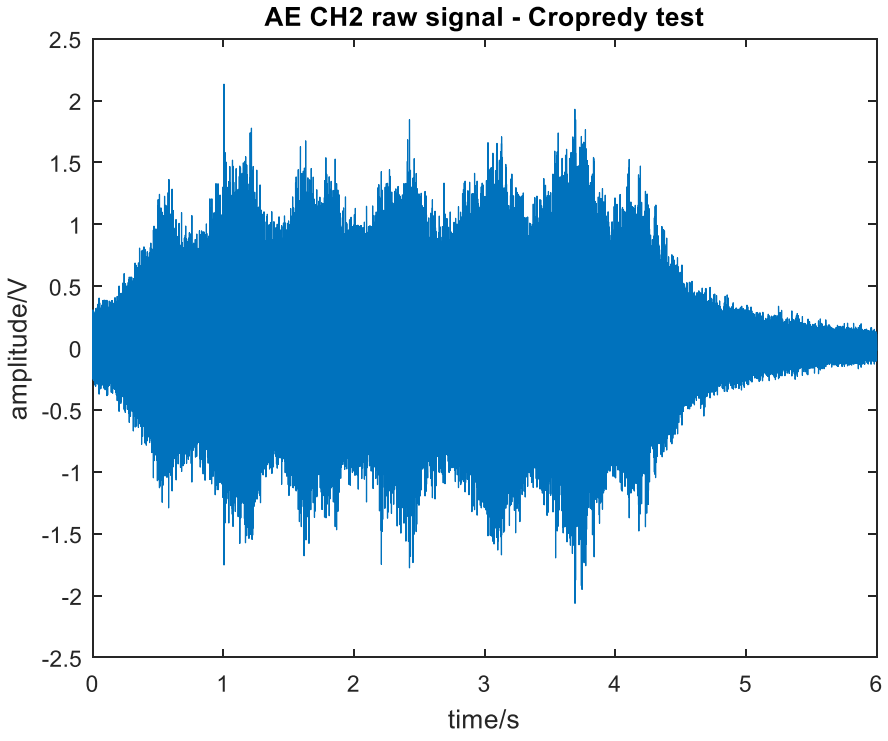

Figure 7-63: Raw acoustic emission signal for Channel 2.

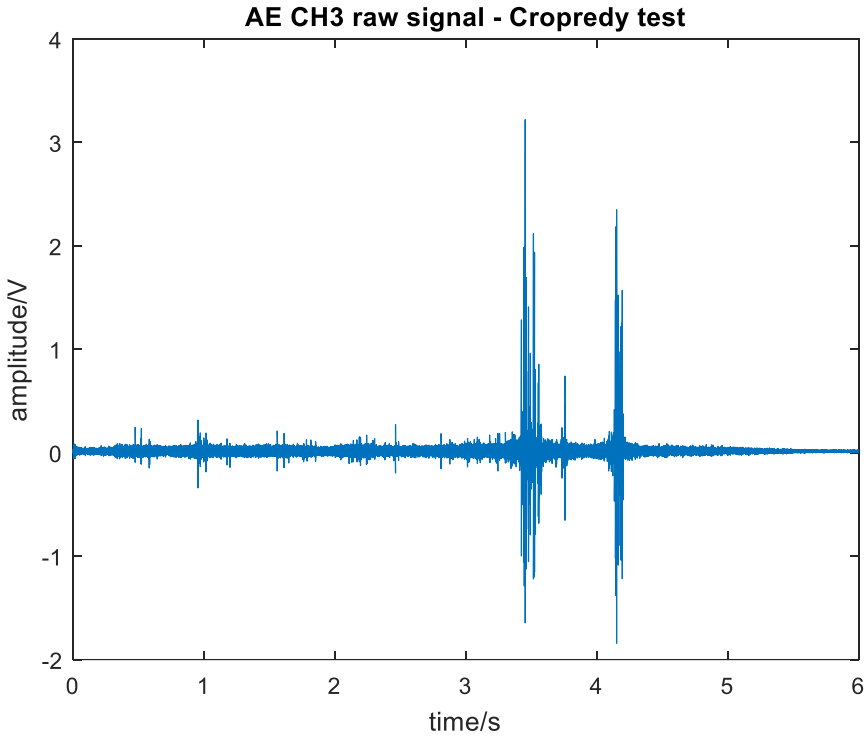

Figure 7-64: Acoustic emission raw signal for Channel 3.

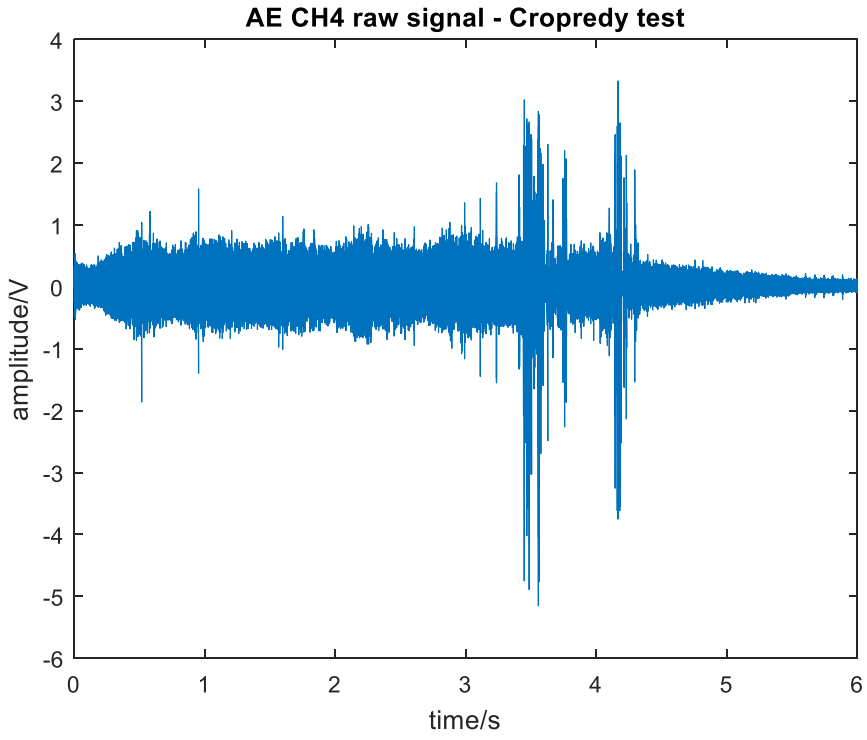

Figure 7-65: Raw acoustic emission signal for Channel 4.

Sensor fusion is carried out in several aspects:

1. By comparing the correlation of two acoustic emission sensors at either side, any defective sensor can be identified. It provides the function of sensor self-test. The threshold value is pre-determined depending on the characteristics of sensor used.

In this scenario, the threshold value is set to be $2.8e^5$. The cross-correlation result for the CH1 & CH2 side is $3.08e^4$, while for the other side is calculated to be $3.9e^5$. Therefore, a warning is provided to the user that one of the sensors may be defective in CH1 & CH2 side.

2. By applying data fusion to two acoustic emission sensors at the same location at either side, namely CH1 & CH3 and CH2 & CH4, the envelope of a fused signal can be constructed as shown in Figure 7-66. Such a fused signal can be used to obtain more information about the condition of the wheelsets of the measured trains.

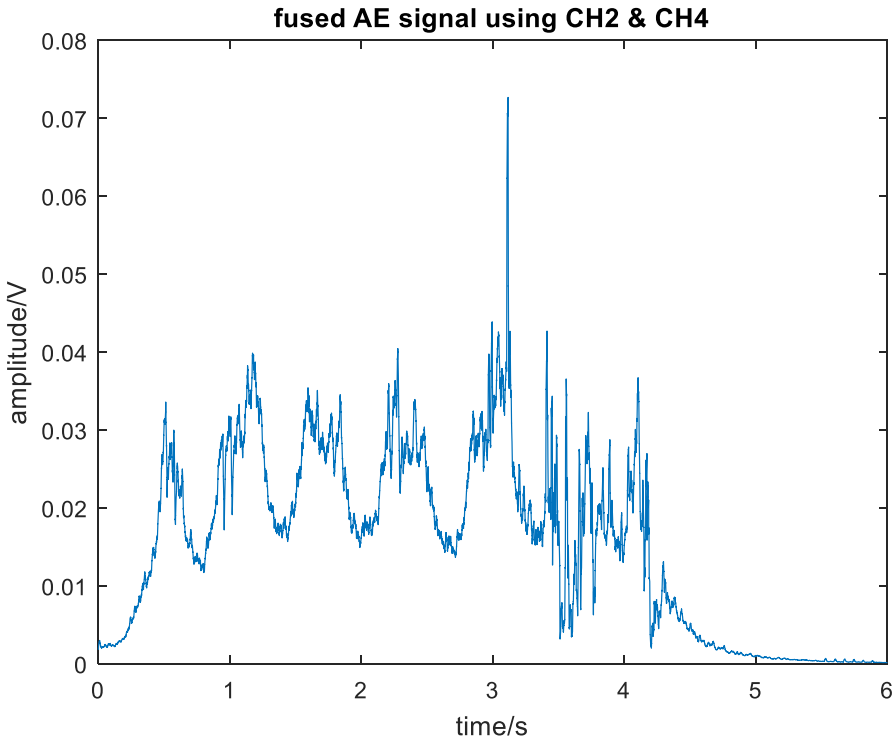

Figure 7-66: Envelope of the fused acoustic emission signal using CH2 & CH4.

The first step is to find all possible peaks that can be generated by each wheel. This is achieved by using local maxima analysis. All the potential peaks are shown in Figure 7-67. The result is then refined with predefined rules to eliminate false values, including minimum peak value, minimum peak distance and minimum peak prominence.

For example, since the maximum line speed is known to be 160 km/h (44.44 m/s) and the interval between two wheels is 2.6 m for Chiltern Class 168 passenger train, the minimum peak distance can be calculated as 0.058 s. In addition, the number of carriages for the passing train can be identified with dynamic local minima analysis, as shown in Figure 7-67 with red asterisk.

When the first wheel of the train passes over the treadle, it triggers the data acquisition. When the same wheel arrives at the first sensor, it generates the first local maxima value. Therefore, the train speed can be calculated with the time instance of the first maximum peak and the distance from the treadle to the first sensor as shown next:

$$v = {}^{d}/_{t} = \frac{18.5}{0.5128} = 36.08 \text{ m/s}$$

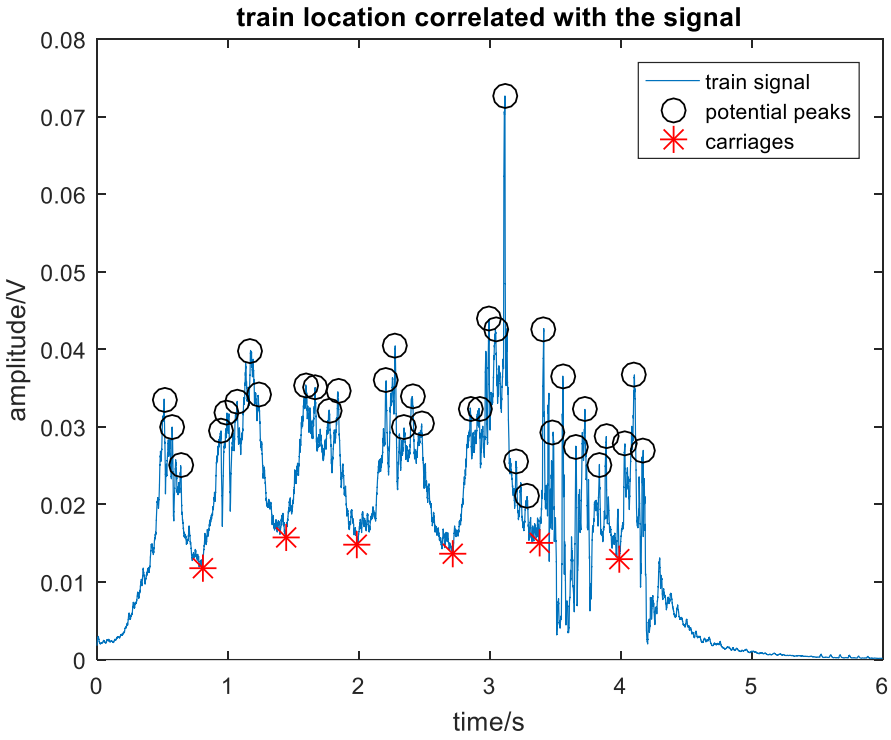

Figure 7-67: Peaks potentially generated by each wheelset.

Figure 7-69 shows location of each bogie annotated in the fused signal. The yellow asterisk represents the location of each wheel and the red line is bogie position. The findings can be validated with the train dimension of Chiltern Class 168 provided in Appendix D.

Table *7-2* shows the values calculated versus the values listed in the data sheet (Figure 7-68).

	Value calculated from fused data	Value listed in the datasheet
1	13.45 m	13.4 m
2	2.57 m	2.6 m
3	4.69 m	5.01 m

Table 7-2: Comparison of train dimensions

The sensor fusion technique discussed herewith can provide the same capability as the optical sensor to identify the position of the train with the fused signal.

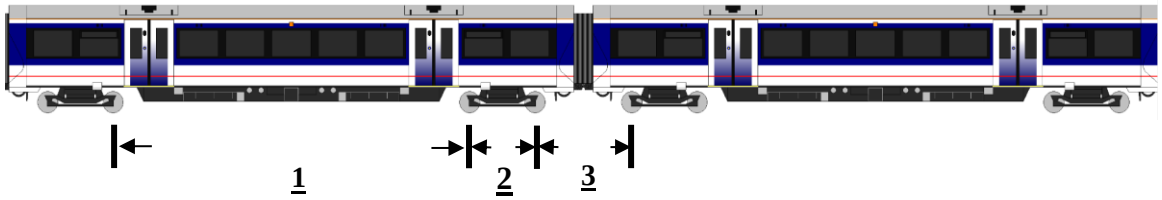

Figure 7-68: Diagram showing the configuration of Class 168 passenger train operated by Chiltern Railway.

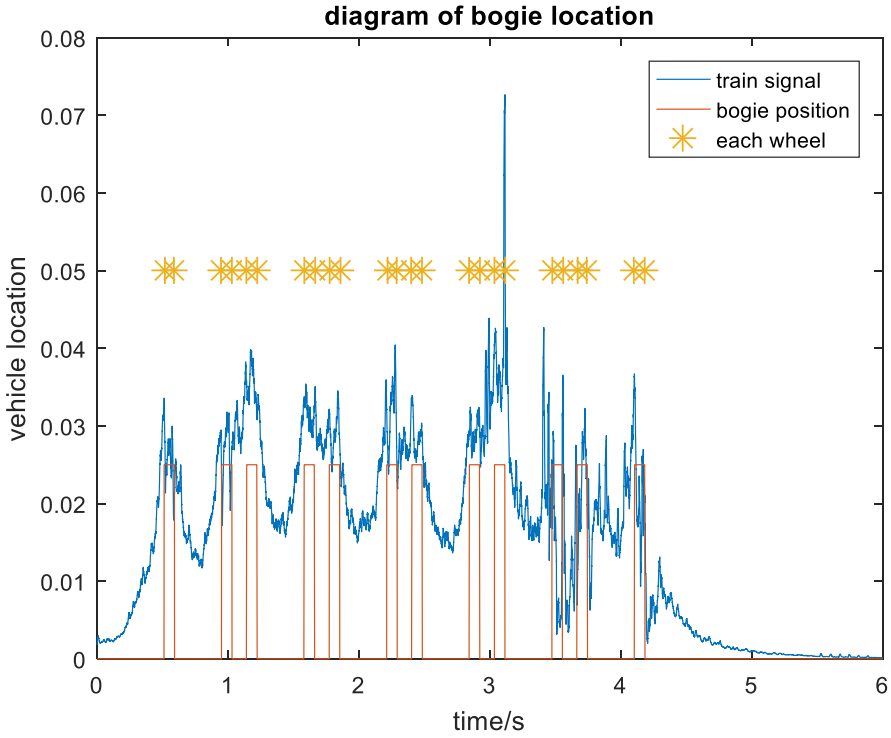

Figure 7-69: diagram of each bogie location correlated to the fused signal

Figure 7-70 provides a summary of the effectiveness of the sensor fusion technique in data analysis. As it can be seen, the sensor fusion technique considered in this study can be used to calculate the train speed as well as the time when each wheelset passed over one of the acoustic emission sensors. Moreover, it provides the ability to truncate the signal of interest from the raw data, which greatly reduces the size of the file to be processed.

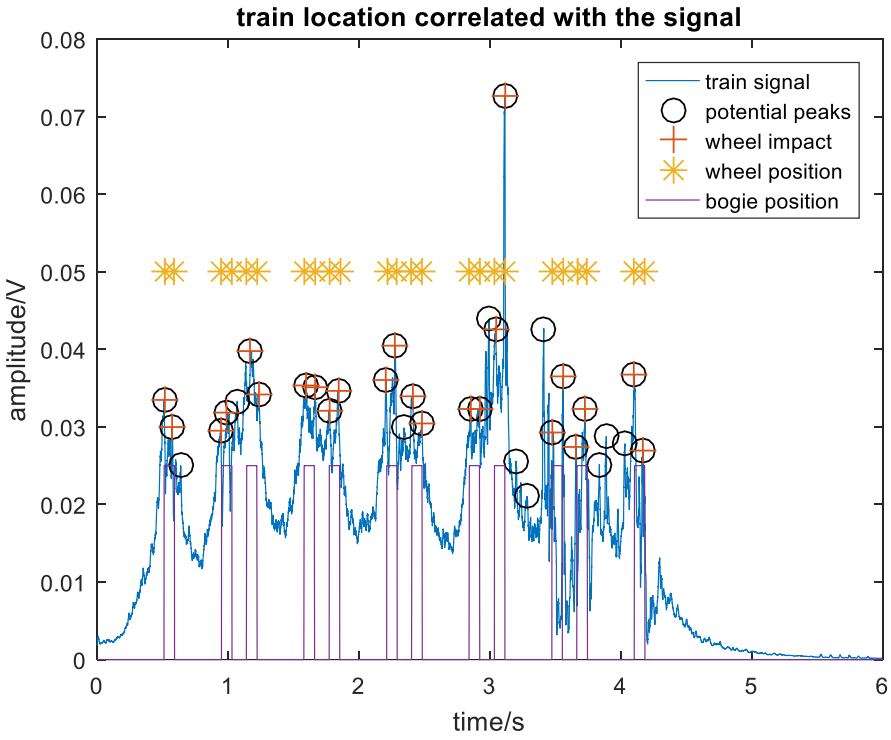

Figure 7-70: Graph showing the location of wheelsets, bogies and corresponding peaks from the fused signal.

Axle load imbalance can be identified by calculating the correlation of two acoustic emission sensors at the same location at either side.

3. The methodology is the same as described earlier, by setting threshold in advance for axle load imbalance. In this example, the threshold is determined to be $3.5e^6$. The cross-correlation result is $2.8e^6$ for CH2 & CH4, which indicates the imbalance of axle load. The conclusion can be easily confirmed from the difference of raw signal of CH2 and CH4.

7.6.2 Object-focused correlation

As explained in the previous chapter, object-focused correlation can greatly improve the reliability of detection and provide comprehensive information about the target from different

perspective. A case study based on rolling stock condition monitoring is proposed here to explain the idea of object-focus correlation.

The rolling stock can be monitored by considering acoustic emission, temperature and vibration signals. Currently in order to achieve this, different types of wayside systems need to be included, such as the customised monitoring system, HABD and WILD. The capability of acoustic emission signals in detecting bearing and wheel defects has already been proven as discussed earlier in the present chapter. The effectiveness of vibration analysis needs to be investigated in more depth.

Figure 7-71 shows the wayside vibration signal obtained for the axle bearings with severe lubricant contamination. It can be seen that vibration is less sensitive to the bearing defect than acoustic emission. This is due to the fact that the accelerometer measures the vibration movement rather than the elastic stress waves propagating through the structures. As long as the bearing defect does not generate abnormal vibration, axle bearing defects are hard to be identified using accelerometers. The peak in the vibration graph corresponds to wheel impacts as they go over the rail joints present on the test track before re-railing.

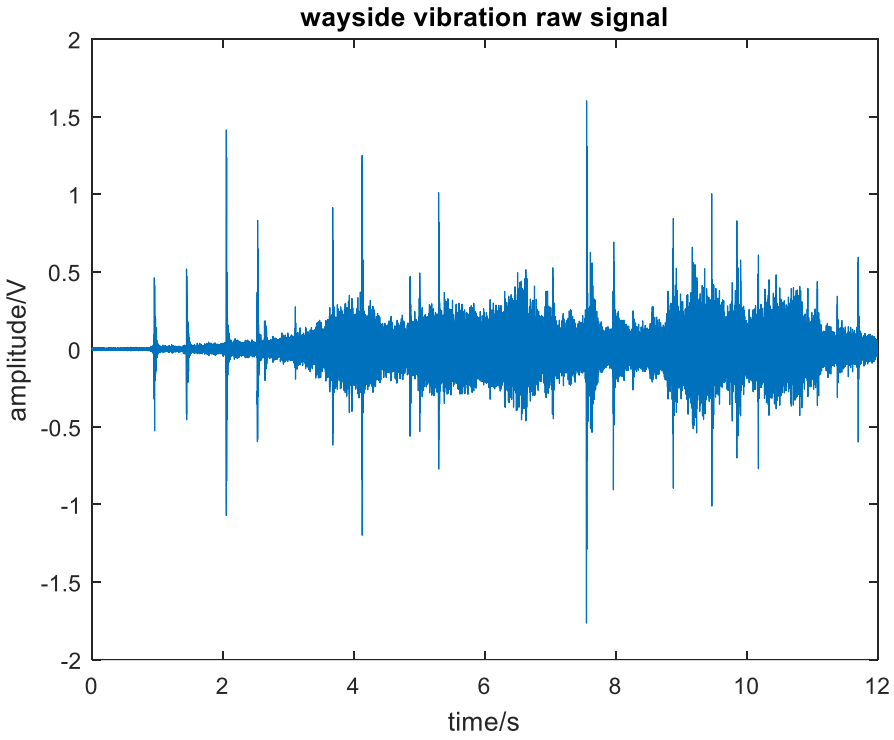

Figure 7-71: Wayside vibration raw signal for the test involving the axle bearing with lubricant contamination.

Nonetheless, accelerometers are very sensitive to wheel flat impacts. As shown in Figure 7-72, a high-amplitude peak is visible at around 6.8 s. It is more distinguishable after moving RMS processing has been carried as shown in the plots presented in Figure 7-73 and Figure 7-74.

As the two datasets were carried out under the same condition, the shape of the waveform remains similar, despite the difference caused by different train speed and the peak of the wheel flat at 6.8 s. As a result, acoustic emission is able to identify both bearing defects and wheel flat, while vibration is more applicable at detecting wheel flats, but fails to detect bearing defects unless damage have reached critical level and affects wheel rotation significantly.

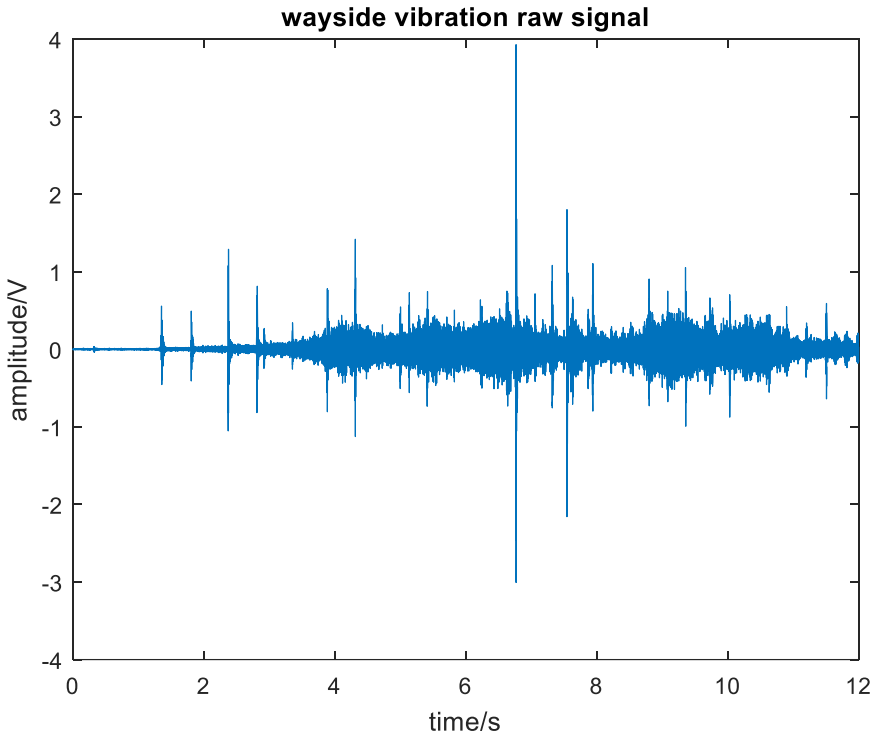

Figure 7-72: Wayside vibration raw signal for bearing contamination defect with wheel flat.

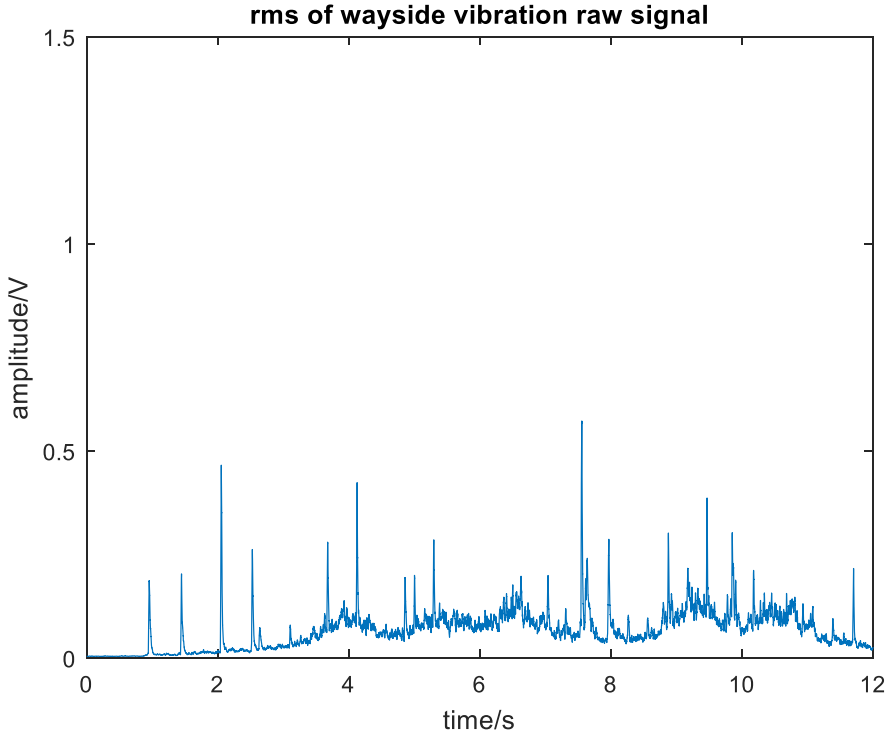

Figure 7-73: Moving RMS result for bearing contamination defect.

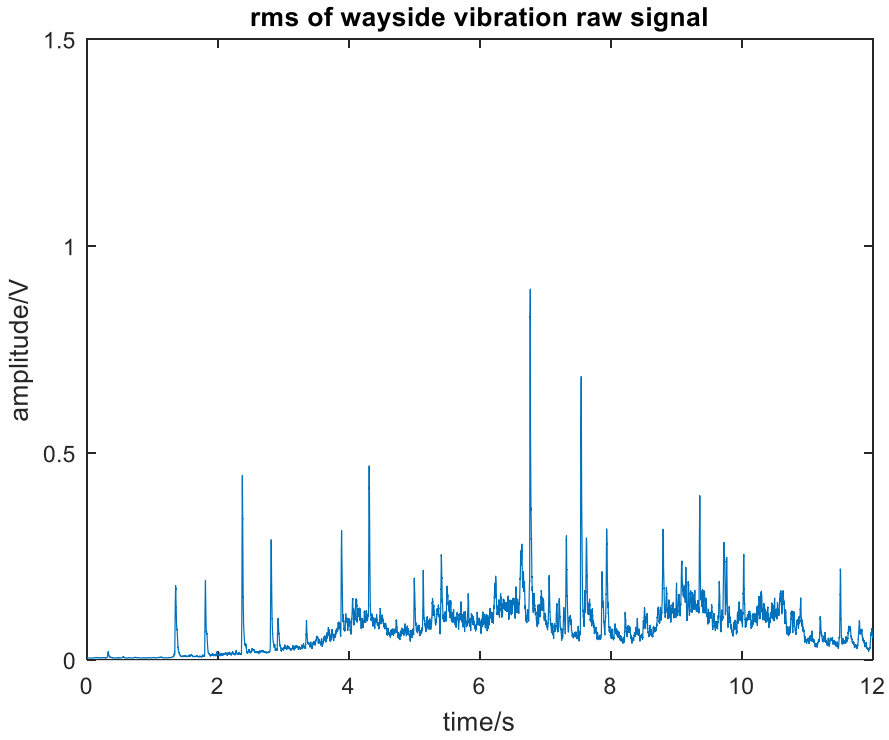

Figure 7-74: Moving RMS result for bearing contamination defect with wheel flat also present.

The HABD and WILD can only provide single value readings. Some typical results are included in the Appendix provided at the end of this thesis. By installing these systems together, it becomes possible to cross-correlate and cross-validate the results obtained from different RCM systems. For example, if the HABD gives a warning, the result from the acoustic emission system can be used to validate the alarm so that it can reduce the number of false alarms. In addition, it is able to distinguish bearing and wheel defect by integrating the acoustic emission and vibration signals, as explained with the example of bearing contamination defect and wheel flat.

7.6.3 System-level correlation

As described earlier, the crack growth signal is generated by the loading event of each wheel passed over the instrumented crossing. Acoustic emission sensors will inevitably record unwanted signals form the vehicle, such as wheel impact and noise form the engine. If such

interferences can be minimised, the signal-to-noise ratio (SNR) will be greatly improved so that the damage evolution in the affected crossing can be evaluated more accurately.

Such information is collected by the same customised RCM system installed at Cropredy to monitor the condition of wheelsets of passing rolling stock. By correlating these two systems together, it becomes possible to remove the background noise interference generated from the vehicle itself. In this way, the spectral distribution of the crossing crack growth signal can be isolated enabling more accurate analysis. Techniques based on machine learning and adaptive filter design could be applied as possible ways of addressing this particular problem in the future. However, before such techniques can be used reliably in railway RCM technologies several technical challenges should be addressed first.

Chapter 8:

Conclusions and future work

Chapter 8: Conclusions and future work

8.1 Conclusions

The importance of effective RCM for the rail industry is undeniable. The opportunities of inspection and maintenance will gradually become scarcer as global demand for rail transport intensifies rapidly. The rail industry at the moment at least is not ready to accommodate a rapid increase in passenger numbers and freight tonnage. A significant percentage of the existing maximum capacity of the rail networks around the world has already been used up. The construction of new lines and the implementation of upgrades through track renewals even if it is affordable cannot keep up with current growth trends and is already lacking behind the overall demand. It is thus absolutely critical that existing infrastructure operation is optimised by introducing new systems and innovation that promote higher traffic density and ensure operational RAMS. At the same time inspection and maintenance campaigns should be minimised to allow the rail network to be used as much as possible by passenger and freight trains. However, in order to achieve this it is essential that effective RCM and decision support tools are in place to ensure reliability and safety of both rail infrastructure and rolling stock.

This research has looked into the development of a customised high-frequency acoustic emission and vibration analysis capable of monitoring critical rolling stock and infrastructure components. Tests have been carried out under laboratory and actual railway operational conditions, whilst a Certificate of Acceptance for testing the customised RCM system on the rail network was obtained from Network Rail. Tests in the field were carried out under controlled conditions at the Long Marston test track as well as at various sites on the UK rail network with a permanently installed system at Cropredy. The Cropredy installation has been

active since September 2015, monitoring the wheelsets of about 200 trains passing through the instrumented site every day.

For the analysis of the acoustic emission and vibration signals acquired by the customised system various signal processing techniques have been considered including moving RMS, HFRT and correlation processing based on selection of appropriate templates and feature extraction. A decision support tool has been implemented to be used in combination with the data generated by the customised RCM system.

The results obtained have clearly shown that the technique developed during this study can be used for the effective online evaluation of axle bearing and wheel defects in rolling stock and propagating cracks in cast manganese crossings. This has been supported by appropriate tests carried out under laboratory conditions as well as in the field under actual operational conditions.

8.2 Future work

In this work, a prototype of novel wayside RCM system has been designed. There are still a lot can be done to improve the performance of such system from the perspective of hardware, software and advanced data processing techniques.

The current system can be expended to measure more parameters to achieve the goal of data integration and system correlation. It is also suggested to upgrade the DAQ unit in order to handle real time data processing. In addition, the customised software can be improved so that signal conditioning, preliminary data analysis and data acquisition can be carried out at the same time. The author highly recommends implementing more advanced signal processing technique with machine deep learning to improve the accuracy of fault detection.

Moreover, research on various levels of system correlation needs to be carried out to investigate the interconnection of different components in the wheel-rail dynamics. A more sophisticated database system is also recommended.

References

ADAMS, M. L. 2000. *Rotating machinery vibration: from analysis to troubleshooting*, CRC Press.

ALFARO, S. C. A. & CAYO, E. H. 2012. Sensoring fusion data from the optic and acoustic emissions of electric arcs in the GMAW-S process for welding quality assessment. *Sensors,* 12**,** 6953-6966.

AMINI, A. 2016. *Online Condition Monitoring Of Railway Wheelsets.* Ph.D, Univeristy of Birmingham.

AMINI, A., ENTEZAMI, M. & PAPAELIAS, M. 2016. Onboard detection of railway axle bearing defects using envelope analysis of high frequency acoustic emission signals. *Case Studies in Nondestructive Testing and Evaluation,* 6**,** 8-16.

AMINI, A., HUANG, Z., ENTEZAMI, M. & PAPAELIAS, M. 2017. Evaluation of the effect of speed and defect size on high-frequency acoustic emission and vibration condition monitoring of railway axle bearings. *Insight-Non-Destructive Testing and Condition Monitoring,* 59**,** 184-188.

ANASTASOPOULOS, A., BOLLAS, K., PAPASALOUROS, D. & KOUROUSIS, D. Acoustic emission on-line inspection of rail wheels. Proc. 29th Eur. Conf. Acoust. Emission Testing, 2010. 1-8.

ANDERSEN, T. 2011. Analysis of past derailments: Information from data bases, investigation reports and surveys. DNV presentation.

ANDERSSON, C. & DAHLBERG, T. 1998. Wheel/rail impacts at a railway turnout crossing. *Proceedings of the Institution of Mechanical Engineers, Part F: Journal of Rail and Rapid Transit,* 212**,** 123-134.

BARKE, D. & CHIU, W. 2005. Structural health monitoring in the railway industry: a review. *Structural Health Monitoring,* 4**,** 81-93.

BENTLY, D. E., GOLDMAN, P. & YU, J. 2001. Rolling element bearing defect detection and diagnostics using REBAM® Probes. *Orbit,* 22**,** 12-25.

BLADON, K. & HUDD, R. Wayside monitoring of metro lines. Railway Condition Monitoring, 2008 4th IET International Conference on, 2008. IET, 1-8.

BLADON, K., RENNISON, D., IZBINSKY, G., TRACY, R. & BLADON, T. Predictive condition monitoring of railway rolling stock. Proc., Conference on Railway Engineering, 2004.

BLAKENEY, A. 2001. Hot axle bearing detection,. London: Reference number :GE/RT8014,Railway Safety.

BOLLAS, K., PAPASALOUROS, D., KOUROUSIS, D. & ANASTASOPOULOS, A. 2010. Acoustic emission inspection of rail wheels. *J. Acoust. Emission,* 28**,** 215-228.

BOSSO, N., ZAMPIERI, N. & GUGLIOTTA, A. 2012. A modular monitoring system for onboard vehicle diagnostic. *Material Evaluation***,** 78-85.

BRECKENRIDGE, F. R., TSCHIEGG, C. E. & GREENSPAN, M. 1975. Acoustic emission: some applications of Lamb's problem. *The Journal of the Acoustical Society of America,* 57**,** 626-631.

BRICKLE, B., MORGAN, R., SMITH, E., BROSSEAU, J. & PINNEY, C. 2008. Wheelset Condition Monitoring-RSSB Report for Task T607. *TTCI (UK), Ltd*.

BURSTOW, M. 2010. Management of rail and wheel deterioration. *In:* SCHMID, F. (ed.) *Wheel-Rail Best Practice Handbook.* Birmingham University Press, A.N. Harris.

CAESARENDRA, W., KOSASIH, B., TIEU, A. K., ZHU, H., MOODIE, C. A. & ZHU, Q.

2016. Acoustic emission-based condition monitoring methods: Review and application for low speed slew bearing. *Mechanical Systems and Signal Processing,* 72**,** 134-159.
CANNON, D., EDEL, K. O., GRASSIE, S. & SAWLEY, K. 2003. Rail defects: an overview. *Fatigue & Fracture of Engineering Materials & Structures,* 26**,** 865-886.
CARTER, G. C., KNAPP, C. H. & NUTTALL, A. H. 1973. Estimation of the magnitude-squared coherence function via overlapped fast Fourier transform processing. *Audio and Electroacoustics, IEEE Transactions on,* 21**,** 337-344.
CASTANEDO, F. 2013. A review of data fusion techniques. *The Scientific World Journal,* 2013.
CHACON, J. L. F., KAPPATOS, V., BALACHANDRAN, W. & GAN, T.-H. 2015. A novel approach for incipient defect detection in rolling bearings using acoustic emission technique. *Applied Acoustics,* 89**,** 88-100.
CHATTOPADHYAY, G. & KUMAR, S. 2008. Parameter estimation for rail degradation model. *International Journal of Performability Engineering*.
COPE, D. & ELLIS, J. 2002. British railway track 7th edition, Volume 5: Switch and crossing maintenance. *Derby, UK: The Permanent Way Institution*.
CURTIS, G. 1974. Acoustic emission—4: Spectral analysis of acoustic emission. *Non-Destructive Testing,* 7**,** 82-91.
DANNESKIOLD-SAMSOE, U., GRAMTORP, J., MADSEN, A.-H. T. & HAURE, T.-M. A. 1993. Plant for track-based detection of the wheel profile of train wheels. Google Patents.
DELAY ATTRIBUTION BOARD 2015. Delay Attribution Guide. *Delay Attribution Board, London.*
DHILLON, B. 2011. Weighted Multi-sensor Data Level Fusion Method of Vibration Signal Based on Correlation Function. *Chinese Journal of Mechanical Engineering,* 5**,** 025.
DONG, J., ZHUANG, D., HUANG, Y. & FU, J. 2009. Advances in multi-sensor data fusion: Algorithms and applications. *Sensors,* 9**,** 7771-7784.
DUKKIPATI, R. & DONG, R. 1999. Impact Loads due to Wheel Flats and Shells. *Vehicle System Dynamics,,* 31**,** 1-22.
EFTEKHARNEJAD, B., CARRASCO, M., CHARNLEY, B. & MBA, D. 2011. The application of spectral kurtosis on Acoustic Emission and vibrations from a defective bearing. *Mechanical Systems and Signal Processing,* 25**,** 266-284.
EKBERG, A. & SOTKOVSZKI, P. 2001. Anisotropy and rolling contact fatigue of railway wheels. *International journal of fatigue,* 23**,** 29-43.
ELASHA, F., GREAVES, M., MBA, D. & FANG, D. 2016. A comparative study of the effectiveness of vibration and acoustic emission in diagnosing a defective bearing in a planetry gearbox. *Applied Acoustics,* 115**,** 181-195.
EN 15313 2007. Railway applications — In-service wheelset operation requirements and inservice and off-vehicle wheelset maintanance
FAIZ, R. & SINGH, S. Condition monitoring of track geometry in UK rail. Computing, Engineering and Information, 2009. ICC'09. International Conference on, 2009. IEEE, 182-190.
FELTEN, D. 2003. *Understanding Bearing Vibration Frequencies* [Online]. Available: http://electromotores.com/PDF/InfoT%C3%A9cnica/EASA/Understanding%20Bearing%20Vibration%20Frequencies.pdf, [Accessed June 2013] [Accessed].
FU, G. 2005. *Inspection and monitoring techniques for bridges and civil structures*, Elsevier.
FU, Z.-F. & HE, J. 2001. *Modal analysis*, Butterworth-Heinemann.
GAO, L., ZAI, F., SU, S., WANG, H., CHEN, P. & LIU, L. 2011. Study and application of

acoustic emission testing in fault diagnosis of low-speed heavy-duty gears. *Sensors,* 11**,** 599-611.
GRASSIE, S. 2012. Squats and squat-type defects in rails: the understanding to date. *Proceedings of the Institution of Mechanical Engineers, Part F: Journal of Rail and Rapid Transit,* 226**,** 235-242.
GRASSIE, S. L. 2005. Rolling contact fatigue on the British railway system: treatment. *Wear,* 258**,** 1310-1318.
GROSSE, C. U., FINCK, F., KURZ, J. H. & REINHARDT, H. W. 2004. Improvements of AE technique using wavelet algorithms, coherence functions and automatic data analysis. *Construction and building Materials,* 18**,** 203-213.
GROSSE, C. U. & LINZER, L. M. 2008. Signal-based AE analysis. *Acoustic emission testing.* Springer Science & Business Media.
GROSSE, C. U. & OHTSU, M. 2008. *Acoustic emission testing*, Springer Science & Business Media.
HAJIBABAI, L., SAAT, M., OUYANG, Y., BARKAN, C., YANG, Z., BOWLING, K., SOMANI, K., LAURO, D. & LI, X. Wayside defect detector data mining to predict potential WILD train stops. Annual Conference and Exposition of the American Railway Engineering and Maintenance-of-Way Association (AREMA), Chicago, Illinois, 2012.
HALL, D. L. & LLINAS, J. 1997. An introduction to multisensor data fusion. *Proceedings of the IEEE,* 85**,** 6-23.
HASE, A., MISHINA, H. & WADA, M. 2012. Correlation between features of acoustic emission signals and mechanical wear mechanisms. *Wear,* 292**,** 144-150.
HENG, R. & NOR, M. 1998. Statistical analysis of sound and vibration signals for monitoring rolling element bearing condition. *Applied Acoustics,* 53**,** 211-226.
HOWARD, I. 1994. A Review of Rolling Element Bearing Vibration'Detection, Diagnosis and Prognosis'. DTIC Document.
HUANG, Z., AMINI, A., WANG, L., KEYKYRAS, S. & PAPAEILAS, M. online evaluation of railway axle bearing faults using acoustic emission and vibration analysis. BINDT, 2014 Manchester.
HUANG, Z., VALLELY, P., AMINI, A., SHI, S. & PAPAELIAS, M. 2015. Structural health monitoring of cast manganese crossing using acoustic emission techniques. Birmingham Centre for Railway Research and Education.
INDEPENDENT INVESTIGATION BOARD 2006. Train Derailment at Hartfield: A Final Report by the Independent Investigation Board.
JAMES LI, C. & LI, S. 1995. Acoustic emission analysis for bearing condition monitoring. *Wear,* 185**,** 67-74.
JARDINE, A. K., LIN, D. & BANJEVIC, D. 2006. A review on machinery diagnostics and prognostics implementing condition-based maintenance. *Mechanical systems and signal processing,* 20**,** 1483-1510.
JAYASWAL, P., VERMA, S. & WADHWANI, A. 2011. Development of EBP-Artificial neural network expert system for rolling element bearing fault diagnosis. *Journal of Vibration and Control,* 17**,** 1131-1148.
JONES, C. J. C. & JONES, R. 2010. Management of noise and vibration. *In:* SCHMID, F. (ed.) *Wheel-Rail Best Practice Handbook.* Birmingham University Press, A.N. Harris.
JONES, M. & SOUTHCOMBE, J. 2015. *Track condition monitoring using service trains* [Online]. [Accessed].
KAPHLE, M., TAN, A. C., THAMBIRATNAM, D. P. & CHAN, T. H. 2012. A Study on the

Use of Acoustic Emission Technique as a Structural Health Monitoring Tool. *Engineering Asset Management and Infrastructure Sustainability.* Springer.
KEYSIGHT TECHNOLOGIES. 2009. *U2500A Series USB Simultaneous Sampling Multifunction Data Acquisition User's Guide* [Online]. Available: http://www.keysight.com/en/pd-1250130-pn-U2531A/2msa-s-usb-modular-simultaneous-data-acquisition?pm=PL&nid=-33238.739734&cc=GB&lc=eng [Accessed].
KONSTANTIN-HANSEN, H. & HERLUFSEN, H. 2010. Envelope and cepstrum analyses for machinery fault identification. *Sound and Vibration,* 44**,** 10.
KOYO 2010. Rolling bearings: failures, causes and countermeasures.
KSCHISCHANG, F. R. 2006. The hilbert transform. *University of Toronto*.
KUMAR, B. V., MAHALANOBIS, A. & JUDAY, R. D. 2005. *Correlation pattern recognition,* Cambridge University Press.
LACEY, S. 2008. An overview of bearing vibration analysis. *Maintenance & Asset Management,* 23**,** 32-42.
LAGNEBÄCK, R. 2007. *Evaluation of wayside condition monitoring technologies for condition-based maintenance of railway vehicles*, Lule å University of Technology.
LAMARI, A. C. 2008. *Rolling stock bearing condition monitoring systems.* University of Southern Queensland.
LEBOLD, M., MCCLINTIC, K., CAMPBELL, R., BYINGTON, C. & MAYNARD, K. Review of vibration analysis methods for gearbox diagnostics and prognostics. Proceedings of the 54th meeting of the society for machinery failure prevention technology, Virginia Beach, VA, 2000. 623-634.
LEWIS, J. Fast normalized cross-correlation. Vision interface, 1995. 120-123.
LEWIS, R. & OLOFSSON, U. 2009. *Wheel-rail interface handbook*, Elsevier.
LI, B., CHOW, M.-Y., TIPSUWAN, Y. & HUNG, J. C. 2000. Neural-network-based motor rolling bearing fault diagnosis. *IEEE transactions on industrial electronics,* 47**,** 1060-1069.
LI, X. 2002. A brief review: acoustic emission method for tool wear monitoring during turning. *International Journal of Machine Tools and Manufacture,* 42**,** 157-165.
LIDÉN, T. 2016. *Towards concurrent planning of railway maintenance and train services*, Linköping University Electronic Press.
LIGGINS II, M., HALL, D. & LLINAS, J. 2008. *Handbook of multisensor data fusion: theory and practice*, CRC press.
MADEJSKI, J. 2006. Automatic detection of flats on the rolling stock wheels. *Journal of Achievements in materials and manufacturing Engineering,* 16**,** 160-163.
MALY, T., RUMPLER, M., SCHWEINZER, H. & SCHOEBEL, A. New development of an overall train inspection system for increased operational safety. Intelligent Transportation Systems, 2005. Proceedings. 2005 IEEE, 2005. IEEE, 188-193.
MALY, T. & SCHOBEL, A. Concept for crossborder data exchange on wayside train monitoring systems. Intelligent Transport Systems Telecommunications,(ITST), 2009 9th International Conference on, 2009. IEEE, 315-319.
MARFO, A., CHEN, Z. & LI, J. 2013. Acoustic emission analysis of fatigue crack growth in steel structures. *Journal of Civil Engineering,* 4**,** 239-249.
MARQUEZ, F. P. G., LEWIS, R. W., TOBIAS, A. M. & ROBERTS, C. 2008. Life cycle costs for railway condition monitoring. *Transportation Research Part E: Logistics and Transportation Review,* 44**,** 1175-1187.
MBA, D. & HALL, L. 2002. The transmission of acoustic emission across large-scale turbine rotors. *NDT & E International,* 35**,** 529-539.

MCFADDEN, P. & SMITH, J. 1984. Vibration monitoring of rolling element bearings by the high-frequency resonance technique—a review. *Tribology International,* 17**,** 3-10.
MCINERNY, S. & DAI, Y. 2003. Basic vibration signal processing for bearing fault detection. *Education, IEEE Transactions on,* 46**,** 149-156.
MCLASKEY, G. C. & GLASER, S. D. 2012. Acoustic emission sensor calibration for absolute source measurements. *Journal of Nondestructive Evaluation,* 31**,** 157-168.
MIETTINEN, J. & PATANIITTY, P. Acoustic emission in monitoring extremely slowly rotating rolling bearing. Proceedings of 12th International Congress on Condition Monitoring and Diagnostic Engineering Management, COMADEM, 1999. 289-297.
MILLER, R. K. & MCINTIRE, P. 1987. Nondestructive Testing Handbook. Vol. 5: Acoustic Emission Testing. *American Society for Nondestructive Testing, 4153 Arlingate Plaza, Caller# 28518, Columbus, Ohio 43228, USA, 1987. 603*.
MISTRAS. 2011. *R50α Product Data sheet* [Online]. Available: http://www.physicalacoustics.com/content/literature/sensors/Model_R50a.pdf [Accessed 2015].
MUSZYŃSKA, A. 1989. Misalignment and shaft crack–related phase relationships for 1X and 2X vibration components of rotor responses. *Orbit,* 10**,** 4-8.
NETWORK RAIL 2007. Signal Maintenance Specifications. *Treadles - General.*
NGIGI, R., PISLARU, C., BALL, A. & GU, F. Modern techniques for condition monitoring of railway vehicle dynamics. Journal of Physics: Conference Series, 2012. IOP Publishing, 012016.
NIELSEN, J. C. & JOHANSSON, A. 2000. Out-of-round railway wheels-a literature survey. *Proceedings of the Institution of Mechanical Engineers, Part F: Journal of Rail and Rapid Transit,* 214**,** 79-91.
OKAMOTO, I. 1998. How bogies work. *Japan Railway & Transport Review,* 18**,** 52-61.
ONO, K. 2005. Current understanding of mechanisms of acoustic emission. *The Journal of Strain Analysis for Engineering Design,* 40**,** 1-15.
OUYANG, Y., LI, X., BARKAN, C. P., KAWPRASERT, A. & LAI, Y. C. 2009. Optimal locations of railroad wayside defect detection installations. *Computer‐Aided Civil and Infrastructure Engineering,* 24**,** 309-319.
PALO, M., GALAR, D., NORDMARK, T., ASPLUND, M. & LARSSON, D. 2014. Condition monitoring at the wheel/rail interface for decision-making support. *Proceedings of the Institution of Mechanical Engineers, Part F: Journal of Rail and Rapid Transit,* 228**,** 705-715.
PANDYA, D., UPADHYAY, S. & HARSHA, S. 2013. Fault diagnosis of rolling element bearing with intrinsic mode function of acoustic emission data using APF-KNN. *Expert Systems with Applications,* 40**,** 4137-4145.
PAO, Y. H., GAJEWSKI, R. R. & CERANOGLU, A. N. 1979. Acoustic emission and transient waves in an elastic plate. *The Journal of the Acoustical Society of America,* 65**,** 96-105.
PAPAELIAS, M. 2009. Effect of defective wheels on rail, Saferail report, Reference number :SCP7-GA-2008-218674,.
PAPAELIAS, M. 2013. Train wheelsets and wayside condition monitoring. Engineering Applications Seminar: The University of Birmingham.
PAPAELIAS, M., AMINI, A., HUANG, Z., VALLELY, P., DIAS, D. C. & KERKYRAS, S. 2014. Online condition monitoring of rolling stock wheels and axle bearings. *Proceedings of the Institution of Mechanical Engineers, Part F: Journal of Rail and Rapid Transit***,** 0954409714559758.

PAPAELIAS, M., PAPAILIAS, F., KERKYRAS, S. & GRAHAM, K. The Future of Rail Inspection Technology and the INTERAIL FP7 Project. the British Institute NDT 2012 International Conference, 11-13 September 2012 Daventry, UK.

PAPAELIAS, M. P., ROBERTS, C. & DAVIS, C. 2008. A review on non-destructive evaluation of rails: state-of-the-art and future development. *Proceedings of the Institution of Mechanical Engineers, Part F: Journal of Rail and rapid transit,* 222**,** 367-384.

PATIL, M. A. V., KUMAR, B. & BARJIBHE, R. 2016. An Extensive Review on the Use of Acoustic Emission Technique for Continuous Monitoring.

RADU, C. 2010. The Most Common Causes of Bearing Failure and the Importance of Bearing Lubrication. *RKB Technical Review-February*.

RAIL ACCIDENT INVESTIGATION BRANCH 2010. Derailment in Summit Tunnel.

RAILWAY GAZZETTE 2009. Wheelset troubles strike again. *Railway Gazzette.*

RANDALL, R. B. & ANTONI, J. 2011. Rolling element bearing diagnostics—a tutorial. *Mechanical Systems and Signal Processing,* 25**,** 485-520.

RINGSBERG, J. W. 2001. Life prediction of rolling contact fatigue crack initiation. *International Journal of fatigue,* 23**,** 575-586.

ROBERTS, T. & TALEBZADEH, M. 2003. Acoustic emission monitoring of fatigue crack propagation. *Journal of Constructional Steel Research,* 59**,** 695-712.

ROGERS, L. 1979. The application of vibration signature analysis and acoustic emission source location to on-line condition monitoring of anti-friction bearings. *Tribology international,* 12**,** 51-58.

RUIZ-CÁRCEL, C., HERNANI-ROS, E., CAO, Y. & MBA, D. 2014. Use of Spectral Kurtosis for Improving Signal to Noise Ratio of Acoustic Emission Signal from Defective Bearings. *Journal of Failure Analysis and Prevention,* 14**,** 363-371.

SALVAN, S., PARKIN, R., COY, J. & LI, W. Intelligent Condition Monitoring of Bearings in Mail Processing Machines using Acoustic Emission. Proceedings of COMADEM, 2001. 67-74.

SCHMID, F. 2010. *Wheel-rail Best Practice Handbook*.

SCHÖBEL, A. & MIRKOVIĆ, S. 2010. Flat Wheel Detection as a Part of Wayside Train Monitoring Systems. *Acta facultatis medicae Naissensis,* 27.

SEGLA, M., WANG, S. & WANG, F. Bearing fault diagnosis with an improved high frequency resonance technique. Industrial Informatics (INDIN), 2012 10th IEEE International Conference on, 2012. IEEE, 580-585.

SEKER, S. 2000. Determination of air-gap eccentricity in electric motors using coherence analysis. *IEEE Power Engineering Review,* 20**,** 48-50.

SHI, S. 2015. *Online structural integrity monitoring of railway infrastructure using acoustic emission.* Ph.D. progress report, The University of Birmingham.

SHIROISHI, J., LI, Y., LIANG, S., KURFESS, T. & DANYLUK, S. 1997. Bearing condition diagnostics via vibration and acoustic emission measurements. *Mechanical Systems and Signal Processing,* 11**,** 693-705.

SIDDIQUE, A., YADAVA, G. & SINGH, B. Applications of artificial intelligence techniques for induction machine stator fault diagnostics: review. Diagnostics for Electric Machines, Power Electronics and Drives, 2003. SDEMPED 2003. 4th IEEE International Symposium on, 2003. IEEE, 29-34.

SKF 1994. SKF Product Information 401: Bearing failures and causes.

SKF. 2010. *SKF Axletronic sensors for the railway industry* [Online]. www.skf.com. Available: http://www.skf.com/binary/21-57366/11007-EN.pdf [Accessed].

SOUTHERN, C., RENNISON, D. & KOPKE, U. 2004. RailBAM-an advanced bearing acoustic monitor: initial operational performance results. *CORE 2004: New Horizons for Rail*, 23.
STEINBERG, A. N., BOWMAN, C. L. & WHITE, F. E. Revisions to the JDL data fusion model. AeroSense'99, 1999. International Society for Optics and Photonics, 430-441.
STRATMAN, B., LIU, Y. & MAHADEVAN, S. 2007. Structural health monitoring of railroad wheels using wheel impact load detectors. *Journal of Failure Analysis and Prevention*, 7, 218-225.
SWIFT, M., AURISICCHIO, G. & PACE, P. New practices for railway condition monitoring and predictive analysis. Railway Condition Monitoring and Non-Destructive Testing (RCM 2011), 5th IET Conference on, 2011. IET, 1-6.
TAHA, M. R., NOURELDIN, A., LUCERO, J. & BACA, T. 2006. Wavelet transform for structural health monitoring: a compendium of uses and features. *Structural Health Monitoring*, 5, 267-295.
TANDON, N. & CHOUDHURY, A. 1999. A review of vibration and acoustic measurement methods for the detection of defects in rolling element bearings. *Tribology International*, 32, 469-480.
TANDON, N. & NAKRA, B. 1992. Comparison of vibration and acoustic measurement techniques for the condition monitoring of rolling element bearings. *Tribology International*, 25, 205-212.
TAYLOR, J. I. 1994. *The vibration analysis handbook*, Vibration Consultants.
TIMKEN 2015. AP™ Bearings,Size and Dimensional Data.
TSLG 2012. Railway Technical Strategy 2012.
TUCKER, G. & HALL, A. Breaking down the barriers to more cross-industry Remote Condition Monitoring (RCM). Railway Condition Monitoring (RCM 2014), 6th IET Conference on, 2014. IET, 1-6.
UIC, R. R. 2015. Railway Statistics 2015.
UNIFE 2016. World Rail Market Study.
USGAME, H. M., PEDRAZA, C. A., QUIROGA, J., 2013. Acoustic emission-based early detection in tapered roller bearings. *Ingenieria e Investigacion*, 33, 5-10.
VALE, C. 2014. Advanced Approaches for Axle Bearing Condition Monitoring, . *Faculty of Engineering, University of Porto, Portugal*.
VALLELY, P. 2015. *A holistic approach to remote condition monitoring for the accurate evaluation of railway infrastructure and rolling stock.* Ph.D. progress report, The University of Birmingham.
VALLEN, H. 2002. AE testing fundamentals, equipment, applications. *Journal of Nondestructive Testing(Germany)*, 7, 1-30.
VALLEN SYSTEME. 2015a. *Acoustic Emission Preamplifiers* [Online]. Available: http://www.vallen.de/zdownload/pdf/Pre1504.pdf [Accessed].
VALLEN SYSTEME. 2015b. *Acoustic Emission Sensors Specification* [Online]. Available: http://www.vallen.de/zdownload/pdf/sov1507.pdf [Accessed].
VIKTOROV, I. A. 2014. Rayleigh and lamb waves: physical theory and applications (ultrasonic technology).
WADLEY, H., SCRUBY, C. & SPEAKE, J. 1980. Acoustic emission for physical examination of metals. *International Metals Reviews*, 25, 41-64.
WASIWITONO, U., ZHENG, D. & CHIU, W. How useful is track acceleration for monitoring impact loads generated by wheel defects? 5th Australasian Congress on

Applied Mechanics (ACAM 2007), 2007. Engineers Australia, 502-507.
WATSON, M., SHELDON, J., AMIN, S., LEE, H., BYINGTON, C. & BEGIN, M. A comprehensive high frequency vibration monitoring system for incipient fault detection and isolation of gears, bearings and shafts/couplings in turbine engines and accessories. ASME Turbo Expo, 2007.
WESTON, M., WRIGHT, B., LIAPTSIS, D., KNIGHT-GREGSON, B. & RANTATALO, M. Reliable sub-surface ultrasonic inspection of cast manganese steel crossings. Railway Condition Monitoring (RCM 2014), 6th IET Conference on, 2014. IET, 1-3.
XU, M. 1999. Spike Energy™ Measurement and Case Histories. *ENTEK IRD International Corporation Technical Report, Online: http://domino. automation. rockwell. com/applications/gs/region/EntekWe bST. nsf/files/Xu99. pdf/$ file/Xu99. pdf*.
XUEJUN, L., GUANGFU, B. & DHILLON, B. S. A new method of multi-sensor vibration signals data fusion based on correlation function. Computer Science and Information Engineering, 2009 WRI World Congress on, 2009. IEEE, 170-174.
YAM, R., TSE, P., LI, L. & TU, P. 2001. Intelligent predictive decision support system for condition-based maintenance. *The International Journal of Advanced Manufacturing Technology,* 17**,** 383-391.
YANG, C., L, S. & TOURNEAU 2005. Learning to predict train wheel failures. *Proceedings of the eleventh ACM SIGKDD international conference on Knowledge discovery in data mining.* Chicago, Illinois, USA: ACM.
YILMAZ, M. & ÇETİN, O. T. S. Y. M. 2004. Titreşimin Fiziksel Prensipleri ve Ölçme Teknikleri. *Gaziosmanpaşa Üniversitesi Ziraat Fakültesi Dergisi,* 2004.
YILMAZER, P., AMINI, A. & PAPAELIAS, M. The structural health condition monitoring of rail steel using acoustic emission techniques. BINDT 2012 Conference, 2012 UK.
ZARETSKY, E. V. 2010. Rolling bearing life prediction, theory, and application. *Recent Developments in Wear Prevention, Friction and Lubrication,* 37**,** 2.
ZHANG, Y.-J. 2011. Rail Vehicle Bearing Defects Detection.
ZUBAIR, M., HARTMANN, K. & LOFFELD, O. 2012. A Correlation Based Sensor Fusion Method for Multi-Channel Seismic Network. *International Journal of Computer and Electrical Engineering,* 4**,** 363.

Appendix A: datasheet for bearing characteristic frequencies

99591-99100 freq results

Rotating Inner Race or Rotating Outer Race Operating at 60 RPM

Bearing: Inner ring 99591

Bearing Geometry Constants

Number of Rollers (Z): 21

1/2 Incl. Roller CL Angle for TRB

(contact angle for non-TRB): 13.6 deg

Pitch Diameter: 200.7 mm

Mean Roller Diameter: 23.6 mm

Frequency Coefficients - multiply by RPM / 60 to calculate frequency

BPFI - Roller/Ball Pass Frequency Inner Race: 11.7 Hz / (Rev/Sec)

BPFO - Roller/Ball Pass Frequency Outer Race: 9.3 Hz / (Rev/Sec)

BSF - Roller/Ball Spin Frequency: 4.198 Hz / (Rev/Sec)

FTFI - Fundamental Train Frequency Inner Race Rotation: 0.443 Hz / (Rev/Sec)

FTFO - Fundamental Train Frequency Outer Race Rotation: 0.557 Hz / (Rev/Sec)

Bearing Relative Component Speeds (Revs/Sec)

Inner/Outer Race or Outer/Inner Race:	1
Cage/Outer Race:	0.443
Cage/Inner Race:	0.557
Roller/Cage:	4.198

Frequencies Resulting From Component Irregularities		
1 Hertz (Revolutions Per Second) – Inner Race or Outer Race		
Possible Source of Vibration	**Frequency (Hz)**	**Other Common Terminology**
Eccentricity Of Rotating Member	f_0 = 1	
Out-Of-Round Of Rotating Member	f_1 = 1	
Roller Irregularity (e.g., nick or spall)	f_2 = 8.396	
	4.198	BSF- Roller/Ball Spin Freq
Inner Race Irregularity (e.g., nick or spall)	f_3 = 11.7	BPFI - Roller/Ball Pass Freq Inner Race
Outer Race Irregularity (e.g., nick or spall)	f_4 = 9.3	BPFO - Roller/Ball Pass Freq Outer Race
Roller Size Variations (Rotating Inner Race)	f_5 = 0.443	FTFI - Fundamental Train Freq Inner Race
Roller Size Variations (Rotating Outer Race)	f_6 = 0.557	FTFO – Fundamental Train Freq Outer Race

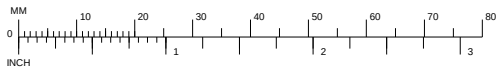

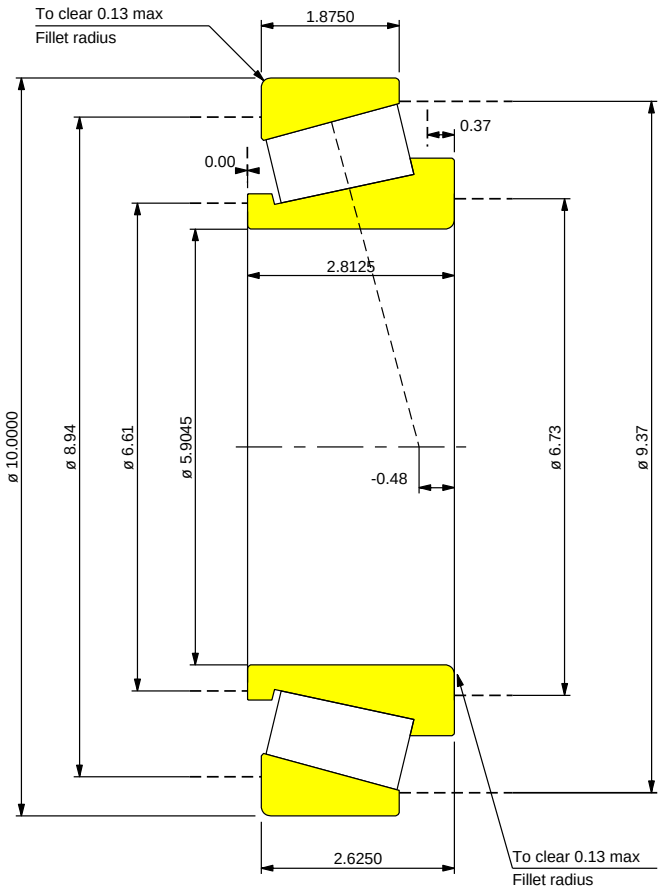

IMPERIAL UNITS

SUPERSEDES

PROJECTION | ORIGINAL SCALE **1 : 2**

Max shaft fillet radius - R	0.13	in
Max housing fillet radius - r	0.13	in
ISO factor - e	0.41	
ISO factor - Y	1.47	
Bearing Weight (with cage)	28.76	lb
Number of rollers per row	21	
Effective center a / Cone back face	-0.48	in

TIMKEN

THE TIMKEN COMPANY

CANTON, OHIO USA

99591 - 99100

TS BEARING ASSEMBLY

K factor	1.43
Dynamic Radial Rating, C90	34100 lbf
Dynamic Thrust Rating, Ca90	23800 lbf
Static Radial Rating, C0	211000 lbf
Radial Rating (1E6 Rev.), C1	132000 lbf

DRAWN	CHECKED	APPROVED	DATE
GST			12/03/2014

*** COMPUTER GENERATED ***

FOR DISCUSSION ONLY

Appendix B: typical results from HABDs

6R45 17/8/11

Train number : 10399

~~~~~~

17.08.2011 11:15:41 Manton Wood Up (R)(T2)standard dir axles: 106

speed : 69 km/hRef1: +032Mirror1: 011 016 016 017RR: 106

Ambient : +020 ℃Ref2: +033Mirror2: 002 002 002 002MK: 106

Train end recognized Ref3: +035Mirror3: 004 006 005 005GR: 106

~~~~~~

Alarm 0018 1 01 0 +085 axle info: +085 +020 +045 xxxx +071 Difference hot alarm

InfoAlarm telegrams: HOAL 1 HOAR 0 FBOA1 0 FBOA2 0

InfoFÜS-Softwarerelease 6.2.0

alarm temperatures HOA120.056.0xxxxxxxxxxHOA Standard

Infoaverage temperature +28.15 +23.73 +55.84 xxxxx All

Infoaverage temperature +28.15 +23.73 +55.84 xxxxx other

Train Start :+62 km/h

Vmin : Axle 87 +69 km/h

Vmax : Axle 1 +72 km/h

Difference :3 km/h4 %

AXLETEMPERATURE AXL |TEMPERATURE AXLFBOA

NUMBERHOA 1 ℃|HOA 2 in ℃in ℃

-----------------------------------|--

1 26xxxxxx|xxxxx 21 68

2 26xxxxxx|xxxxxx 24 56

3 26xxxxxx|xxxxx 21 57

4 25xxxxxx|xxxxx 23 73

5	26xxxxxx|xxxxxx 27	72
6	25xxxxxx|xxxxxx 24	76
7	23xxxxx|xxxxx 22	75
8	23xxxxx|xxxxx 22	78
9	27xxxxxx|xxxxxx 25	24
10	26xxxxxx|xxxxx 22	24
11	31xxxxxxx|xxxxxx 27	131
12	25xxxxxx|xxxxx 23	128
13	38xxxxxxxxx|xxxxxx 26	123
14	29xxxxxxx|xxxxxxx 29	128
15	23xxxxx|xxxxx 22	76
16	22xxxxx|xxxxx 22	73
17	25xxxxxx|xxxxx 23	24
18	85[J] DDDDDDD|xxxxx 20	45
19	26xxxxxx|xxxxx 23	126
20	29xxxxxxx|xxxxxx 24	111
21	26xxxxxx|xxxxx 21	117
22	38xxxxxxxxx|xxxxxxx 29	133
23	25xxxxxx|xxxxx 22	87
24	33xxxxxxxx|xxxxxx 26	25
25	30xxxxxxx|xxxxxx 26	24
26	33xxxxxxxx|xxxxxx 26	25
27	25xxxxxx|xxxxx 23	139
28	29xxxxxxx|xxxxx 22	97
29	28xxxxxxx|xxxxxx 26	123
30	24xxxxxx|xxxxx 21	114
31	25xxxxxx|xxxxx 21	69
32	27xxxxxx|xxxxxx 24	65

Appendix C: typical results from WILDs

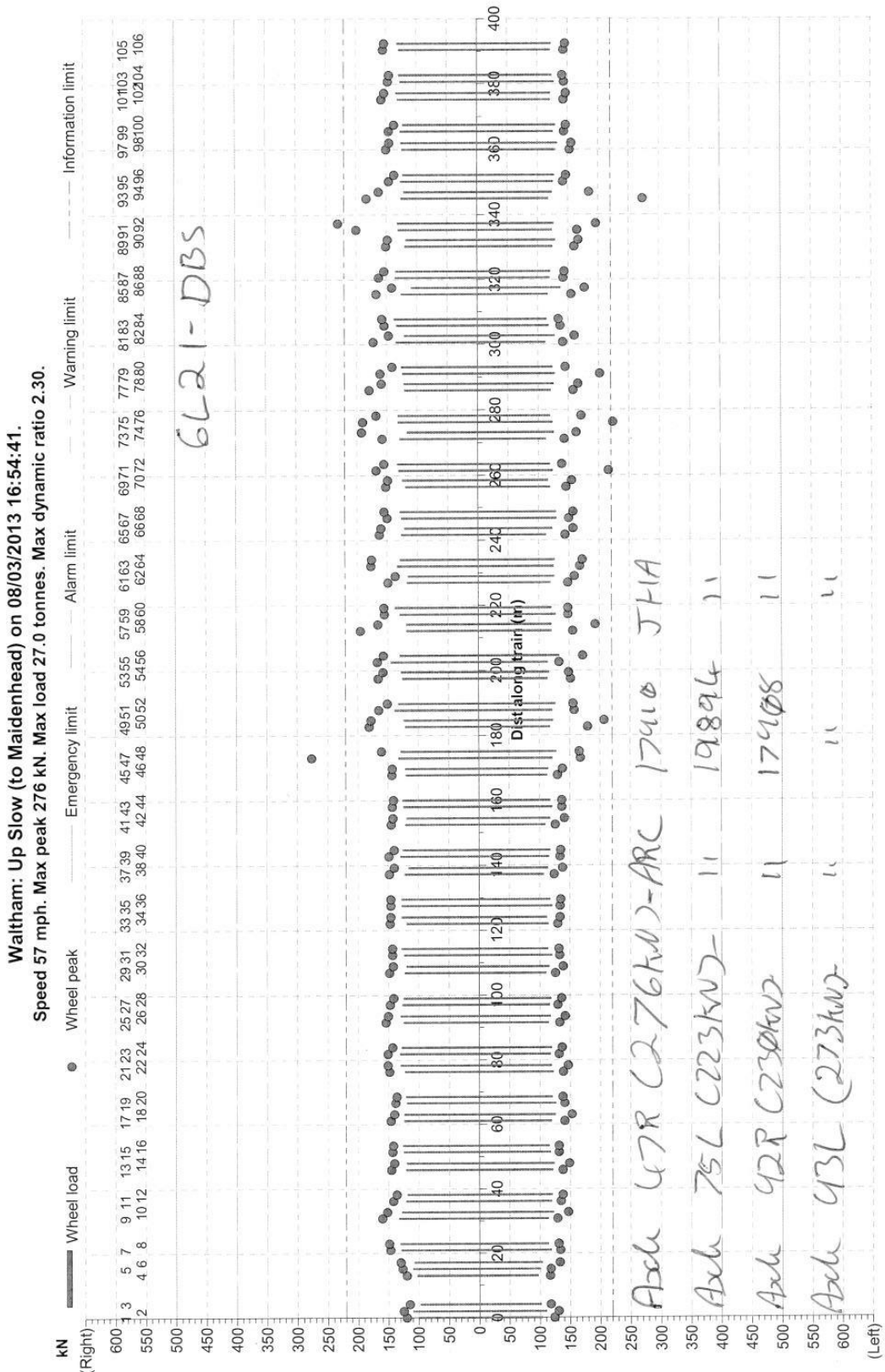

Appendix D: vehicle diagram for Class 168